ELECTROCHEMICAL CHIRAL BIOSENSORS

RUZNIZA MOHD-ZAWAWI

ELECTROCHEMICAL CHIRAL BIOSENSORS

RUZNIZA MOHD ZAWAWI

A thesis submitted in part fulfilment

of the requirements for the degree of

Doctor of Philosophy.

Department of Chemistry

Durham University

2011

ABSTRACT

Recognition of chiral molecules in biological assemblies has been a subject of extensive research. The aim of this work was to fabricate and characterise biocompatible composite materials suitable for chiral recognition. Collagen, the most abundant chiral, extracellular protein, was chosen as a possible matrix. The chiral recognition properties were evaluated by a comparative study in collagen, collagen incorporated in tetramethyl orthosilicate (TMOS) and TMOS. In electrochemical studies, ferrocene was incorporated to facilitate electron transfer. The recognition characteristics of two chiral enzymes, L-lactate oxidase and D-glucose oxidase were tested using circular dichroism (CD), Fourier Transform Infra-Red (FTIR) spectroscopy and electrochemical methods. A surprising result revealed an inversion of chiral selectivity. The effect of various parameters such as immobilisation, temperature, chemical modification, solvent systems, on enantioselectivity is well known. Stereoinversions caused by the 'sergeants and soldiers' effect in gel-forming p-conjugated molecules caused by co-assembly has been reported by several groups. The inversion of stereoselectivity observed in this study is probably due to a combination of the microenvironment and electrostatic interactions of the enzyme, mediator and substrate with the chiral collagen matrix. The results may have important implications for biosensing, asymmetric syntheses and understanding the nature of chiral interactions in biological systems.

Declaration

The work described in this thesis was carried out in the Department of Chemistry at Durham University between January 2007 and July 2010, under the supervision of Dr. Ritu Kataky. All the work is my own, unless otherwise stated, and has not been submitted previously for a degree at this or any other university.

Ruzniza Mohd Zawawi

Statement of Copyright

To my beloved daughters,

Nurin Insyirah & Nurzara Arissa..

ACKNOWLEDGEMENT

No one came across my mind when it comes to acknowledgement section, but a great woman named Ritu Kataky. She is the one who helped me the most since the first day I stepped into this top leading university in UK, Durham University. When I feel down with my work, her words always restore my spirit to keep up a good work till the end of this journey. For that reason, I am most grateful to Dr Ritu Kataky, who served as my supervisor, without whose help, patience, guidance and encouragement; this would not have been possible.

Also many thanks to all the group members, Aidan, Francisco, Yusran, Alice, Anil, Ioanna, Quan, Paula and Rui who really helpful and make the group a fun and comfortable to be. I also thank Dr Helen Riggs for technical assistance during the characterizing properties using ESEM, Mr Doug Carswell for thermogravimetry analysis, and Dr Richard Thompson for invaluable guidance in using atomic force microscope (AFM), although the results obtained are not really good to be included in this thesis. To the electron microscope team in Biology and Physics Departments, thank you for the great SEM and TEM services provided. Indirectly, there are so many new techniques that I have learned through out my studies here. To the Department of Chemistry, Durham University, thank you so much for the scholarship and supports. Not forget to my sponsors, Ministry of Higher Education, Malaysia and Universiti Putra Malaysia for giving me the opportunity to further my studies in UK.

Personally, to my husband, thank you so much for your courage and understanding. Also to my mum, dad and my auntie ‘makngah’, thank you for your continuous support behind me.

Finally, thank you to all the people who have given their support and shared their knowledge and friendship that I forgot to mention in this section. The enjoying time in Durham will be in my memory forever.

Ruzniza

PUBLICATIONS

Ritu Kataky and Ruzniza Mohd Zawawi. 'Modification of the Chiral Selectivity of D-glucose oxidase and L-lactate oxidase in a Collagen Matrix'. *Phys. Chem. Chem. Phys.*, 2010, **12**, 9183-9187.

Ritu Kataky and Ruzniza Mohd Zawawi. 'Simultaneous Detection of L- and D-lactate in Dairy Products by Chiral Lactate Biosensor'. *Analytical Chemistry.* (submitted).

TABLE OF CONTENTS

LIST OF SYMBOLS AND ABBREVIATIONS

A	Ampere
A	Surface area
A	Absorbance
Å	Angstrom
C	Capacitance
C	Concentration
C_d	Double layer capacitance
D	Diffusion coefficient
e^-	Electron
E	Potential
E_p	Peak potential
E_{pa}	Anodic peak potential
E_{pc}	Cathodic peak potential
ΔE	Peak separation ($E_{pa} - E_{pc}$)
$E°$	Formal potential / Standard potential
f	Frequency
F	Faraday constant
i_p	Peak current
i_{pa}	Anodic peak current
i_{pc}	Cathodic peak current
J	Flux
k'_{ME}	Effective heterogeneous rate constant
K_M	Michaelis-Menten constant

mV	milivolt
O	Oxidized spesies
q	Charge
R	Reduced species
R	Universal gas constant
R	Resistance
R_s	Ohmic resistance of the electrolyte solution
R_p	Polarization resistance
R_{ct}	Charge transfer resistance
[S]	Concentration of substrate
t	time
T	Absolute temperature
v_0	Initial rate of reaction
V	Rate of enzyme-catalyzed reaction
V_{max}	Maximum rate of reaction
W	Warburg impedance
Z	Impedance
Z'	Real impedance
Z''	Imaginary impedance
$\nu^{1/2}$	Square Root of Scan Rate
λ	Wavelength
ϕ	Wrapping angle
ϕ	Phase shift
ω	Radial frequency
η	Overvoltage
θ	Ellipticity
1,2-DCE	1,2-Dichloroethane

Ag/AgCl	Silver/Silver Chloride Reference Electrode
CA	Chronoamperometry
CC	Chronocoulometry
CD	Circular Dichroism
CE	Counter electrode
CV	Cyclic Voltammetry / Cyclic Voltammogram
CNTs	Carbon Nanotubes
DMF	Dimethylformamide
DNA	Dioxyribonucleic acid
DPV	Differential Pulse Voltammetry
EIS	Electrochemical Impedance Spectroscopy
ESEM	Environmental Scanning Electron Microscopy
FAD	Flavin Adenine Dinucleotide
$FADH_2$	1,5-dihydro-Flavin Adenine Dinucleotide
Fc	Ferrocene
Fc^+	Ferrocenium ion
FMN	Flavin mononucleotide
$FMNH_2$	Dihydro-flavin mononucleotide
FTIR	Fourier Transform Infra-Red
GCE	Glassy Carbon Electrode
GOx	Glucose oxidase
GPs	Graphite particles
HCl	Hidrochloric Acid
ICP-OES	Inductively Coupled Plasma-Optical Emission Spectrometer
IHP	Inner Helmholtz Plane
IPE	Ideal Polarized Electrode

IR	Infra-Red
KCl	Potassium chloride
KH_2PO_4	Potassium dihydrogen phosphate
K_2HPO_4	Dipotassium hydrogen phosphate
LOx	Lactate oxidase
MWCNTs	Multi-walled Carbon Nanotubes
OHP	Outer Helmholtz Plane
ORD	Optical rotatory dispersion
PBS	Phosphate Buffer Solution
RE	Reference Electrode
SEM	Scanning Electron Microscopy
SPCs	Spherical porous carbons
SWCNTs	Single-walled Carbon Nanotubes
SWV	Square Wave Voltammetry
TEM	Transmission Electron Microscopy
TGA	Thermogravimetry Analysis
TMOS	Tetramethyl orthosilicate
WE	Working Electrode

LIST OF FIGURES

CHAPTER 1

CHAPTER 2

CHAPTER 3

FIGURE

CHAPTER 4

FIGURE

CHAPTER 5

FIGURE

CHAPTER 6

FIGURE

LIST OF TABLES

CHAPTER 4

CHAPTER 5

CHAPTER 6

CHAPTER 1

INTRODUCTION

1.1 Introduction to General Biosensors

The term biosensor has been variously applied to a number of devices either used to monitor living systems or incorporating biotic elements. Generally, a biosensor is a sensing device that incorporates a biological entity as a fundamental part of the sensing process. This can be enzymes, antibody, bacteria tissues, nucleic acids, proteins, drug, small organic molecules *etc*. The usual aim of a biosensor is to convert the biological recognition reaction into a measurable electronic signals, which under ideal circumstances, are proportional to the concentration of a single analyte or a related group of analytes.[1-2] Enzymes are the biological components most commonly used in biosensors, while electrochemical transduction is the most popular method, often employing potentiometric or amperometric methods. The analytical information from the biorecognition process is obtained in the form of potential (potentiometric) or current (amperometric) signals, depending on the sensoric devices. An amperometric biosensor may be more attractive nowadays due to its high sensitivity and wide linear range,[3] leading the presently available biosensor systems.

Over the past 20 years, research and development in the sensors area has expanded exponentially in terms of number of papers published, the financial investment and also the number of active researchers worldwide. In addition, the sensors have also gained momentum from the enormous commercial potential and are quickly becoming a useful tool in medicine, food quality control, environmental monitoring and other practical fields.[3-5] The wide uses of biosensors are mainly due to their favourable analytical characteristics, such as selectivity, sensitivity, portability, speed, low cost and potential for miniaturization.[4-5] Indeed, the selectivity of the biosensor for the target analyte is mainly determined by the biorecognition element, whilst its sensitivity is greatly influenced by the transducer.

It was during the 1980s, however, that large-scale commercial success was first achieved by introducing the glucose sensor.[6] At that time, the basic problem lay largely with the cost of producing the biosensors, which made most of the company involves in the biosensor sector uncompetitive with the other technologies widely used in the massive rapid testing sector. It was within this sector that the hopes were pinned, since it was and still is a huge market. Steady progress looks likely in the years ahead, with most of the research and development (R&D) work being undertaken to address niche markets. While fascinating, the research required to develop these technologies still lacks the impetus provided by mass-market potential.

Biosensor applications are expected to be successful where they can fulfil an industry-wide need such as food safety in rapid detection of pathogenic organisms such as *E. coli* or sugar measurement in drink products. There are enormous number of possible biosensor applications in the agriculture sector such as monitoring crop diseases, plant nutrients, and pesticides. However, there seems to be a consensus in the research community that many of these applications are still too specialized for commercial viability.

Previous study shows that medical applications overshadow the other seemingly important applications areas. Glucose sensing has been the first to become a commercial success in mass-market biosensor nowadays. The increasing rate of obesity and the alarming rise in the rate of diabetes in the industrialized world is driving a need for more biosensors to monitor diabetic patients' glucose levels. Amperometric glucose biosensors are today widely used as portable, low cost devices, which give the possibility of self-testing at home for diabetic patients. Biosensors have made their most significant commercial inroads with the portable glucose sensors used by diabetics to measure blood sugar. These have been available around for over 30 years. The first commercial biosensor was marketed in 1974 by the Yellow Springs Instrument Company (YSI).[6] Subsequently, YSI appear to have withdrawn from this market to the more recent development of a glucose biosensor based on a ferrocene mediator by MediSense (Cambridge, USA). The devices such as the Glucose Pen employ an enzyme that catalyses a particular kind of chemical reaction. In this case, the glucose oxidase is used, which catalyses the oxidation of glucose. This oxidation reaction produces a transfer of electrons between the target and an enzyme in close proximity to an

electrode within the device. As a result, it can be translated into a measurable electrical signal.

MediSense's sales showed exponential growth reaching US$175 million by 1996 when they were purchased by Abbott. Boehringer, Mannheim and Bayer now have competing mediated biosensors and the combined sales of the three companies dominate 85% of the world market for biosensors and are rapidly displacing conventional reflectance photometry technology for home diagnostics.[6] Still, upwards of 90% of the biosensor industry is focused solely on glucose sensing, even though the technology could potentially serve a wide range of niche markets.

Beside glucose biosensors, many other compounds of biomedical importance are targeted for the development of biosensors and lactate is one of them. The lactate blood concentration is important for athletes, since elevated levels of blood lactate decrease the blood pH resulting in muscular fatigue or cramps. The pharmaceutical research industry is also driving the need for new rapid assay biosensors to speed the progress of drug discovery. The use on-the-spot biosensors could enable analytical results to be obtained within seconds or minutes at most.

While the main commercial impetus for such technology comes from the medical sector, there are many other areas where it could provide considerable cost savings. In the food industry, for example, there is interest in developing electronic systems able to automatically confirm the freshness or correct smell or flavour of different foodstuffs and ingredients. Another area of demand is environmental monitoring, which biosensors are used by public to detect the presence of pollutants in the water supply. There is an enormous range of potential analytes in air, water, soils and other situations. Things like BOD, acidity, pesticides, fertilizers and industrial wastes require extensive analyses. In addition to the obvious pollution applications, farming, gardening, veterinary science and mining are potential areas where biosensors could be used for environmental monitoring.

Advances in areas such as materials science and molecular chemistry are enabling the development of novel and useful biosensor technologies. Biosensors exploit the incredible specificity and sensitivity of biological molecules such antibodies and enzymes. An antibody, for example, will tend to bind with only one other type of molecule, or antigen. It has a remarkable affinity for this antigen, which provides the basis for a technology that promises to enable the development of highly accurate

instruments with notable advantages over existing laboratory measurement systems, particularly with respect to speed, portability and ease of manufacture.

Developing biosensors that meet accurate technical standards is a crucial issue that manufacturers need to address immediately. At the commercial scale, a series of associated problems such as sterilization, selectivity, reproducibility, reliability, and cost of manufacture also exist. These technology-commercial considerations delay the product launches as well as prevent the mass production of many newly developed biosensors. As demand for various biosensors continues to increase and investors streamline the commercial manufacturing aspects ensuring higher long-term growth, the impact of this challenge is likely to reduce. Rapid miniaturization is going to be a key consideration while developing biosensors. High performance miniature biosensors are not only expected to quicken commercialization but also allow biosensors to penetrate several untapped markets.

A recent survey of the sensor marketplace identified medical applications as being a major contribution for the development of emerging sensor technologies. Projected market volumes for clinical testing products in the European market up to 1990s indicate a market size greater that $4000 million per annum.[7]

Previous study by Fuji-Keizai USA, Inc. (2004)[8] estimates that the market size for worldwide biosensors at year end 2003 was about $7.3 billion. The market is projected to improve and grow to about $10.8 billion in 2007 with a growth rate of about 10.4%. Biosensors, particularly glucose sensors, accounted for nearly all of the market in 2003. Sales of other biosensor devices are projected to increase significantly over the next five years. Biomedical and life sciences applications were found to dominate the market, accounting for 99% with environmental monitoring and remediation applications a distant second.

Due to their speed, low cost and sensitive nature, scientists are now trying to use sensor technology in every aspect of life. Environmental monitoring will require rugged sensors to measure the biological, chemical and physical properties of the atmosphere, landmass and oceans including the detection of pollution and toxic chemicals. Because of their automated and continuous, remote and in-situ monitoring will be increasingly required in every aspect of life. This technology will be needed to provide early diagnosis of disease and to maximize the benefits of treatment in healthcare and will be incorporated into applications throughout science and engineering research. Also in

future, processing the data from arrays of sensors will require access to faster, cheaper and more flexible real-time data processing, combined with the best available data transmission and storage systems. Scientists therefore are trying to develop sensed data system technology.[9]

1.2 Chiral Biosensors

1.2.1 Principle of Chirality

Stereoisomers are compounds whose atoms are connected in the same order but with a different geometry. There are two kinds of stereoisomers, which are enantiomers and diastereomers. Enantiomers are pairs of isomers that are non-superimposable mirror images of each other. Two compounds that are enantiomers of each other have the same physical properties, but different in the direction in which they rotate polarized light and how they interact with different optical isomers of other compounds. In nature, only one enantiomer of chiral biological compounds, such as amino acids (except glycine, which is achiral), is commonly present. As a result, different enantiomers of a compound may have substantially different biological effects.

Diastereomers are stereoisomers that are not related through a reflection operation. They are neither mirror images nor superimposable to each other. These include *cis-trans* (*E-Z*) isomers, and non-enantiomeric optical isomers. Unlike enantiomers, diastereomers seldom have the same physical properties.

The existence of enantiomeric pairs is known as chirality and molecules capable of existing as enantiomers are called chiral molecules. They have the property of rotating the plane of polarisation of plane-polarised monochromatic light that is passed through it. This phenomenon is called optical activity. Because the difference between right and left hands is universally known and easy to observe, many pairs of enantiomers are designated as “right-” and “left-handed”, which assigned conventionally as D- and L-enantiomers, respectively.

A simplified rule applies to tetrahedrally-bonded carbon, as shown in Figure 1.1. If all four substituents are different, the molecule is chiral. A chiral molecule is not necessarily asymmetric, that is, devoid of any symmetry elements, as it can have, for example, rotational symmetry. A non-chiral object is called achiral and can be superimposed on its mirror image.

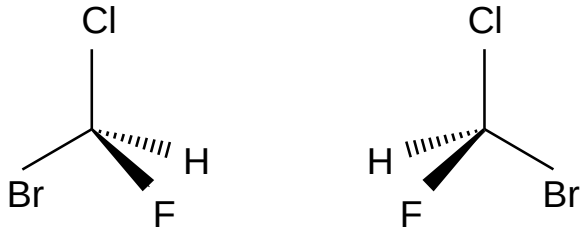

Figure 1.1: The two enantiomers of bromochlorofluoromethane.

1.2.2 Chirality and Optical Activity in Biomolecules

The phenomenon of chirality is especially important in biochemistry because many biomolecules are chiral. In biological systems, there is usually a selection for one of a pair of enantiomers. For example most amino acids in living systems are L-enantiomers with D-enantiomers occurring only very rarely (*e.g.* in antibiotic peptides). Similarly, most monosaccharides are D-enantiomers. By contrast, most chemical reactions carried out in solution result in a 50:50 mixture of D- and L-enantiomers. Such a mixture is called a racemic mixture that shows zero optical rotation because the positive rotation from one enantiomer exactly cancels the negative rotation from the other.

Enzymes are biocatalysts that are made from amino acids. Since almost all amino acids are chiral, enzymes also are chiral catalysts. They are able to assert a dramatic chiral influence on the reaction due to the chiral active site they own. The reactant molecules are bound to the active site where the reaction takes place. In kinetic resolution-catalyzed by enzymes, only one enantiomer of a chiral reactant fit to the active site properly and is able to undergo the reaction while the second enantiomer is

left unreacted and in enantiomerically pure form. Consequently, a prochiral substrate may be transformed into an optically active product and both enantiomers of a racemic substrate may react at different rates.

Each enantiomer of an optically active molecule interacts differently with left and right circularly polarised light. An enantiomer will absorb left- and right-circularly polarised light to differing degrees. This is the basis of circular dichroism (CD) spectroscopy. Usually the difference in absorptivity is relatively small (parts per thousand). CD spectroscopy is a powerful analytical technique for investigating the secondary structure of proteins and for determining the absolute configurations of chiral compounds, in particular, transition metal complexes.

1.2.3 Chiral Recognition in Biological Molecules

Chiral recognition is a fundamental property of many biological molecules. Many examples have been reported in the literature[10-11] showing its theoretical and practical interest. This topic has been studied extensively especially in recognition of substrates to chiral receptor molecules with macromolecular systems such as polymers,[12] and chiral surfaces[13]. The resulting chiroselective binding processes were widely applied in chiral separations.[14-15] Chiroselectivity have been also observed in the association of optically active transition metal complexes to DNA[16-17] and enantioselective electron transfer in the DNA microenvironment.[18]

The concept of chirality can also been studied in the application of biosensors. In biosensors, an enzyme, which is used as the bioreceptor have a structure that does not allowed a direct electron transfer between the enzyme and the electrode surface. The deeply buried redox center of the enzyme does not permit electron transfer, thus making the oxidation of the redox active site inefficient. In order to facilitate the electron transfer between enzyme and the electrode surface, the enzyme layer has to modify with electron-tunnelling groups so that it can efficiently oxidize for use in an electrochemical biosensors.

Electron transfer mediators provide a means to establish electrical communication between redox proteins and electrode surfaces.[19] Ferrocene derivatives, for example, were widely applied as electron transfer mediators for flavin-containing oxidoreductases such as glucose oxidase[19] and lactate oxidase[20-21]. In the case of chiral biosensors, chiroselective mediated electron-transfer has been studied intensively using diffusional chiral electron mediators. The enantiomeric electron relays (S)- and (*R*)*N*,*N*-dimethyl-1-ferrocenyl-ethylamine were reported to stimulate chiroselective bioelectrocatalyzed oxidation of glucose in the presence of glucose oxidase.[14] The bioelectrocatalyzed oxidation of glucose was ca. 2-fold enhanced in the presence of the (*S*)-isomer as compared to (*R*)-isomer.

The concept of enantioselective electrical contacting of redox-enzymes and electrode surfaces was also developed by the organization of a chiral electron-transfer mediator as a monolayer on an electrode surface.[22] (*R*)- and (*S*)-2-methylferrocene carboxylic acid were assembled as monolayers on Au-electrodes. The monolayer-mediated oxidation of glucose in the presence of glucose oxidase showed a ca. 1.9-fold enhancement at the electrode functionalized by the (*S*)-enantiomer over the electrode functionalized by the (*R*)-enantiomer. The reversal of chiral specificity was also reported by cytochrome c peroxidase with two ferrocene enantiomers.[23] The enantiomeric selectivity is reversed by a single site specific change in the surface charge of the enzyme.

All of the research explained above involved chiral mediators as a chiroselective agent to biosensors. However, there is still no research involves achiral mediators as artificial electron transfer to the oxidation of both enantiomers of specific analytes. Thus, the key idea of this research is to develop a chiral glucose and lactate biosensors by using ferrocene-modified glassy carbon electrodes in the presence of collagen and collagen/sol-gel matrixes as immobilizing agents to both glucose oxidase and lactate oxidase enzymes. Collagen matrix is the key idea in this research as it is a chiral molecule and biocompatible with biological substances. This work provides an explanation on how collagen can affect the chiral selectivity in both glucose and lactate in order to develop an interesting effect in simultaneous detection of both enantiomers.

This thesis covers seven chapters including introduction in first chapter and conclusion of the research in the seventh chapter. The second chapter gives an elucidation of the basic in electrochemical principles, giving a good background of the

concepts of electrochemistry that have been used as the key understanding to the topic given. The details of the materials used and the basic principle of the methods used in this research are explained in chapter three.

The fourth chapter describes fundamental studies in developing electrochemical biosensors used in this work. This chapter is focused on the development of glucose biosensors based on collagen and collagen/sol-gel as the matrix for immobilizing glucose oxidase at the electrode surface. The glucose oxidase system was chosen in the first instance as it is a well characterised system in terms of its physical and electrochemical behaviour. Ferrocene was used as mediator to electron transfer reaction at the surface of glassy carbon electrodes.

The fifth chapter focuses on elucidating the unusual chiral effects of collagen to glucose and lactate oxidase. The respective enzymes, D-glucose oxidase and L-lactate oxidase were immobilized within tetramethyl orthosilicate (TMOS) sol-gel, collagen and/or TMOS sol-gel matrixes in the presence of ferrocene as the electron shuttle to the electrode surface. Because collagen is a chiral molecule, the effect of collagen to enantioselectivity of D- and L-glucose as well as L- and D-lactate was intensively investigated in further detail.

The sixth chapter describes the application of chiral lactate biosensor to dairy products such as milk and yogurt. Both L- and D-lactate contained in the dairy products can be detected simultaneously by using the constructed biosensors and the results obtained were compared with previously reported lactate biosensors in literature.

Finally, the seventh chapter states the conclusion of this research and the ongoing research that can be done in the future.

References

(1) Turner, A. P. F., Karube, I., and Wilson, G.S. *Biosensors: Fundamentals and Applications*; Oxford University Press: Oxford, **1987**.

(2) Freire, R. S.; Pessoa, C. A.; Mello, L. D.; Kubota, L. T. *Journal of the Brazilian Chemical Society.* **2003**, *14*, 230.

(3) Wang, J. *J. Pharm. Biomed. Anal.* **1999**, *19*, 47.

(4) Vo-Dinh, T.; Cullum, B. *Fresenius J. Anal. Chem.* **2000**, *366*, 540.

(5) Rosatto, S. S.; Freire, R. S.; Duran, N.; Kubota, L. T. *Quim. Nova.* **2001**, *24*, 77.

(6) Eggins, B. R. *Biosensors: An Introduction*; John Wiley & Sons Inc.: USA, **1996**.

(7) Frost and Sullivan, Inc.: *Trends and Forecast for The World Sensor Marketplace*; New York, **1995**.

(8) Fuji-Keizai USA, Inc.: *U.S. & Worldwide Biosensor Market, R&D and Commercial Application*; **2004**.

(9) Toko, K. *Biomometic Sensor Technology*; 1st edition ed.; Cambridge University Press: London, **2000**.

(10) Fersht, A. R.; Shi, J. P.; Wilkinson, A. J.; Blow, D. M.; Carter, P.; Waye, M. M. Y.; Winter, G. P. *Angew. Chem.-Int. Edit. Engl.* **1984**, *23*, 467.

(11) Casella, L.; Poli, S.; Gullotti, M.; Selvaggini, C.; Beringhelli, T.; Marchesini, A. *Biochemistry.* **1994**, *33*, 6377.

(12) Qian, P.; Matsuda, M.; Miyashita, T. *J. Am. Chem. Soc.* **1993**, *115*, 5624.

(13) Avnir, D.; Wellner, E.; Ottolenghi, M. *J. Am. Chem. Soc.* **1989**, *111*, 2001.

(14) Marxtibbon, S.; Katz, E.; Willner, I. *J. Am. Chem. Soc.* **1995**, *117*, 9925.

(15) Tamai, Y.; Qian, P.; Matsunaga, K.; Miyano, S. *Bull. Chem. Soc. Jpn.* **1992**, *65*, 817.

(16) Pyle, A. M.; Morii, T.; Barton, J. K. *J. Am. Chem. Soc.* **1990**, *112*, 9432.

(17) Turro, N. J.; Barton, J. K.; Tomalia, D. A. *Accounts Chem. Res.* **1991**, *24*, 332.

(18) Purugganan, M. D.; Kumar, C. V.; Turro, N. J.; Barton, J. K. *Science.* **1988**, *241*, 1645.

(19) Cass, A. E. G.; Davis, G.; Francis, G. D.; Hill, H. A. O.; Aston, W. J.; Higgins, I. J.; Plotkin, E. V.; Scott, L. D. L.; Turner, A. P. F. *Anal. Chem.* **1984**, *56*, 667.

(20) Iwasawa, K.; Eguchi, M.; Uno, K.; Yabuki, S. *Electrochemistry.* **2008**, *76*, 552.

(21) Zheng, H. T.; Zhou, J. L.; Okezaki, Y. S.; Suye, S. I. *Electroanalysis.* **2008**, *20*, 2685.

(22) Tao, G. L.; Katz, E.; Willner, I. *Chem. Commun.* **1997**, 2073.

(23) Sadeghi, S. J.; Gilardi, G.; Nicolosi, G.; Cass, A. E. G. *Chem. Commun.* **1997**, 517.

CHAPTER 2

INTRODUCTION TO ELECTROCHEMISTRY AND ELECTROCHEMICAL BIOSENSORS

2.1 Processes at Electrodes: Faradaic and Nonfaradaic Processes

The special kind of process that occurs at the electrode surface is the transfer of electrons. The electrons transfer process can be divided into two types, which are faradaic and nonfaradaic processes. The faradaic processes are referred to processes that involve electrons or charges transfer across the metal-solution interface. Electrodes at which faradaic processes occur are sometimes called charge-transfer electrodes and the processes cause oxidation or reduction reactions to occur.

The phenomena of the faradaic processes can be explained in terms of Fermi level, E_F^{α}. The Fermi level represents the average energy of available electrons in phase α and is related to the chemical potential of electrons in that phase, μ_e^{α}, and the inner potential of α. The Fermi level of a metal or semiconductor depends on the work function of the material. For a solution phase, it is a function of the electrochemical potentials of the dissolved oxidized and reduced species. For an inert metal in contact with a solution, the condition for electrical equilibrium is that the Fermi levels of the two phases be equal, that is, $E_F^s = E_F^M$. This condition is equivalent to saying that the average energies of available electrons are the same in both phases. The equality is attained by the transfer of electrons between the phases, with electrons flowing from the phase with the higher Fermi level (more energetic electrons) to the phase with the lower Fermi level. This electron flow causes the potential difference between the phases or the electrode potential to shift.

Figure 2.1 shows the relationship between electronic states at an interface between a metal electrode and a solution containing O and R species at equal concentrations.

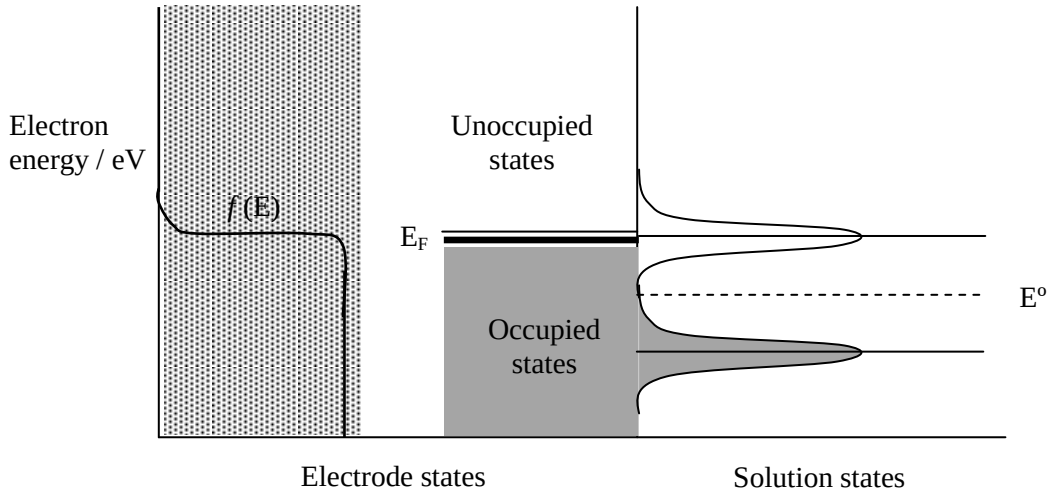

Figure 2.1: A model based on distribution of energy states at an interface between a metal electrode and a solution containing species O and R at equal concentrations.

The vertical axis in Figure 2.1 is electron energy, E, on the absolute scale. Filled states are denoted on both sides of the interface by dark shadding. Since filled electrode states overlap with empty O states, reduction can proceed. Since the filled R states overlap only with filled electrode states, oxidation is blocked.

The main idea of this model is that an electron transfer can take place from any occupied energy state that is matched in energy, E, with an unoccupied receiving state. If the process is a reduction, the occupied state is on the electrode and the receiving state is on an electroreactant, O. For an oxidation, the occupied state is on species R in solution and the receiving state is on the electrode. In general, the eligible states extend over a range of energies, and the total rate is an integral of the rates at each energy.

There is another condition where the electrode-solution interface will show a range of potentials where no charge-transfer reactions occur because such reactions are thermodynamically or kinetically unfavourable. However, processes such as adsorption and desorption can occur, and the structure of the electrode-solution interface can change with changing potential or solution composition.[1] Although charge does not cross the interface, external currents can flow when the potential, electrode area, or solution composition changes. These kinds of processes are called nonfaradaic processes.

Both faradaic and nonfaradaic processes occur when electrode reactions take place. Even though the faradaic processes are usually of primary interest in the investigation of an electrode reaction, the effects of the nonfaradaic processes must be taken into account in using electrochemical data to obtain information about the charge transfer and associated reactions.

2.1.1 Nonfaradaic Processes and the Nature of Electrical Double Layer

In nonfaradaic processes, there is no charge transfer across the electrode-solution interface. The electrode used in this process, is called the *ideal polarized electrode* (IPE). Since charge cannot across the IPE interface when the potential across it is changed, the behaviour of the electrode-solution interface is analogous to that of a capacitor.[2] For an ideal capacitor, the charge, q stored on the capacitor (in coulombs, C) is directly proportional to the potential difference as shown in Equation. 2.1:

$$q = CE \tag{2.1}$$

where C is the capacitance (in farads, F) and E is the potential across the capacitor (in volts, V). When a potential is applied to the capacitor, the charge will accumulate on the surface and the charging current will flow.

The process occuring at the electrode-solution interface has been shown to behave like a capacitor. The model that attemps to describe the electrode/electrolyte interface is called the electrical double layer. The double layer is comprised of layers closest to the electrode surface that reflects the ionic zones formed in the solution. A positively charged electrode attracts a layer of negative ions, and vice versa. The interface must be neutral, so excess charge of the electrode (q_e) plus the charge of the ions in the nearby solution (q_s) must be equal to zero. According to this theory, such a counterlayer must consists of ions with opposite sign than that of the electrode.

The electrical double layer has a complex structure of several distinct parts as illustrated in Figure 2.2:

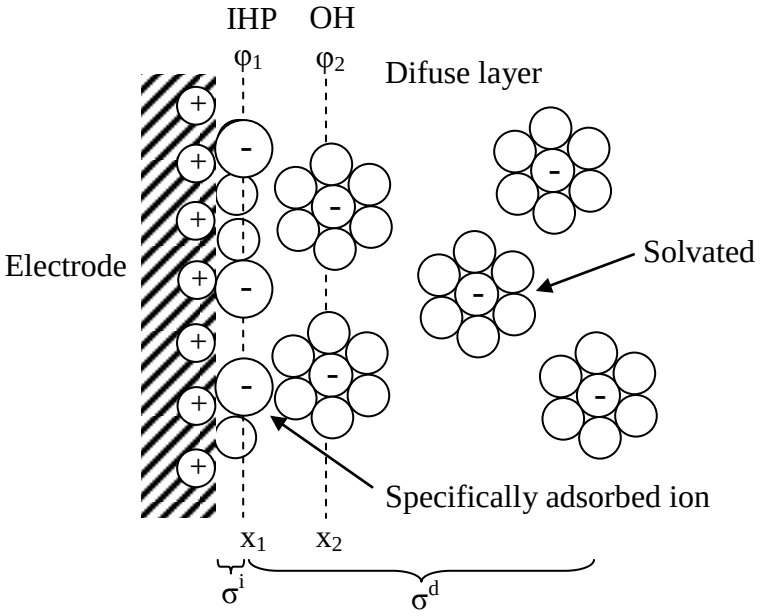

Figure 2.2: Schematic diagram of the electrical double layer model.

The inner layer closest to the electrode contains solvent molecules and specifically adsorbed ions. It is defined by the electrical center of the specifically adsorbed ions, known as the *inner Helmholz plane* (IHP), which is at a distance x_1. The total charge density from these specifically adsorbed ions is σ^i ($\mu C\ cm^{-2}$). The next layer beside the IHP is called the *outer Helmholz plane* (OHP), defined by the center of the nearest solvated ions, which can approach the electrode only to a distance x_2. The solvated ions are non-specifically adsorbed and attracted to the electrode surface by only long-range electrostatic forces.

Both IHP and OHP layers represent the compact layer in which the charges are strongly held by the electrode. Beyond the compact layer, there is the diffuse layer, which is a three-dimensional region of scattered ions. It extends from the OHP into the bulk solution. The thickness of the diffuse layer depends on the total ionic concentration in the solution. Such ionic distribution reflects the counterbalance between ordering forces of the electrical field and the disorder caused by a random thermal motion. In accordance with the Boltzmann Equation;

$$C(x) = C(0)\exp(-zF\Phi)\,/RT) \qquad (2.2)$$

the concentration of ionic species at a given distance from the surface, $C(x)$, decays exponentially with the ratio between the electrostatic energy ($zF\Phi$) and the thermal energy (RT). The total excess charge density on the solution side of the double layer is equals to the total charge of the compact and diffuse layers, as given by Equation 2.3:

$$\sigma^S = \sigma^i + \sigma^d \tag{2.3}$$

The potential-distance profile across the double layer region involves two segments, with a linear decrease until the OHP and an exponential one within the diffuse layer, as displayed in Figure 2.3.

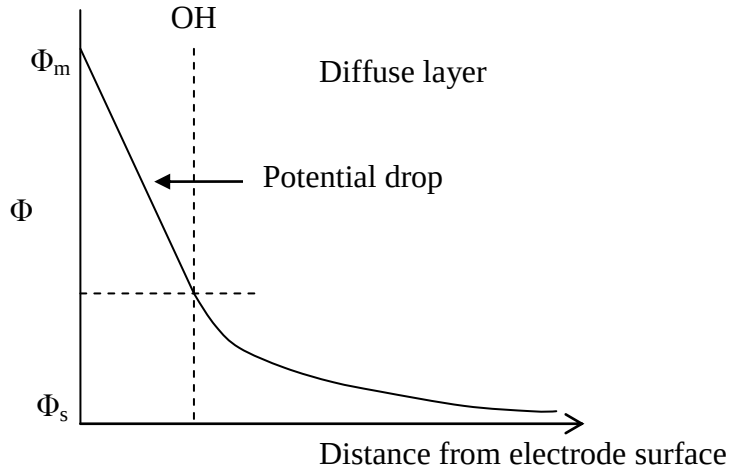

Figure 2.3: Schematic diagram of the potential drop across the interface.

The structure of the double layer can affect the rates of electrode processes. Sometimes one can neglect double layer effects in considering electrode reaction kinetics. Usually, one cannot neglect the existence of the double layer capacitance or the presence of a charging current in electrochemical process. Indeed, during electrode reaction involving very low concentrations of electroactive species, the charging current can be much larger than the faradaic current for the oxidation or reduction reaction.[2]

2.1.2 Faradaic Processes

Faradaic processes involve reactions that occur in a potential region that makes the electron transfer thermodynamically and kinetically favourable. The transfer of electron during the redox reaction of the analyte can be shown as Equation 2.4 as follows:

$$O + ne^- \rightleftharpoons R \qquad (2.4)$$

where O and R are the oxidized and reduced forms, respectively of the redox couple. According to Nernst equation (Equation 2.5), the potential of the electrode can be used to establish the concentration of the electroactive species at the electrode surface at equilibrium:

$$E = E^\circ + \frac{2.3RT}{nF}\log\frac{C_O(0,t)}{C_R(0,t)} \qquad (2.5)$$

where $C_O(0,t)$ and $C_R(0,t)$ are the bulk concentrations of oxidized and reduced forms, respectively at the electrode surface and time t, E^o is the formal potential, R is the universal gas constant (8.314 $JK^{-1}mol^{-1}$), T is the Kelvin temperature, n is the number of electrons transferred in the reaction and F is the Faraday constant (96,487 C). The current resulting from a change in oxidation state of the electroactive species is called faradaic current. The faradaic current is the direct measure of the rate of the redox reaction.

The rate of the electrode reactions can be determined by the slowest step in the series of several steps. Generally, the electrode reactions can involve several processes.[2] A simple reaction can involve only mass transport of the electroactive species to the electrode surface, electron transfer across the interface, and mass transport of the product back to bulk solution. More complex reaction might involve a series of electron transfer and protonations, branching mechanisms or modification of the electrode surface. The pathway of a general electrode reaction is shown in Figure 2.4:

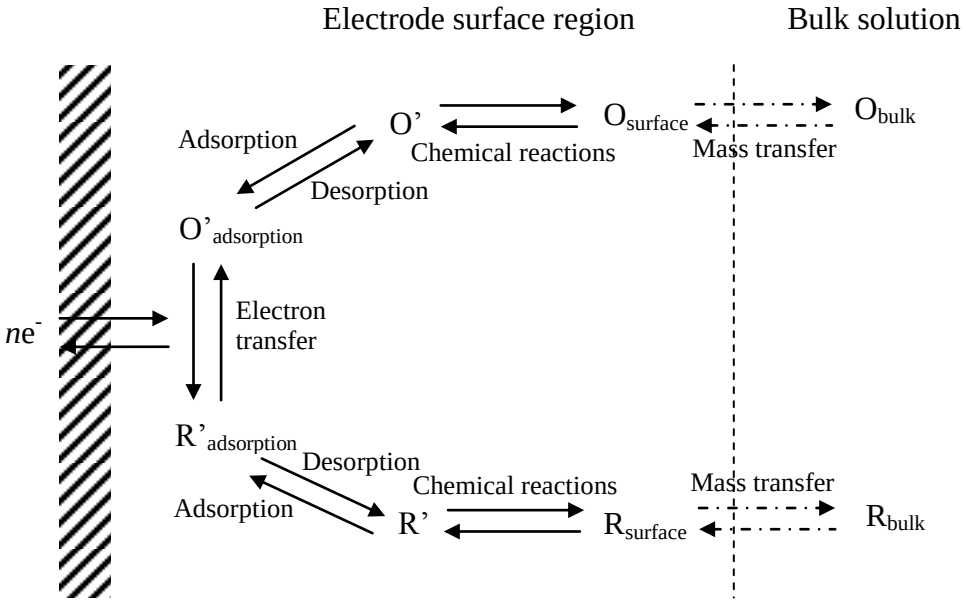

Figure 2.4: Pathway of a general electrode reaction.[2]

Whether such a reaction is controlled by mass transport or electron transfer, the more sluggish process will be the rate-determining step. The more facile reactions are held back from their maximum rates by the slowness with which a rate-determining step disposes of their products or creates their reactants.

2.1.2.1 Mass Transport-Controlled Reactions

Mass transport plays a big role in electrochemical dynamics. It is a movement of a material from one location in solution to another that arises from the differences in electrical or chemical potential at the two interfaces. The process of mass transport at the electrode/solution interface is known to occur by three modes, as follows:

- Diffusion. It arises from the spontaneous movement under the influence of concentration gradient, from high concentrations regions to low concentration regions. The process aims to minimize the concentration differences between two interfaces.

- Migration. It is a movement of a charged particle under the influence of an electric field.
- Convection. It is a transport to the electrode due to the gross physical movement. Convection occurs when an external mechanical energy force associated with stirring, pumping, gas bubbling or flowing in solution, rotating or vibrating the electrode. Beside the force convection, natural convection can also occurs as a result of density or thermal gradients within the solution.

The common measure of the rate of mass transport of electroactive material at a fixed point is the *flux* (*J*). It is defined as the number of molecules penetrating a unit area of an imaginary plane in a unit of time with a unit of mol cm^{-2} s^{-1}. The *flux* to the electrode is described as the *Nernst-Planck equation*, given here as follows:

$$J(x,t) = -D\frac{\partial C(x,t)}{\partial x} - \frac{zFDC}{RT}\frac{\partial \phi(x,t)}{\partial x} + C(x,t)V(x,t) \qquad (2.6)$$

Diffusion Migration Convection

where *D* is the diffusion coefficient (cm^2 s^{-1}), $[\partial C(x,t)]/\partial x$ is the concentration gradient (at distance x and time t), $[\partial \varphi(x,t)]/\partial x$ is the potential gradient, *z* and *C* is the charge (dimensionless) and concentration (mol cm^{-3}), respectively, of the electroactive species, and *V*(x,t) is the hydrodynamic velocity (cm s^{-1}) with which a volume element in solution moves in the x direction.

However, when the three modes of mass transport occur simultaneously, the situation becomes so complex giving rise to difficulties in the data interpretation. To simplify this situation, the electrochemical systems are usually designed so that one or more of the factors to mass transport are negligible. For example, the migration component can be reduced by suppressing the electromigration through the addition of excess inert supporting electrolyte, compared to the concentration of electroactive ions. A slight redistribution of the different cations and anions from the supporting electrolyte takes place to maintain the electrical neutrality near the interfacial region. Beside this, the addition of supporting electrolyte might also increase the solution conductivity

making it less resistive to the current flow, and also provide a constant ionic strength of the solution through out the electrolysis process.

Convection effects can be eliminated by using a quiescent solution. This can be done by avoiding stirring solution and vibrations in the electrochemical cells. In the absence of migration and convection effects, transfer of the electroactive species is limited by diffusion (Equation 2.7). So, the reaction occurring at the electrode surface generates concentration gradients adjacent to the surface.

According to Fick's first law, the rate of diffusional *flux* is directly proportional to the slope of the concentration gradient:

$$J(x,t) = -D\frac{\partial C(x,t)}{\partial x} \tag{2.7}$$

It is known that current (i) is directly proportional to the *flux* and the surface area (A):

$$i = -nFAJ \tag{2.8}$$

Combining the Equation 2.7 and 2.8 gives a general expression for the current response:

$$i = nFAD\frac{\partial C(x,t)}{\partial x} \tag{2.9}$$

Hence, we can say that the current at any time is proportional to the concentration gradient of the electroactive species.

2.1.2.2 The Rate of Electron Transfer-Controlled Reactions

A reaction with sufficient fast mass transport is the reaction in which the current is controlled by the electron transfer rate. It is different from the previously discussed mass-transport-controlled reactions.

Considering the electron transfer reaction;

$$O + ne^- \rightleftharpoons R \tag{2.4}$$

The rate of the forward reaction, V_f is first-order in O:

$$V_f = k_f C_O(0,t) \tag{2.10}$$

while that of the reversed reaction V_r, is first-order in R:

$$V_f = k_r C_R(0,t) \tag{2.11}$$

where k_f and k_r are the forward and reverse heterogeneous rate constants, respectively. These rate constants depend on the operating potential according to the following exponential relationship:

$$k_f = k^\circ \exp[-\alpha nF(E-E^\circ)/RT] \tag{2.12}$$

$$k_r = k^\circ \exp[(1-\alpha)nF(E-E^\circ)/RT] \tag{2.13}$$

where k^o (cm s^{-1}) is the standard heterogeneous rate constant that reflects the reaction between the particular reactant and the electrode material used, and α is the transfer coefficient that reflects the symmetry of the free-energy curve with respect to the reactants and products. In general, Equation 2.12 and 2.13 indicate that by changing the applied potential, k_f and k_r are change exponentially.

As the forward and reverse currents are proportional to V_f and V_r, respectively

$$i_f = nFAV_f \tag{2.14}$$

$$i_r = nFAV_r \tag{2.15}$$

and the net reaction rate is:

$$V_{net} = V_f - V_r \tag{2.16}$$

$$= k_f C_O(0,t) - k_r C_R(0,t) \tag{2.17}$$

The overall current is given by the difference between the currents due to the forward and reverse reactions:

$$i_{net} = i_f - i_r = nFA[k_f C_O(0,t) - k_r C_R(0,t)] \tag{2.18}$$

From Equation 2.11 and 2.12, respectively, the expression for k_f and k_r can be substituted to obtain the *Butler-Volmer equation* (Equation 2.19). It describes the current-potential relationship for reactions controlled by the rate of electron transfer.

$$i = nFAk^{\circ}\left\{C_O(0,t)\exp\left[-\frac{\alpha nF(E-E^{\circ})}{RT}\right] - C_R(0,t)\exp\left[\frac{(1-\alpha)nF(E-E^{\circ})}{RT}\right]\right\} \tag{2.19}$$

There is a special case in which the interface is at equilibrium with a solution in which C_O is equal to C_R. In this situation, $E = E^o$ and $k_f C_O = k_r C_R$, so that $k_f = k_r$. Thus, E^o is the potential where the forward and reverse rate constants have the same value, called the *standard rate constant*, k^o. This situation is dynamic with continuous movement of charge carriers in both directions and with equal opposing anodic and

cathodic current components. The absolute magnitude of these components at E^o is the exchange current, i_o, which is directly proportional to the *standard rate constant*, k^o.

$$i_o = i_c = i_a = nFAk°C \tag{2.20}$$

The *Butler-Volmer equation* can be written in terms of the exchange current:

$$i = i_0[\exp\left(-\frac{\alpha nF\eta}{RT}\right) - \exp\left(\frac{(1-\alpha)nF\eta}{RT}\right)] \tag{2.21}$$

where $\eta = E_{appl} - E$ is the overvoltage, where E is given by the *Nernst* Equation and E_{appl} is the applied potential.

2.2 Electrochemical Biosensors

2.2.1 Principle of Biosensors

Biosensor is the term used for a whole class of sensors that utilize a biochemical reaction to determine a specific compound. Generally, a biosensor is an analytical device that responds to an analyte in an appropriate sample and interprets its concentration as an electrical signal via a suitable combination of a biological recognition system and an electrochemical transducer.

A schematic of a biosensor can be seen on the Figure 2.5. The main component of a biosensor is the receptor (*i.e.* enzymes, antibodies, lipid layers and immobilized cells), that plays a role of a molecular recognition device and transform the analyte in some way. In the presence of the analyte under study, it must produce a physicochemical effect that is detectable by the transducer. The receptor is also responsible for the selectivity of the sensor.

The other main component of a biosensor is the transducer (*i.e.* pH-electrode, oxygen electrode, hydrogen peroxide-sensor, ion selective electrode, *etc*.), which exploits the biochemical modification of the substrate by transforming it into an

electrical signal. The choice of transducer depends on the type of biochemical modification, and it should give a signal that is sensitive, easily monitored and has minimal background noise. Low background noise reduces the detection limit and improves the biosensor performance.

An amperometric biosensor is based on measuring the current produced at a fixed potential. When a species is oxidized or reduced at an electrode under certain condition, the current produced is directly related to the concentration of the species. For this purpose, it is necessary for the interest species is electroactive at the electrode material at a reasonable potential value where neither solvent nor electrolyte decomposition occur.

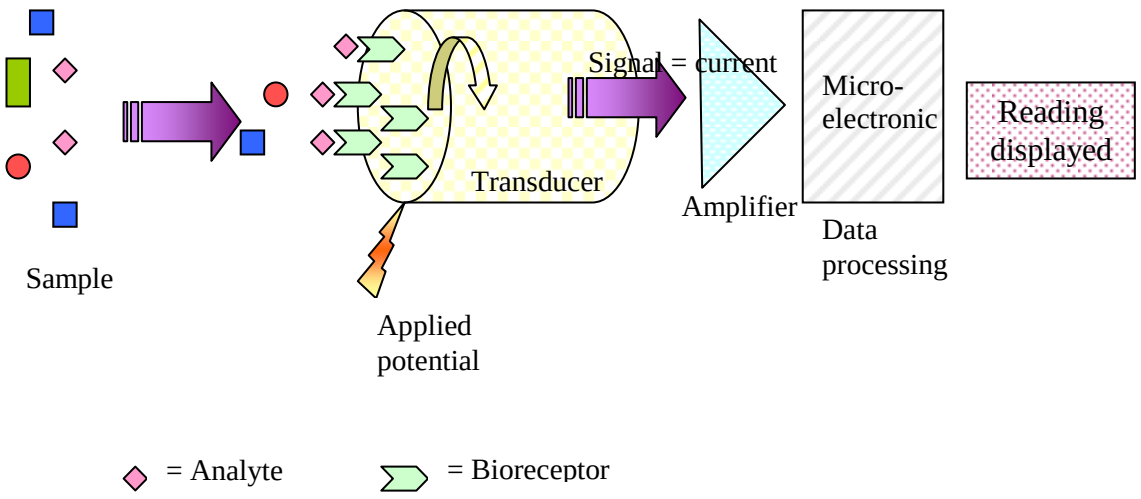

Figure 2.5: Schematic diagram showing the main components of a biosensor. The bioreceptor converts the analyte to product. This reaction is determined by the transducer which converts it to an electrical signal. The output from the transducer is amplified, processed and displayed.

2.2.2 Reaction Mechanism involved in a Biosensor System

Cyclic voltammetry (CV) is the most widely used technique to obtain qualitative information about electrochemical reactions. It is often the first experiment performed

in an electroanalytical study. One of the most important applications of CV is for qualitative diagnosis of chemical reaction mechanisms that proceed the redox process.[3-4] Changes in the shape of the cyclic voltammogram, resulting from the chemical competition for the electrochemical species, can be very useful for elucidating these reaction pathways and for providing reliable chemical information about reactive intermediates.[3]

Reactions involve in some of the biosensors are said to have the EC′ mechanism, due to the presence of enzyme as a biocatalyst in the chemical reaction. The letter E refers to electron transfer reaction, whereas C′ represents a catalytic process. The EC′ mechanism can be summarized by the following general kinetic scheme:

$$A + e^- \rightleftharpoons B \tag{2.22}$$

$$B + Z \xrightarrow{k_2} A + Y \tag{2.23}$$

where k_2 is the rate constant.

The ‘catalytic’ term arises from the chemical reaction which regenerates the starting material A from the product of the electrode reaction B, whereas Z is converted to final product Y. In this case, Y and Z are electroactive at the operating potential. Figure 2.6 shows a typical cyclic voltammogram in a biosensor system to illustrate the different between those two voltammograms in the (i) absence or (ii) presence of the substrate. An increase in the current is observed as the homogeneous reaction regenerates A, which then can be reduced again to B at the electrode surface. The height of the catalytic current detected is dependent on the amount of substrate present in solution and the rate of the reaction between B and Z.[5]

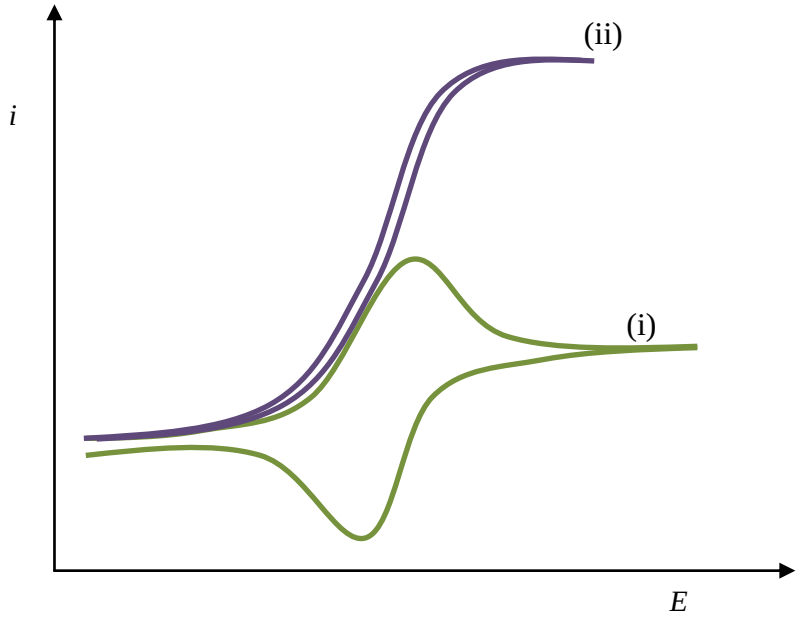

Figure 2.6: Cyclic voltammograms for EC′ mechanism reaction.

Figure 2.6 also can represent the different in the shape of cyclic voltammogram when the rate constant, k_2 is increased from (i) to (ii). It is proved that at low rate constants the cyclic voltammogram showed an unperturbed A / B reductive process. When the k_2 is increases to a larger value, a steady state current is reached rather than the peak current. There is also a large amount of Z present to sustain the catalytic cycle. These characteristics are consistent with the following reaction consuming B and regenerating A.

2.2.3 Types of Biosensors

2.2.3.1 Enzyme-based Electrodes

Enzyme electrodes are based on the coupling of a layer of an enzyme with an appropriate electrode as a transducer. Enzymes are proteins that catalyze chemical reactions in living systems. These biocatalysts are very efficient and extremely selective. Thus, coupling the enzyme with an appropriate electrode has shown to be very useful for monitoring a wide variety of substrates.

Theoretically, the immobilized enzyme layer at the electrode surface is used to catalyze a reaction to consume or generate a detectable species:

$$S+C \xrightarrow{enzyme} P+C' \tag{2.24}$$

where S and C are the substrate and cofactor, respectively and P and C' are the corresponding products.

Figure 2.7 shows a schematic diagram of an enzyme electrode. The enzyme which in an immobilized form, is placed onto an electrode which is then measures either the decrease of the reactants or the increase of the products. It is assumed that there is no mass transfer across the enzyme-electrode interface. The external surface of the biocatalytic layer is immersed in a solution containing the substrate under study. The substrate diffuses into the enzyme layer on the electrode surface, producing or consuming an electroactive substance when the reaction catalyzed by the enzyme. The electrode reaction at this layer is sensed by the base electrode and the current produced by this reaction is correlated with the concentration of the substance assayed.

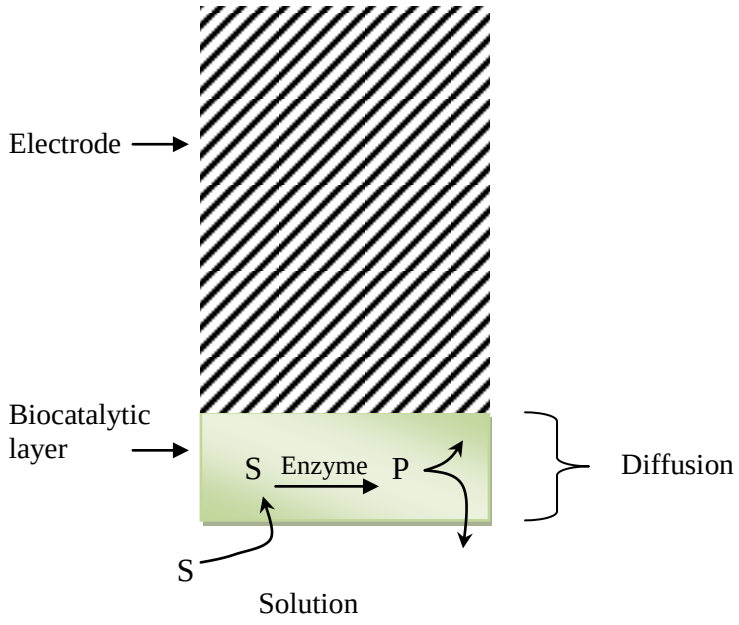

Figure 2.7: Schematic diagram represents the steps involved at the enzyme-based electrode.

In conclusion, the steps involved during the operation of enzyme electrode are as follows; first, substrate is transported from the bulk solution towards the enzymatic layer. This substrate is then diffused within this layer and the enzymatic transformation of the substrate to the reaction product will occur, followed by migration of the product towards the transducer. Finally, conversion of the concentration of the product at this interface into an electrical signal will produce.

2.2.3.2 Microbial Sensors

Since the first microbial sensor was studied by Krube *et al*. (1977)[6], many types of microbial cell sensors have been developed as analytical tools in bioanalysis. Microbial sensors are a class of the cell-based sensors produced as a result from the combination of a microorganism as a sensing element with a transducer capable of detecting the metabolite involved. In this case, microorganisms possess enzymatic systems that effect biological transformations. The characteristics of microbial sensors are a complete different to those of enzyme sensors or immunosensors, which are highly specific for the substrates of interest, although the specificity of the microbial sensor has been improved by genetic modification of the microorganism used as the sensing element.

The use of microorganisms in biosensor systems requires their immobilization around the transducer surface. Microorganisms are often immobilized by physical entrapment in gels, or using dialysis membrane.[7] Potentiometric or amperometric electrodes such as pCO_2, pNH_3 and pO_2 are particularly useful because they already have a gas-permeable hydrophobic membrane. The microorganism is inserted between this membrane and an electrode surface provides a method whereby cells are immobilized very gently. Cell entrapment within membranes made from carbohydrate polymers such as cellulose and alginate has been employed.[8] The construction of biosensors by immobilizing microorganisms on transducers is attractive because it eliminates extraction and purification processes. The enzyme involved is also maintained in its natural environment thus avoiding problems like the regeneration of

cofactors.[7] In contrast to enzymes, once the microorganism is immobilized, it must be kept in a basal medium to maintain its activity.

Microbial sensors are potentially reusable, due to the ability to replenish the cells. The biocatalytic activity of some microbial sensors can be restored by placing the spent electrodes into nutrient growth medium and the new cells then grow in situ.[8]

The main electrochemical transducers used nowadays in the construction of microbial sensors are gas sensors, ion-selective membrane electrodes and ISFET (ion-sensitive field-effect transistor) sensor.[8-10] The oxygen gas electrode is the most used because of the large number of sensing systems based on the metabolic activity of the microorganisms which increases in respiratory activity caused by assimilation of substrates and are recorded as a decrease in oxygen tension.[8]

Microbial sensors have been reported to have attractive applications in bioanalysis. For example, in the analysis of glucose, mediator type amperometric microbial sensors were prepared based on the use of whole cells of *Aspergillus niger* containing glucose oxidase.[11] The microorganism immobilized on a Milipore type HA membrane filter, was either attached to the surface of a Pt or C paste electrode, or incorporated directly into the carbon paste bulk.

A microbial sensor based on an oxygen electrode was constructed by cultivating *Pseudomonas putida* in a medium containing L-lactic acid as the sole carbon source. This sensor was used to determine the concentration of lactic acid in wine.[12] The sensor responses to wine samples (n=6) from 0.5 to 5 mmol/L concentration range. The lifetime of the sensor was 10 days.

Microbial cell sensors have the advantages of tolerance to measuring conditions, a long lifetime, and good cost performance. However, it has the main disadvantage created by the high diffusion resistance of the cell and sub-cellular membranes, which increases the response time of the sensor.[10,13] This is because it varies with both the thickness of the active layer and the diffusion coefficient of the substrate, which change during the operation of a microbial sensor.

The sensor also must be reliable and reproducible. Loss in enzymatic activity upon use of viable cells was considered counterbalances by the growth of the biomass. In practice, this growth is difficult to control because it depends on a large number of physicochemical parameters. Furthermore, the biocatalytic matrix is not solid enough to

contain the growth of the microbial population in the presence of its substrate. This result in a leak of cells and contamination of the sample medium. The microbial sensor is thus inappropriate for in-vivo measurements.

2.2.3.3 Immunological Sensors

Immunoassays are among the most specific of the analytical techniques, provide extremely low detection limits and can be used for a wide range of substances. Such assays become extremely useful for identifying and quantitating proteins. Immunological sensors (immunosensors) are based on immunological reactions involving miniaturized measuring devices that exploit the recognition involved in the coupling of an antigen with an antibody for triggering useful electrical signals. The main reaction that is taking place at the membrane-solution interface of the immunosensor is:

$$Ag + Ab \leftrightarrow [Ag\text{---}Ab] \tag{2.25}$$

where Ag is the antigen, Ab is the antibody and Ag---Ab is the form of antigen/antibody complex. The Ab is a globular protein produced by an organism to bind to foreign molecules, namely antigens, and mark them for elimination from the organism. The Ab is an extraordinarily selective and versatile reagent. Ab binding leads to a variation in optical properties, electric charge, mass, or heat, which can be detected directly or indirectly by a variety of transducers. Therefore, it is necessary to select the type of the transducer in concordance with the sensitivity of the immunoassay that will occur at the electrode surface. The reproducibility of the construction of the membrane plays an important role in the reliability of response characteristics of the electrode. It was proved for different types of membrane electrodes that the best reproducibility can be obtained using carbon paste electrodes.[10]

Due to the fact that the quality of the immunosensors is directly related to the affinity of the Ab for the target analyte, special attention should be given to the selection of the Ab. Consequently, detection units for single-use and quasi-continuous measuring

devices are presently preferred. An important future development is seen in the field of multi-analyte sensors. The most attractive application is based on Abs with sufficiently different cross-reactivities. The response pattern provides information on the presence and concentration of structurally similar analytes, as they are found for instance in pesticide groups such as the *s*-triazines.[14] It is obvious that this development will be significantly accelerated by applying recombinant techniques for Ab production. The next step is directed toward the generation of recombinant Ab libraries, which will provide a huge repertoire, generated at the DNA level, for new Ab types.

Similar to enzyme biosensors, it is first necessary to immobilize an Ab onto the surface of a transducer in order to develop an immunosensor. This can be carried out by physical adsorption, electrostatic entrapment in a conducting polymer matrix like polypyrrole and chemical immobilization by covalent binding. Ab immobilization can significantly change its reactivity. Therefore, careful attention was given to achieve oriented coupling of antibodies on solid supports that can increase the Ag binding capacity.[10] However, covalent binding leads to a decrease in reactivity.

Instead of immobilizing the antibody onto the transducer, it is possible to use a bare (amperometric or potentiometric) electrode for probing enzyme immunoassay reaction.[15] In this case, the content of the immunoassay reaction vessel is injected into an appropriate flow system containing an electrochemical detector, or the electrode can be inserted into the reaction vessel. Remarkably low detection limits (femtomolar) have been reported in connection to the use of this technique.[15]

In addition to antibodies, it is possible to use artificial nucleic acids ligands, known as aptamers, for the selective detection of proteins. The tight binding properties make aptamers attractive as molecular recognition elements in a wide range of bioassays and for the development of protein arrays. The interaction between aptamer and protein has been monitored by electronic detection.[16]

2.2.4 Immobilization of Bioreceptor for Development of Biosensors

Immobilization of biomolecules to act as bioreceptor has become the most important area of research in the development of biosensor. The main target is to obtain

the optimum bio-stability and reaction efficiencies of the biomolecules. As to achieve this, the preferred host matrix appears to be one that isolates the biomolecule, protecting it from self-aggregation and microbial attack, while providing essentially the same local aqueous microenvironment as in biological media.[17]

Several facts must be taken into account when immobilizing the bioreceptors. The most important is the choice of the biomolecules in terms of its activity and its stability. The activity of the biomolecules must be preserved and the specificity must not be reduced. Its stability also has to be maintained or preferably increased to ensure the stability of the biosensor in terms of reusability and long term storage.

The types of matrix where the biomolecules will be immobilized also have to be taken into account. The choice and condition of matrix must be suitable for the biomolecules to retain their activity. Extreme conditions (*e.g*., pH, temperature) should be avoided for long term exposure.

Direct or indirect immobilization of biologically active proteins on transducers can be used to ensure maximal contact and response. Immobilization steps should be ensure that no nonspecific binding can occur as a consequence of the procedures used. An easy to perform and highly reproducible method would be ideal in large-scale production of the biosensors.

A number of established immobilization procedures are now used. They can be divided into two types of enzyme immobilization; (i) physical immobilization, and (ii) chemical immobilization:

(i) Physical immobilization.

- **Physical adsorption on to a solid surface.**

  This immobilization technique is not reproducible and reliable method of biomolecule attachment to sensing surfaces because of the problems associated with leaching during long-term storage. Glass, plastic and cellulose have been known to adsorb proteins via binding forces such as van der Waals forces, hydrogen bonds, and hydrophobic interactions. Such forces are not very stable and can be easily disrupted by changes in pH, temperature of ionic strength.[18] Unstable multiple layers can also be form by the excess protein at the electrode surface.

- **Use of membranes.**

  Membranes of various porosities can be used to retain the biomolecule close to the electrode surface. This method uses the idea of immobilizing an enzyme on a membrane, and attaching the membrane to the transducer. The step avoids the constraints of direct enzymatic immobilization of the transducer, and allows mass production, which improves the reproducibility of the biosensor signal. Soft membranes for example, can be obtained by coreticulation of the enzyme with a load protein like albumin or collagen.[7] These membranes can therefore be attached simultaneously to the same electrode, which is then the electrochemical transducer of the biosensor.

- **Electromagnetic immobilization.**

  The magnetic particles containing enzymes can be immobilized on the electrode surface by applying a magnetic field produced by passing a continuous current through a solenoid.[19-20] The current is regulated to give a homogeneous distribution of the magnetic particles and homogeneous distribution of the enzyme is obtained when the signal stops fluctuating because the magnetic interactions have stabilized. This method has an advantage of that the biocatalytic component can be changed regularly by releasing the enzyme when the current in the solenoid is stopped. However, it also has several disadvantages which include the difficulty in the fixation of the enzyme to the magnetic particles, the fragility and reversibility of the biospecific interaction and the enzyme may be easily released under certain conditions of pH or ionic strength.

- **Entrapment using a gel films.**

  A useful and simple immobilization based on trapping the enzyme between an inner cellulose acetate film and a collagen can be done by casting the films at the tip of electrode.[3] Encapsulation of enzyme onto sol-gel films also can be used as this method is a mild technique that can be done at low temperature condition. Such coverage with the coating serves to extend the linear range by reduction of the local substrate concentration and to eliminate potential interferences (*e.g.* coexisting electroactive species).

(ii) Chemical immobilization.

- **Covalent attachment.**

  Chemical coupling of biomolecules may provide stable biosensing surfaces that are resistant to wide ranges of pH, temperature and ions to ensure a greater long-term enzymatic stability.[20-21] Three types of supports have been used, which are inorganics, natural and synthetic polymers. However, a covalent bond of the enzyme to the matrix will decrease its activity. Thus, the binding process must occur under conditions that do not denature the biomolecule.

- **Use of crosslinking reagents.**

  Crosslinking is a process that uses a bifunctional agent to form a bridge between different biocatalytic proteins. The process results in increasing in molecular weight, and the aggregates formed are insoluble. Glutaraldehyde is one example of crosslinking reagents that give greater stability to the immobilized protein although inevitably, some inactivation does occur as the crosslinking chemicals may interact with the active site, in the case of enzyme. This bifunctional agent has two aldehyde groups which react with the amine group on the enzyme to form derivatives that are analogues of Schiff bases (Equation 2.26).[20]

  Polymers also can be used to crosslink in the presence of the substance to be immobilized. Polymeric films such as polypyrrole or Nafion maybe used to entrap the enzyme via casting or polymerization. Before the enzyme is bound on nylon, the nylon must have a special treatment.[10] The porosity and degree of crosslinking can also be controlled. Care should be taken to ensure that the crosslinks retain the molecule and the leaching does not occur.

$$\begin{array}{l} \text{E}-\text{N}H_2 \;+\; \text{OCH-}(\text{CH}_2)_3\text{-CHO} \;+\; \text{H}_2\text{N}-\text{P} \\ \qquad\qquad\qquad\qquad \downarrow \\ \text{E}-\text{N}=\text{CH-}(\text{CH}_2)_3\text{-CH}=\text{N}-\text{P} \end{array} \qquad (2.26)$$

2.2.5 Mediators

When an enzyme is immobilized on the transducer, the cofactor is trapped at the active site of the enzyme which is situated at some distance within enzyme, and cannot make close contact with the electrode. In this case, a mediator is necessary to transfer the electrons by acting as a bridge or a shuttle between the cofactor and the electrode. The mediator is reduced to M_{red} by the cofactor, and then oxidized back into M_{ox} when it comes into contact with the anode, which is polarized at the appropriate potential.

As a result of using artificial electron-carrying mediators, measurements become insensitive to oxygen fluctuation and can be carried out at lower potentials that do not provoke interfering reactions from coexisting electroactive species.[3] A variety of electron acceptors have been used as mediators, for example, quinones, organic dyes and ferricyanide.[22] However, their use is limited because they have to be added to the sample, and are toxic, pH-dependent and often undergo auto-oxidation. One good widely used mediator nowadays is organometallic derivatives. Ferrocene and its derivatives such as dimethylferrocene and ferrocene carboxylic acid have the advantage of being hydrophobic, which means that they can simply be absorbed onto a carbon electrode. An electrode that uses ferrocene as a mediator gives a current that is virtually independent of both pH and oxygen partial pressure.[23] However, this electrode has a number of disadvantages, notably its instability and short lifetime.

In order to ensure the electron transfer, the mediator must be present in both oxidized and reduced forms. This means the mediator must remain immobilized near the electrode. It also should have a rate constant for the reaction with enzymes that is sufficiently competitive with that of oxygen, the natural electron acceptor. In order to obtain these conditions, the mediator can be made less soluble through the use of conducting polymers.

2.2.6 Wired Enzymes

The electrical contact between the redox centre of an enzyme and the electrode surface can be further improves by wiring the enzyme with a redox polymer. Heller's group[24-25] has developed an interesting non-diffusional route for establishing electrical communication between GOx enzyme and the electrodes. This was accomplished by wiring the enzyme to the electrode surface with a long flexible hydrophilic polymer backbone [poly(vinylpyridine], having a dense array of covalently linked osmium(bipyridyl) electron relays. The redox polymer penetrates and binds the enzyme to form a three-dimensional network that adheres to the surface. Such a polymeric chain is flexible enough to fold along the enzyme structure resulting to reduce the distance between the redox centers of the polymer and the FAD center of the enzyme. The film thus conducts electrons and is permeable to the substrate and product of the enzymatic reaction. The resulting three-dimensional redox-polymer/enzyme network offers high current outputs and stabilizes the mediator to the surface.

The mechanism of electron diffusion through redox hydrogels, which electrically 'wire' redox centers of enzymes to electrodes has been clarified by Aoki *et al*. (1995)[26]. It is thought that electrons diffuse in redox hydrogels through electron-transferring collisions between fast redox centers attached to the hydrated polymer network. The electron-diffusion coefficients increase when the gels are hydrated because of hydration that leads to an increase in the amplitude of the colliding polymer chain segments. In electrodes made with redox hydrogels, formation of an electrostatic complex between the enzyme and the gel-forming redox polyelectrolyte is essential for electrical wiring when the redox centers are deeply buried in the enzyme protein (for example in glucose oxidase), but not when the redox centers are at, or near the surface (for example in peroxidase).[27]

Nanomaterials can also be used for effective electrical wiring of redox enzymes. Various nanomaterials, such as carbon nanotubes or gold nanoparticles, have been used as electrical connectors between the electrode and the redox centre of enzyme. Xiao's group (2003)[28] for example, have been reconstituted an apo-glucose oxidase on a 1.4 nm gold nanocrystal functionalized with the FAD cofactor. The gold nanoparticle

immobilized onto the gold electrode by means of a dithiol linker, thus acts as an 'electrical nanoplug' for the electrical wiring of its redox-active center. This leads to a high electron-transfer turnover rate of ~5000 per second.

Carbon nanotubes also can be coupled to enzymes to provide a favourable surface orientation and act as an electrical connector between their redox center and the electrode surface. Willner's group[29] demonstrated that aligned reconstituted GOx on the edge of a single wall carbon nanotubes (SWCNTs) can be linked to an electrode surface. The enzyme reconstitution on the end of carbon nanotubes represents an extremely efficient approach for 'plugging' an electrode into GOx. Electrons were thus transported along distances higher than 150 nm with the length of the SWCNTs controlling the rate of electron transport. This efficient direct electrical connection to GOx property was also reported by Gooding's group in connection to aligned SWCNTs array.[30]

2.2.7 Enzyme Kinetics: Michaelis-Menten Kinetic Mechanism

Michaelis and Menten (1913)[31] proposed the steady-state enzyme kinetics which is based on the assumption that the substrate is first forms a complex with the enzyme in a reversible process and that equilibrium is maintained between the enzyme, E and substrate, S and the enzyme-substrate complex, ES. The irreversible breakdown of this enzyme-substrate complex then produces the product, P and liberates the enzyme.

$$\mathrm{E+S} \overset{K_M}{\leftrightarrow} \mathrm{ES} \overset{k_{cat}}{\longrightarrow} \mathrm{E+P} \tag{2.27}$$

At a fixed enzyme concentration, the rate of the enzyme-catalyzed reaction, *V* is given by the Michaelis-Menten equation:

$$V = V_{max}\,[\mathrm{S}]/(K_{\mathrm{M}} + [\mathrm{S}]) \tag{2.28}$$

where K_M is the Michaelis-Menten constant, [S] is the substrate concentration, and V_{max} is the maximum rate of the reaction (when [S] = ∞).

The Michaelis-Menten constant (K_M) is defined as the substrate concentration at which the enzyme catalyzes the reaction at ½ V_{max}. K_M is often referred to as the enzyme dissociation constant. Maximum velocity (V_{max}) represents the rate when 100% of the enzyme is occupied by substrate in the process of catalysis, which occurs if concentration of substrate, [S] is high enough. In the construction of enzyme electrodes, it is desirable to obtain the lowest K_M and the highest V_{max}. However, when the apparent K_M is much larger than its value for soluble enzyme, it means either that a significant substrate diffusion barrier is present between the sample and reaction layer, or that the rate of reaction to the co-substrate with the enzyme is increased.[10]

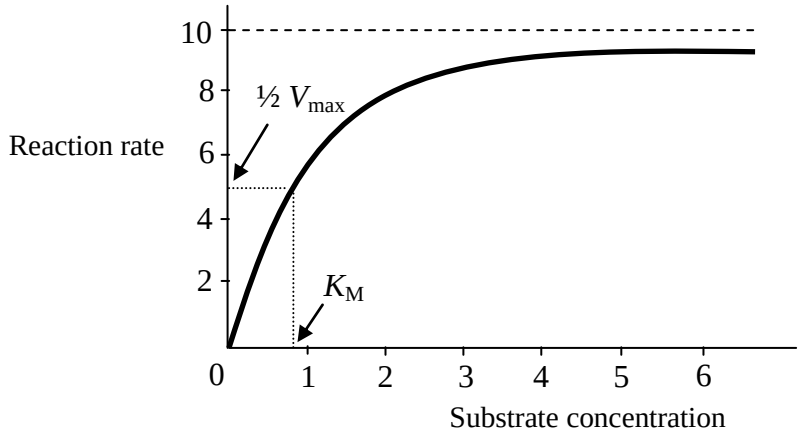

Figure 2.8: Michaelis-Menten saturation curve of an enzyme reaction.

Figure 2.8 shows the typical plot of dependency of the reaction rate on the substrate concentration. The initial rate increases linearly with substrate concentration, until a non-limiting excess of substrate is reached because at this region, S<<K_M. And then, further increase in concentration of substrate (S>>K_M), will cause no further increase in the rate and k_{cat} is known to independent of substrate concentration. k_{cat} (in unit sec^{-1}) is called the 'turnover number', which is the number of substrate molecule converted to product in one second by one molecule of enzyme. By Equation 2.29,

$$k_{cat} = \frac{V_{max}}{[Enzyme\ ]} \tag{2.29}$$

k_{cat} shows the potential of an enzyme as a catalyst. The relationship between k_{cat} and K_M can be explained in terms of 'specificity constant' of the free enzyme and substrate. The term k_{cat}/ K_M is a measure of how efficiently an enzyme converts a substrate into a product. Thus, the specificity constant is an effective bimolecular rate constant for free enzyme to react with free substrate to form product. The specificity constant also can be obtained by the slope of the Michaelis-Menten equation at low concentration of substrate (when [S] << K_M).

In order to solve the value of the K_M and V_{max}, Michaelis-Menten equation (Equation 2.28) can be rewritten in several different ways to yield straight line plots. By using the straight line model y = mx + c (where m is the slope of the line and c is the y-axis intercept), K_M can be obtained from the Lineweaver-Burk plot and Hanes-Hoolf plot as shown in Figure 2.9 and 2.10, respectively.

The Lineweaver-Burk plot or double reciprocal plot is common way of illustrating kinetic data. This is produced by taking the reciprocal of both sides of the Michaelis–Menten equation. As shown below, this is a linear form of the Michaelis–Menten equation and produces a straight line with the equation y = mx + c with a y-intercept equivalent to $1/V_{max}$ and an x-intercept of the graph representing $-1/K_M$.

$$\frac{1}{v_0} = \frac{K_M}{V_{max}} \frac{1}{[S]} + \frac{1}{V_{max}} \tag{2.30}$$

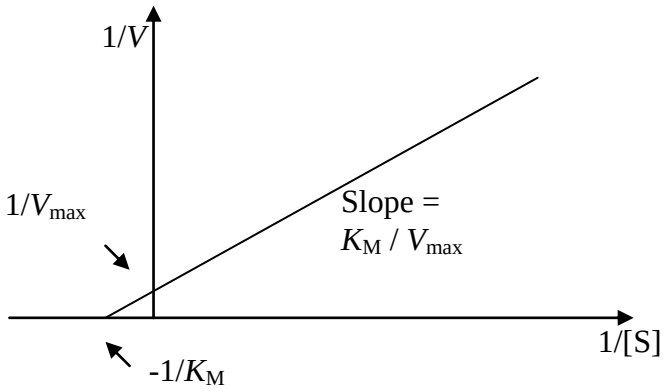

Figure 2.9: Lineweaver-Burk plot.

Although the Lineweaver-Burk plot is the simplest way to analyze enzyme kinetic data, it also has a significant drawback. Because it is a double reciprocal plot, the errors associated with the data at low substrate concentration are greatly influenced and, if a simple least squares analysis is used, it can lead to significant errors in the estimates of K_M value.

The Hanes-Woolf plot is also widely used to determine the important terms in enzyme kinetics, such as K_M and V_{max}, as the y-intercept of such a graph is equivalent to the inverse of K_M/V_{max} and the slope of the graph represents $1/V_{max}$. The Hanes-Woolf plot has advantages over the Lineweaver-Burk plot, that it avoids taking reciprocal concentrations, so that the determination of the V_{max} value is more accurate than that from the Lineweaver-Burk plot. Thus, it is the preferred method for statistical correctness of data analysis.

Starting from the Michaelis-Menten equation,

$$V = V_{max}\,[\mathrm{S}]/(K_M + [\mathrm{S}]) \tag{2.28}$$

Multiply both sides by [S],

$$\frac{[S]}{v_0} = \frac{[S](K_M + [S]}{V_{max}\,[S]} = \frac{K_M + [S]}{V_{max}} \tag{2.31}$$

and rearrange the equation to get:

$$\frac{[S]}{v_0} = \frac{K_M}{V_{max}} + \frac{1}{V_{max}}[S] \tag{2.32}$$

Plot of [S] / v_0 on y-axis and [S] on x-axis gives the Hanes-Woolf plot as shown in Figure 2.10:

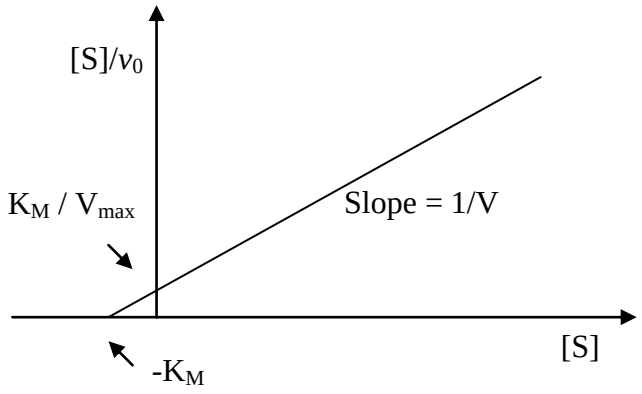

Figure 2.10: Hanes-Woolf Plot.

A uniform series of concentrations in the experiment gives a uniformly spaced set of points in the data because the x-axis in the Hanes-Woolf plot is simply [S], not in reciprocal form. The rightmost points relate to the larger and more accurate values of [S] and v_0, so there is no exaggeration of error on the right.

The analysis of Hanes-Woolf plot can be used to analyse the enzyme electrode data according to the method described by Albery and Bartlett.[32] This method is used for analysing amperometric enzyme kinetics where the enzyme is entrapped behind a membrane as shown in Equation 2.33, which is similar in form to the Hanes plot frequently used in the analysis of homogeneous enzyme kinetic data.

$$\frac{S_\infty}{j} = \frac{1}{k'_{ME}}\left[1 + \frac{S_\infty}{K_{ME}}\left(1 - \frac{j}{k_s S_\infty}\right)\right] \quad (2.33)$$

where

$$1/k_{\mathrm{ME}}' = K_{\mathrm{M}}/\mathrm{e}_{\Sigma} L k_{cat} + 1/k_s' \quad (2.34)$$

is the effective heterogeneous rate constant for the enzyme membrane electrode and

$$K_{\mathrm{ME}} = [K_{\mathrm{M}}(Lk_{cat})^{-1} + \mathrm{e}_{\Sigma}(k_s')^{-1}]/[(Lk_{cat})^{-1} + (k')^{-1}] \quad (2.35)$$

where S_∞ is the bulk substrate concentration, j is the flux, k'_{ME} is the effective heterogeneous rate constant and K_{ME} is similar to the Michaelis–Menten constant in homogeneous enzyme kinetics. When the concentration of substrate is less that K_{ME} the system is unsaturated; the current is then proportional to the substrate concentration and is governed by the rate constant k'_{ME}. When the concentration of substrate is greater than K_{ME} the system becomes saturated and the current, as a function of substrate concentration, reaches a plateau.

The great advantage of this method is that it allows the rate limiting steps to be identified, which in turn means that rational steps can be taken to optimize or improve the electrode design and performance.[32]

References

(1) Bard, A. J., and Faulkner, L.R. *Electrochemical Methods: Fundamentals and Applications*; 2nd edition ed.; John Wiley & Sons Inc.: USA, 2001.

(2) Bard, A. J., and Faulkner, L.R. *Electrochemical Methods: Fundamentals and Applications*; 2nd edition ed.; John Wiley & Sons Inc., 2000.

(3) Wang, J. *Analytical Electrochemistry*; 3rd edition ed.; John Wiley & Sons, Inc.: Hoboken, New Jersey., 2006.

(4) Nicholson, R. S.; Shain, I. *Anal. Chem.* **1964**, *36*, 706.

(5) Fisher, A. C. *Electrode Dynamics*; Oxford University Press: Oxford, 1996.

(6) Karube, I.; Matsunaga, T.; Mitsuda, S.; Suzuki, S. *Biotechnol. Bioeng.* **1977**, *19*, 1535.
(7) Tran, M. C. *Biosensors*; Chapman & Hall: London, 1993.
(8) McCormack, T., Keating, G., Killard, A., Manning, B.M. and O'Kennedy, R. In *Principle of Chemical and Biological Sensors*; Diamond, D., Ed.; John Wiley & Sons, Inc.: New York, USA, 1998.
(9) Scheller, F. W.; Hintsche, R.; Pfeiffer, D.; Schubert, F.; Riedel, K.; Kindervater, R. *Sens. Actuator B-Chem.* **1991**, *4*, 197.
(10) Stefan, R.-I., van Staden, J-F., and Aboul-Enein, H.Y. *Electrochemical Sensors in Bioanalysis*; Marcel Dekker, Inc.: New York, 2001.
(11) Katrlik, J.; Brandsteter, R.; Svorc, J.; Rosenberg, M.; Miertus, S. *Anal. Chim. Acta* **1997**, *356*, 217.
(12) Ukeda, H.; Yamamoto, N.; Sawamura, M.; Kusunose, H. *Anal. Sci.* **1995**, *11*, 941.
(13) Shimomura-Shimizu, M.; Karube, I. In *Whole Cell Sensing Systems Ii*; Springer-Verlag Berlin: Berlin, 2010; Vol. 118, p 1.
(14) Hock, B. *Anal. Chim. Acta* **1997**, *347*, 177.
(15) Heineman, W. R.; Halsall, H. B. *Anal. Chem.* **1985**, *57*, 1321.
(16) Xiao, Y.; Lubin, A. A.; Heeger, A. J.; Plaxco, K. W. *Angew. Chem.-Int. Edit.* **2005**, *44*, 5456.
(17) Gupta, R.; Chaudhury, N. K. *Biosens. Bioelectron.* **2007**, *22*, 2387.
(18) Diamond, D. *Principle of Chemical and Biological Sensors*; John Wiley & Sons Inc.: USA, 1998.
(19) Miyabayashi, A.; Mattiasson, B. *Anal. Chim. Acta* **1988**, *213*, 121.
(20) Canh, T. M. *Biosensors*; Chapman & Hall: London, 1993.
(21) Mascini, M.; Guilbault, G. G. *Biosensors* **1986**, *2*, 147.
(22) Mahenc, J.; Aussaresses, H. *Comptes Rendus Hebdomadaires Des Seances De L Academie Des Sciences Serie C.* **1979**, *289*, 357.
(23) Cass, A. E. G.; Davis, G.; Francis, G. D.; Hill, H. A. O.; Aston, W. J.; Higgins, I. J.; Plotkin, E. V.; Scott, L. D. L.; Turner, A. P. F. *Anal. Chem.* **1984**, *56*, 667.
(24) Degani, Y.; Heller, A. *J. Phys. Chem.* **1987**, *91*, 1285.
(25) Pishko, M. V.; Katakis, I.; Lindquist, S. E.; Ye, L.; Gregg, B. A.; Heller, A. *Angew. Chem. Int. Ed. Engl.* **1990**, *29*, 82.
(26) Aoki, A.; Rajagopalan, R.; Heller, A. *J. Phys. Chem.* **1995**, *99*, 5102.
(27) Katakis, I.; Ye, L.; Heller, A. *J. Am. Chem. Soc.* **1994**, *116*, 3617.
(28) Xiao, Y.; Patolsky, F.; Katz, E.; Hainfeld, J. F.; Willner, I. *Science* **2003**, *299*, 1877.
(29) Patolsky, F.; Weizmann, Y.; Willner, I. *Angew. Chem. Int. Ed.* **2004**, *43*, 2113.
(30) Liu, J. Q.; Chou, A.; Rahmat, W.; Paddon-Row, M. N.; Gooding, J. J. *Electroanalysis* **2005**, *17*, 38.
(31) Michaelis, L.; Menten, M. L. *Biochem. Z.* **1913**, *49*, 333.
(32) Albery, W. J.; Bartlett, P. N. *J. Electroanal. Chem.* **1985**, *194*, 211.

CHAPTER 3

MATERIALS AND EXPERIMENTAL TECHNIQUES

3.1 Biocomposite Materials used for making the Biosensors.

3.1.1 Glucose oxidase Enzyme as the Bioreceptor of Biosensors.

Glucose oxidase (GOx) is an enzyme that commonly used as a benchmark system in the development of biosensors.[1-7] It has favourable attributes that contribute to its common usage, which include excellent selectivity, high turnover rate, good pH and thermal stability and low cost.[8] GOx is a dimeric protein that made up of two identical subunits, each containing a molecule of flavin adenine dinucleotide (FAD) coenzyme. The dimer contains two disulphide bridges that link the two subunits of GOx together. It has a molecular weight of 160 kDa and a size of 70 Å x 55 Å x 80 Å.[9-11]

The isolation of GOx from a number of sources has been reported, include red algae,[12] citrus fruits,[13] and bacteria[14]. One of the most commonly used GOx in the field of biosensor nowadays is the one that isolated from bacteria *Aspergillus niger*. The GOx from *Aspergillus niger* is a glycoprotein with high-mannose content of 10 to 16% of its molecular weight.[15-16] The latter group has proposed that the carbohydrate content ranges from 8 to 12%.[17-18] The carbohydrate moieties are N- and O-glycosidically linked to the protein.[19] The different ranges in carbohydrate content leads to variations in the isoelectric point between 3.9 and 4.3. Elsewhere the isoelectric point has been quoted as 4.2,[20] which means that GOx is an anionic enzyme at physiological pH.[21]

GOx has a high content of secondary structure with 28% helix and 18% sheet.[11] Two distinctly different β-sheet systems has characterized the tertiary structure of the enzyme; one of that forms part of the FAD binding domain and the second is a large six stranded anti-parallel β-sheet supported by four α-helices.[11] This β-sheet forms one side of the active site which are located near the interface between the two subunits of GOx monomers. A structure of GOx is shown in Figure 3.1.

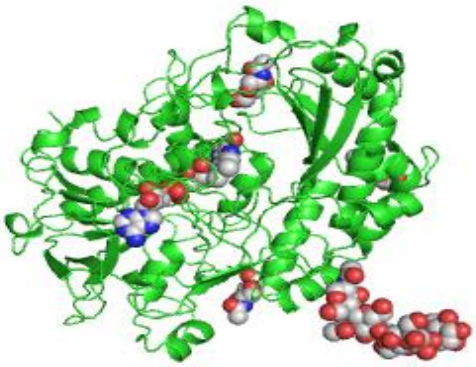

Figure 3.1: Glucose oxidase structure from *Aspergillus niger*. Structure created using polyview. FAD is showed as the blue-red-grey space-fill, which grey is corresponds to carbon atom, blue is nitrogen atom and red is oxygen atom. The α-helix and β-sheet secondary structures of glucose oxidase are showed as the green chains.

The active site of the enzyme GOx contains the FAD coenzyme molecule. As seen in Figure 3.1, the FAD is showed as the blue-red-grey space-fill, which is tightly attached but not covalently bound to the enzyme that can be released from the enzyme by partial unfolding of the protein without permanently denaturing it.[8-9] The crystal structure of GOx has shows that the FAD group sits in a cleft at the bottom of a deep cavity.[9,18] Access to the flavin system in the active site is provided by a large deep pocket which is shaped like a funnel and is formed on one side by residues of the second molecule of the dimer.[11] FAD is the reaction site where the oxidation of glucose occurs catalyzed by GOx. It works efficiently as a cofactor because of its reversible electrochemistry. The fully oxidized state of FAD can be fully reduced to $FADH_2$ by addition of two hydrogen atoms as shown in Figure 3.2.

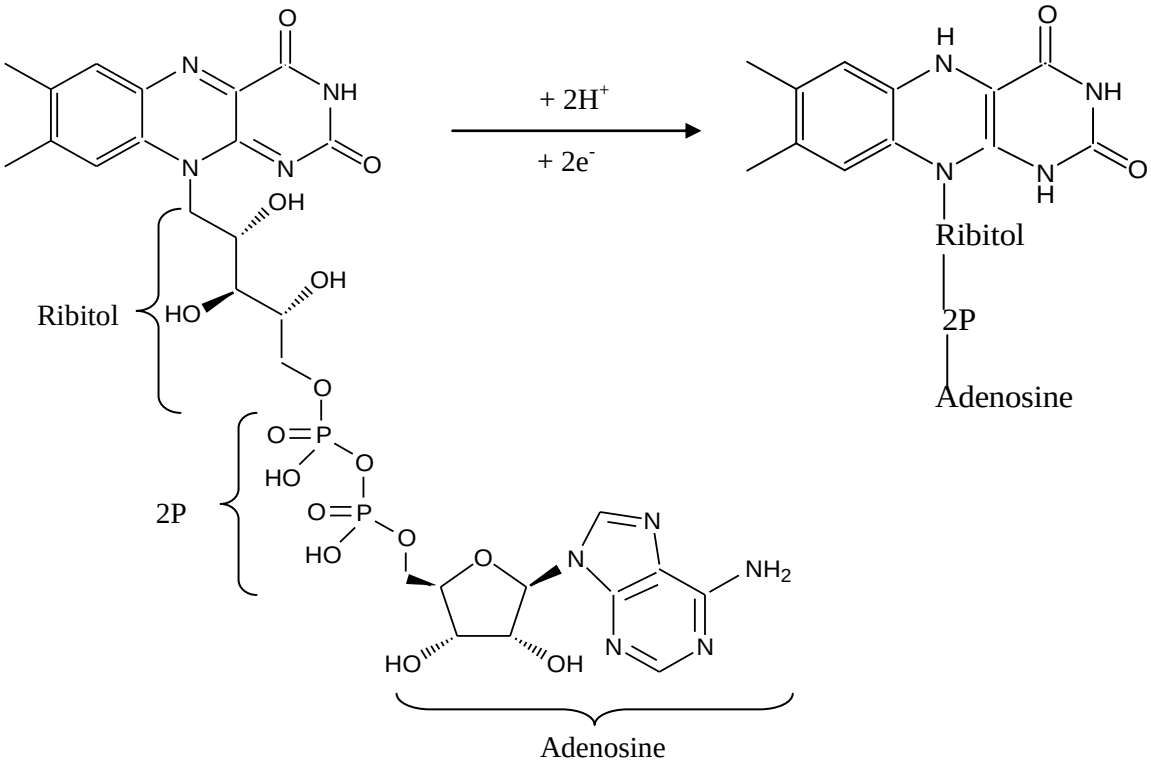

Figure 3.2: Reduction of FAD to $FADH_2$.

To re-oxidized $FADH_2$ back to FAD, molecular oxygen reacts non-enzymatically to produce hydrogen peroxide as shown in Figure 3.3.[10]

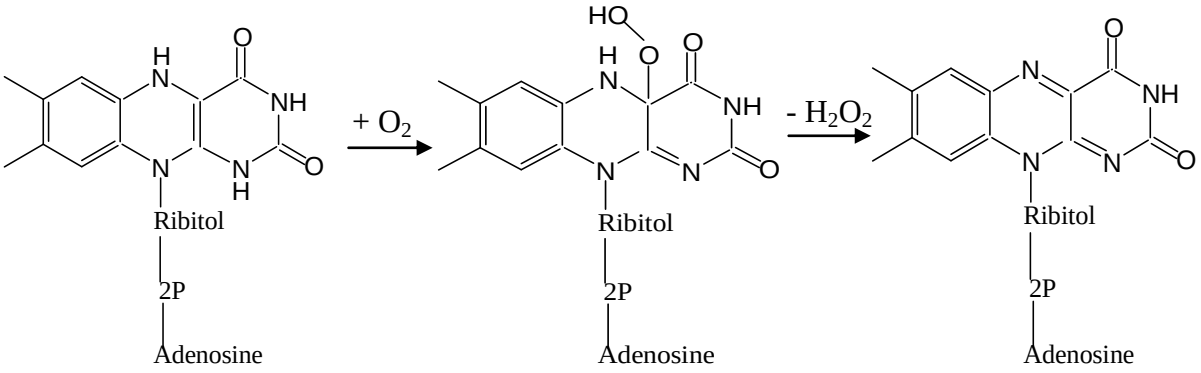

Figure 3.3: Oxidation of $FADH_2$ by the natural electron acceptor O_2.

GOx shows a high specificity for β-D-glucose. In the presence of glucose, FAD via GOx will efficiently oxidize glucose by shuttling electrons from glucose to dissolved oxygen in solution as mediator,[10] as shown in Equations 3.1 and 3.2. FAD oxidizes glucose to produce $FADH_2$ and gluconolactone. The $FADH_2$ is then regenerated by oxygen to produce hydrogen peroxide, H_2O_2 and returning the enzyme in the form of FAD.

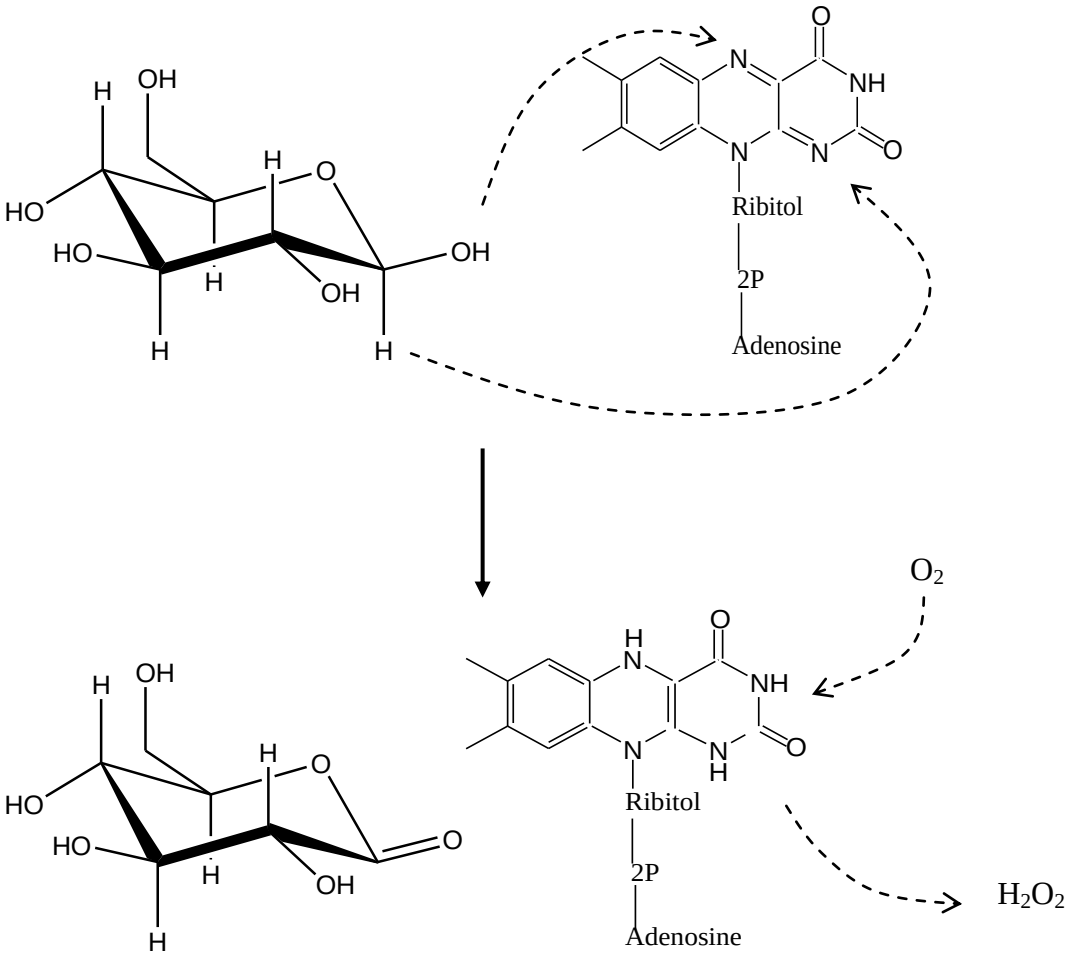

$$FAD + C_6H_{12}O_6 \rightarrow FADH_2 + C_6H_{10}O_6 \quad (3.1)$$

$$FADH_2 + O_2 \rightarrow FAD + H_2O_2 \quad (3.2)$$

Due to the orientation of the FAD molecule in a deep cavity thick layer of GOx, the FAD oxidation by an electrode becomes inefficient. According to Marcus *et al*. (1985)[22], the low efficiency of the oxidation of an enzyme is due to the limited distance that an electron can tunnel between enzyme and the electrode. As the distance gets larger, the intrinsic barrier to direct electron transfer is introduced so that the oxidation of the FAD become kinetically unfavourable and is unlikely to occur. In order to facilitate the electron transfer between enzyme and the electrode surface, the enzyme layer has to modify with electron-tunnelling groups so that it can efficiently oxidize for use in an electrochemical biosensors.

3.1.2 Lactate oxidase

While GOx was used as a benchmark of the biosensor system, lactate oxidase (LOx) was then be used in lactate detection as the test case of several biological applications in industries. Because of their chirality, LOx can be present as D-lactate oxidase (D-LOx) or L-lactate oxidase (L-LOx) depending to their sources of origin. In this study, the scope of this research has been specific to L-LOx. L-LOx belongs to the family of flavoproteins that catalyze the oxidation of α-hydroxyacids.[23-24] It is an enzyme that contains a flavin mononucleotide (FMN) group as the cofactor to catalyse the conversion of L-lactate to pyruvate. This enzyme displays a high level of substrate specificity.[25]

The overall structure of LOx contains two tightly packed tetramers. Each tetramer has a dimension of 50 Å x 100 Å x 100 Å.[23] As found in many other flavin family proteins, each monomer of LOx has a typical eight α-helices and eight β-strands, with the FMN-binding site and the active site are formed on the C-terminal end of the β-strands[25] as shown in Figure 3.4. These individual monomers of LOx are superimposed well onto each other.

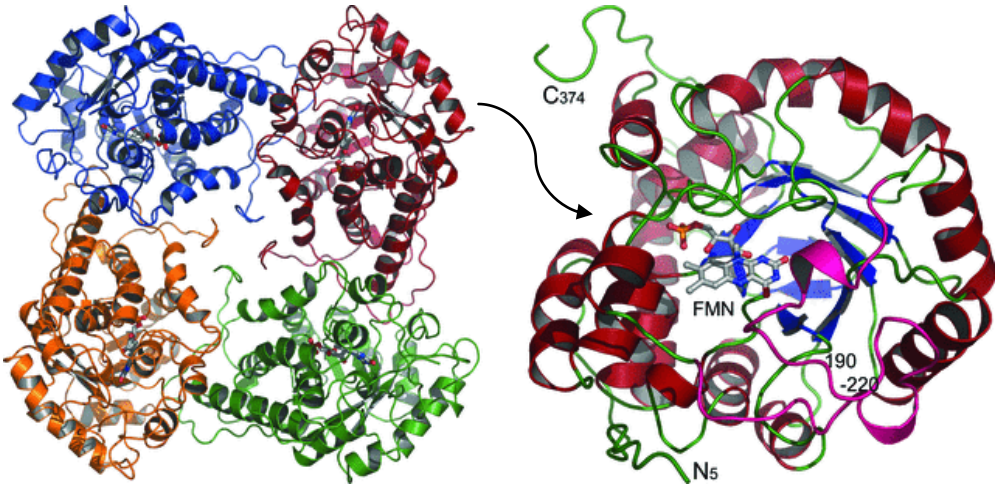

(a) (b)

Figure 3.4: The tetramer structure (a) with each monomer is depicted in different colour, and the monomer structure (b) of L-LOx showing the FMN cofactor located on the tip of the β-barrel and residues 190-220 (in pink) form a lid over the active site. Red is α-helices, and blue is β-strand.[23]

The FMN is the oxidative cofactor of the active site in LOx. It is positioned deep down in the funnel-shaped substrate binding site, behind the substrate when it is bound. The interaction of FMN with the respective substrate is found to determine the substrate specificity and the reaction mechanism.

Like any other α-hydroxy acid-oxidizing enzymes, the enzymatic reaction of lactate oxidation was found to follows a 'ping-pong' mechanism with sequential reductive and oxidative steps.[24,26] The reductive half reaction mechanism of LOx is believed to involve either carbanion formation or hydride transfer. The mechanism involves the formation of a carbanion intermediate when the catalytic histidine (His265) in LOx deprotonated the α-carbon hydrogen in lactate as a proton. This reaction subsequently transfers the reducing substrate to the flavin, to yield the $FMNH_2$ and pyruvate. Alternatively, for the hydride transfer mechanism to occur, the catalytic base His265 will deprotonated the α-hydroxyl group in lactate and then transfer the α-hydrogen to FMN as a hydride. Figure 3.5 shows the mechanism involves in FMN group in the presence of L-lactate as the substrate to L-LOx.[24]

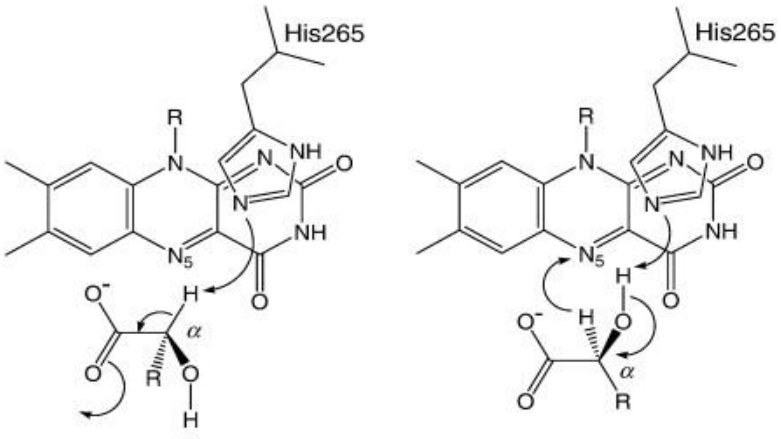

(a) (b)

Figure 3.5: Chemical mechanisms for substrate oxidation by an α−hydroxy acid oxidase. (a) The carbanion formation mechanism, and (b) the hydride transfer mechanism.

The following mechanism (Figure 3.6) was proposed by Furuichi *et al.* (2008)[24] when the L-lactate is presence to the L-LOx system. The mechanism starts with the disruption of α-carbon hydrogen (C^{α}-H) and the α-carbon hydroxyl (C^{α}-OH) bonds in L-lactate. At the same time, FMN is reduced and the histidine (His265) residue is protonated and flipped out, followed by introduction of molecular oxygen to the complex. Alternatively, the product pyruvate is releasing at the end of the half-reaction. After the completion of the reductive half-reaction, the oxidative half-reaction starts as the molecular oxygen moves to the substrate-binding site, as the second substrate by flipping back of His265, and the molecular oxygen is placed in the same location as the C^{α} and keto-oxygen atoms of the pyruvate molecule in the LOx-pyruvate complex. This arrangement of the molecular oxygen in the active site promotes the reverse reaction; that is, the reduced FMN functions as the hydride donor, and the protonated His265 acts as the active site acid. The hydrogen peroxide is then produced from the molecular oxygen and exits from the complex. At the same time, FMN is re-oxidized and His265 is deprotonated, so that they are ready for the next reaction cycle.

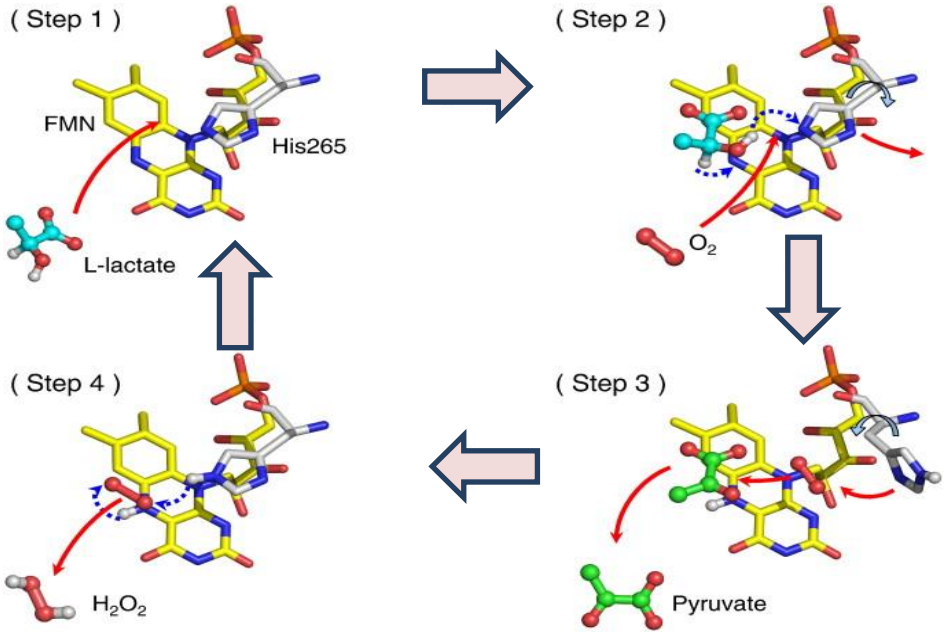

Figure 3.6: The mechanism of L-lactate oxidation proposed by Furuichi *et al*. (2008).[24] The two hydrogen atoms involved in L-lactate oxidation are depicted as gray balls. Hydrogen transfer and hydride transfer are shown by blue broken arrows.

$$\text{Lactate} + \text{LOx}_{\text{ox}} \rightarrow \text{Pyruvate} + \text{LOx}_{\text{red}} \tag{3.3}$$

$$\text{LOx}_{\text{red}} + \text{O}_2 \rightarrow \text{LOx}_{\text{ox}} + \text{H}_2\text{O}_2 \tag{3.4}$$

$$\text{H}_2\text{O}_2 \rightarrow \text{O}_2 + 2\text{e}^- \tag{3.5}$$

As shown in Equation 3.3 to 3.5, the overall reaction involves the transfer of two electrons and two protons from the reduced cofactor to molecular oxygen to generate hydrogen peroxide and pyruvate and ultimately regenerate the oxidized cofactor.

3.1.3 Ferrocene as Mediator.

Ferrocenes or bis(cyclopentadienyl)iron(II) are a class of mediators that frequently used as electroactive residue in supramolecular electrochemistry because of its reproducible redox properties. They have a wide range of redox potentials, are easy to derivatize, and have fast electron transfer kinetics.[10] Ferrocene undergoes one-electron oxidation at a low potential, around 0.5 V vs. a saturated calomel electrode (SCE) to yield the cationic ferrocenium species. It is a stable 18-electron system. The oxidized and reduced forms of ferrocene are stable in most organic solvents, but decompose quickly in aqueous media, especially in basic conditions. Ferrocene also can be used as an internal reference (known as a reference redox couple) for electrochemical experiments performed in low dielectric solvents that do not permit use of a standard reference electrode.[27]

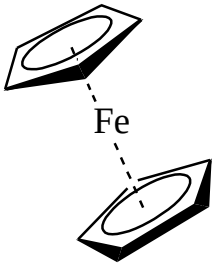

Figure 3.7: Structure of ferrocene.

Several groups have demonstrated that ferrocene-derivatives can mediate the oxidation of analyte in GOx[8,28-29] and LOx systems.[30-31]

3.1.4 Enzyme-Electrode Immobilization Matrix.

3.1.4.1 Collagen

Collagen is a long, fibrous structural protein whose functions are quite different from those of globular proteins. It is an important biomaterial in medical applications due to its special characteristics, such as biocompatibility, biodegradability and weak antigenecity. In animals, collagen plays critical roles in tissue architecture, tissue strength, and cell to cell relationships. In major component of all connective tissue matrixes, collagen is presence in all tissues and organs where it provides the framework that gives the tissues their form and structural strength. Its high concentration was found presence in all organs such as skin (74%), cornea (64%), cartilage (50%), aorta (12-24%), whole bone (23%), lung (10%) and liver (4%).[32] Thus, collagen has been used in drug delivery systems and tissue engineering.

Collagen contains large amounts of glycine (33%) and proline (13%), as well as two amino acids that are not inserted directly by ribosomes, which are 4-hydroxyproline (9%) and 5-hydroxylysine (0.6%) (Figure 3.8). These two derivatives of proline and lysine play important roles in the stabilisation of the collagen sub-unit called tropocollagen globular structure as well as the final fibre shaped structure by forming covalent bonds. Collagens are glycoproteins with carbohydrate covalently bonded to the derived amino acid, 5-hydroxylysine by an O-glycosidic bond through the δ-carbon hydroxyl group. Formation of 5-hydroxylysine and addition of the carbohydrate occur after polypeptide chain formation but prior to the folding of the collagen chains into their unique supercoiled structure.[32] This resulting structure is called a collagen triple helix.

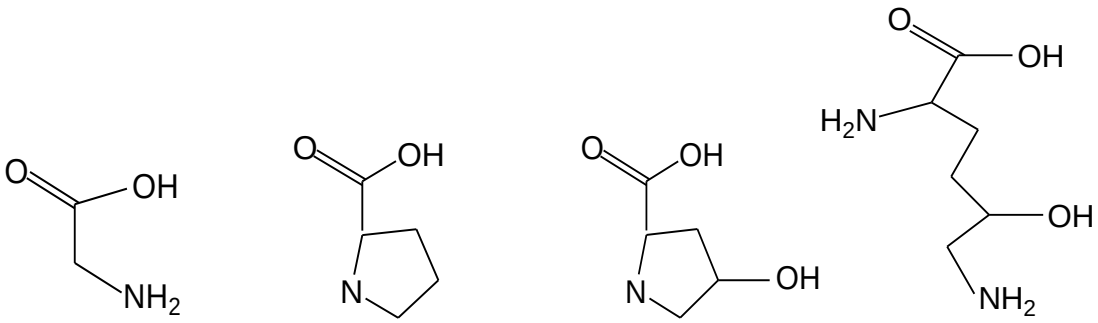

(a) (b) (c) (d)

Figure 3.8: The four amino acids that form the structure of a collagen molecule. (a) Glycine, (b) proline, (c) 4-hydroxyproline, and (d) 5-hydroxylysine.

There are ten known forms of collagen, because of differences in functional requirements and chemical environments and compositions. All forms of collagen share the same basic structure, which is three polypeptide chains coiled together to form a triple helix. The collagens fibres consist of globular units of tropocollagen spontaneously arrange themselves under physiological conditions into staggered array structures stabilised by numerous hydrogen and covalent bonds. Tropocollagen sub-units are left-handed triple helices where each strand is, further, a right-handed helix itself. Figure 3.9 shows the structure of collagen triple helix.

(a)

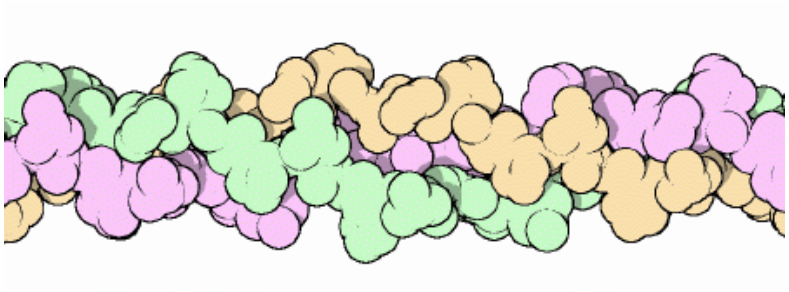

(b)

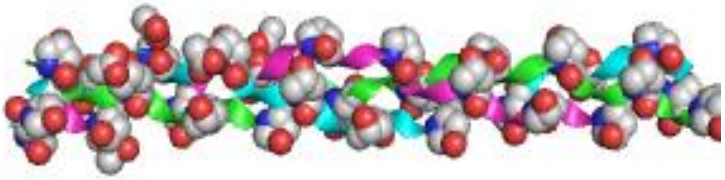

Figure 3.9: Diagram of collagen obtained from RCSB Protein Data Bank, (entry ID: pdb1bkv). (a) Ribbon model of supercoiled structure of collagen with each individual chain (depicted by different colours) in a polyproline type II helix. (b) Structure of collagen type I created by polyview.

Collagen is also one of the biopolymers most extensively used to construct hybrid complexes.[33] There were reports on construction of organic-inorganic hybrid[34] and nano-bio hybrid complexes[35-36] using sol-gel and carbon nanotubes, respectively in combination with collagen. However, their applications to development of biosensors have not been studied extensively.

Collagen proved to be an attractive material for biomolecules immobilization because it has large pores (0.7 – 1.6 μm in 0.4 – 2.0 ng/mL gels),[37] simple gel formation and have a high mechanical strength.

3.1.4.2 Sol-gel

The enzyme immobilization technique that has been used in this study was entrapment of enzyme using a gel. Sol-gel glass offers a better way to immobilize enzyme within its porous optically transparent matrix. This is due to simple sol-gel processing conditions which can be conducted under near ambient temperature and neutral conditions, and also possibility of tailoring for specific requirements. This

approach is unique because entrapment is based on the growing of siloxane polymer chains around the enzyme within an inorganic oxide network. Furthermore, because of the porous nature of the sol-gel network, entrapped species remains accessible and can interact with external analytes.[38-39]

As aging progresses, cross-linking of the network increases and the internal solvent is expelled from the matrix. This might cause the internal polarity and viscosity to change and the average pore size to decrease that can led to entrapped species inaccessible to external analyte.[39] According to MacCraith *et al*. (1995),[40] sol-gel derived thin films are always preferred for immobilizing the biomolecules to act as a biosensor because of the basic requirement of short diffusion path for quick interaction and detection of the analyte molecule.

Sol-gel refers to a process whereby inorganic polymers are involved in a transition from sol composition in a form of liquid 'sol' into a solid 'gel' phase.[41-42] A 'sol' is a dispersion of colloidal particles in a liquid and a 'gel' is a rigid, interconnected polymeric network formed by the assembly of the sol.[43]

The sol-gel method is a low temperature technique in which a precursor alkoxide under goes hydrolysis and condensation to form optically transparent glass after a period of time. After a sol is gelled, an enzyme can be entrapped within a polymeric network of the porous gel.[44] The enzyme molecules become entrapped in the covalent network rather than being chemically bound to the inorganic matrix as chemical bonding of the substrate may inactivate the molecule.

In the sol-gel process, the precursors for preparation of a colloid consist of a metal or metalloid element surrounded by various ligands. For example, common precursors for aluminium oxide include inorganic salts such as $Al(NO_3)_3$ or organic materials such as $Al(OC_4H_9)_3$. The latter is an alkoxide, the example of class of precursors most widely used in sol-gel research because they react readily with water.[45] Metal alkoxides are members of the family of metal organic compounds, which have an organic ligand attached to a metal or metalloid atom. This reaction involves known as hydrolysis and described as the following reaction.[45]

$$\equiv Si - OR + H_2O \xleftrightarrow[esterification]{hydrolysis} \equiv Si - OH + ROH \qquad (3.6)$$

Depending on the amount of water and catalyst present, hydrolysis may go to completion as follows:

$$\equiv Si-OR+4H_2O \equiv \xleftrightarrow[esterification]{hydrolysis} Si(OH)_4+4ROH \quad (3.7)$$

The size of the sol particles and the cross-linking within the particles depend upon the pH and *R* ratio ($R = [H_2O]/[Si(OR)_4]$). In general, under stoichiometric addition of water ($R < 2$), the alcohol condensation process become dominant (Equation 3.8), whereas ($R \geq 2$), water condensation process is more favoured (Equation 3.9).

$$\equiv Si-OR+HO-Si \equiv \xleftrightarrow[alcoholysis]{alcohol\ condensation} \equiv Si-O-Si \equiv +ROH \quad (3.8)$$

$$\equiv Si-OH+HO-Si \equiv \xleftrightarrow[hydrolysis]{water\ condensation} \equiv Si-O-Si \equiv +H_2O \quad (3.9)$$

Various researchers have shown that variations in the synthesis conditions such as the value of *R*, the concentration and the type of catalyst and the solvent used can cause modifications in the structure and properties of the polysilicate product. Acid-catalysed hydrolysis with low H_2O:Si ratios produced weekly branched polymeric sols, whereas base-catalysed hydrolysis with large H_2O:Si ratios will produces highly condensed particulate sols. Intermediate conditions will produce the intermediate structures of these sols.[45] Acid or base catalysts were found play an important role in the structure of the sol-gel product.

The gelation of the colloidal suspension then occurs as the the gel point is achieved. This is defined as the point at which the entire solid mass becomes inter-connected in three-dimentional network (Figure 3.10). At the initial stages of polymerization, the silanol functional groups at the surface of the growing particles are partly deprotonated, and their negative charge provides a repulsion barrier that stabilizes the sol.[46] The solvent will be evaporated later on and the consumption of water by alkoxysilanes will hydrolyse the concentrated solution and destabilizes the suspension.

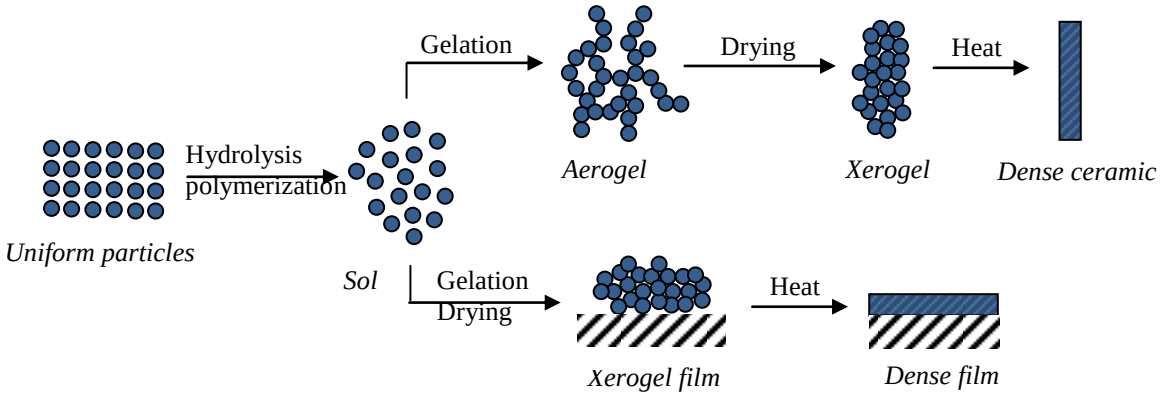

Figure 3.10: The sol-gel process.

During continuous drying phase, water and organic solvent are evaporated from the interconnected pore network and the solid matrix obtained will shrinks gradually. At this time, some of the larger pores are emptied while smaller pores remain wetted by the solvent, producing a porous glasslike structure called xerogel. Xerogel is the desirable end product for sensing application, as dopants can remain physically encapsulated within the porous structure but maintain their ability to interact with external species that diffuse into the matrix.[47]

There are many factors that have a great influence in the quality of the sol-gel formation, such as the choice of precursors, solvent and co-solvent, pressure, temperature, aging and drying conditions. It also reported that the intrinsic properties of sol-gel matrix, porosity, surface area, rigidity and polarity are greatly dependent on the progress of hydrolysis and condensation reactions.[48-49]

The sol-gel used in this studies was a low molecular weight alkoxysilane, named tetramethyl orthosilicate (TMOS), which is a tetrahedral molecule with the formula of $Si(OCH_3)_4$. The hydrolysis of TMOS is an example of sol-gel process which produce methanol as the side product. The reaction proceeds via a series of condensation reactions that convert the TMOS molecule into a mineral-like solid via the formation of Si-O-Si linkages. Rates of this conversion are sensitive to the presence of acids, which serve as catalysts.

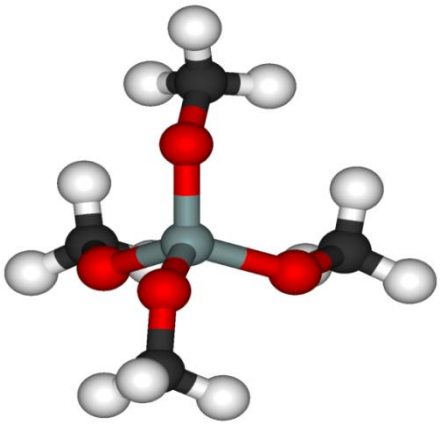

Figure 3.11: The structure of tetramethyl orthosilicate (TMOS).

3.1.4.3 Collagen/Sol-gel Hybrid Complex

Hybrid material is prepared by using collagen solutions as templates. The preparation method was inspired by Carturan *et al*.,[50] that based on the vapour diffusion of a volatile alkoxysilane which hydrolyses at the hydrated surface of the protein, then diffuses and condenses in the bulk template. Collagen solution and TMOS solution are mixed together at the ratio of 1:2 in a tightly closed glass vessel. The mixture was then used as an immobilization matrix to the tested enzyme prior to gelation at the electrode surface.

Preliminary studies indicate that both hydrogen bonding and attractive electrostatic interactions may have an effect on the interaction between the silica and collagen interface. The hybrid material was prepared at neutral pH because it was known that the electrostatic interactions may be effective during the collagen gel silicification, where silicates are negatively charged, and favouring silica deposition on collagen fibre complex. This hybrid material has been reported to have bi-refringence property and the long-range organization is maintained in the solid glassy hybrid.[34]

3.1.5 Carbon Nanotubes

Carbon nanotubes (CNTs) are new and interesting types of carbon derivatives offering unique geometrical, mechanical, electronic and chemical properties.[51]The bonding in carbon nanotubes is sp^2, with each atom joined to three neighbours, as in graphite. The tubes can therefore be considered as rolled-up graphene sheets in the cylindrical form, which is as individual graphite layer as shown in Figure 3.12.

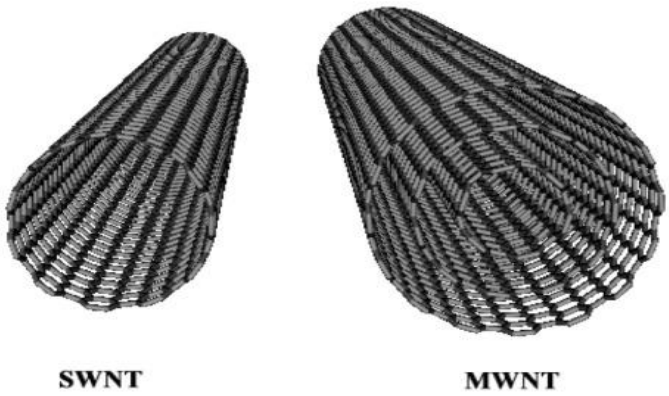

Figure 3.12: Models of SWCNT and MWCNT. Source: ibmc.u-strasbg.fr/ict/vectorisation/

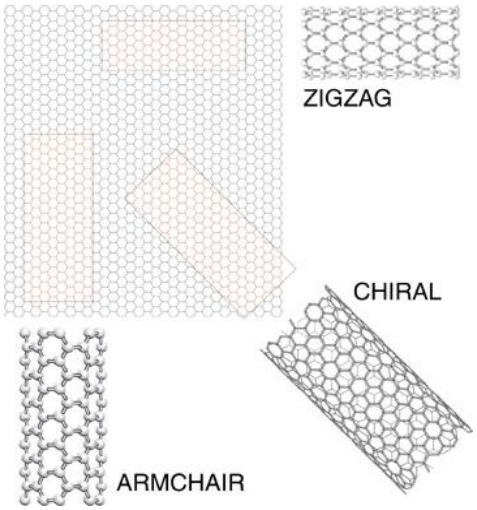

Figure 3.13: 3D model of three types of single wall carbon nanotubes, zig-zag, chiral and armchair. Source:seas.upenn.edu/mse/research/nanotubes

The chirality of CNTs can in turn affects the conductance of the nanotube, its density and its lattice structure. Carbon nanotubes can form three different types, which can be described by the chiral vector (*n*, *m*), where *n* and *m* are integers of the vector equation $R = na_1 + ma_2$. Based on the wrapping angle, ϕ formed between R and the 'Armchair' line, the CNTs can be divided into three types, which are called an armchair nanotube (when $\phi=0^o$), zigzag nanotube (when $\phi=30^o$) and chiral nanotube (when $0^o<\phi<30^o$).[52] Figure 3.13 shows the 3D model of the three types of SWCNTs.

Carbon nanotubes are molecular-scale wires with high electrical conductivity, high chemical stability and extremely high mechanical strength and modulus.[53] Generally, CNTs can be composed of single-walled carbon nanotubes (SWCNTs) or several shells multi-walled carbon nanotubes (MWCNTs). Their electronic properties suggest that CNTs have the ability to promote electron transfer reactions when used in the electrochemical measurement of biosensors.

However, a major barrier for developing the CNTs-modified electrode is the insolubility of CNTs in most solvents. Many efforts have been made to disperse CNTs into suitable solvents such as dimethylformamide (DMF) or concentrated acid solutions to improve their solubility.[54] But these solvents are not compatible with immobilization of biomolecules. Hence for successful application of amperometric biosensors, it is pertinent to explore and develop a simple and reliable method to fabricate electrode surfaces with CNTs and enzymes.

3.2 Techniques used for Analysis of Biosensors

3.2.1 Electrochemical Techniques

The electrochemical techniques used for controlled-potential experiments in biosensors analysis usually required a basic instrumentation which is relatively inexpensive and readily available in market. These include a three electrode cell, a voltammetric analyzer and a plotter. The instruments involve should be located in a place that is free from major electrical interferences, vibrations and drastic fluctuations in temperature.

The three electrode cells usually involve the three electrodes, which are working, reference and counter electrodes that are immersed in the sample solution in a beaker (cell) of 5-50mL volume. The working electrode is the electrode under study where the electron transfer occurs. It is usually made of carbon, mercury or noble metals such as gold and platinum. The selection of working electrode is primarily depends on the redox behaviour of the target analyte and the background current over the potential region required for the measurement.

The reference electrode provides a stable and reproducible potential, against which the potential of the working electrode is compared. While the applied potential is controlled by the reference electrode, the current flows through the solution between the working and counter electrodes is then measured. The counter electrode is always chosen so that it does not produce substances by electrolysis process that will reach the working electrode surface and cause interfering reactions.[55] Figure 3.14 shows the three electrode cells arrangement used in most electrochemical measurement.

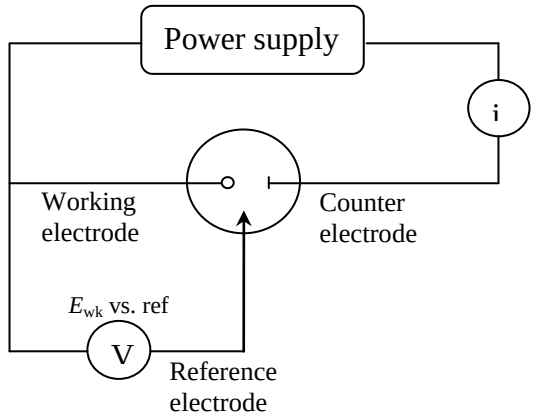

Figure 3.14: The three electrode cell.

Voltammetry is a method that used to study the kinetics processes at the working electrode surface. It is an electrochemical technique in which a faradaic current passing through the electrolysis solution is measured while an appropriate potential is applied to the polarizable or indicator electrode. In voltammetry, the current in an electrochemical cell is measured under conditions of complete concentration polarization in which the rate of oxidation or reduction of the analyte is limited by the rate of mass transfer of the

analyte to the electrode surface. Thus, information about an analyte and their concentration can be obtained by measuring the current as the potential is varied.

Voltammetry is extensively used in various fields of fundamental studies that involve the oxidation and reduction process in various media, the adsorption processes on surfaces and also in study of electron transfer mechanisms at chemically modified electrode surfaces. [56]

3.2.1.1 Cyclic Voltammetry

Cyclic voltammetry is a type of potentiodynamic electrochemical measurement that is widely used for obtaining qualitative information about electrochemical reactions. This technique provides a fast and simple method for initial characterization of a redox-active system and interfacial structure. In addition to providing an estimate of the redox potential, it can also provide information about the rate of electron transfer between the electrode and the analyte, and the stability of the analyte in the electrolyzed oxidation states.

The basic cyclic voltammetry scheme gives the electrode potential follows a linearly ramping potential *vs*. time as shown in Figure 3.15.

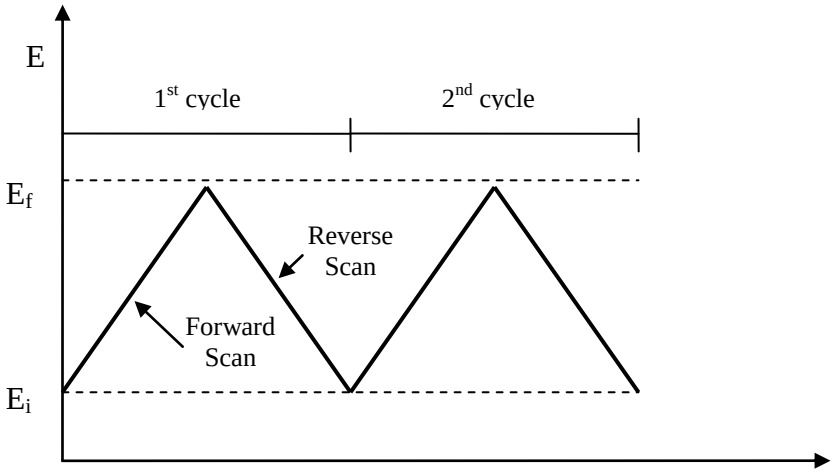

Figure 3.15: Triangular potential waveform for cyclic voltammetry.

As the waveform shows, the forward scan produces a current peak for an analyte that can be reduced through the range of the potential scan. The current will increase as the potential reaches the reduction potential of the analyte, but then falls off as the concentration of the analyte is depleted close to the electrode surface. As the applied potential is reversed, it will reach a potential that will re-oxidize the product formed in the first reduction reaction, and produce a current of reverse polarity from the forward scan. This oxidation peak will usually have a similar shape to the reduction peak. As a result, information about the redox potential and electrochemical reaction rates of the compounds is obtained.

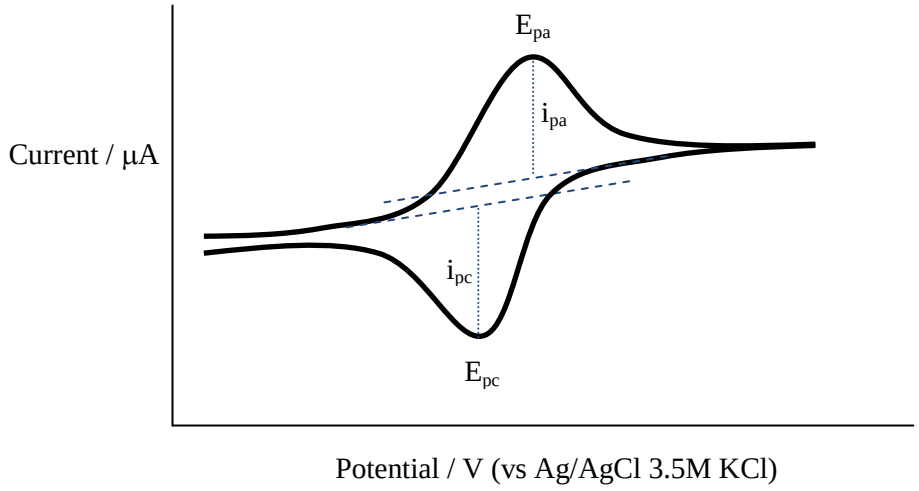

Figure 3.16: Typical cyclic voltammogram for a macrolectrode at a reversible reaction.

In a cyclic voltammetry experiment, the three-electrode method is the most widely used because the electrical potential of reference does not change easily during the measurement. The potential is measured between the reference electrode and the working electrode and the current is measured between the working electrode and the counter electrode. When the potentiostat applied a potential to the system, the Faradaic current response due to the redox reaction of an electroactive species is measured as well as the double layer charge called Capacitive current. This data is then plotted as current (*i*) *vs*. potential (*E*) (Figure 3.16). For instance if the electronic transfer at the surface is fast and the current is limited by the diffusion of species to the electrode

surface, then the current peak will be proportional to the square root of the scan rate. The dependence of the peak current to the scan rate is given by the Randles-Sevcik equation.[57]

$$i_p = 2.69\text{x}10^5 \text{n}^{3/2} D^{1/2} C v^{1/2} A \quad (3.10)$$

where i_p is the peak current, n is the number of electrons involved in redox reaction, D is the diffusion coefficient (cm^2/s), C is the bulk concentration (mol/cm^3), v is the scan rate (V/s) and A is the electrode area (cm^2). For a reversible electron-transfer (Nernstian) process, the following information can be obtained from a cyclic voltammogram using macroelectrodes:

- The cathodic peak current (i_{pc}) is equal to the anodic peak current (i_{pa}), which is $i_{pc} = i_{pa}$
- The peak potentials (E_{pc} and E_{pa}) are independent of the scan rate (v).
- The formal potential (E^o) is centred between E_{pc} and E_{pa}, which is $E^o = (E_{pc} + E_{pa})/2$.
- The peak current (i_p) is proportional to the square root of the scan rate ($v^{1/2}$).
- The separation between the peak potentials (ΔE) is 59/n mV for an n-electron couple. This information can be used to determine the number of electrons transferred, and as a criterion for a Nernstian behaviour.

For an irreversible reaction, the individual peaks are reduced and become widely separated. This system is characterized by a shift of the peak potential with the scan rate to obtain a more drown out cyclic voltammogram. The peak current in irreversible reaction is given by:

$$i_p = (2.99\text{x}10^5)\text{n}(\alpha\text{n})^{1/2} A C D^{1/2} v^{1/2} \quad (3.11)$$

where α is the transfer coefficient. From the Equation 3.11, the peak current is still proportional to the bulk concentration, but will be lower in height depending on the value of α.

Intermediate case for reversible and irreversible reactions can also exist in between of these reactions. It was called the quasi-reversible reaction. For a quarsi-reversible reaction, the current is controlled by both the charge transfer and mass transport.[58] A reverse peak of similar magnitude of the forward peak is observed on the reverse sweep, but the separation of the two peaks is dependent on the scan rate and the peak current is not proportional to the square root of the scan rate (unlike to the case of reversible reaction).

Besides the qualitative information about electrochemical reaction at the electrode obtain from the cyclic voltammogram, multiple cyclic voltammetry experiments can be also used for a variety of applications include:

- The number of electrons transferred in an oxidation or reduction processes.
- The determination of Nernstian (reversible) and non-Nernstian (irreversible) behaviour of redox couple.
- Formal potentials.
- Rate constants.
- Formation constants.
- Reaction mechanisms.
- Diffusion coefficients.

3.2.1.2 Chronoamperometry

The basis of the step techniques is to measure the current response to an applied potential after the capacitive current has died away as the electroactive species near the electrode surface. There are two types of step techniques, which are Chronoamperometry (CA) when the potential is applied and the current response is

measured with time, and Chronocoulometry (CC) when the current is applied to the working electrode and the charge response is measured with time. However in this study, only chronoamperometry technique is used and will be explained in further.

Chronoamperometry is a technique where the electrode potential is stepped to a region where the analyte is electroactive and the decaying current reflects the growth of the diffusion layer with time.[59] Figure 3.17 shows the waveform for a step experiment in which is the basis concept in chronoamperometry experiment. The potential of the working electrode is stepped from a value E_1 at which the oxidized or reduced species is electroinactive (no faradaic reaction occurs), to the value of E_2 where the oxidation or reduction process could occurs. At this time the surface concentration of the electroactive species is effectively zero.

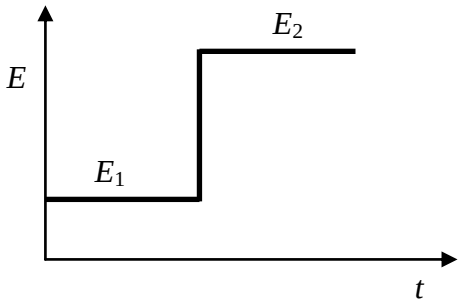

Figure 3.17: The variation of applied potential in a potential step experiment.

At the same time, a large current is detected which falls steadily with time (Figure 3.18(a)). This arises since the mass transport under this condition is controlled by the rate of diffusion of the electroactive species to the electrode surface. The initial process has created an extremely large concentration gradient as well as large flowing current, since there has been little time for any depletion of the electroactive species. We can say that the current produced is proportional to the concentration gradient at the electrode surface. But then, as depletion occurs gradually, the diffusion layer thickness increases and the slope of the concentration profile decline with time. Accordingly, the flowing current decays as time progresses.

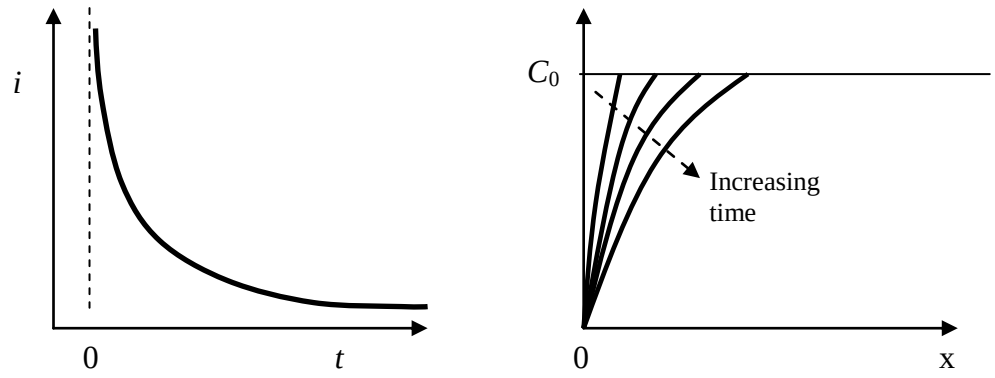

(a) (b)

Figure 3.18: The current response *vs*. time (a), and concentration profile (b) at the electrode in a potential step experiment.

Chronoamperometry is often used to measure the diffusion coefficient of electroactive species or the surface area of the working electrode according to the *Cottrell* equation:

$$i = \mathrm{n}FACD^{1/2}\pi^{-1/2}t^{-1/2} \tag{3.12}$$

where n is the number of electrons involved in redox reaction, *F* is the Faraday constant (96,500 C/mol), *A* is the electrode area (cm^2), *C* is the bulk concentration (mol/cm^3), *D* is the diffusion coefficient (cm^2/s) and *t* is the time (s). However, this *Cottrell* equation only valid for mass transport-limited currents. It also can be applied to study the mechanisms of electrode processes. To this application, a reversal double-step choronoamperometry experiment will need to be performed, where the second step is used to probe the fate of a species generated in the first one.[58]

3.2.1.3 Pulse Voltammetry

Pulse voltammetric techniques are aimed to lower the detection limits of the voltammetric measurements by increasing the ratio between the faradaic and nonfaradaic currents. The most commonly used pulse techniques are the Differential Pulse Voltammetry (DPV) and Square Wave Voltammetry (SWV). The difference

between the various pulse techniques is the excitation waveform and the current sampling region

Differential pulse voltammetry (DPV) is considered as a series of regular potential pulses superimposed on a linearly changing potential are applied to the working electrode at a time just before the end of the drop. The resulting current is measured between the ramped baseline potential and the pulse potential. A digital staircase potential is commonly used as the ramped baseline. DPV sampled the current twice in each pulse period, just before the pulse and at the end of the pulse application, at which when the charging current has decayed (Figure 3.19).

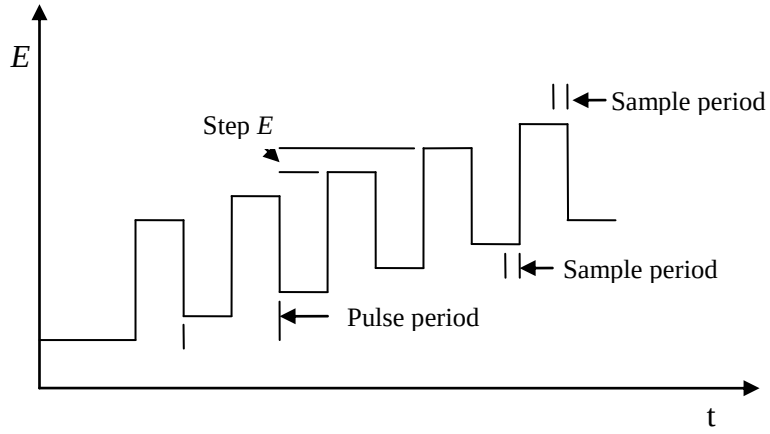

Figure 3.19: The potential waveform of differential pulse voltammetry.

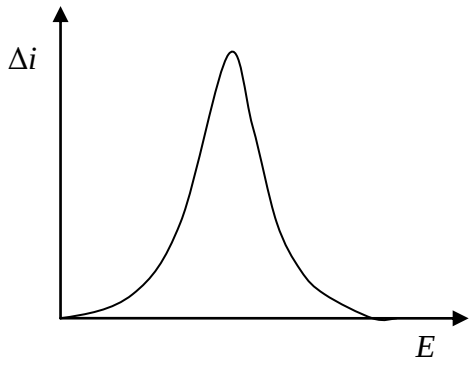

Figure 3.20: Schematic differential pulse voltammogram.

The difference between these two current values [$\Delta i = i(t_2) - i(t_1)$] is recorded and plotted against the applied potential (Figure 3.20). The resulting differential pulse voltammogram consists of current peaks with the height of the peak current which is directly proportional to the concentration of the corresponding analytes as shown in Equation 3.13:

$$i_p = \frac{nFA\,D^{1/2}C}{\sqrt{\pi t}}\left(\frac{1-\sigma}{1+\sigma}\right) \tag{3.13}$$

where $\sigma = \exp\left(\frac{nF}{RT}\frac{\Delta E}{2}\right)$, and ΔE is the pulse amplitude. The maximum value of the quotient (1-σ)/(1+σ), obtained for large pulse amplitudes is unity.[58,60]

By measuring currents at the time when the charging current is decays to approach zero, this nonfaradaic current is thus greatly reduced and the signal-to-noise ratio is larger. Thus, thee greater sensitivity of DPV technique can be attributed by an enhancement of the faradaic current or a decrease in the charging current.

Other pulse technique is the square wave voltammetry. Square wave voltammetry (SWV) is a differential technique that involves a large amplitude in which a waveform composed of a symmetrical square wave, superimposed on a base staircase potential applied to the working electrode.[58] In SWV, the current is sampled twice at the end of each half-cycle. This means, the current measured on the reverse half-cycle (i_r) is subtracted from the current measured on the forward half-cycle (i_f). This difference current ($\Delta i = i_f - i_r$) is displayed as a function of the applied potential.

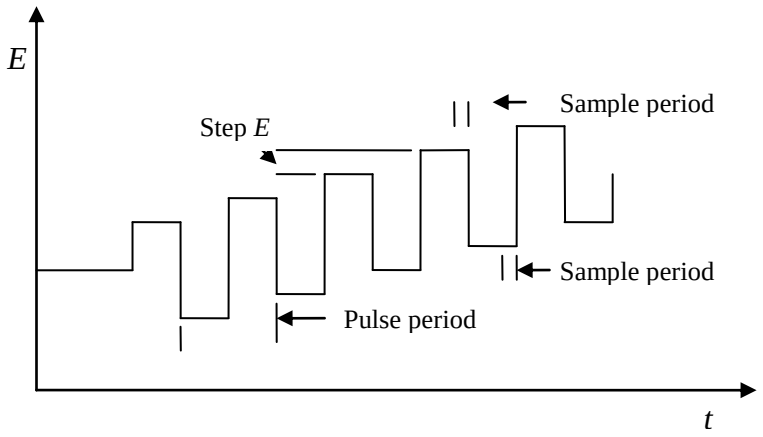

Figure 3.21: The potential waveform of square wave voltammetry.

SWV have the advantages over the other pulse techniques. It is a fast technique that does not interfere with the limiting current which due to dissolved species such as oxygen. Kinetic studies can be done from the rapid scanning capability and the reversal nature of this technique. Furthermore, because of the ability to analyze both the forward and reverse currents as well as the net current, information about reaction reversibility and electrode structure can be obtained easily.

3.2.2 Electrochemical Impedance Spectroscopy

3.2.2.1 The concept of Impedance

Impedance can be understands to have a similar concept of electrical resistance. Electrical resistance is the ability of a circuit element to resist the flow of electrical current. According to Ohm's law, resistance is defined in terms of the ratio between voltage, *E* and current, *I*:

$$R = \frac{E}{I} \tag{3.14}$$

This relationship is only limited to only one circuit element which is the ideal resistor. However, the real world may contain circuit elements that exhibit much more complex behaviour. In this case, we use impedance, which is a measure of the ability of a circuit to resist the flow of electrical current that made of combinations of resistors, capacitors or inductors.

Electrochemical impedance is usually measured by applying an AC potential to an electrochemical cell and measuring the current through the cell. By applying a sinusoidal potential, E_t, to a simple capacitor, we can get the response in an AC current signal.

$$E_t = E_0 \sin(\omega t) \tag{3.15}$$

where E_t is the potential at time t, and E_0 is the maximum potential amplitude. The radial frequency, ω (in radians/s) can be expressed in terms of frequency, f (in Hertz) as follows:

$$\omega = 2\pi f \tag{3.16}$$

In a linear system, the response current signal, i_t is shifted in phase, θ:

$$i_t = i_0 \sin(\omega t + \theta) \tag{3.17}$$

where i_t is the current at time t, i_0 is the maximum current amplitude and θ is the phase different between the applied potential and detected current. Figure 3.22 shows the current response to a sinusoidal potential at the same frequency but shifted in phase.

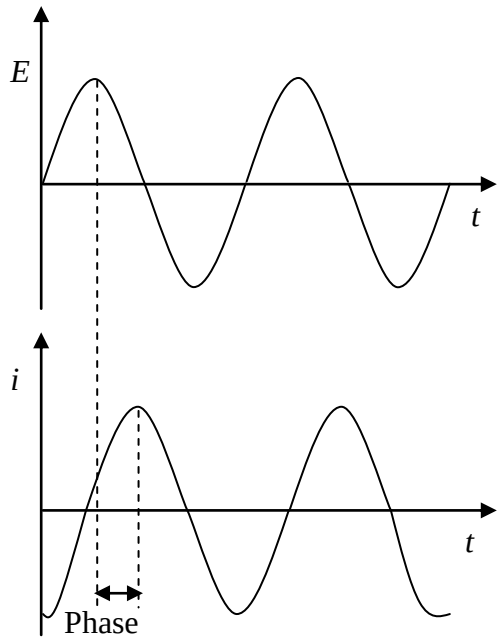

Figure 3.22: Sinusoidal current response to applied potential in a linear system.

The differential capacitance can be related to the current as follows:

$$i = C_d \frac{dE}{dt} = C_d[2\pi f E_0 \cos(2\pi f t)] \tag{3.18}$$

$$i = C_d[2\pi f E_0 \sin(2\pi f t + \pi/2)] \tag{3.19}$$

where $\theta = \pi/2$.

The Ohm's law can be expressed in terms of the impedance, *Z*:

$$Z = \frac{E_t}{i_t} \tag{3.20}$$

And Equation 3.20 can be change by substituted in Equation 3.15 and 3.17:

$$Z = \frac{E_0 \sin(\omega t)}{i_0 \sin(\omega t + \theta)} \tag{3.21}$$

$$Z = Z_0 \frac{\sin(\omega t)}{\sin(\omega t + \theta)} \quad (3.22)$$

Equation 3.22 also can be defined in terms of frequency by substituted in Equation 3.16:

$$Z = Z_0 \frac{\sin(2\pi f t)}{\sin(2\pi f t + \theta)} \quad (3.23)$$

Electrochemical impedance spectroscopy technique uses a three electrodes system of an electrochemical cell that connected to a frequency response analyser, which can generate impedance plots directly. The instrument employs an electronic device to produce the frequencies range from 10^{-2} to 10^{5} Hz.

3.2.2.2 Electrochemical Impedance Spectroscopy

Electrochemical transformations occurring at the electrode-solution interface can be modelled by using components of the electronic equivalent circuit that correspond to the experimental impedance spectra. This interfacial phenomena model is called the Randles and Ershler electronic equivalent-circuit model.[58] The electronic components include in this model is double layer capacitance C_d, the ohmic resistance of the electrolyte solution R_s, the polarization resistance R_p, and the Warburg impedance W, resulting from the diffusion of ions from the bulk solution to the electrode surface. However, when overvoltage, $\eta = 0$, R_p becomes the charge-transfer resistance, R_{ct}.

By deriving from the Ohm's law equation, the impedance of the interface is consists of two parts connected in parallel, a real impedance *Z'* and imaginary impedance, *Z''* as shown in Equation 3.22 and 3.23:

$$Z(\omega) = R_s + \frac{R_p}{1+\omega^2 R_p^2 C_d^2} - \frac{j\omega R_p^2 C_d}{1+\omega^2 R_p^2 C_d^2} \quad (3.22)$$

$$Z(\omega) = Z' + jZ'' \tag{3.23}$$

where $j = \sqrt{-1}$.

Impedance spectroscopy involves the application of a small-amplitude perturbing sinusoidal voltage signal (at a ω frequency) to the electrochemical cell and measuring the current response. The resulting faradaic impedance spectrum can be displayed in different ways as a function of frequency. In a *Nyquist plot*, the plot of imaginary impedance, *Z''* vs real impedance, *Z'* is displayed, while in a *Bode plot*, the absolute value of impedance or phase angle, ϕ are plotted against the frequency (where ϕ is equal to $\tan^{-1}[Z''(\omega) / Z'(\omega)]$).

Nyquist plot contains information about the electrified interface and the electron transfer reaction. This plot commonly includes a semicircle region lying on the axis followed by a straight line. At high frequencies, the frequency dependent term in Equation 3.22 is vanishes, resulting in $Z(\omega) = Z'(\omega) = R_s$, which is an intercept of the $Z'(\omega)$ axis on the high frequency side. For $\omega \rightarrow 0$, Equation 3.22 becomes $Z(\omega) = R_s + R_p$, which is an intercept of the $Z'(\omega)$ axis on the low frequency side.

The diameter of the semicircle is equals to the electron transfer resistance, R_{ct}. At high frequency, the impedance plot shows that the dominant contribution to the total impedance is simply that of the solution resistance. This is due to the double layer that can provide a path of negligible resistance to the current. As the frequency is reduced, this phenomenon is no longer occurs and the effect of R_{ct} in parallel with C_d gives rise to the characteristics of a semicircle plot. Further decrease to lower frequencies, the impedance shows a large increase as modelled by the Warburg impedance due to significant concentration changes induced by the a.c. current which become increasingly difficult to replenish by diffusion as frequencies decreases.[61] The effect of the Warburg element can be important at low frequencies because the mass transport of the electroactive species may limit the electron transfer process. The Warburg impedance can be derived by the following equation:

$$Z(\omega) = R_s + R_p \left[1 + \frac{\lambda}{\sqrt{2}\omega}\right] - R_p^2 \lambda^2 C_d - \frac{j R_p \lambda}{\sqrt{2}\omega} \tag{3.23}$$

and $$\lambda = k_f / \sqrt{D_O} + k_b / \sqrt{D_R}, \quad (3.24)$$

where k_f and k_b are the forward and backward electron transfer rate constants, respectively, and D_O and D_R are the diffusion coefficients for the oxidant O and the reductant R, respectively for the reaction O + $ne^- \leftrightarrow$ R. The frequency-dependent term, $\lambda/\sqrt{2}\omega$ are corresponding to the Warburg impedance. In the presence of the Warburg components, the plot of $Z''(\omega)$ versus $Z'(\omega)$ will have a straight line at the low frequencies with a slope of unity and an intercept of $R_s + R_p - R_p^2 \lambda^2 C_d$.[62]

In *Nyquist plot*, the semicircle region observed at higher frequencies corresponds to the electron transfer-limited process, while the straight line portion at the low frequencies range represents the diffusion-limited process. In the case of very fast electron transfer processes, the impedance spectrum includes only the linear portion, while a very slow electron transfer processes are showed by a large semicircle region.[58]

The *Bode plot* provides the same information as the *Nyquist plot*. The phase shift, ϕ versus log ω plot shows that the impedance responses are resistive primarily at high and low frequencies as indicated by practically no phase shifts, whereas at intermediate frequencies, they are mostly capacitive as their phase shifts get closer to 90°.[62] Thus, both *Nyquist plot* and *Bode plot* can gives all the necessary information regarding the electrode-electrolyte interface and reaction.

The equivalent Randles circuit to represents the electrolytic reactions that taking place at the electrode surface is shown in Figure 3.23.

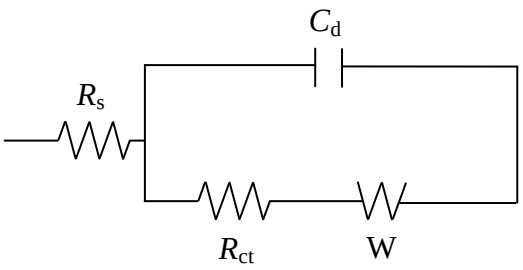

Figure 3.23: The Randles circuit.

3.2.3 Spectroscopic Methods

3.2.3.1 Circular Dichroism

Circular dichroism (CD) is a form of spectroscopy based on the differential absorption of left- and right-handed circularly polarized light. It measures differences in the absorption of left-handed polarized light versus right-handed polarized light which arise due to structural asymmetry. The absence of regular structure results in zero CD intensity, while an ordered structure results in a spectrum which can contain both positive and negative signals.

CD spectra are measured in a spectrophotometer called a CD spectropolarimeter, as shown in Figure 3.24. Selectively exposing sample to right and left circularly polarised light is achieved by passing a beam of plane polarised light through a photoelastic modulator. The differential absorption of right and left circularly polarised light is detected at a photomultiplier and converted into ellipticity, θ which has units of milidegrees. This ellipticity may be converted to units of delta absorbance, ΔA (which is the difference between absorbance of left- and right-handed circularly polarized light) using the following equation:

$$\Delta A = \frac{\theta}{32982} \tag{3.25}$$

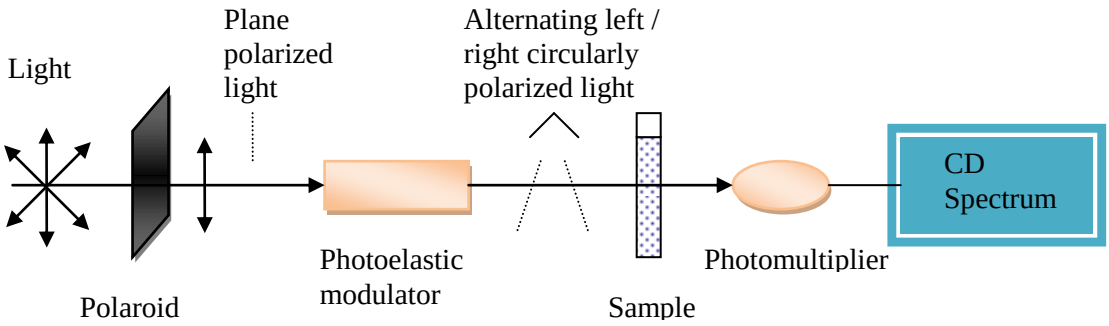

Figure 3.24: Diagram of CD spectropolarimeter.

CD is closely related to the optical rotatory dispersion (ORD) technique.[63] ORD is a consequence of the fact that each enantiomer of an optically active molecule interacts differently with left and right circularly polarised light. Light passing through a chromophore solution may interact with the sample in two main ways. The light may be refracted or delayed on passage through the solution or it may be absorbed. Refraction is quantified by the refractive index, *n*, of the solution while absorption is quantified by the molar extinction coefficient, ε. If the light is plane polarised and the sample is optically active, each enantiomer may interact differently with the left and right circularly polarised components of the light beam.

ORD arises from the fact that there is a specific refractive index for left (n_L) and right (n_R) circularly polarised light, which

$$n_L \neq n_R \tag{3.26}$$

The difference in refractive index at any wavelength may be expressed as Δn. Similarly, optically active samples have distinct molar extinction coefficient for left (ε_L) and right (ε_R) circularly polarised light. This is called circular dichroism, which

$$\varepsilon_L \neq \varepsilon_R \tag{3.27}$$

The difference between ε_L and ε_R may be expressed as $\Delta\varepsilon$. If $\Delta\varepsilon$ or ΔA (where A is the absorbance) are plotted against wavelength (λ), a CD spectrum may be obtained. The CD spectrum of one enantiomer is a mirror image of that of the other and is related to the corresponding ORD spectrum.

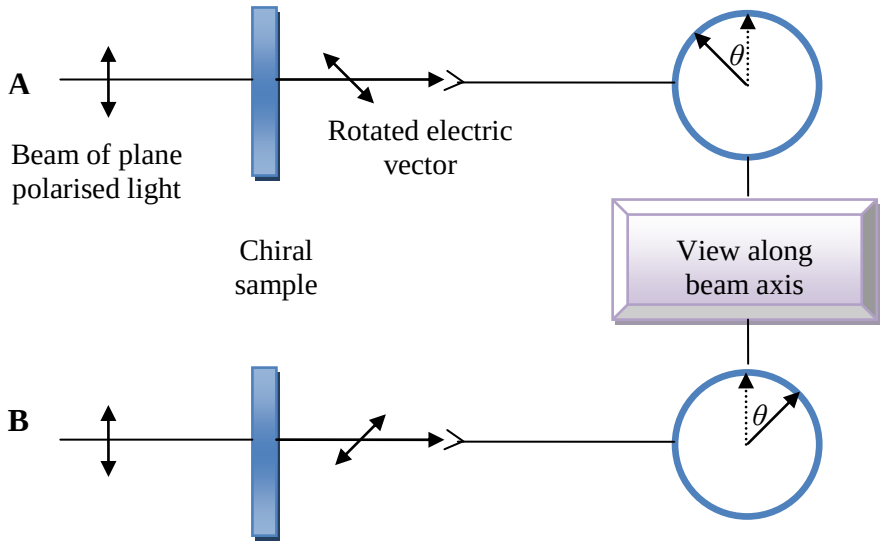

Figure 3.25: Diagram of the principle of Optical Rotatory Dispersion (ORD).

When a beam of plane polarised light is passed through a sample of a single enantiomer (*i.e* a chiral sample), the plane of polarisation is rotated through an angle θ. L-enantiomer (A in Figure 3.25) rotate the plane to the left, whereas D-enantiomer (B in Figure 3.25) rotate the plane to the right. Equal concentrations of an enantiomer rotate the plane of polarization through equal (though opposite) angles, θ, so that a 50:50 mixture does not rotate the plane at all.

3.2.3.2 Fourier Transform Infra-Red Spectroscopy:

Fourier Transform Infra-Red (FTIR) spectroscopy is a technique to identify the types of chemical bonds in a molecule by producing an infrared (IR) absorption spectrum. The IR region of the electromagentic spectrum can be divided into three

regions, the near-, mid- and far-IR. The useful IR region is at the mid-infrared region at about 4000 to 400 cm^{-1} that can be used to study the rotational-vibrational structure of a molecule.

The IR spectroscopy is based on the fact that molecules have specific frequencies at which they rotate or vibrate corresponding to discrete energy levels. Since each frequency absorbed by a molecule corresponds to a specific molecular motion, the kind of motions a molecule can be determined by measuring its IR spectrum. By interpreting those motions, the types of bonding based on the functional groups present in the molecule can be found out.[64]

In FTIR, infra-red radiation is passed through a sample. Some of the infra-red radiation is absorbed by the sample and some of it is transmitted. The resulting spectrum represents the molecular absorption and transmission, creating a molecular fingerprint of the sample. Because of this uniqueness characteristic, FTIR can be utilized to quantitate some components of an unknown mixture. It also can provide various useful information including identification of unknown materials, determination of the quality or consistency of a sample and also the amount of components in a mixture.[65]

The FTIR spectrometry was developed in order to overcome the limitations encountered with dispersive instruments which involve a very slow scanning process. A very simple optical device called an interferometer was employed to measure all of the infrared frequencies simultaneously, rather than individual measurement. Most interferometer employs a beam splitter which takes the incident infrared beam and divides it into two optical beams. Figure 3.26 shows a simple instrumentation in FTIR.

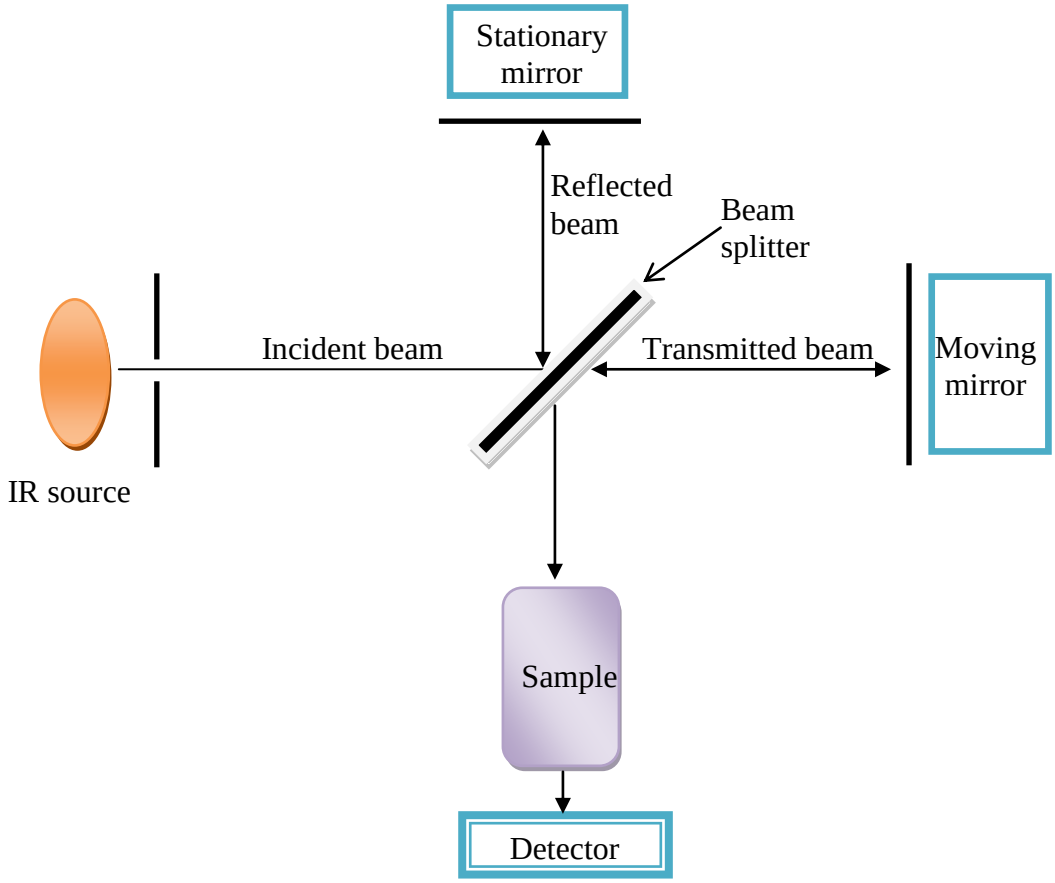

Figure 3.26: The instrumentation in the FTIR spectroscopy.

The basic design of the FTIR instrumentation involves the splitting of the incident beam through a beam splitter, which will transmit half of the light and reflect the other half. The two beams are reflected by the stationary and moving mirrors, respectively and recombine to form a resultant beam. The process is called constructive interference occurs when the two beams are in phase to produce the resultant beam as the sum of the two beams. Otherwise, if both beams are out of phase, the resultant beam is weaker than the sum of the two beams. This process is called destructive interference.[63] These two processes occur depends on the relative positions of the two mirrors at any moment in time. The interference patterns obtained then are added together and analysed by a mathematical tool called the Fourier transform.

FTIR spectroscopy is essentially a technique that based on the interference patterns obtained while measuring absorptions. This technique is applicable to most classes of biomolecules such as lipids, glycolipids and oligosaccharides. It is proved to have a particularly useful in the study of the structure and dynamic properties of

proteins and peptides as each molecule gives a characteristics FTIR spectrum which reflects its chemical structure. Hydrogen bonding between peptide bonds for example underlies secondary structure in proteins.

In the case of collagen, FTIR measurements can also be used for the identification of α-helices, β-sheets and turns secondary structure in collagen. Particularly, the secondary structures in collagen might change due to alterations in pH, ionic strength, pressure, temperature, ligand binding, aggregation and folding. These changes can be detected and analysed by FTIR. The technique has become standard for the study of biomolecules and yields structural information complementary to that available from other methods such as circular dichroism technique.[63]

3.2.3.3 Raman Spectroscopy

Raman spectroscopy is a spectroscopic technique used to study vibrational, rotational and other low-frequency transitions in molecules. This technique is based on inelastic scattering, or Raman scattering of monochromatic light, usually from a laser in the visible, near infrared, or near ultraviolet range. Photons of the laser light are absorbed by the sample and then reemitted. Frequency of the reemitted photons is shifted up or down in comparison with original monochromatic frequency, which is called Raman effect. This shift in energy gives information about the vibrational modes in the system.

The Raman effect occurs when light impinges upon a molecule and interacts with the electron cloud and the bonds of that molecule. For the spontaneous Raman effect (Raman scattering), a photon excites the molecule from the ground state to the energy state. When the molecule relaxes, it emits a photon and returns to a different rotational or vibrational state. The difference in energy between the original state and this new state leads to a shift in the emitted photon's frequency away from the excitation wavelength.

While IR is an absorption spectroscopy, which measures the transmitted light, Raman spectroscopy is a technique that measures the scattered light (Figure 3.27). There are three types of scattered lights, which are Rayleigh scattering, Stokes

scattering and Anti-Stokes scattering. Rayleigh scattering is an elastic scattering where there is no energy exchange between the incident light and the molecule. Stokes scattering happens when there is an energy absorption from the incident light. If the final vibrational state of the molecule is more energetic than the initial state, then the emitted photon will be shifted to a lower frequency in order for the total energy of the system to remain balanced. This shift in frequency is assigned as a Stokes shift. If the final vibrational state is less energetic that the initial state, then the emitted photon will be shifted to a higher frequency, and this is assigned as an Anti-Stokes shift. Stokes and Anti-Stokes scattering are called Raman scattering, which can provide the vibration/rotation information.

About 99.999% of all incident photons in spontaneous Raman undergo elastic Rayleigh scattering. This type of signal is useless for practical purposes of molecular characterization. Only about 0.001% of the incident light produces inelastic Raman signal. Spontaneous Raman scattering is very weak and special measures should be taken to distinguish it from the predominant Rayleigh scattering. Instruments such as notch filter, tunable filter, laser stop apertures, double and triple spectrometric systems are used to reduce Rayleigh scattering and obtain high-quality Raman spectra.

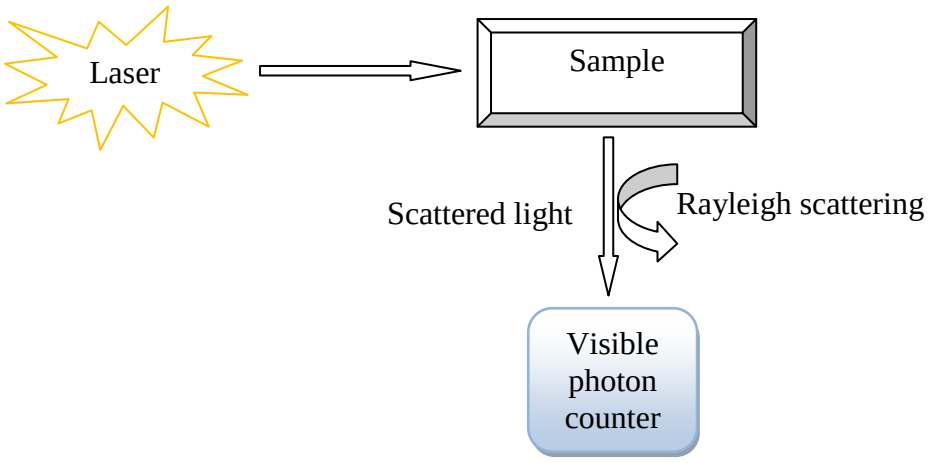

Figure 3.27: Schematic diagram for Raman spectroscopy.

3.2.4 Electron Microscopic Techniques

The electron microscopic technique is an imaging technique that uses a particle beam of electrons to illuminate the specimen to create a magnified image of it. The microscope has a greater magnification than the optical microscope because it uses electrons that have wavelengths about 100,000 times shorter than the visible light. Thus, the electron microscope can achieve magnifications of up to 1,000,000x, whereas light microscopes are limited to 1000x magnification.

The electron microscope uses electrostatic and electromagnetic lenses to control the electron beam and focus it to form an image. It can be classified into two major groups; the first one is transmission electron microscope (TEM), which are used to explore the internal structure of the specimen and second one is scanning electron microscope (SEM), which are mainly used to study surface morphology.

3.2.4.1 Transmission Electron Microscopy

Transmission electron microscopy (TEM) is a microscopy technique in which a beam of electrons is transmitted through an ultra thin specimen, interacting with the specimen as it passes through it. An image is formed from the electrons transmitted through the specimen, magnified and focused by an objective lens and appears on an imaging screen.

The TEM uses a high energy electron beam transmitted through a very thin sample to image and analyze the microstructure of materials with atomic scale resolution. The electrons are focused with electromagnetic lenses and the image is observed on a fluorescent screen, or recorded on film or digital camera. The electrons are accelerated at several hundred kV, giving wavelengths much smaller than that of light, *i.e* 200 kV electrons have a wavelength of 0.025 Å. However, the resolution of the the electron microscope is limited by aberrations inherent in electromagnetic lenses; to about 1-2 Å. Figure 3.28 shows the typical diagram of TEM instrumentation.

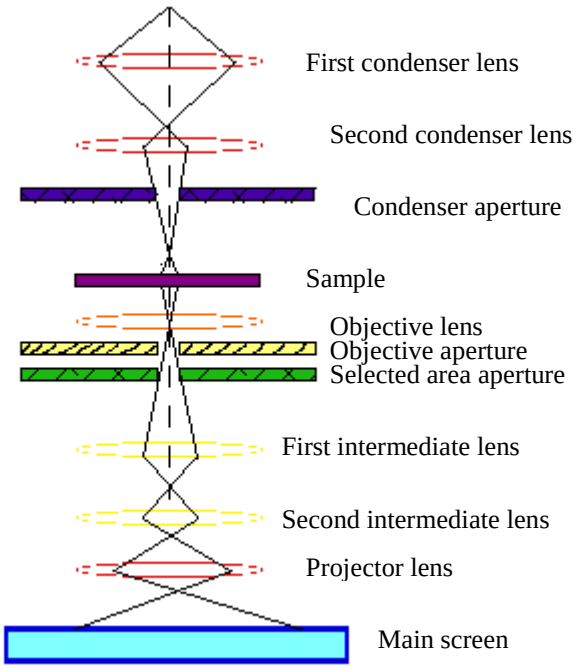

Figure 3.28: Typical diagram for TEM system.

The TEM is used to characterize the microstructure of materials with very high spatial resolution. Information about the morphology, crystal structure and defects, crystal phases and composition, and magnetic microstructure can be obtained by a combination of electron-optical imaging (2.4 Å point resolution), electron diffraction, and small probe (20 Å) capabilities. The trade-off for this diverse range of structural information and high resolution is the challenge of producing very thin samples for electron transmission.

3.2.4.2 Scanning Electron Microscopy

The Scanning Electron Microscopy (SEM) is primarily used to study the surface topography of solid samples. It is the usual method for direct and high-resolution imaging of solid surface. In SEM, a finely focused electron probe is used to scan all over the surface of a bulk specimen and transforms the geometrical arrangement point-by-point into a chronological sequence. The specimen structure is then reconstructed as

an image on the screen of a monitor and collected by using detector and amplifier. The image magnification is the ratio of the scanned monitor range to the scanned sample range. The principle of SEM can be represents in the Figure 3.29:

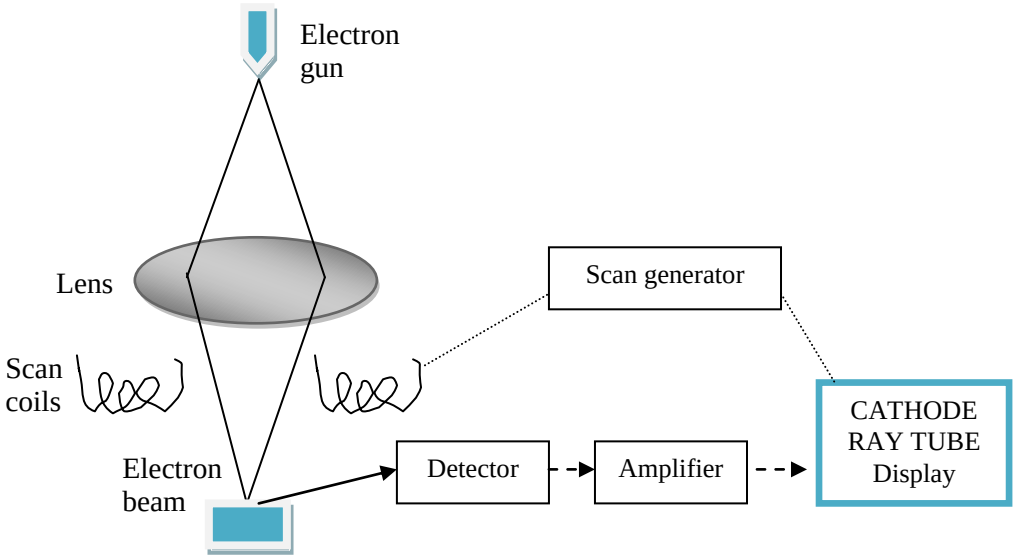

Figure 3.29: The components in a scanning electron microscope, SEM.

A fine beam of electrons passing through an evacuated column is focused by electromagnetic lenses onto the specimen surface. The beam is scanned across the surface of the specimen in synchronism with the spot of the cathode ray tube (CRT) display screen. A detector monitors the intensity of a chosen secondary signal from the specimen and the brightness of the CRT spot is controlled by an amplified version of the detected signal.[66] The signal is controls the brightness of individual positions on the monitor screen, related to these of the original points on the sample surface. The images produce then are readily interpreted because they contain light and shade in much the same way as images which are familiar to the eyes.

The SEM imaging has to be done in a vacuum, in order to achieve proper creation, control and detection of the electron beam. The surface of the samples must be very conductive so that a good contrast and resolution images is obtained. Generally, the image resolution of an SEM is between 1.5 to 3 nm, which is approximately two

orders of magnitude better than optical microscopes and an order of magnitude less than that of TEM.[67] However, because the SEM image relies on surface processes rather than transmission, it is able to image bulk samples up to many centimetres in size and has a great depth of field, and so can produce images that are good representations of the three-dimensional shape of the specimen.

One of the advantages of SEM is the high depth of field, resulting in an apparently three-dimensional image. This is caused by the low irradiation aperture and it allows the investigation of rough material surfaces.[68] However, this technique also has several disadvantages, that it can only view the surface rather than through the specimen. In addition, the SEM operates under high vacuum and therefore is unsuitable imaging of materials in liquid forms without suitable drying methods.

3.2.4.3 Environmental Scanning Electron Microscopy

SEM technique is not suitable for imaging materials in liquid form. Due to this limitation, the Environmental Scanning Electron Microscopy (ESEM) is used to overcome this problem. It employs a scanned electron beam and electromagnetic lenses to focus and direct the beam on the specimen surface in an identical way as SEM. Although ESEM has lower resolution compared to SEM, it can be used for imaging of specimens in liquid or solution form because it allows hydrated samples to view in a low-pressure gaseous, wet environment. Another advantage of using the ESEM is that it can used to image non-conductive materials by coating the samples with a very thin layer of conductive material in a sputtering machine. As a result, specimens can be examined more easily and faster without needs to complex and time consuming preparation methods of modifying the natural surface, as of SEM.

3.3 Experimental

3.3.1 Materials and Reagents

Glassy carbon electrode was obtained from Bioanalytical Systems (Warwickshire, UK). Ferrocene (98%), 1,2-dichloroethane, N,N-dimethylformamide, acetone, ethanol, D- and L-glucose, D- and L-lactate, D-glucose oxidase (β-D-glucose:oxygen 1-oxidoreductase 1.1.3.4 from *Aspergillus niger* type II-S; 39,800 unit g^{-1}), L-lactate oxidase (from *Pediococcus sp*.; 20 units mg^{-1}), graphite carbon (GC), collagen type I (from rat tail), tetramethyl orthosilicate (TMOS), KCl, K_2HPO_4 and KH_2PO_4 were purchased from Sigma Aldrich, UK. The single-wall carbon nanotubes (SWCNTs), double-wall carbon nanotubes (DWCNTs) and multi-wall carbon nanotubes (MWCNTs) were purchased from Shenzhen Nanotech. Port. Co., Ltd. (Shenzhen, China), while spherical porous carbon (SPC) was obtained from MASTcarbon (Guildford, UK). The purity of the carbon samples were analyzed by Inductively Coupled Plasma-Optical Emission Spectrometry (ICP-OES) and Raman Spectroscopy (LabRam 300 (Horiba Jobin Yvon Ltd. UK)) using the LabSpec 4.14 programme.

Ferrocene (0.1 M) was prepared directly in 1,2-dichloroethane (1,2-DCE). Phosphate buffer solution, 0.1 M made from K_2HPO_4 and KH_2PO_4 (in KCl) and adjusted the pH to 7 was employed as supporting electrolyte. Deionized water was used throughout the experiments. The solutions of enzymes, (GOx and LOx) and analytes (D- and L-glucose, and D- and L-lactate), respectively were also prepared in 0.1 mM PBS (pH 7) to obtain 1 mg/mL enzyme or analyte stock solutions. All stock solutions were stored at 4 ºC for 24 hours before use. Collagen type I (BioReagent grade) was solubilised in 0.5 mM acetic acid to obtain a 1mg/mL stock solution. The acidic solution of collagen (pH 2.5) was maintained as to prevent fibrillogenesis.[69] The sol-gel stock solution was prepared by mixing 14.9 ml of TMOS, 3.39 ml deionised water and 0.22 ml HCl (0.04 mol dm^{-1} aqueous) in a glass vial. The vial was sonicated in an ultrasonic bath containing ice for 15-20 min until the mixture turned homogeneous. The sol was then diluted (1:4) in water. It was stored in the fridge at 4 ºC and can be used for up to 2 weeks before it solidified to gel.

3.3.2 Methodology

All electrochemical measurements were carried out with a conventional three-electrode system. The working electrodes were the modified glassy carbon electrode and a platinum plate was used as a counter electrode. An Ag/AgCl (3.5 M KCl) reference electrode was used for all measurements, and all the potentials were reported in this thesis are against the potential of this reference electrode (potential 222 mV versus standard hydrogen electrode). The electrochemical measurements were performed using the potentiostat model 263 (EG&G Princeton Applied Research, USA). For amperometric measurements, the analyte solution was stirred for 2 seconds for proper mixing before measurement without stirring. The cell was places in a Faraday cage to eliminate external interference. All experimental solutions were deoxygenated by bubbling highly pure nitrogen for 15 min and maintained under nitrogen atmosphere during measurements. All electrochemical measurements were done in triplicate.

Electrochemical impedance measurements were carried out in the same electrochemical cell with a PC-controlled Solartron SI 1260 Impedance/Gain-Phase Analyzer (Solartron Analytical, UK) using Zplot 3.1c software. Sinusoidal voltage pertubation amplitude 10 mV was applied, scanning from 10 kHz to 0.1 Hz. Fitting to equivalent circuits was performed with Zview 3.1c software.

The conformation of the collagen and its interaction with enzymes and analytes was verified by recording circular dichroism (CD) spectra. CD measurements and titrations were performed using a spectropolarimeter model J-810 Jasco (Japan). The solution was scanned at the wavelength range from 190 to 250 nm at 25 ºC at the scan rate of 10 nm/min, data pitch of 0.5 nm for 10 scans, using 0.1 cm path-length quartz cells. CD spectra were recorded for pure samples and their mixtures after substraction of buffer spectrum to account for the baseline. Titrations of collagen sample were done by setting up the ratio of collagen to enzymes from 1:0 to 1:5 followed by stepwise addition of the analytes for the ratio from 1:5:0 to 1:5:6 (collagen:enzymes:D- or L-analytes). The difference in ellipticity values obtained from the mixture of collagen/enzyme/D-analyte and collagen/enzyme/L-analyte were calculated.

Fourier transform infra-red (FTIR) spectra were collected on a Thermo Nicolet Nexus 670 FTIR spectrophotometer (Nexus Instrument Corp., USA) equipped with a liquid nitrogen-cooled mercury-cadmium-telluride (MCT) detector and a KBr beam splitter. One hundred scans were acquired with a spectral resolution of 4 cm^{-1}. To obtain more detailed information about the secondary structure of macromolecules, the curve fitting of the overlapping components under the amide I counter bands were carried out. The curve fitting was performed with origin pro 7.5 (Origin-Lab, USA), using a linear baseline and Gaussian multipeak-fit components.

Transmission electron microscopy (TEM) images of collagen samples (staining with uranyl acetate) were obtained by using H-7600 TEM (Hitachi, USA), while scanning electron microscopy (SEM) was carried out by using Ultra-high resolution S-5200 SEM (Hitachi, USA). Thermogravimetry analysis (TGA) was performed in air by using thermogravimetric analyzer Pyris 1 TGA (Perkin Elmer, USA), while Raman spectra were recorded using a Jobin Yvon Horiba LabRam spectrometer in a back scattered confocal configuration using He/Ne laser excitation (632.8 nm, 1.96 eV).

3.3.2.1 Preparation of the Modified GC Electrodes

The glassy carbon electrodes (GCE, 3 mm diameter) were polished before each experiment with 0.05 μm alumina slurry (Bioanalytical systems, Inc., UK), rinsed thoroughly with doubly distilled water and then sonicated in water bath before allowed to dry at room temperature. For the preparation of collagen-silica hybrid complex, 1 mL of the collagen solution and 2 mL of TMOS were mixed in a tightly closed 30 mL glass vial and the apparatus kept at 4 °C for 6 days.

The clean GCE was modified by applying 6 μL ferrocene (Fc) on the electrode surface, let it dry for 1 minute before it washed thoroughly to remove the excess ferrocene. The enzyme solutions were mixed with collagen suspension or collagen-silica complex (2:3) as the immobilization matrices in ultrasonication for 15 minutes at 4 ºC. 10 μL of enzyme/collagen suspension and enzyme/collagen-silica hybrid complex were then deposited separately on the Fc-modified GCE surface to obtain the Fc/GOx or LOx/collagen and Fc/GOx or LOx/collagen-silica hybrid modified electrodes. The

enzyme modified electrodes were allowed to dry at room temperature to obtain the gel film. Prior to electrochemical experiments, the electrode was rinsed thoroughly with doubly distilled water and kept in 0.1 M phosphate buffer solution (PBS) pH 7 at 4 °C.

For the preparation of the CNTs-based modified electrodes, the CNTs suspension was firstly prepared by dispersing 0.1, 0.5 or 2 mg (to obtain different concentrations) of both SWCNTs and MWCNTs, respectively in 1 mL Fc solution (0.1 M in 1,2-dichloroethane) with sufficient ultrasonication for about 1 hour. The suspension was allowed to stabilize for 24 hours at room temperature. The solvent was then allowed to dry to obtain the modified CNTs. The Fc-modified CNTs were dispersed in collagen and collagen-silica hybrid complex, respectively and allowed to mix by ultrasonication for 1 hour and allowed to stabilize for 24 hours.

7.5 μL of Fc/CNTs/collagen suspension or Fc/CNTs/collagen-silica hybrid complex and 7.5 μL of GOx solution were deposited on GC electrode surface to obtain the GOx/Fc/CNTs/collagen and GOx/Fc/CNTs/collagen-silica hybrid modified electrodes. The modified electrodes were allowed to dry at room temperature to obtain the gel film. Prior to electrochemical experiments, the electrode was rinsed thoroughly with doubly distilled water and kept in 0.1 M phosphate buffer solution (PBS) pH 7 at 4 °C.

References

(1) Battaglini, F.; Calvo, E. J. *J. Chem. Soc.-Faraday Trans.* **1994**, *90*, 987.
(2) Adeloju, S. B.; Moline, A. N. *Biosens. Bioelectron.* **2001**, *16*, 133.
(3) Calvo, E. J.; Danilowicz, C.; Diaz, L. *J. Chem. Soc.-Faraday Trans.* **1993**, *89*, 377.
(4) Sakslund, H.; Wang, J.; Lu, F.; Hammerich, O. *J. Electroanal. Chem.* **1995**, *397*, 149.
(5) Dicks, J. M.; Hattori, S.; Karube, I.; Turner, A. P. F.; Yokozawa, T. *Ann. Biol. Clin.* **1989**, *47*, 607.
(6) Hodak, J.; Etchenique, R.; Calvo, E. J.; Singhal, K.; Bartlett, P. N. *Langmuir*. **1997**, *13*, 2708.
(7) Yonzon, C. R.; Haynes, C. L.; Zhang, X. Y.; Walsh, J. T.; Van Duyne, R. P. *Anal. Chem.* **2004**, *76*, 78.
(8) Wilson, R.; Turner, A. P. F. *Biosens. Bioelectron.* **1992**, *7*, 165.
(9) Wohlfahrt, G.; Witt, S.; Hendle, J.; Schomburg, D.; Kalisz, H. M.; Hecht, H. J. *Acta Crystallogr. Sect. D-Biol. Crystallogr.* **1999**, *55*, 969.

(10) Katz, E., Shipway, A.N., and Willner, I. *Bioelectrochemistry*; Wiley-VCH: Weinheim, Germany, 2002; Vol. 9.
(11) Hecht, H. J.; Schomburg, D.; Kalisz, H.; Schmid, R. D. *Biosens. Bioelectron.* **1993**, *8*, 197.
(12) Bean, R. C.; Hassid, W. Z. *J. Biol. Chem.* **1956**, *218*, 425.
(13) Bean, R. C.; Porter, G. G.; Steinber.Bm *J. Biol. Chem.* **1961**, *236*, 1235.
(14) Dowling, J. H.; Levine, H. B. *J. Bacteriol.* **1956**, *72*, 555.
(15) Pazur, J. H.; Kleppe, K.; Cepure, A. *Arch. Biochem. Biophys.* **1965**, *111*, 351.
(16) Tsuge, H.; Natsuaki, O.; Ohashi, K. *J. Biochem.* **1975**, *78*, 835.
(17) Hayashi, S.; Nakamura, S. *Biochim. Biophys. Acta.* **1981**, *657*, 40.
(18) Hecht, H. J.; Kalisz, H. M.; Hendle, J.; Schmid, R. D.; Schomburg, D. *J. Mol. Biol.* **1993**, *229*, 153.
(19) Takegawa, K.; Fujiwara, K.; Iwahara, S.; Yamamoto, K.; Tochikura, T. *Agricultural and Biological Chemistry*. **1991**, *55*, 883.
(20) Swoboda, B. E. P.; Massey, V. *J. Biol. Chem.* **1965**, *240*, 2209.
(21) Voet, J. G.; Andersen, E. C. *Arch. Biochem. Biophys.* **1984**, *233*, 88.
(22) Marcus, R. A.; Sutin, N. *Biochimica Et Biophysica Acta.* **1985**, *811*, 265.
(23) Leiros, I.; Wang, E.; Rasmussen, T.; Oksanen, E.; Repo, H.; Petersen, S. B.; Heikinheimo, P.; Hough, E. *Acta Crystallogr. F-Struct. Biol. Cryst. Commun.* **2006**, *62*, 1185.
(24) Furuichi, M.; Suzuki, N.; Dhakshnamoorhty, B.; Minagawa, H.; Yamagishi, R.; Watanabe, Y.; Goto, Y.; Kaneko, H.; Yoshida, Y.; Yagi, H.; Waga, I.; Kumar, P. K. R.; Mizuno, H. *J. Mol. Biol.* **2008**, *378*, 436.
(25) Umena, Y.; Yorita, K.; Matsuoka, T.; Kita, A.; Fukui, K.; Morimoto, Y. *Biochem. Biophys. Res. Commun.* **2006**, *350*, 249.
(26) Macheroux, P.; Mulrooney, S. B.; Williams, C. H.; Massey, V. *Biochimica Et Biophysica Acta.* **1992**, *1132*, 11.
(27) Kaifer, A., and Gomez-Kaifer, M. *Supramolecular Electrochemistry*; Wiley-VCH: USA, 2001.
(28) Cass, A. E. G.; Davis, G.; Francis, G. D.; Hill, H. A. O.; Aston, W. J.; Higgins, I. J.; Plotkin, E. V.; Scott, L. D. L.; Turner, A. P. F. *Anal. Chem.* **1984**, *56*, 667.
(29) Godet, C.; Boujtita, M.; El Murr, N. *New J. Chem.* **1999**, *23*, 795.
(30) Iwasawa, K.; Eguchi, M.; Uno, K.; Yabuki, S. *Electrochemistry.* **2008**, *76*, 552.
(31) Kobayashi, Y.; Hoshi, T.; Anzai, J. *Chem. Pharm. Bull.* **2001**, *49*, 755.
(32) Devlin, T. M. *Textbook of Biochemistry with Clinical Correlations*; 5th edition ed.; John Wiley & Sons Inc.: New York, 2002.
(33) Zong, S. Z.; Cao, Y.; Zhou, Y. M.; Ju, H. X. *Anal. Chim. Acta.* **2007**, *582*, 361.
(34) Eglin, D.; Mosser, G.; Giraud-Guille, M. M.; Livage, J.; Coradin, T. *Soft Matter.* **2005**, *1*, 129.
(35) Bhattacharyya, S.; Salvetat, J. P.; Saboungi, M. L. *Appl. Phys. Lett.* **2006**, *88*.
(36) Bhattacharyya, S.; Salvetat, J. P.; Roy, D.; Heresanu, V.; Launois, P.; Saboungi, M. L. *Chem. Commun.* **2007**, 4248.
(37) Stefan, R.-I., van Staden, J-F., and Aboul-Enein, H.Y. *Electrochemical Sensors in Bioanalysis*; Marcel Dekker, Inc.: New York, 2001.
(38) Flora, K. K.; Brennan, J. D. *J. Phys. Chem. B.* **2001**, *105*, 12003.
(39) Flora, K. K.; Brennan, J. D. *Chem. Mat.* **2001**, *13*, 4170.
(40) Maccraith, B. D.; McDonagh, C. M.; Okeeffe, G.; McEvoy, A. K.; Butler, T.; Sheridan, F. R. *Sens. Actuator B-Chem.* **1995**, *29*, 51.
(41) Hench, L. L.; West, J. K. *Chem. Rev.* **1990**, *90*, 33.
(42) Gupta, R.; Chaudhury, N. K. *Biosens. Bioelectron.* **2007**, *22*, 2387.

(43) Laughlin, J. B.; Sarquis, J. L.; Jones, V. M.; Cox, J. A. *Journal of Chemical Education.* **2000**, *77*, 77.
(44) Singh, S.; Singhal, R.; Malhotra, B. D. *Anal. Chim. Acta.* **2007**, *582*, 335.
(45) Brinker, C. J., and Scherer, G.W. *Sol-Gel Science: The Physics and Chemistry of Sol-Gel Processing*; Academic Press: San Diego, California, 1990.
(46) Aurobind, S. V.; Amirthalingam, K. P.; Gomathi, H. *Advances in Colloid and Interface Science.* **2006**, *121*, 1.
(47) Rabinovich, L.; Lev, O. *Electroanalysis.* **2001**, *13*, 265.
(48) Lev, O.; Tsionsky, M.; Rabinovich, L.; Glezer, V.; Sampath, S.; Pankratov, I.; Gun, J. *Anal. Chem.* **1995**, *67*, A22.
(49) Winter, R.; Hua, D. W.; Song, X.; Mantulin, W.; Jonas, J. *J. Phys. Chem.* **1990**, *94*, 2706.
(50) Carturan, G.; Dal Toso, R.; Boninsegna, S.; Dal Monte, R. *J. Mater. Chem.* **2004**, *14*, 2087.
(51) Iijima, S. *Nature***1991**, *354*, 56.
(52) Wilder, J. W. G., Venema, L.C., Rinzler, A.G., Smalley, R.E., and Dekker, C. *Nature.* **1998**, *391*, 59.
(53) Wu, K. B.; Ji, X. B.; Fei, J. J.; Hu, S. S. *Nanotechnology.* **2004**, *15*, 287.
(54) Song, Z.; Huang, J. D.; Wu, B. Y.; Shi, H. B.; Anzai, J. I.; Chen, Q. *Sens. Actuator B-Chem.* **2006**, *115*, 626.
(55) Bard, A. J., and Faulkner, L.R. *Electrochemical Methods: Fundamentals and Applications*; 2nd edition ed.; John Wiley & Sons Inc.: USA, 2001.
(56) Skoog, D. A., West, D.M., and Holler, J.F. *Fundamentals of Analytical Chemistry*; 8th edition ed.; Brooks/Cole, 2003.
(57) Bard, A. J., and Faulkner, L.R. *Electrochemical Methods: Fundamentals and Applications*; 2nd edition ed.; John Wiley & Sons Inc., 2000.
(58) Wang, J. *Analytical Electrochemistry*; 3rd edition ed.; John Wiley & Sons, Inc.: Hoboken, New Jersey., 2006.
(59) Edmonds, T. E. *Chemical Sensors*; Blackie and Sons, 1988.
(60) Parry, E. P.; Osteryoung, R. A. *Anal. Chem.* **1964**, *36*, 1366.
(61) Fisher, A. C. *Electrode Dynamics*; Oxford University Press: Oxford, 1996.
(62) Park, S. M.; Yoo, J. S. *Anal. Chem.* **2003**, *75*, 455A.
(63) Sheehan, D. *Physical Biochemistry: Principles and Applications*; John Wiley & Sons Ltd.: England, 2000.
(64) McMurry, J. *Organic Chemistry*; 6th edition ed.; Thomson Learning, Inc.: USA, 2004.
(65) Thermo Nicolet: 2001.
(66) Chescoe, D., and Goodhew, P.J. *The Operation of Transmission and Scanning Electron Mixroscopes*; Oxford University Press: Oxford, England, 1990.
(67) Goodhew, P. J., Humphreys, F.J., and Beanland, R. *Electron Microscopy And Analysis* 3rd edition ed.; Taylor & Francis: London & New York, 2001.
(68) Wetzig, K. In *In Situ Scanning Electron Microscopy in Materials Research*; Wetzig, K., and Schulze, D., Ed.; Akademie Verlag GmbH: Berlin, Germany, 1995.
(69) Deniset-Besseau, A.; Duboisset, J.; Benichou, E.; Hache, F.; Brevet, P. F.; Schanne-Klein, M. C. *J. Phys. Chem. B.* **2009**, *113*, 13437.
(70) Wu, M. Z.; Yao, L. Z.; Cai, W. L.; Jiang, G. W.; Li, X. G.; Yao, Z. *J. Mater. Sci. Technol.* **2004**, *20*, 11.
(71) Greene, L. E.; Law, M.; Goldberger, J.; Kim, F.; Johnson, J. C.; Zhang, Y. F.; Saykally, R. J.; Yang, P. D. *Angew. Chem.-Int. Edit.* **2003**, *42*, 3031.

CHAPTER 4

ELECTROCHEMICAL GLUCOSE BIOSENSORS

4.1 Introduction to Electrochemical Glucose Biosensors

The concept of an enzyme biosensing electrode involves placement of an enzyme in close proximity to an electrode surface. The enzyme involved here must have the ability to catalyze a reaction involving the analyte with the consumption of an electroactive reactant and/or the production of an electroactive product. The depletion or production process is then monitored amperometrically and gives a direct measurement of the analyte concentration.

Based on this concept, the first enzyme electrode was achieved with glucose sensor. The first glucose biosensors were developed by Clark and Lyons in 1962 and implemented by Updike and Hicks, who then introduced the term enzyme electrode.[1-2] Typically, a thin layer of oxireductase enzyme, such as glucose oxidase (GO_x), is entrapped over an oxygen electrode via a semipermeable dialysis membrane. The enzyme was selectively oxidized the analyte by the reduction of O_2 to H_2O_2. The consumption of oxygen or the formation of hydrogen peroxide were then measured at a platinum electrode by the enzyme-catalyzed reactions.[3]

Measurements were made based on the monitoring of the oxygen consumed by the enzyme-catalyzed reaction:

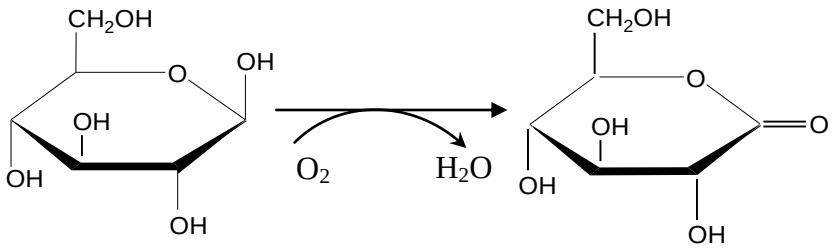

(4.1)

$$O_2 + 4H^+ + 4e^- \rightarrow 2H_2O \qquad (4.2)$$

or $$H_2O_2 \rightarrow O_2 + 2H^+ + 2e^- \qquad (4.3)$$

Amperometric biosensors have been divided into three generations as sketched in Figure 4.1.

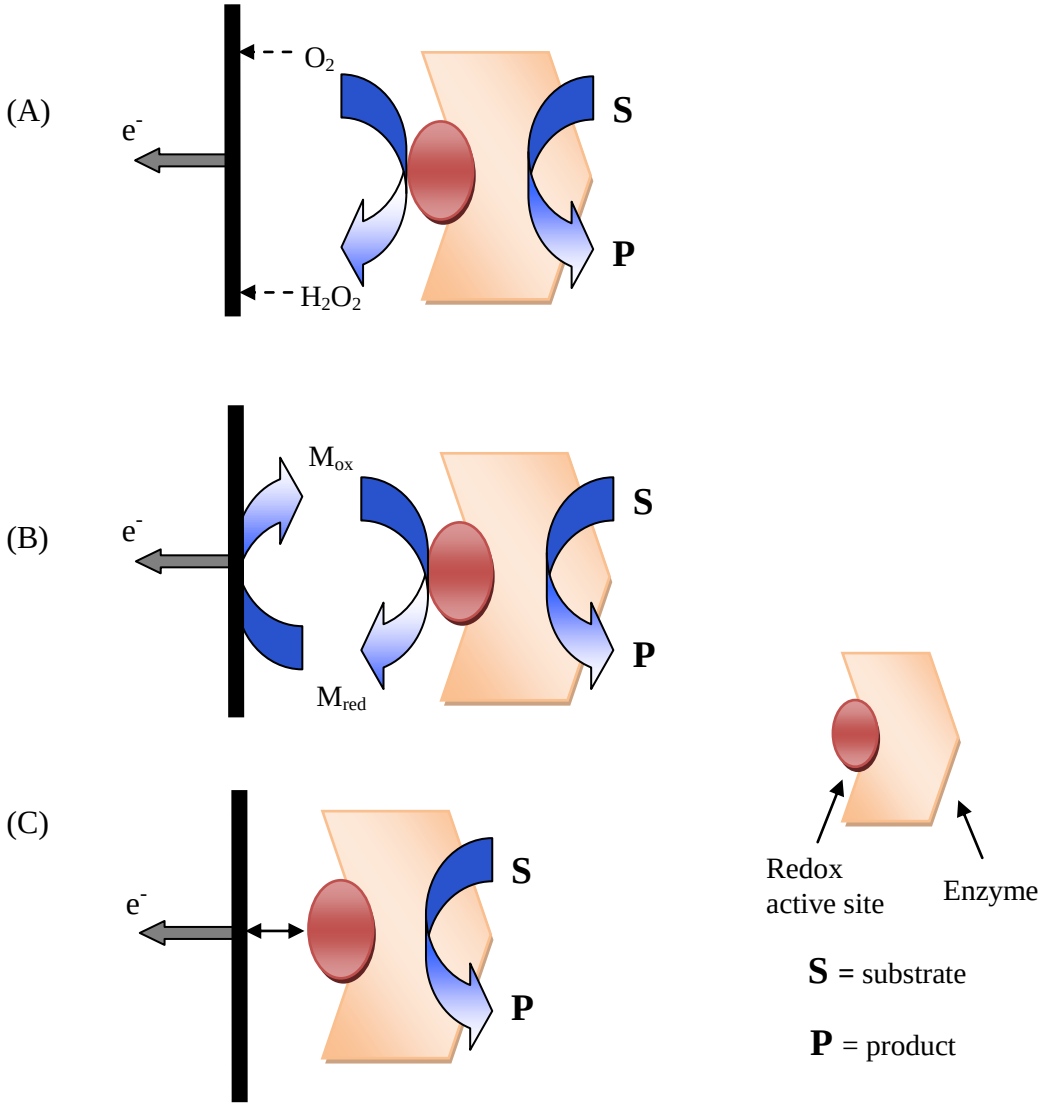

Figure 4.1: Three generations of amperometric enzyme electrodes for glucose based on the use of natural oxygen cofactor (A), artificial redox mediators (B), or direct electron transfer between enzyme and the electrode surface (C).

First-generation glucose biosensors use natural oxygen as a co-substrate and detect the generation of hydrogen peroxide. The biocatalytic reaction involves reduction of the flavin adenine dinucleotide (FAD), the redox active site in the enzyme by reaction with glucose to give the reduced form of the enzyme ($FADH_2$) followed by reoxidation of the flavin by molecular oxygen to regenerate the oxidized form of the enzyme GOx(FAD). These measurements are commonly carried out on a platinum electrode at anodic potential of around +0.6 V (vs Ag/AgCl).[4]

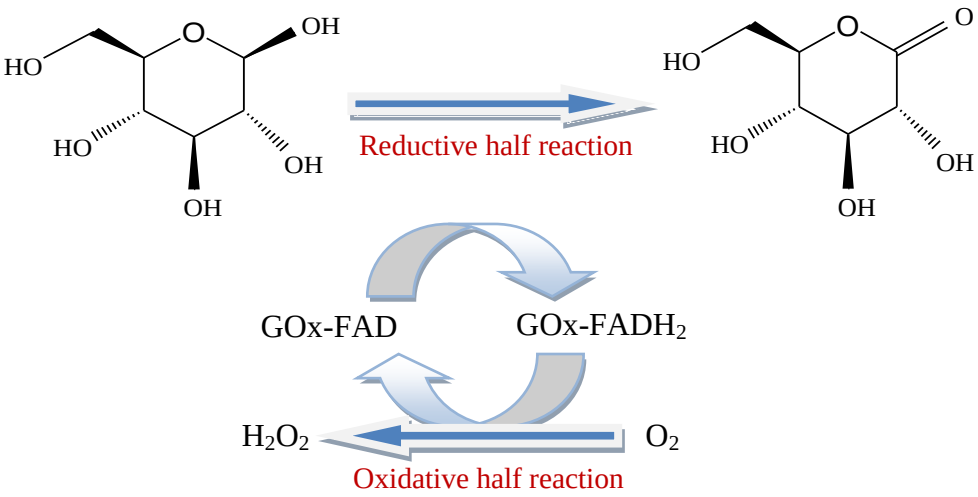

Figure 4.2: Reaction involves in first generation of glucose biosensors.

There is a problem with this biosensor arrangement, which is the loss in selectivity between the biorecognition active site and the amperometric H_2O_2 detection. The highly oxidizing potential (700 mV versus Ag/AgCl) is necessary for H_2O_2 oxidation results in substantial interference from the oxidation of other compounds in complex matrixes.

Several limitations were also reported with O_2 / H_2O_2 monitoring in sensor design. H_2O_2 can be consumed by impurities in the enzyme preparation, thus can arise to an error results. Furthermore, H_2O_2 is a strong oxidant and at high local concentrations may deactivate certain enzymes.

The electron transfer between GOx and the surface of the electrode can be improved by placing the oxygen with a non-physiological electron acceptor capable of

shuttling electrons from the redox centre of the enzyme to the electrode surface. The electron transfer between the GOx active site and the surface of the electrode is the limiting factor in the system of amperometric glucose biosensors. GOx is an enzyme that does not transfer the electrons directly to the electrode because of a thick layer surrounding its flavin adenine dinucleotide (FAD) redox centre and introducing an intrinsic barrier to direct electron transfer (Figure 4.3).

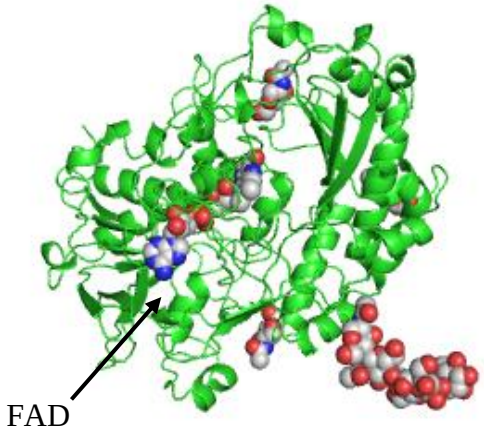

Figure 4.3: Glucose oxidase (GOx) from *Aspergillus niger* showing the flavin adenine dinucleotide (FAD) molecule. Structure created using polyview.

Second-generation glucose biosensors use an artificial electron mediator, which replaces O_2 as the electron shuttle between the FAD centre and the electrode surface by the following scheme:

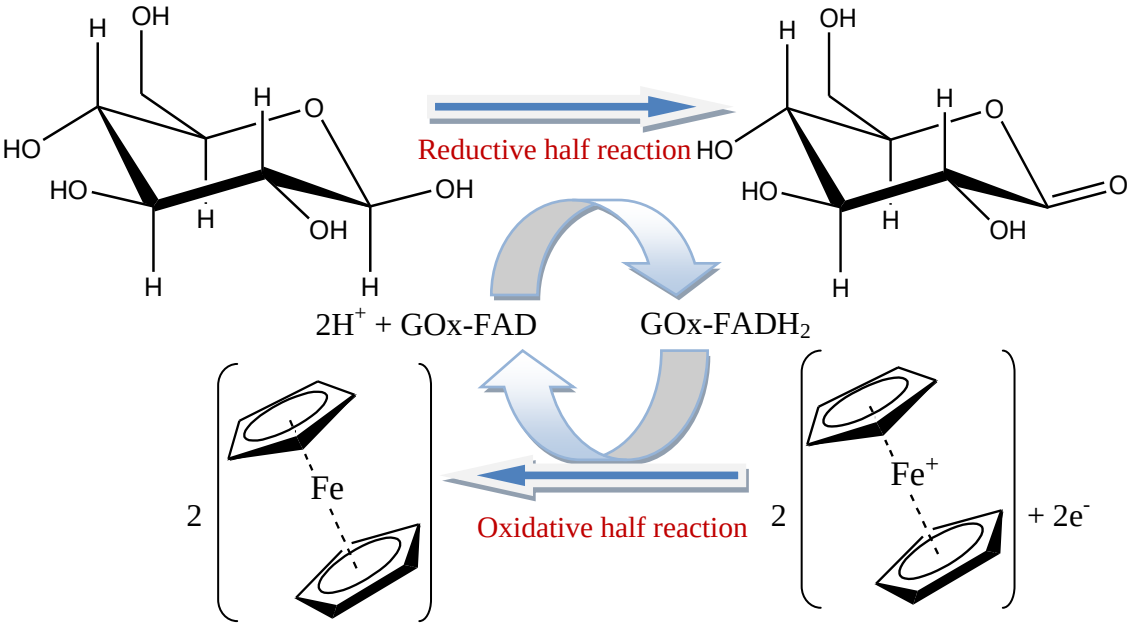

Figure 4.4: Reaction involves in second generation of glucose biosensors.

where Fc and Fc^+ have been used as an example of the reduced and oxidized forms of the mediator, respectively. When the reduced form of the mediator is reoxidized at the electrode (Figure 4.4), a current signal is produced that proportional to the glucose concentration presence. This then will regenerate the oxidized form of the mediator.

Ferrocene derivatives, quinones, organic conducting salts, and transition-metal complexes, have been particularly useful to electrically contact GOx.[4] By using these electron mediators, amperometric measurements become independent of oxygen partial pressure and could be carried out at lower potentials that do not provoke interfering reactions from coexisting electroactive species.

Third-generation glucose biosensors were developed by the progression from use of a freely diffusing mediator (O_2 or artificial) to a system where enzyme and mediator are co-immobilized at an electrode surface, making the biorecognition component an integral part of the electrode transducer. Co-immobilization of enzyme and mediator can be accomplished by redox mediator labelling of the enzyme followed by enzyme immobilization in a redox polymer, or enzyme and mediator immobilization in a conducting polymer. There are even reported cases of direct electrical contact of enzyme to electrode.[4]

$$FADH_2\text{-oxidase} \rightarrow FAD\text{-oxidase} + 2H^+ + 2e^- \quad (4.4)$$

Third-generation biosensors offer all the benefits of second-generation sensors and some new ones as well. The latter arise from the self-contained nature of the sensor. Since neither mediator nor enzyme must be added, this design facilitates repeated measurements. Sensor use for multiple analyses minimizes cost pressures on sensor design. It also follows that such a sensor could allow for continuous analyte monitoring.

4.2 Fundamental Study: Ferrocene-modified GC Electrodes.

Research on electrochemical glucose biosensors was started with fundamental study on the electrochemical behaviour of ferrocene as mediator to electron transfer reaction at the surface of glassy carbon electrodes (GCE). Figure 4.5 shows the cyclic voltammograms (CVs) of bare GCE and GCE modified with ferrocene (0.1 M in 1,2-dichloroethane) in phosphate buffer solution (pH 7) at 50 mV/s. No peaks were observed on bare GCE (blue line). But when the GCE was modified with ferrocene, the CV (red line) shows a pair of well-defined reversible redox peaks with the formal potential located at 0.283 V vs Ag/AgCl (reduction and oxidation peaks at 0.2 V and 0.366 V, respectively). It is clearly to conclude that ferrocene can be used as a mediator in the electron transfer process. A fully reversible CV was obtained with the GCE coated with ferrocene. Otherwise, a base line CV was obtained with a bare CV in the absence of ferrocene as mediator.

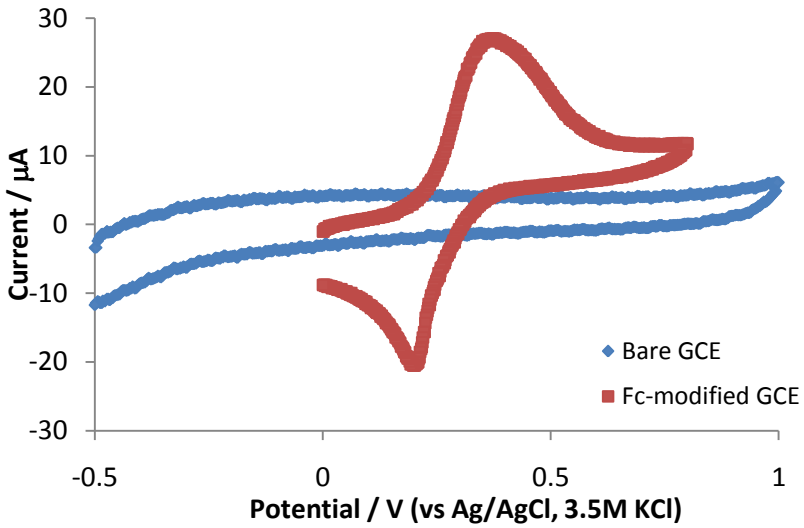

Figure 4.5: CVs of bare and ferrocene-modified GC electrode in phosphate buffer solution, 0.1 M (pH 7). Scan rate 50 mV/s.

Ferrocene is a suitable mediator in this process since it is easily be reduced, and also easily be re-oxidized back to its original form. It gives a stable voltammogram with a reversible one-electron oxidation and reduction reactions at the surface of the GC electrode. At the electrode surface, a fast heterogeneous reaction occurs as the oxidation of the Fc to Fc^+ on the forward scan at 0.366V. As the scan is reversed back to the initial potential, the reduction of Fc^+ to Fc is observed.

$$Fc \leftrightarrow Fc^+ + e^- \tag{4.5}$$

In the electrochemical glucose biosensor systems, at which the electron transfer reaction is mediated by the ferrocene, the Fc^+ will be reduced by the GOx presence in a homogeneous reaction. At the same time, glucose is then oxidized by GOx to produce gluconolactone.

$$Fc \xrightarrow{electrode} Fc^+ + e^- \tag{4.6}$$

$$2Fc^+ + \mathrm{GOx(FADH_2)} \xrightarrow{k} \mathrm{GOx(FAD)} + 2Fc \tag{4.7}$$

$$\mathrm{GOx(FAD)} + \mathrm{Glucose} \leftrightarrow \mathrm{GOx(FAD)\text{-}Glucose} \leftrightarrow \mathrm{GOx(FADH_2)} + \mathrm{Gluconolactone} \tag{4.8}$$

Figure 4.6(A) shows the CVs of GCE doped with ferrocene as mediator in phosphate buffer solution, scan at 2, 10, 25, 50 and 100 mV/s. Plots of peak current versus square root of scan rate (Figure 4.6(B)) show linear correlation was observed in these CVs.

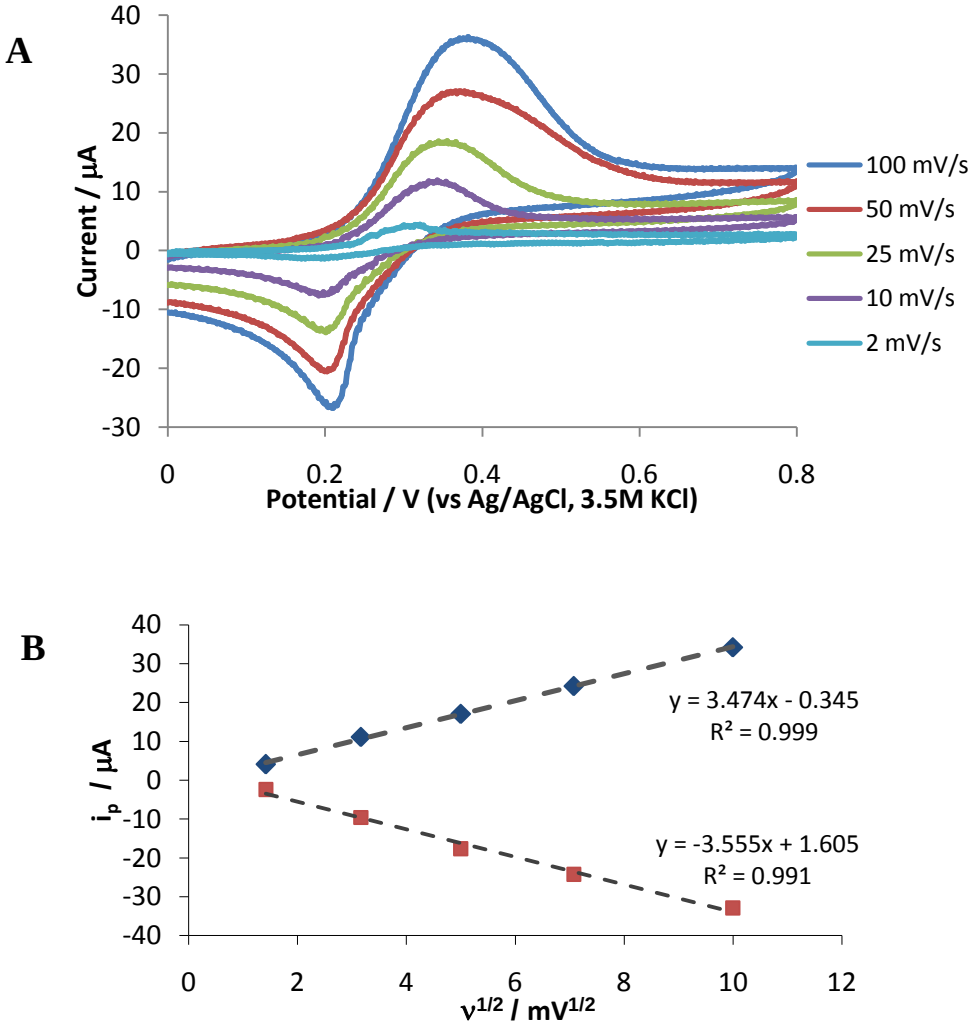

Figure 4.6: (A) CVs obtained at the GC electrode modified with ferrocene (0.1 M in 1,2-dichloroethane) in phosphate buffer solution, 0.1 M (pH 7). Scan rate (from inner to outer) 2, 10, 25, 50 and 100 mV/s. (B) Plots of peak currents versus $\nu^{1/2}$.

As shown in Figure 4.6(B), the plots of peak currents versus square root of scan rates gave a linear line which suggests that the electron transfer process in ferrocene is diffusional control process. The peak to peak separation (ΔE) was calculated be in the range of 0.10 to 0.14 V dependent to the scan rates. According to Randles-Sevcik equation, $i_p = (2.69 \times 10^5) n^{3/2} A C D^{1/2} \nu^{1/2}$ the value of diffusion coefficient, D was determine to be 8.1×10^{-7} cm^2/s. This value is in good agreement with previously published literature that the D value should be on the order of ~ 10^{-7} cm^2/s at 298 ºC.[5-7]

4.3 Carbons-based GC Electrodes

The ferrocene-modified GC electrodes were used for the next study. At this section, the GC electrode was further modified with various forms of carbon particles, including spherical porous carbons (SPCs), graphite particles (GPs), single-wall carbon nanotubes (SWCNTs) and multi-wall carbon nanotubes (MWCNTs). Each of the carbon sources were dispersed in N,N-dimethylformamide (2 mg/mL) solution with ultrasonic agitation for about 1 hour to form a black solution.

The GC electrode was first deposited with ferrocene for approximately 1 min prior to modification with carbon films. The carbon films were prepared by dropping a solution of various forms of carbon (7.5 µl) on the GC electrode surface and then evaporating the solvent at room temperature. After modification, the electrodes were rinsed with deionised water to remove the loosely adsorbed carbon. The immobilization of glucose oxidase at the sol-gel composite on the surface of electrode was obtained by carefully mix the sol solution and enzyme solution (1:1, v/v), and then pipette onto each surface of bare and carbon modified GCE and dried for 30 min at room temperature. The sol-gel was used as the immobilization matrix due to its several advantages as reported in Section 2.2.4. The resulting glucose sensor was then transferred and immersed into an electrochemical cell containing 0.1 M phosphate buffer solution at pH 7.0 as electrolyte solution.

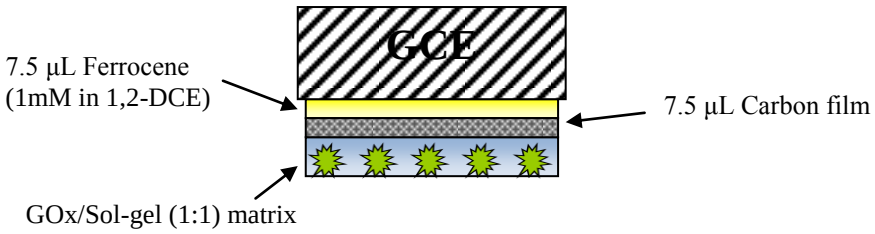

Figure 4.7: Diagram illustrated the layers on the modified GC electrode.

The electrochemical behaviour of each form of carbon films was monitored using CV. It was found that the shape of the CVs obtained were different among all types of carbon films. The shape of the voltammetric signal depends on the type of the electronic conductor used. Figure 4.8 to 4.11 show the cyclic voltammograms of the ferrocene-modified GC electrodes with SPCs, GPs, SWCNTs and MWCNTs, respectively scanned at different rates varied from 2 to 50 mV/s.

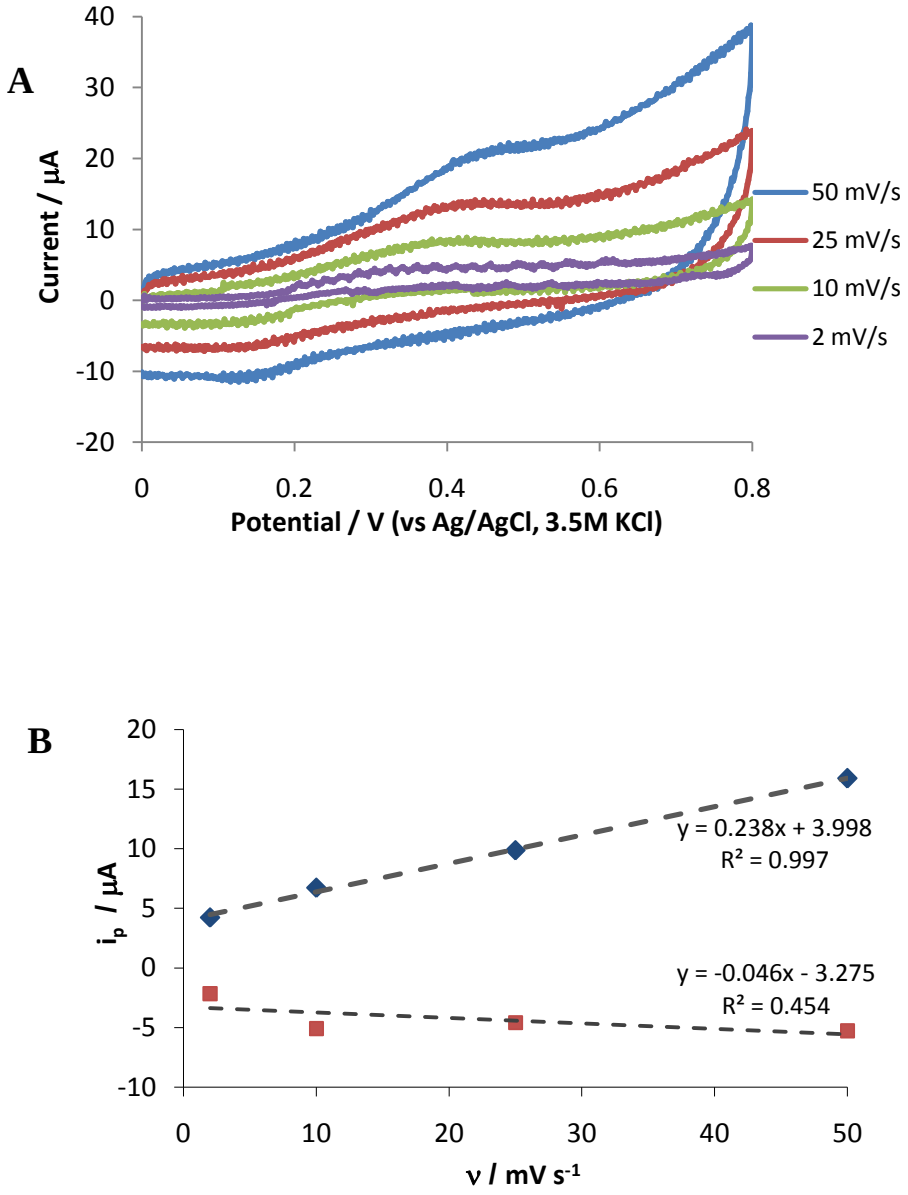

Figure 4.8: CVs (A) and plot of peak currents versus scan rates (B) of Fc/SPCs/sol-gel GC electrodes in 0.1 M PBS (pH 7), scanned at various scan rates.

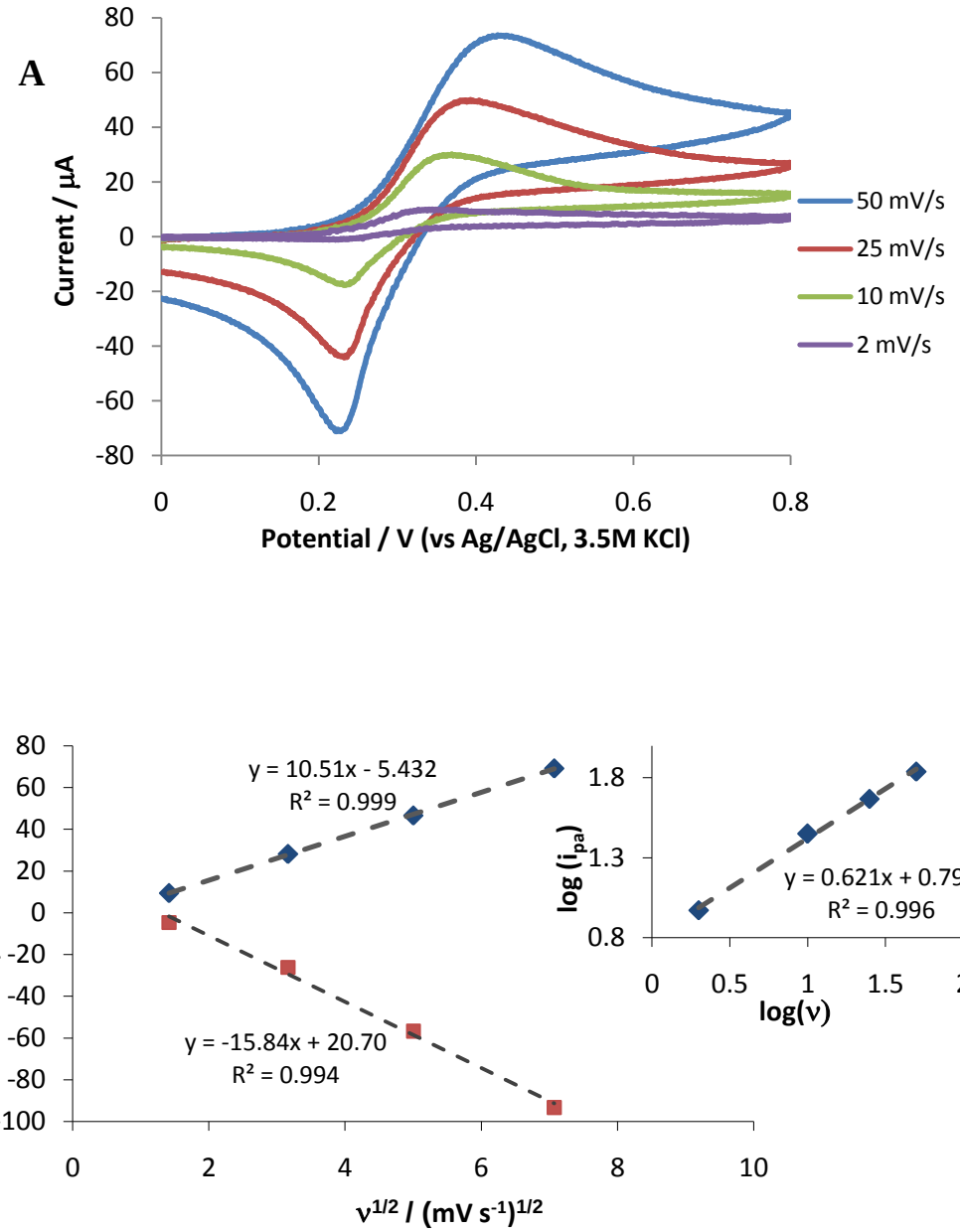

Figure 4.9: CVs (A) and plot of peak currents versus square root of scan rates (B) of Fc/GPs/sol-gel GC electrodes in 0.1 M PBS (pH 7), scanned at various scan rates.

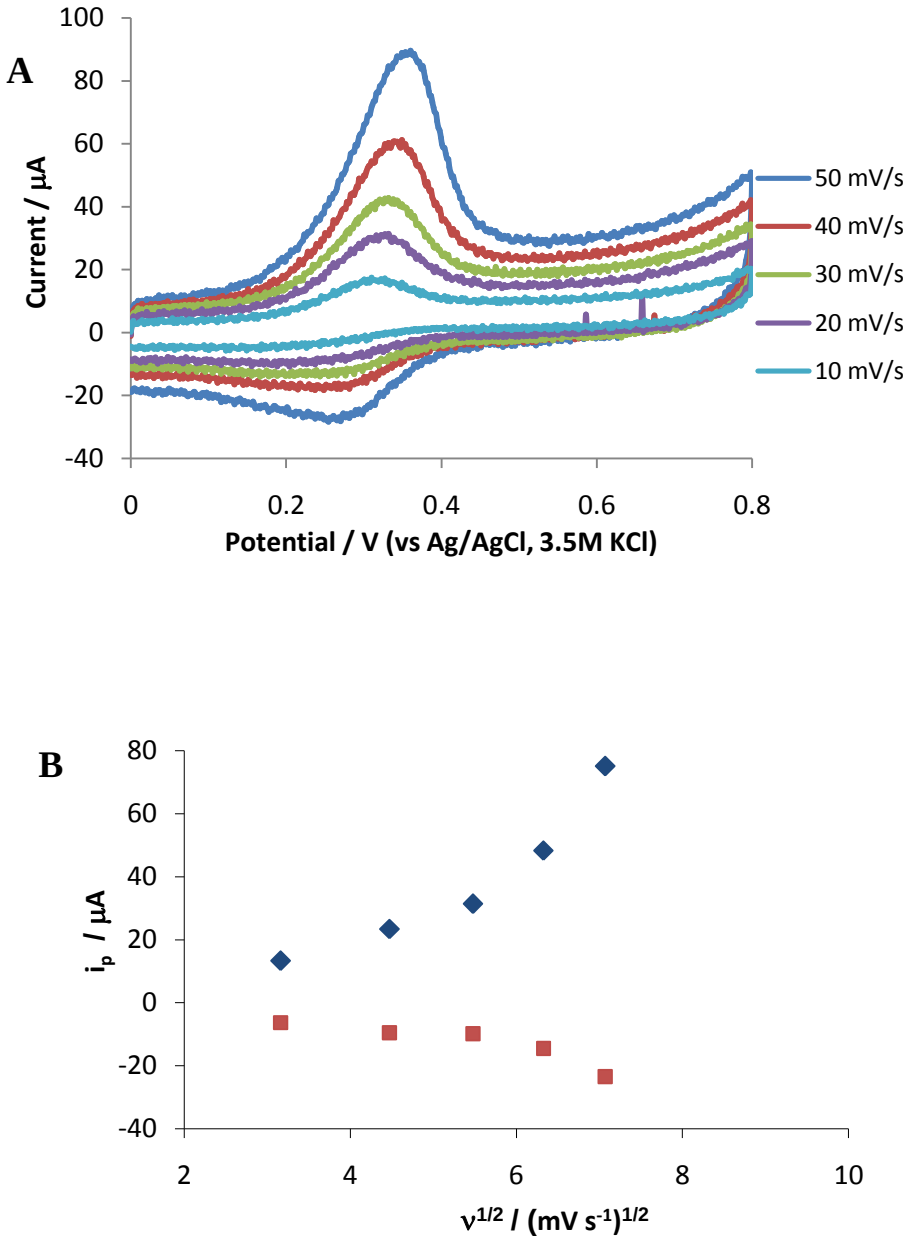

Figure 4.10: CVs (A) and plot of peak currents versus scan rates (B) of Fc/SWCNTs/sol-gel GC electrodes in 0.1 M PBS (pH 7), scanned at various scan rates.

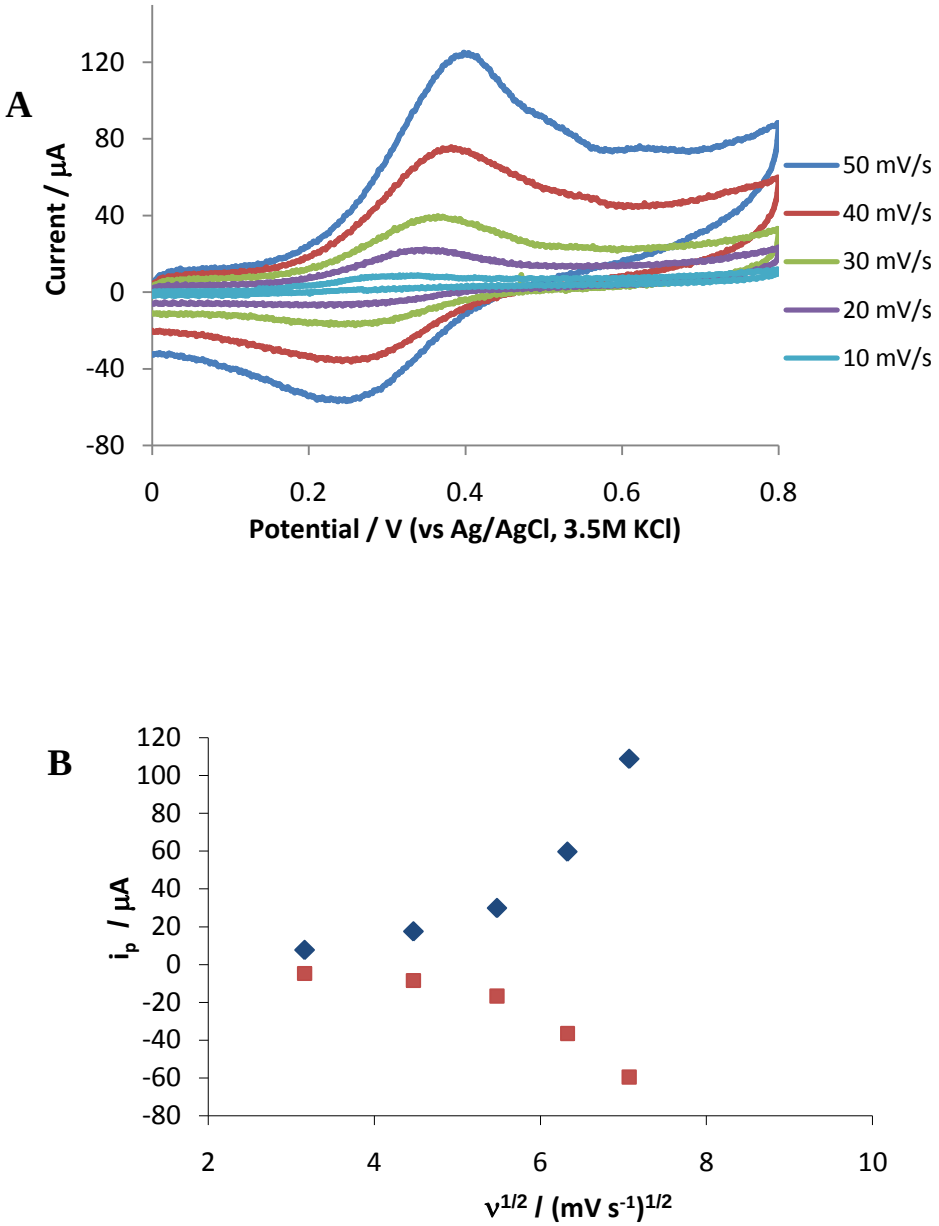

Figure 4.11: CVs (A) and plot of peak currents versus scan rates (B) of Fc/MWCNTs/sol-gel GC electrodes in 0.1 M PBS (pH 7), scanned at various scan rates.

The peak currents in CVs of Fc/SPCs/sol-gel-modified GC electrode (Figure 4.8) were not clearly observed compared to other forms of carbon with wide peak-to-peak separation, (ΔE = 0.343 V). A wide peaks separation could indicate that this modified electrode undergoes an irrversible or quarsi-reversible reaction. In general, a

linear correlation between anodic peak currents (i_{pa}) and the scan rates between 2 to 50 mV/s was obtained suggested that the Fc/SPCs-modified electrode the reaction is a surface-controlled process. The overall redox process confined at the electrode surface can be considered to be relatively slow corresponds to a slow conversion of a surface film without diffusion or kinetically controlled reaction step.

A more clear, well-defined reversible redox peaks were observed in the CVs of Fc/GPs/sol-gel-modified GC electrode as shown in Figure 4.9. The cathodic peaks appear sharper than the anodic peaks. This voltammetric peak shape was also found similar with other carbon paste based electrodes as reported elsewhere.[8] However, the peak separations were found to vary from 90 mV to 178 mV depends on the scan rates. Plot of peak currents (i_p) versus square root of scan rates between 2 to 50 mV/s shows linear relation which suggested a diffusion-controlled redox process. Further analysis of the anodic peak currents can also be used to determine the types of the redox process. The slopes of 0.50 and 1.00 in a linear plot of log (i_{pa}) versus log (ν) are expected for ideal diffusion and surface processes, respectively.[8] In this case, the slope of the log (i_{pa}) versus log (ν) plot (inset in Figure 4.9) gave a value of 0.621, suggesting a mixture of diffusion- and surface-controlled processes which tending towards the diffusion-limited process.

Both Fc/SWCNTs/sol-gel- and Fc/MWCNTs/sol-gel-modified GC electrodes gave well-defined redox peaks as shown in the CVs in Figure 4.10 and 4.11, respectively. High capacitive currents were obtained indicated slow kinetic processes occurs at both CNTs-based electrodes. Non-linear correlation between peak currents and neither the square root of scan rates nor the scan rates were also observed, which can be explained that the process at the electrodes are not diffusional nor surface-controlled processes.

It also can be seen in Figure 4.11 that the Fc/MWCNTs/sol-gel-modified electrode seems to have two i_{pa} values at the scan rates range from 30 to 50 mV/s. These two anodic peaks could be due to the presence of the catalytic impurities in the sample of MWCNTs. This was proved by the ICP analysis that the MWCNTs sample was found to contain 1.66% of cobalt and 2.16% of molybdenum (Table 4.1). These interferences could possibly undergo a catalytic oxidation as well at the surface of the electrode. However, this two anodic peaks behaviour was not observed in the CVs of the same electrode when it was scanned at lower scan rates.

Table 4.1: ICP-OES results for the present of impurities in carbon samples.

Types of carbons	% Impurities present
Single wall carbon nanotubes (SWCNTs)	0.43 % Co, 0.33 % Mo, 0.11 % Fe
Multi wall carbon nanotubes (MWCNTs)	1.66 % Co, 2.16 % Mo
Spherical porous carbons (SPCs)	0.24 % Fe
Graphite particles (GPs)	0.48 % Fe

The response of various forms of carbon-modified GC electrodes can also been clearly seen in Figure 4.12. As shown below, the current responses were enhanced with both Fc/SWCNTs- and MWCNTs/sol-gel-modified GC electrodes compared to Fc/SPCs- and GPs/sol-gel-modified electrodes. This indicates that the electron transfer process in the CNTs-based GC electrodes was enhanced due to the excellent ability of CNTs to promote the electron transfer reaction of the electroactive species. In addition, the special nanostructure of CNTs may act as 'molecular wire' to facilitate the direct electron transfer between ferrocene and the electrode.[9]

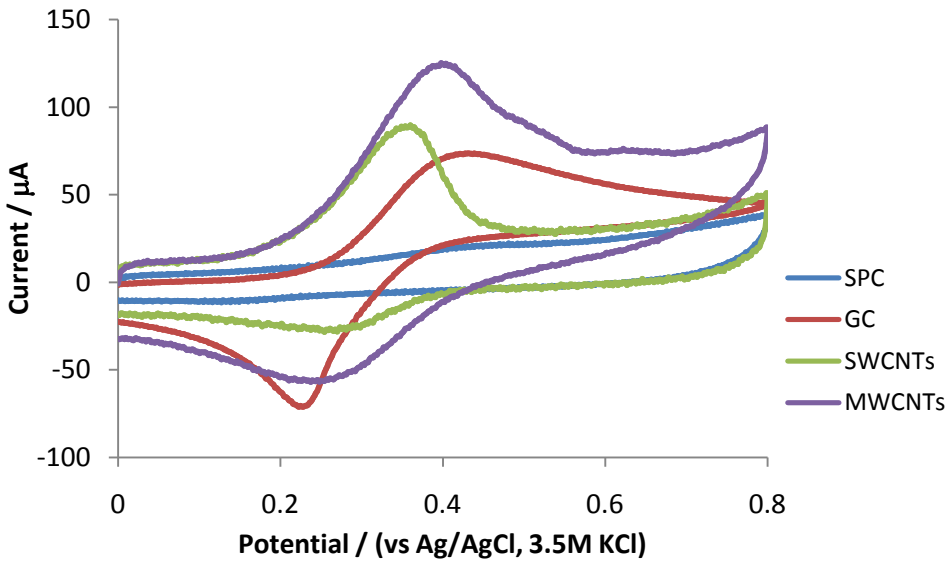

Figure 4.12: CVs of Fc-modified SPCs, GPs, SWCNTs and MWCNTs GC electrodes, respectively in 0.1 M PBS (pH 7). Scan rate 50 mV/s.

As can be seen clearly in the Figure 4.12, the Fc/MWCNTs/sol-gel-modified GC electrode gave the highest anodic peak current (i_{pa}) of 108.82 μA at 0.384 V *vs.* Ag/AgCl (3.5 M) scanned at 50 mV/s. The peaks separation was also lower in the CVs of both CNTs-based GC electrodes. The low peaks distance could support the facts that the CNTs-based electrodes could be the best electrodes under study so far because it attributed to the fast kinetics mechanism of electron transfer reaction at the electrode surface. Thus, further studies on the use of the modified electrodes to the application of glucose biosensors will be focused on the CNTs-based GC electrodes (Section 4.4).

4.4 Ferrocene-modified Carbon Nanotubes Electrodes

4.4.1 Characterization of Ferrocene-modified Carbon Nanotubes Electrodes

Raman spectroscopy is one of the most useful techniques to characterise carbon nanotubes (CNTs). Raman scattering in CNTs involves strong resonance of the incoming and outgoing light and the vibrational states with the electronic energy levels of a tube. The Raman spectra produce therefore carries useful information about the electronic states of CNTs.

Figure 4.13 shows the Raman spectrum of SWCNTs. The different properties of SWCNTs can be determined by examining each peaks in Raman spectrum, including the radial breathing mode (RBM) at around 200 cm^{-1}, the disorder induces mode (D band) at around 1350 cm^{-1} and the high-energy mode (G band) at the Raman shift range between 1550 to 1600 cm^{-1}. The radial breathing mode is a unique peak for SWCNTs. The presence of SWCNTs can be proved by the presence of the radial breathing mode and the double-peak structure of the high energy mode in the Raman spectrum.

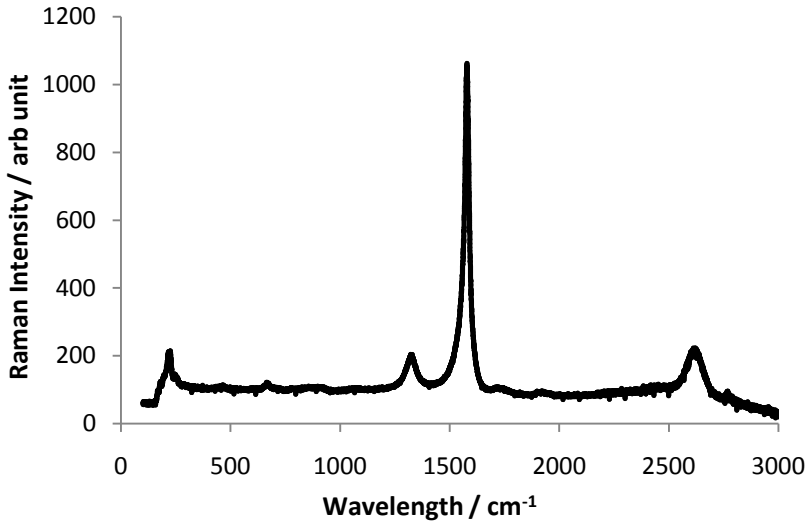

Figure 4.13: Raman spectrum of SWCNTs

The frequency of the RBM is proportional to the inverse of the CNTs diameter. It is by far the easiest and fastest method to determine the diameter of the CNTs. By measuring the RBM frequency, the diameter of CNTs can be estimated. As shown in Figure 4.13, the RBM frequency of this SWCNTs sample is 224.17 cm^{-1} and the tubes are determined to have an average diameter of approximately 1 nm according to the following equation:

$$\text{Diameter of CNTs} = \frac{227}{\omega_{RBM}} \qquad (4.9)$$

$$= \frac{227}{224.17}$$

$$= 1.01 \text{ nm}$$

Raman scattering also can be used to distinguish between metallic and semiconducting CNTs by looking at the peaks at high energy mode in Raman spectrum. In metallic CNTs, the lower high-energy mode is strongly broadened and shifted to smaller energies. However, this lower G band is not observed in the Raman spectrum of our SWCNTs, which indicated the presence of semiconducting nanotubes. The high intensity of G band as compared to D band shown in the spectrum also attributed to the high quality of the SWCNTs sample used in this study.

Other method to characterise the properties of CNTs is by using thermogravimetry analysis (TGA). TGA measures weight changes in a material as a function of temperature (or time) under a controlled atmosphere. The measurement of TGA was carried out in air, and the weight is recorded as a function of increasing temperature. In the particular case of carbon nanotubes, the weight change in an air atmosphere is typically a superposition of the weight loss due to oxidation of carbon into gaseous carbon dioxide and the weight gain due to oxidation of residual metal catalyst into solid oxides. The maximum temperature is selected to 1000 ˚C so that the CNTs weight is stable until the end of the experiment, implying that all chemical reactions are completed.

The TGA provides two important numerical pieces of information, which is ash content in this case is the residual mass, M_{res} and the weight loss onset temperature (T_{onset}). This temperature refers to the temperature of the maximum rate of oxidation. The gradual onset is believed to be due to nanotubes being contaminated with amorphous carbon and other types of carbonaceous impurities that oxidize at temperatures lower than that of nanotubes. In these cases, T_{onset} describes the properties of the impurities rather than the nanotubes.

As shown in Figure 4.14, the T_{onset} of the unmodified SWCNT and MWCNT were 564.27 ˚C and 548.99 ˚C, respectively. These temperatures suggest that the CNTs used in this study were pure with the residual mass started to appear at > 800 ˚C.

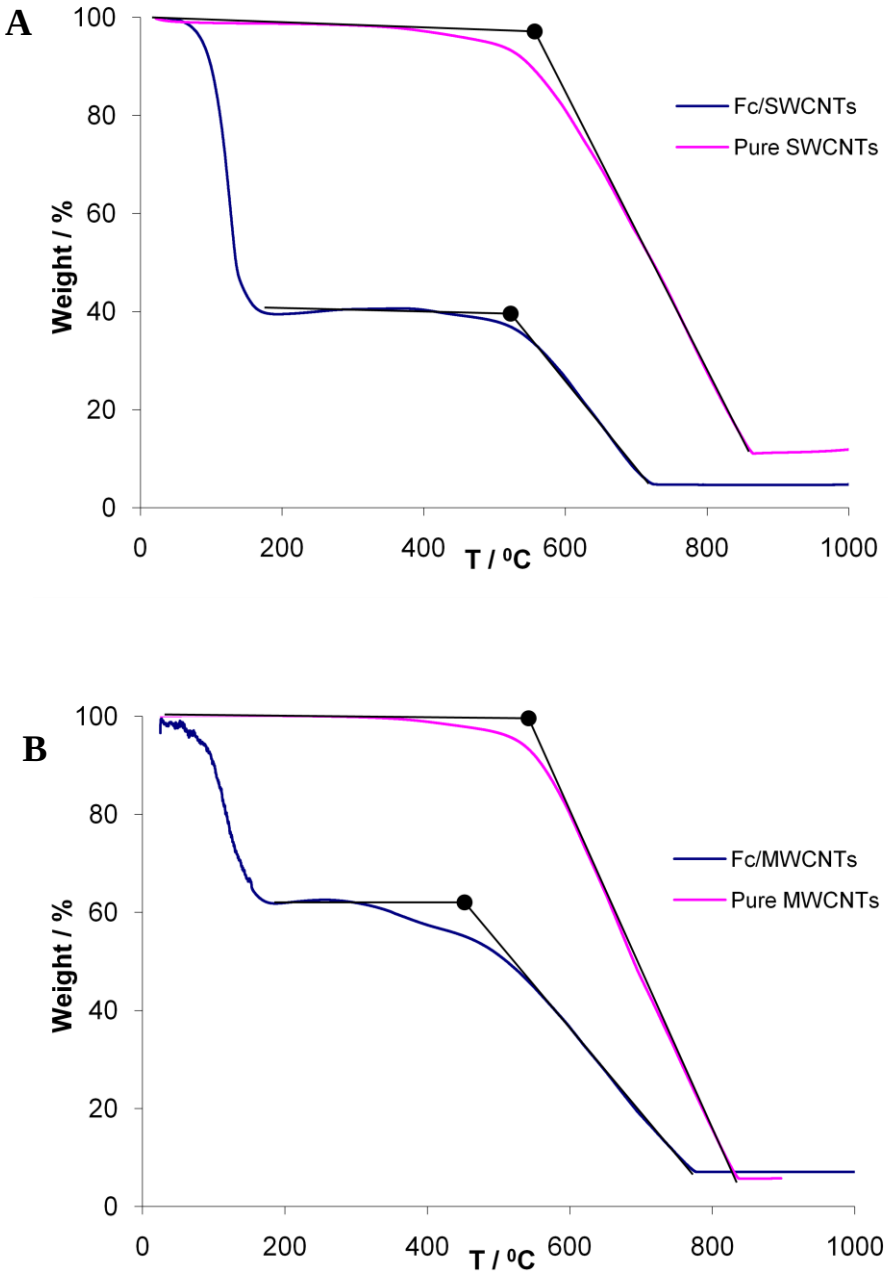

Figure 4.14: The TGA results of pure and ferrocene-modified SWCNT (A) and MWCNT (B).

It was found that there were two points of T_{onset} observed in ferrocene-modified CNTs. The first T_{onset} was observed at approximately 90 ˚C, suggesting the oxidation of ferrocene molecule, while the second T_{onset} observed then was the oxidation of CNTs molecule in the compound of ferrocene-modified CNTs. These results clearly showed

that the ferrocene-modified CNTs had successfully produced to being used later in the next section.

4.4.2 Electrochemical Behaviour of Ferrocene-modified Carbon Nanotubes Electrodes

The electrochemical behaviour of ferrocene-modified SWCNTs and MWCNTs electrodes in the presence of various matrixes was first studied in order to understand the electron transfer of carbon nanotubes after modification with ferrocene. Figure 4.15 and 4.16 shows the cyclic voltammograms (CVs) for the Fc / Fc^+ couple with SWCNTs and MWCNTs, respectively at the (a) sol-gel, (b) collagen and (c) collagen/sol-gel composite electrodes in 0.1 M phosphate buffer solution (PBS) at scan rate of 2 mV/s. It is clearly seen that the CVs of both SWCNTs and MWCNTs-based electrodes showed a couple of redox peaks indicate a reversible redox process occurred in correlated to modification of CNTs with ferrocene.

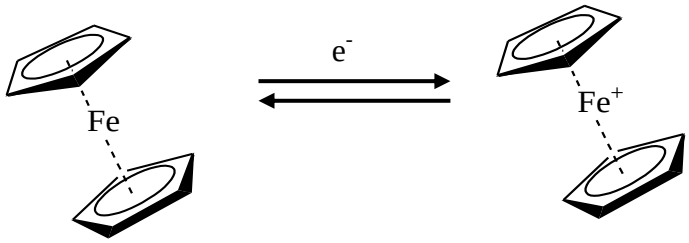

(4.10)

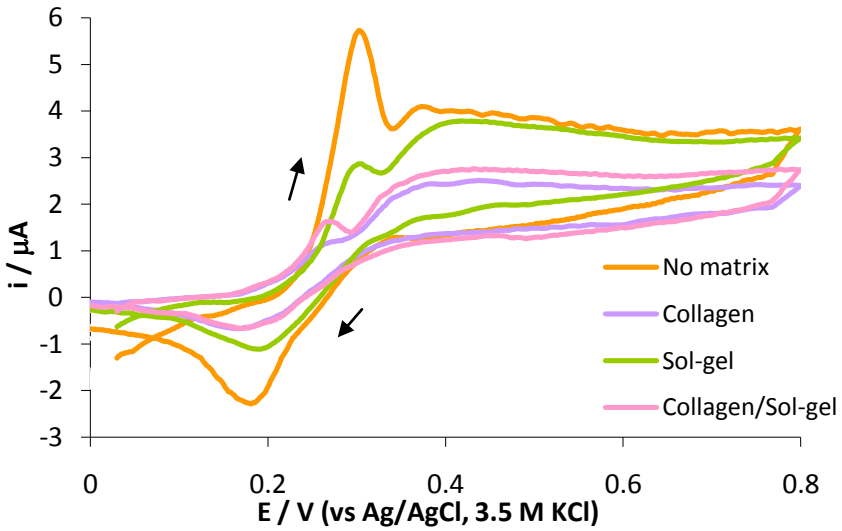

Figure 4.15: CVs for direct immobilized ferrocene-modified SWCNTs (orange line) and ferrocene/SWCNTs immobilized within silica sol-gel (green line), collagen (purple line) and collagen/sol-gel composite (pink line) electrodes in 0.1 M PBS (pH 7). Scan rate 2 mV/s.

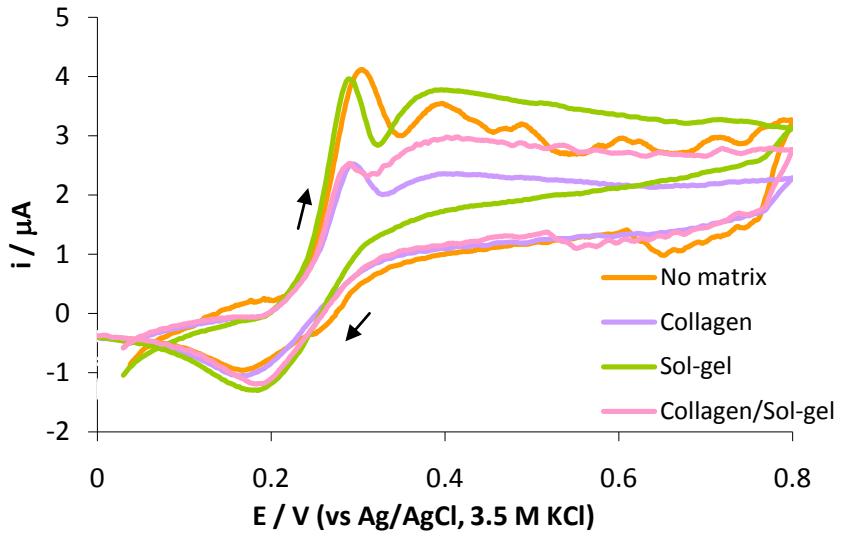

Figure 4.16: CVs for direct immobilized ferrocene-modified MWCNTs (orange line) and ferrocene/MWCNTs immobilized within silica sol-gel (green line), collagen (purple line) and collagen/sol-gel composite (pink line) electrodes in 0.1 M PBS (pH 7). Scan rate 2 mV/s.

A pair of peak currents was observed in the CVs of both SWCNTs and MWCNTs-based electrodes, indicated a linear diffusion-controlled redox process of the Fc / Fc^+ couple at these modified electrodes. However, the ferrocene-modified CNTs showed a sharp 'pre-peak' appears before the phase containing electroactive species voltammetric peak. This phenomenon suggests an oxidation of dissolved Fc to adsorbed Fc^+ molecule.

These adsorption phenomena were not found observed in the CVs of ferrocene-modified glassy carbon electrode (GCE) without the presence of any CNTs and matrixes (Figure 4.6(A)). Often, the electrode materials have to be optimized to minimize the effect of adsorption.[10] Thus, these ferrocene/CNTs-based electrodes were then used to construct glucose biosensor by immobilizing the enzyme within TMOS sol-gel, collagen and collagen/TMOS sol-gel matrixes in order to minimize the effect of adsorption phenomena that appeared strongly in such modified electrode without any matrix.

4.4.2.1 The Effect of Carbon Nanotubes Concentration on the Electrochemical Behaviour of Glucose Biosensors.

The effect of carbon nanotubes concentrations on the behaviour of glucose oxidation was study to obtain the optimum concentration of CNTs that give the highest response to glucose sensors.

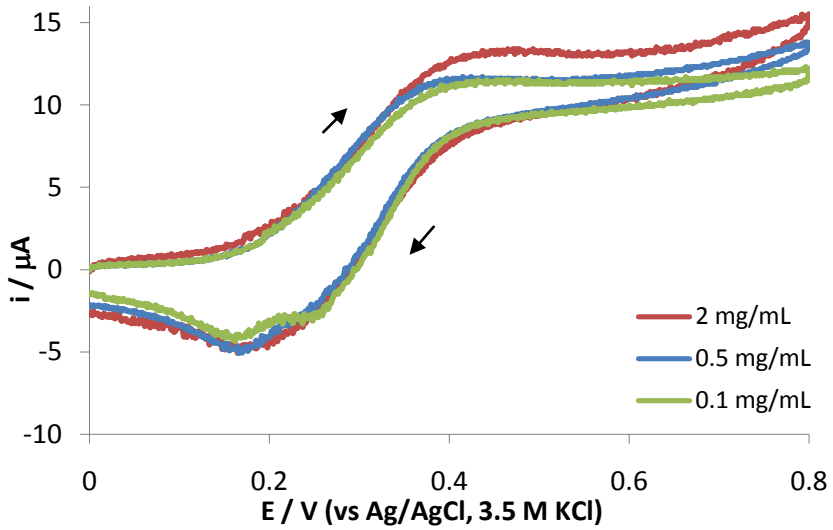

Figure 4.17: CVs obtained at Fc/SWCNTs/GOx/sol-gel GC electrode, in 100 mM PBS (pH 7) containing 10 mM D-glucose. Scan rate, 25 mV/s.

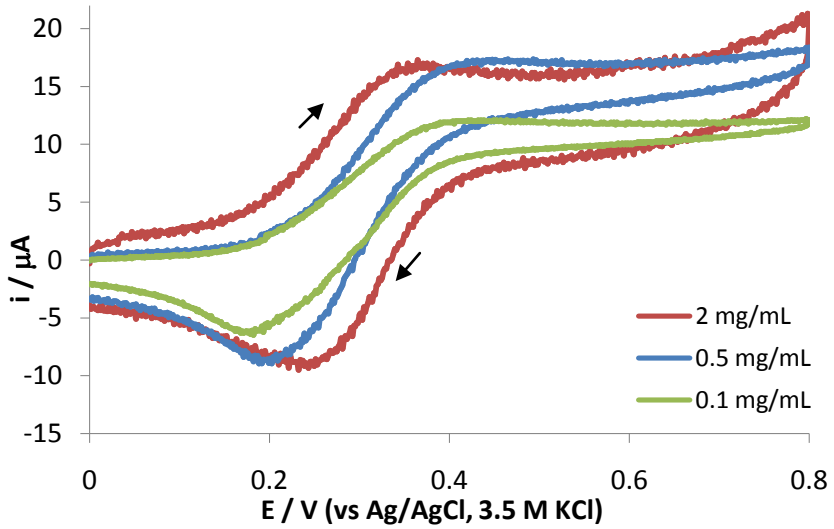

Figure 4.18: CVs obtained at Fc/MWCNTs/GOx/sol-gel GC electrode, in 100 mM PBS (pH 7) containing 10 mM D-glucose. Scan rate, 25 mV/s.

Figure 4.17 and 4.18 show the CVs for Fc/SWCNTs/GOx/sol-gel and Fc/MWCNTs/GOx/sol-gel GC electrodes respectively, in 0.1 M phosphate buffer solution (pH 7) containing 10 mM glucose. The CVs were scanned at 25 mV/s. It is clearly seen that the steady state current responses were obtained with 0.1 and 0.5 mg/mL of both SWCNTs and MWCNTs modified with ferrocene depicting the

characteristic catalytic system for glucose sensors. However, when the content of CNTs initially dispersed in the ferrocene was increased to 2 mg/mL, the CVs obtained for the Fc / Fc^+ redox couple changed, a peak shape behaviour was observed in the CVs.

Both ferrocene-modified SWCNTs and MWCNTs gave an optimum concentration of CNTs of 0.5 mg/mL as shown in Figure 4.17 and 4.18, respectively. The optimum MWCNTs concentration of 0.5 mg/mL also gaves the highest formal potential of 311.25 mV compared to other modified electrodes.

4.5 Ferrocene/Carbon Nanotubes/Collagen-based Glucose Biosensors

4.5.1 Ferrocene-modified SWCNTs with GOx Entrapped within Collagen and Collagen/Sol-gel Matrixes.

Collagen is one of the biopolymers that most extensively used to construct the functionalized hybrid structures. Figure 4.19 shows the CVs of ferrocene-modified SWCNTs with GOx entrapped within sol-gel, collagen and collagen/sol-gel hybrid matrixes that displayed a different shape of the CVs when D- and L-glucose presence, respectively. A steady state anodic current was observed in the CVs of sol-gel, collagen and collagen/sol-gel matrixes when D-glucose presence in the solution (Figure 4.19 (A)). On the other hand, a sharp peak was observed with Fc/SWCNTs/GOx/collagen matrix electrode at the reverse scan, exhibited an adsorption of product to the electrode surface.[10] According to Zou *et al*. (2008),[11-12] the CNTs also have strong adsorptive ability and they can absorb the biomolecules stably.

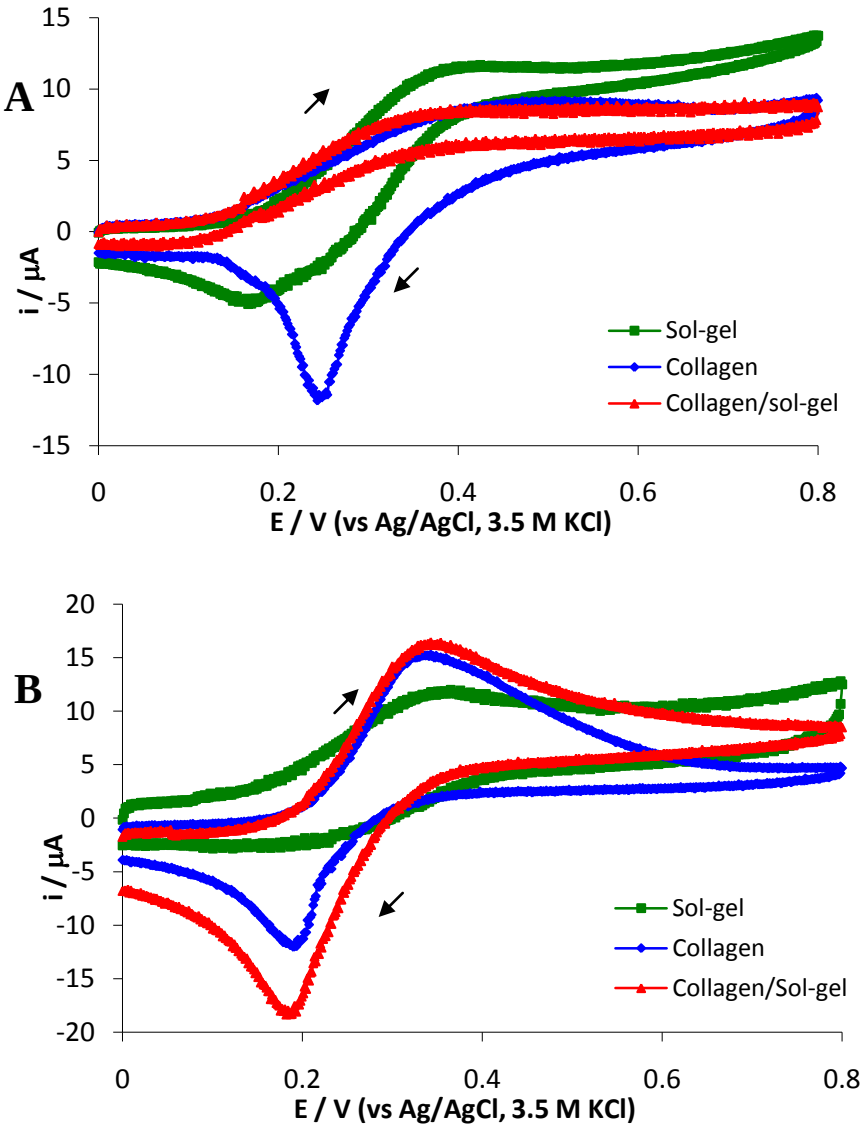

Figure 4.19: CVs of Fc/SWCNTs/GOx entrapped within sol-gel, collagen and collagen/sol-gel matrixes in PBS (0.1 M, pH 7) containing 10 mM (A) D- and (B) L-glucose. Scan rate, 25 mV/s.

Figure 4.19 (A) also showed that GOx enzyme entrapped within sol-gel matrix have a higher ability to oxidize D-glucose to D-gluconolactone compared to other matrixes, as shown by its high anodic peak current, i_{pa}. The chemistry of sol-gel itself yields a matrix that retains the natural conformation and the reactivity of the enzyme, thus increasing its activity.[13] The porous structure of the sol-gel matrix also ensured free

diffusion of glucose and the reaction products through the matrix and thus giving better sensor response.

The same, various types of Fc/SWCNTs/GOx modified electrodes were also tested to the response towards the presence of L-glucose in the solution. However, when L-glucose was used as an analyte, a couple of stable and well-defined redox peaks at approximately 190 and 340 mV at 25 mV/s were obtained (Figure 4.19 (B)). Unlike D-glucose, these systems did not follow EC' mechanism and were attributed to the redox reaction of the electroactive species present. This redox behaviour of ferrocene at the modified electrodes shows a reversible electrochemical response with the highest current response to L-glucose was obtained with Fc/SWCNTs/GOx/collagen/sol-gel electrode. This modified electrode seems to give a good response towards both glucose enantiomers as showed by a well-defined sigmoid catalytic wave corresponds to the presence of D-glucose and a high, well-defined peak shape wave that corresponds to L-glucose containing solution.

Figure 4.20 and 4.21 show the cyclic voltammograms of the ferrocene/SWCNTs/GOx electrodes, entrapped within collagen and collagen/sol-gel matrixes, respectively scan at different rate varies from 2 to 100 mV/s. Plot of peak currents (i_p) versus square root of scan rate ($\nu^{1/2}$) for in the CVs of ferrocene/SWCNTs/GOx electrode, showed a linear correlation in solutions containing D- and L-glucose when the enzyme entrapped within collagen/sol-gel matrix, however with the line passes not through the origin. Such relations of current versus square root of scan rate suggest a poor diffusion of mass transfer kinetics within the SWCNT/collagen/sol-gel electrode.[14] However, when the enzyme was entrapped within collagen matrix, only the anodic peak current (i_{pa}) showed a linear correlation with square root of scan rate ($\nu^{1/2}$) in the D-glucose-containing solution (Figure 4.20(A)). In the solution containing L-glucose, the ferrocene/SWCNTs/collagen GOx electrode showed a non-linear correlation between peak currents and the square root of scan rates nor the scan rates, which can be explained that the process at this modified electrode is not diffusional nor surface confine-controlled processes.

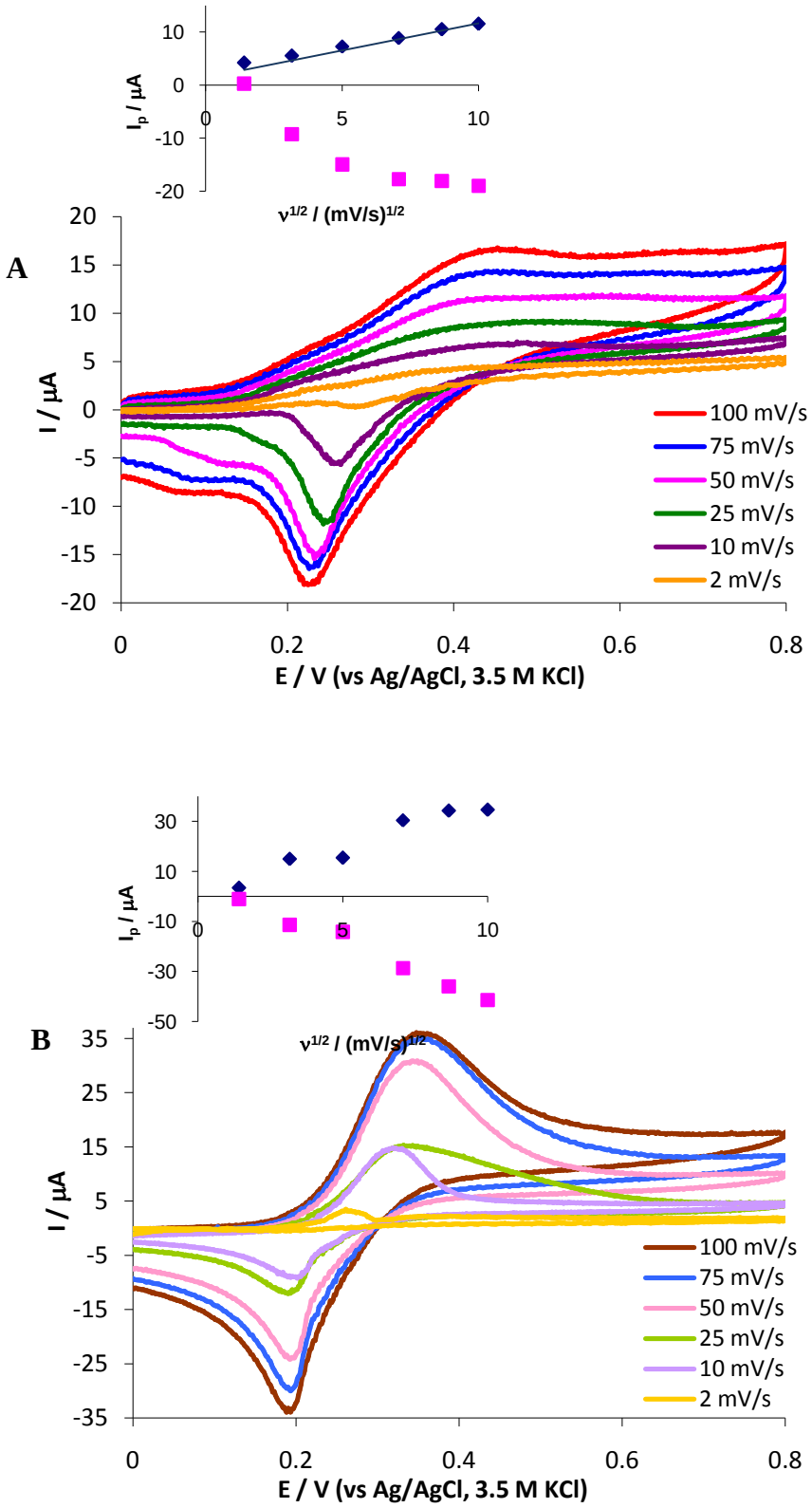

Figure 4.20: CVs of ferrocene-modified SWCNT with GOx entrapped within collagen matrix in 0.1 M PBS (pH 7) containing 10 mM (A) D- and (B) L-glucose. Scan rate: 2, 10, 25, 50, 75, 100 mV/s.

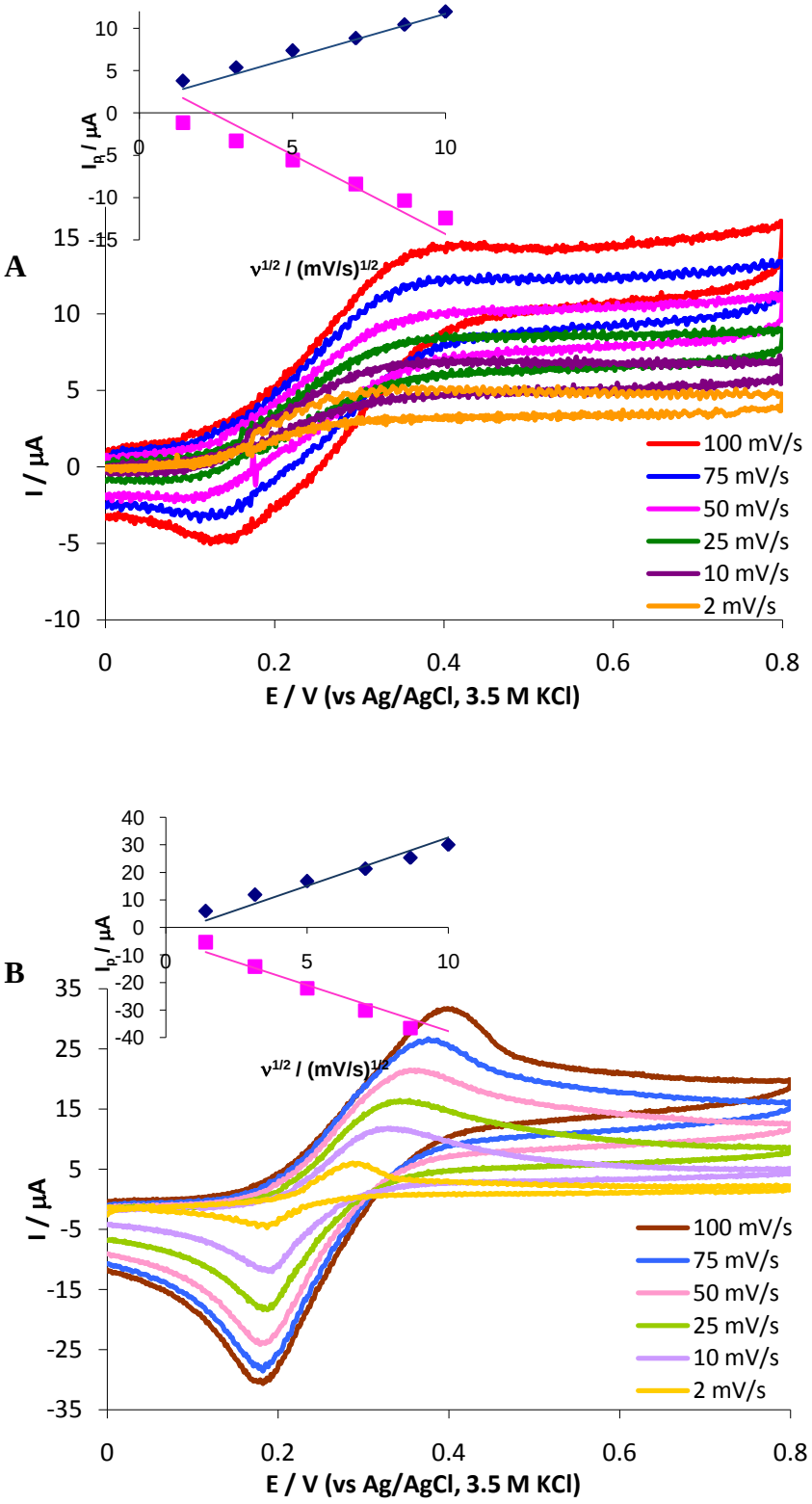

Figure 4.21: CVs of ferrocene-modified SWCNT with GOx entrapped within collagen/sol-gel matrix in 0.1 M PBS (pH 7) containing 10 mM (A) D- and (B) L-glucose. Scan rate: 2, 10, 25, 50, 75, 100 mV/s.

4.5.2 Ferrocene-modified MWCNTs with GOx Entrapped within Collagen and Collagen/Sol-gel Matrixes.

Recent electrochemical studies have shown the ability of CNTs to promote certain types of electron transfer reactions and enhance electrocatalytic activity.[11-12] Figure 4.22 displays CVs of the Fc/MWCNT/GOx entrapped within sol-gel, collagen and collagen/sol-gel matrixes in 0.1 M PBS (pH 7) containing 10 mM (A) D- and (B) L-glucose. Similar to that observed with SWCNT, Fc/MWCNT-modified GC electrodes also showed an enantioselective response towards D-glucose and L-glucose. Both collagen and collagen/sol-gel hybrid matrixes had enhanced the sigmoidal response to D-glucose with steady state current of 7.37 and 11.1 μA for collagen and collagen/sol-gel complex, respectively.

The sigmoidal response to D-glucose was found higher with collagen/sol-gel hybrid electrodes. The porous structure of the silicate matrix and the long-range organization of collagen/sol-gel complex, could lead to the better interaction between the hybrid complex and the GOx. Preliminary studies on the effect of the silicates on the collagen self-assembly process indicate that both hydrogen bonding and attractive electrostatic interactions had been improved by the collagen/silica interface.[15] This electrostatic interaction was effective during the collagen gel silicification at neutral pH, where silicates were negatively charged, that possibly favouring silica deposition on collagen matrix.[16]

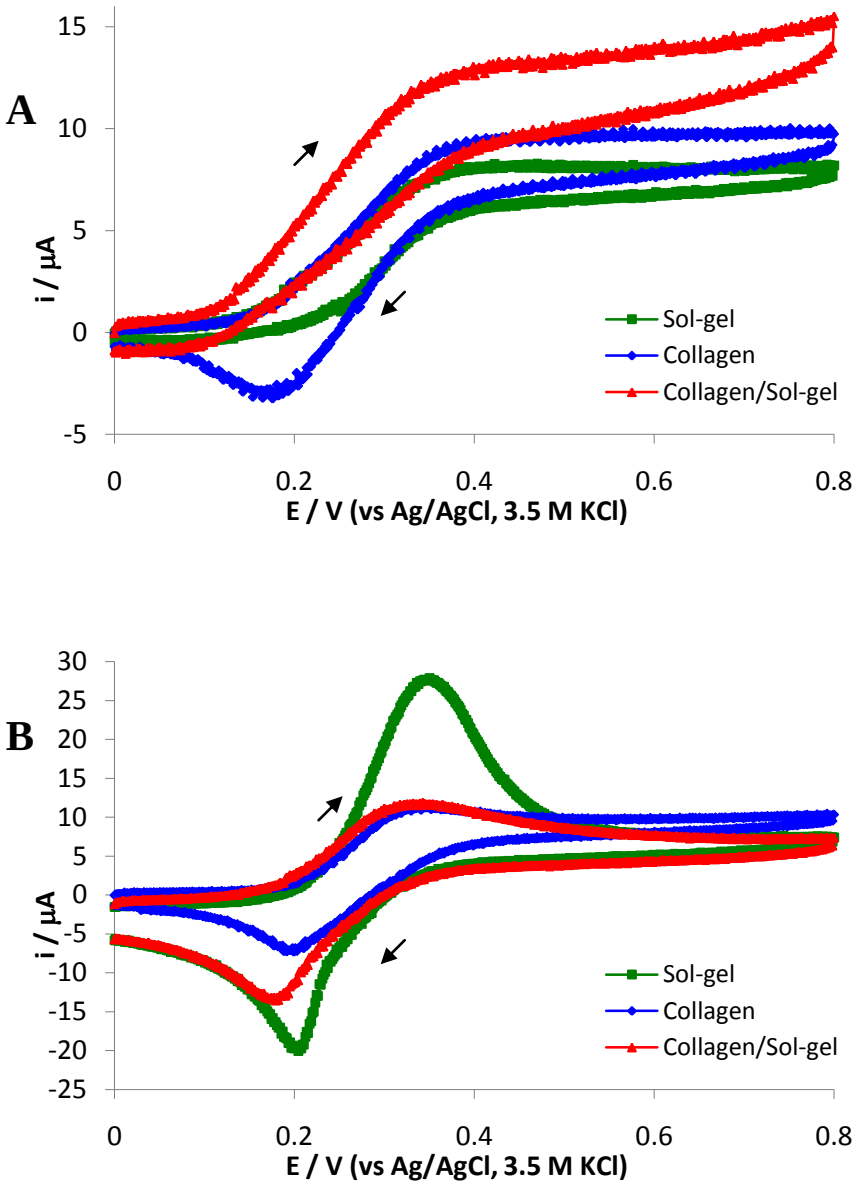

Figure 4.22: CVs of ferrocene-modified MWCNT with GOx entrapped within collagen and collagen/sol-gel matrix in PBS (0.1 M, pH 7) containing 10 mM (A) D- and (B) L-glucose. Scan rate, 25 mV/s.

The CVs exhibit anodic and cathodic peak currents, which can be assigned to the oxidation and reduction of ferrocene, which indicates the redox activity of Fc-GOx on the electrode surface. A pair of well-defined peak was obtained in the CVs containing L-glucose as analyte with E_{pa} and E_{pc} of ~ 350 and 180 mV, respectively. The anodic peak current (i_{pa} = 28.4 µA) was observed higher in the sol-gel matrix compared to that obtained in collagen/sol-gel hybrid complex. However, the minimum

peak to peak separation of 146.25 mV was also observed with Fc/MWCNT/GOx constructed with collagen matrix electrode.

Figure 4.23 shown plot of Fc/MWCNT/GOx entrapped within collagen matrix in 0.1 M PBS (pH 7) containing 10 mM (A) D- and (B) L-glucose, scanned at various scan rates. Non-linear correlation between peak currents (i_p) and square root of scan rate ($v^{1/2}$) was also obtained in these CVs. Thus, the diffusion coefficient (*D*) value couldn't be determined by Randle-Sevcik equation because of these non-linear correlations. This non-linear relationship was also observed in the CVs of Fc/MWCNT/GOx entrapped within collagen/sol-gel matrix in both D- and L-glucose.

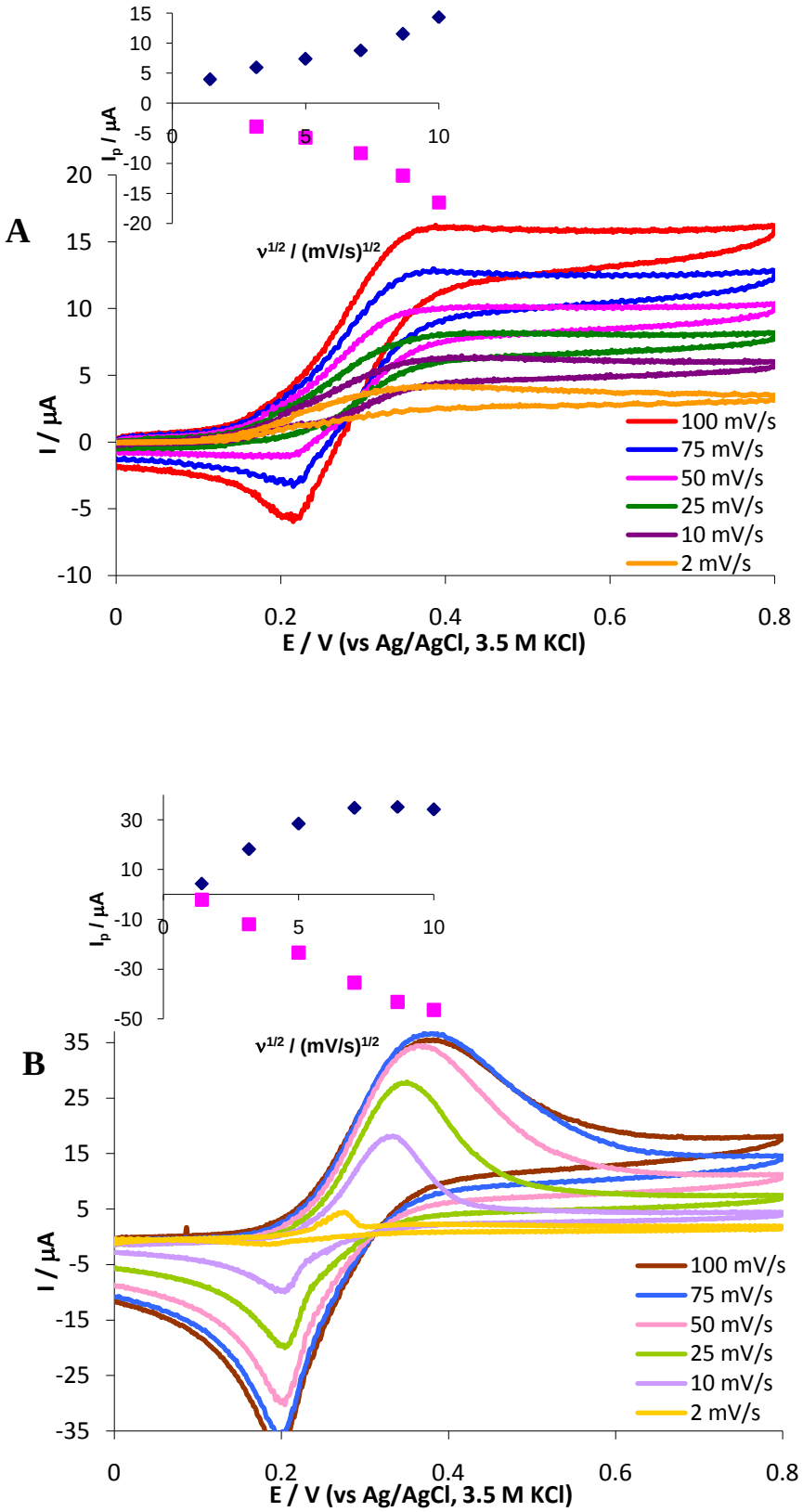

Figure 4.23: CVs of ferrocene-modified MWCNT with GOx entrapped within collagen matrix in 0.1 M PBS (pH 7) containing 10 mM (A) D- and (B) L-glucose. Scan rate (from inner to outer) 2, 10, 25, 50, 75, 100 mV/s.

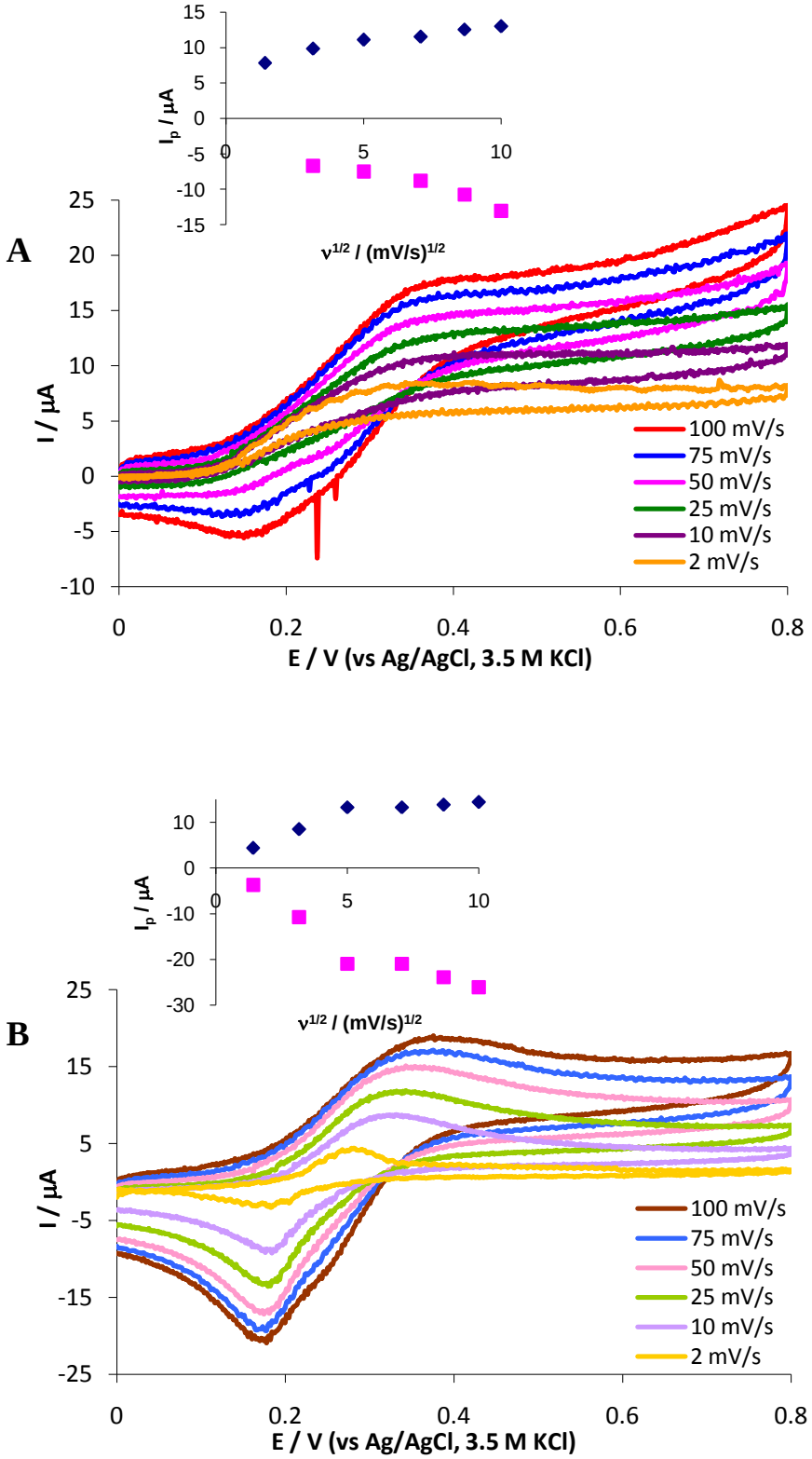

Figure 4.24: CVs of ferrocene-modified MWCNT with GOx entrapped within collagen/sol-gel matrix in 0.1 M PBS (pH 7) containing 10 mM (A) D- and (B) L-glucose. Scan rate (from inner to outer) 2, 10, 25, 50, 75, 100 mV/s.

This section had successfully studied a new approach in bio-sensing by fabrication of two chiral composites of carbon nanotubes. Biocomposite electrodes made of collagen, silica hybrids and ferrocene-modified carbon nanotubes were fabricated by dispersing ferrocene-modified single walled and multi walled carbon nanotubes, into the collagen and collagen/sol-gel hybrid matrixes. The optimum carbon nanotubes loadings were optimized to 0.5 mg/mL for both ferrocene-modified SWCNTs and MWCNTs electrodes.

Electrochemical studies revealed an enantioselective response to D- and L-glucose, which different behaviours of CVs were obtained coresponse to the presence of D- and L-glucose in the tested solution. Both collagen and collagen/sol-gel hybrid matrixes showed sigmoidal shape CVs in response to D-glucose but exhibit peak shape CVs when L-glucose is presence in the solution. These different behaviour in the CVs of both ferrocene-modified SWCNTs and MWCNTs electrodes towards both enantiomer of glucose was further investigated by chronoamperometric technique as will be explained in further details in the next chapter.

References

(1) Clark, L. C.; Lyons, C. *Annals of the New York Academy of Sciences.* **1962**, *102*, 29.
(2) Updike, S. J.; Hicks, G. P. *Nature.* **1967**, *214*, 986.
(3) Guilbaul, G. G.; Lubrano, G. J. *Abstr. Pap. Am. Chem. Soc.* 1973, 12.
(4) Wang, J. *Chem. Rev.* **2008**, *108*, 814.
(5) Katayama, Y.; Yukumoto, M.; Yamagata, M.; Miura, T.; Kishi, T. *Electrochemical behavior of ferrocene in some hydrophobic room temperature molten salt systems*; Shanghai Univ: Shanghai, 2001.
(6) Chanfreau, S.; Cognet, P.; Camy, S.; Condoret, J. S. *J. Electroanal. Chem.* **2007**, *604*, 33.
(7) Qiu, J. D.; Wang, R.; Liang, R. P.; Xia, X. H. *Biosens. Bioelectron.* **2009**, *24*, 2920.
(8) Lawrence, N. S.; Deo, R. P.; Wang, J. *Anal. Chem.* **2004**, *76*, 3735.
(9) Song, Z.; Huang, J. D.; Wu, B. Y.; Shi, H. B.; Anzai, J. I.; Chen, Q. *Sens. Actuator B-Chem.* **2006**, *115*, 626.

(10) Compton, R. G., and Banks, C.E. *Understanding Voltammetry*; World Scientific Publishing Co. Pte. Ltd.: United Kingdom, 2007.
(11) Zou, Y. J.; Xian, C. L.; Sun, L. X.; Xu, F. *Electrochim. Act.* **2008**, *53*, 4089.
(12) Zou, Y. J.; Xiang, C. L.; Sun, L. X.; Xu, F. *Biosens. Bioelectron.* **2008**, *23*, 1010.
(13) Xu, Z.; Chen, X.; Dong, S. J. *Trac-Trends Anal. Chem.* **2006**, *25*, 899.
(14) Pandey, P. C.; Upadhyay, S. *Sens. Actuator B-Chem.* **2001**, *76*, 193.
(15) Eglin, D.; Mosser, G.; Giraud-Guille, M. M.; Livage, J.; Coradin, T. *Soft Matter*. **2005**, *1*, 129.
(16) van Bommel, K. J. C.; Shinkai, S. *Langmuir*. **2002**, *18*, 4544.

CHAPTER 5

CHIRAL GLUCOSE AND LACTATE BIOSENSORS

5.1 Introduction to Chiral Glucose Biosensors

D-Glucose is the most important carbohydrate in human cells. Its concentration in the blood is about 1 g dm^{-3}. The small size and solubility in water of glucose molecules allows them to pass through the cell membrane into the cell.

Glucose ($C_6H_{12}O_6$) contains six carbon atoms, one of which is part of an aldehyde group, and is therefore referred to as an aldohexose. In solution, the glucose molecule can exist in an open-chain (acyclic) and ring (cyclic) form in equilibrium. At pH 7 and in the solid phase, the cyclic form is predominant. Glucose is commonly available in the form of a white substance or as a solid crystal. It can also be commonly found as an aqueous solution.

There are two forms of the cyclic glucose molecule, which are α-glucose and β-glucose. The rearrangement of the cyclic forms produces α-glucose when the hydroxyl group attached to C-1 is positioned trans to the -CH_2OH group at C-5, while β-glucose is produce when it is positioned cis to the -CH_2OH group. Isomers, such as these, which differ only in their configuration about their carbonyl carbon atoms, are called anomers.

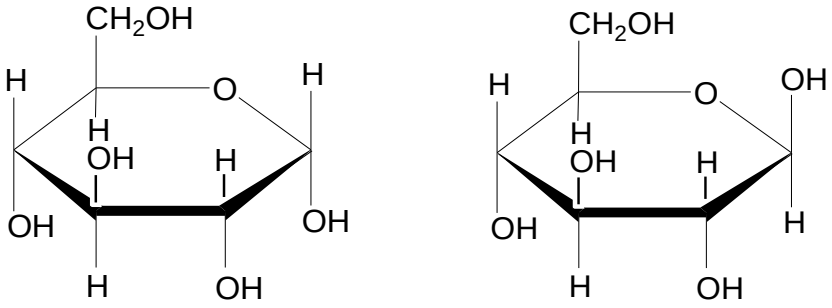

α-D-glucose β-D-glucose

Figure 5.1: The structure of α-D-glucose and β-D-glucose.

Stereoisomers are compounds in which the atoms are linked in the same order but differ in their spatial arrangement. Enantiomers are compounds that are mirror images of each other but are not identical, comparable to left and right. Identical molecules can be made to correspond to each other by flipping and rotating. However, enantiomers cannot be made to correspond to their mirror images by flipping and rotating. The following structures illustrate the difference between D-glucose and L-glucose. Between these two stereoisomers, only D-glucose is biologically active, where as the L-glucose cannot be metabolized by cells in the biochemical process known as glycolysis.

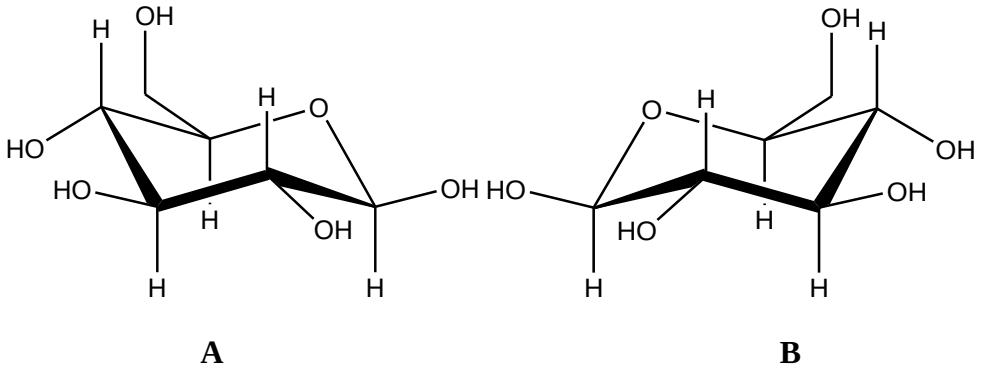

Figure 5.2: The stereoisomers of β-D-(+)-glucose (A), and β-L-(-)-glucose (B).

Glucose has a huge significant importance in public health industry. Diabetes mellitus is a worldwide health problem that arises from insulin deficiency and hyperglycemia. This metabolic disorder is reflected by blood glucose concentrations lower or higher than the normal range of 80-120 mg/dL (4.4-6.6 mM).[1] The complications lead from diabetes is numerous, including higher risks of heart disease, blindness of kidney failure. These complications can be reduced through continuous control of blood glucose levels. Due to this significant importance of testing blood glucose level by diabetic patients, 85% of the entire biosensor market comes from glucose biosensors.[1]

There are some reports involving chiral glucose sensors. Chiroselective mediated electron-transfer has been studied intensively using diffusional chiral electron

mediators. The enantiomeric electron relays (S)- and (*R*)*N*,*N*-dimethyl-1-ferrocenyl-ethylamine were reported to stimulate chiroselective bioelectrocatalyzed oxidation of glucose in the presence of glucose oxidase.[2] The bioelectrocatalyzed oxidation of glucose was ca. 2-fold enhanced in the presence of the (*S*)-isomer as compared to (*R*)-isomer.

The concept of enantioselective electrical contacting of redox-enzymes and electrode surfaces was also developed by the organization of a chiral electron-transfer mediator as a monolayer on an electrode surface.[3] (*R*)- and (*S*)-2-methylferrocene carboxylic acid were assembled as monolayers on Au-electrodes. The monolayer-mediated oxidation of glucose in the presence of glucose oxidase showed a ca. 1.9-fold enhancement at the electrode functionalized by the (*S*)-enantiomer over the electrode functionalized by the (*R*)-enantiomer. All of these researches involved chiral mediators as a chiroselective agent for a glucose sensor. The key idea of this research is to develop a chiral glucose biosensor by using ferrocene-modified GC electrodes in the presence of collagen and collagen/sol-gel matrices as immobilizing agent to glucose oxidase (GOx). The inherent chirality of collagen elicits a chiral recognition.

Figure 5.3 demonstrates the mechanism of chiral glucose biosensors used in this study. In the biosensor development, the immobilized D-GOx oxidizes either D- or L-lactate to gluconolactone in the presence of ferrocene, which acts as an acceptor of electrons generated in the enzymatic reaction and is transformed to its reduced form. This, in turn, diffuses to the electrode, where is reoxidized back into its oxidized form. The magnitude of this catalytic current can be employed as the analytical signal in the determination of the concentration of glucose.

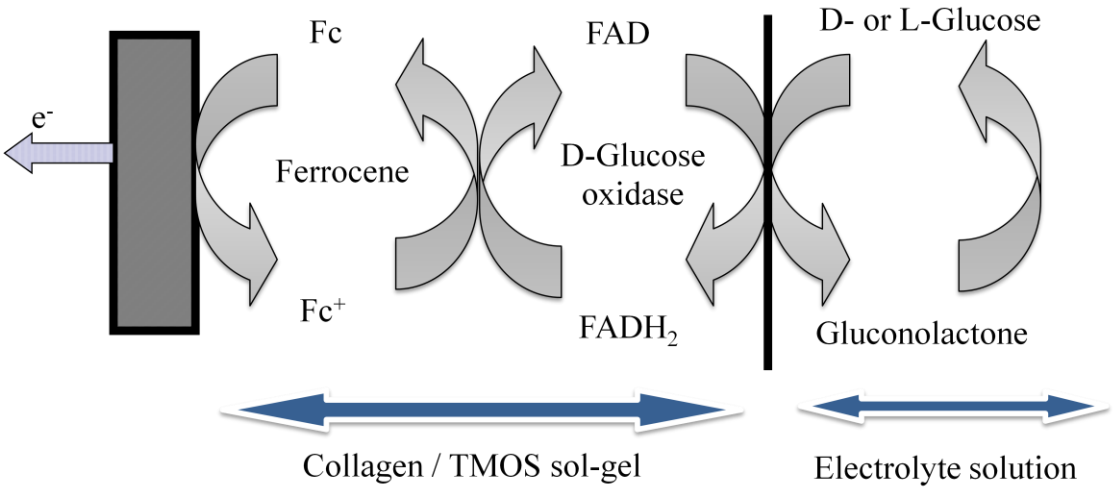

Figure 5.3: The mechanism of chiral glucose biosensors.

5.2 Introduction to Chiral Lactate Biosensors

Lactate, which has a chemical name of 2-hydroxypropanoate, was discovered by Scheele, C. (1780)[4], who isolated it from sour milk. It is the simplest hydroxycarboxylic acid and exist as two stereoisomers due to its asymmetric C2 atom (Figure 5.4). Both enantiomers have similar physical and chemical properties with pK_a of 3.86. At physiological pH, lactate always dissociates freely yielding a lactate ion:lactic acid ratio of 3000:1.[5]

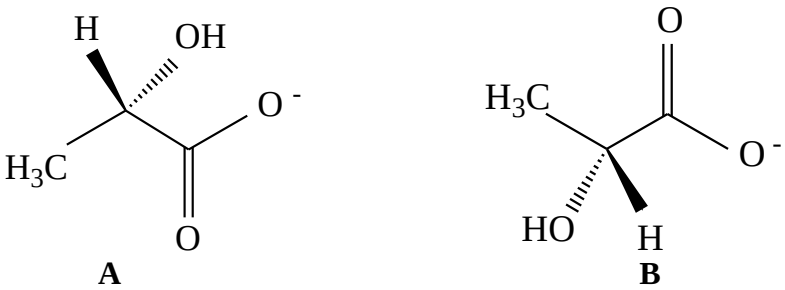

Figure 5.4: The stereoisomers of L-(+)-lactate (A), and D-(-)-lactate (B).

L-Lactate is the key metabolite of the anaerobic glycolytic pathway. Glycolysis is a metabolic process in which one mole of glucose is catabolized to two moles of each pyruvate, NADH and energy in the form of ATP, according to the Equation 5.1:

$$\text{Glucose} + 2\text{ATP} + 2\text{NAD}^+ + 2\text{P}_i \rightarrow 2\text{pyruvate} + 2\text{ATP} + 2\text{NADH} + 2\text{H}^+ \qquad (5.1)$$

Under aerobic conditions, pyruvate is further oxidized by mitochondrial enzymes to CO_2 and H_2O. In the absence of oxygen, the anaerobic glucose metabolism will produce energy by converting glucose to pyruvate using the oxidative potential of NAD^+. This NAD^+ is then regenerated from reduced NADH by the conversion of pyruvate to lactate. Figure 5.5 shows the glycolytic pathway involves in living organisms.

L-Lactate dehydrogenase (LDH) is an enzyme that catalyzes the inter-conversion of pyruvate to lactate. This enzymatic reaction oxidizes NADH and replenishes NAD^+, which is essential for the glycolytic conversion of glucose to pyruvate. In abnormal cells, the glycolysis process is increases in response to hypoxia.[6] Hypoxia is a pathological condition in which the body as a whole (generalized hypoxia) or a region of the body (tissue hypoxia) is deprived of adequate oxygen supply. For example in people with cancer cells, the glycolysis could further undergo with increased production of lactate even in the presence of oxygen.[6] This could contribute to the importance of measurement of lactate content in blood for cancer sufferer.

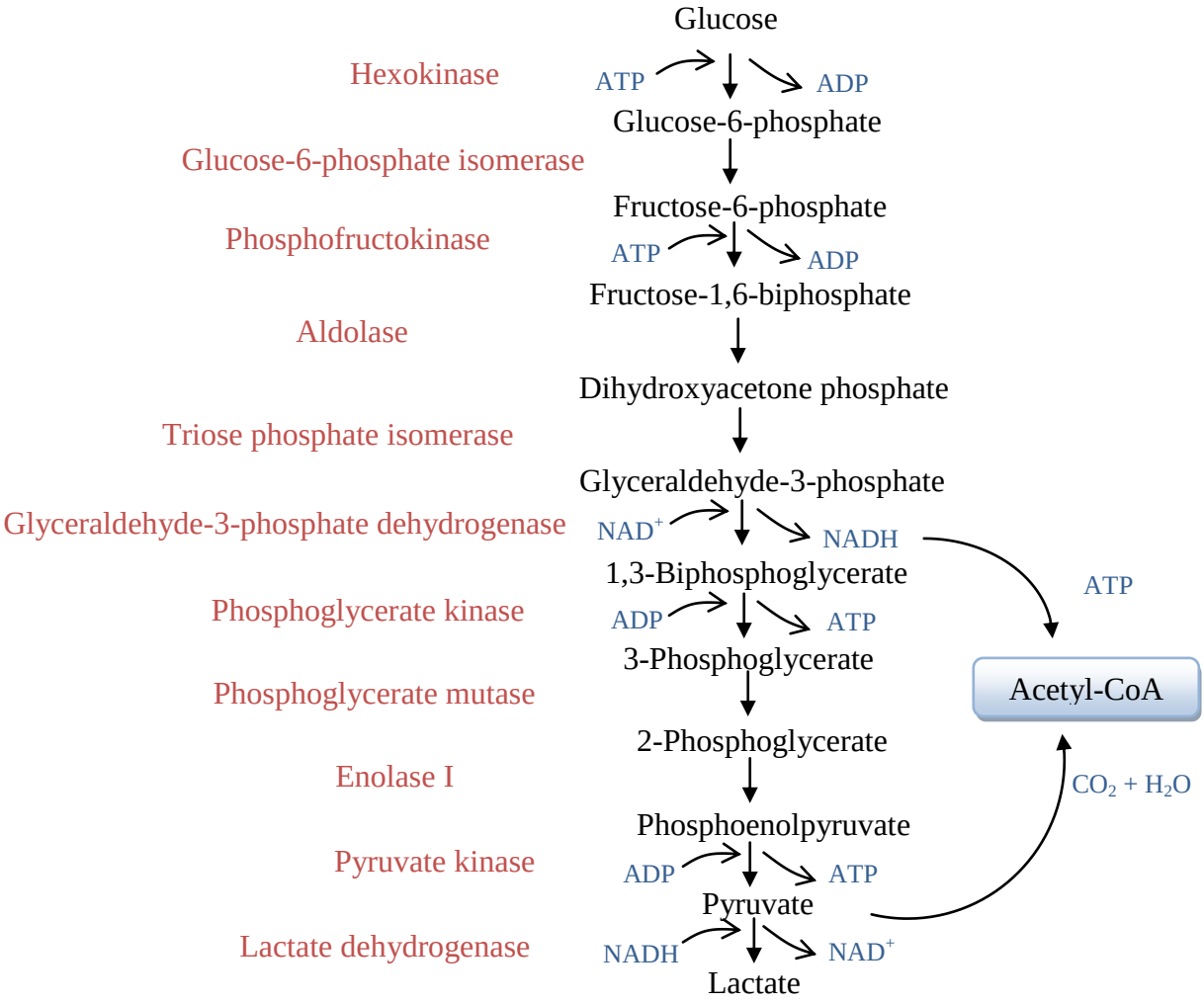

Figure 5.5: The glycolytic pathway.

Lactate is a universal metabolite of nearly all living organisms and a natural or an artificial component of food products. It is a salt of lactic acid that is generated from glucose in many organisms. In mammals, L-lactate is the major stereoisomer formed in the intermediary metabolism, whereas D-lactate present at only about 1-5% of the total lactate concentration. In normal healthy people, the serum L-lactate concentration is approximately 1-2 mmol/L, with the presence of D-lactate formed in nanomolar concentrations via the methylglyoxal pathway.[5] While L-lactate is mainly present in blood, the D- enantiomer is usually found in human physiologic fluids originate from bacterial production in the intestinal tract.[5]

The research on the development of lactate biosensors has been increasing in the past four decades mainly due to the importance of lactate especially in clinical diagnostics, food industry and sports medicine.[7-11] A rapid determination of lactate in blood is important for particular for people in special care unit in hospitals, especially for cardiac patients and those in diabetes control, because the L-lactate level may be used to indicate the oxygen supply for those particular patients. Lactate is always of interest as indicator of many metabolic disorders, including cerebral ischemia of the respective tissue. [12] An elevated lactate level in blood can be used to predict multiple organ failure and death of patient with septic shock. L-lactic acidosis also might occur as a result of the decreased in tissue oxygenation, left ventricular failure, drug toxicity and underlying disease states.[5,7] Although D-lactic acidosis is less common occur in humans, there are circumstances that it can become elevated in the blood of diabetic people that also can be used as a marker of sepsis, ischemia and trauma.[5]

Lactate is also useful in sports medicine, especially for estimating physical conditions of athletes. Blood lactate levels during exercise are used as an indicator for the athletic training status and fitness.[13-14] The normal values of L-lactate in healthy persons will significantly higher at prolonged exercise conditions.[15-16] At anaerobic conditions, muscles use carbohydrates for energy to support the exercise and produce lactic acid, hence increasing the concentration of lactate in blood to certain defined point of exercise, termed the lactate threshold. At this point, lactate is being produced faster than it can be metabolised and then accumulates in blood. Elevated blood lactate levels tend to lower blood pH value and consequentially disturb the metabolism of protein structure. This will further cause the lactate poisoning, which induces some discomfort such as muscle ache or fatigue.[17] Thus it is therefore important to monitor lactate levels in athletes during and after training, hence increase the importance to carry out this measurement in a continuous mode, which can be achieve by using biosensors.

The importance of D- and L-lactate also can be found in many food and fermentative industry. Both D- and L-lactate can be produced naturally by a group of bacteria known as lactic acid bacteria (LAB).[18] These type of bacteria produce lactate as the main metabolic end product of carbohydrate fermentation.[19] Fermentative products such as wine, cured meat and fish and also pickled vegetables produce a mixture of both enantiomers of lactate. Due to this fact, L- and D-lactate is commonly used as a specific indicator to the presence of bacteria fermentation, thus as an indicator for the freshness

and quality of the food.[18] Many other applications of lactate measurements in food industry will be explained in further detail in Chapter 7.

As mentioned above, it is clear that lactate is a metabolite that have a great interest in many industries, thus it is important to detect and measure the existence of both L- and D-lactate in various media. The development of electrochemical biosensor as an alternative method for lactate detection has received considerable interest because of their simplicity, high sensitivity and fast response. To date, many studies dealing with L- and D-lactate electrochemical biosensors have been reported.[11,14,20-26] Basically, most lactate biosensors reported in literature are based on the immobilized enzymes lactate oxidase (LOx) or lactate dehydrogenase (LDH). In this research, LOx from *Pediococcus* sp. is used as the enzyme that catalyzes the oxidation of lactate to pyruvate and hydrogen peroxide, which can be oxidized at the electrode surface according to the Equation 5.2. Therefore, LOx was preferred over LDH due to its simple reaction, which involves aerobic oxidation of lactate to pyruvate and H_2O_2.

$$\text{Lactate} + \text{LOx}_{\text{ox}} \rightarrow \text{Pyruvate} + \text{LOx}_{\text{red}} \qquad (5.2)$$

$$\text{LOx}_{\text{red}} + O_2 \rightarrow \text{LOx}_{\text{ox}} + H_2O_2$$

$$H_2O_2 \rightarrow O_2 + 2e^-$$

However, the determination of enzymatically produced hydrogen peroxide needs to be obtained at a high oxidation potential at an unmodified electrode, which causes severe interference arising from easily electro-oxidizable species. Furthermore, the fluctuation of O_2 concentration in the solution brings the system complexity, and affects the detection limit. Mediator-based lactate sensors have been further developed to overcome from fluctuation of O_2 concentration.[27] In this study, the immobilized L-LOx enzyme within various matrixes will oxidizes either L- or D-lactate to pyruvate in the presence of ferrocene, which act as a stationary mediator on the surface of the GC electrode. In the presence of lactate, the enzymatic reaction occurs according to the following pathways:

$$\text{Lactate} + \text{LOx}_{\text{ox}} \rightarrow \text{Pyruvate} + \text{LOx}_{\text{red}} \quad (5.3)$$

$$\text{LOx}_{\text{red}} + Fc^{+} \rightarrow \text{LOx}_{ox} + Fc$$

$$Fc \rightarrow Fc^{+} + e^{-}$$

Figure 5.6 demonstrates the mechanism of chiral lactate biosensors used in this study. In the biosensor assembly developed, the immobilized L-LOx oxidizes either L- or D-lactate to pyruvate in the presence of ferrocene, which acts as an acceptor of electrons generated in the enzymatic reaction and is transformed to its reduced form. This, in turn, diffuses to the electrode, where is re-oxidized back into its oxidized form. The electrode serves as a secondary acceptor of electrons able to regenerate the redox mediator used in the enzymatic reaction, so the magnitude of this catalytic current can be employed as the analytical signal in the determination of the lactate concentration.

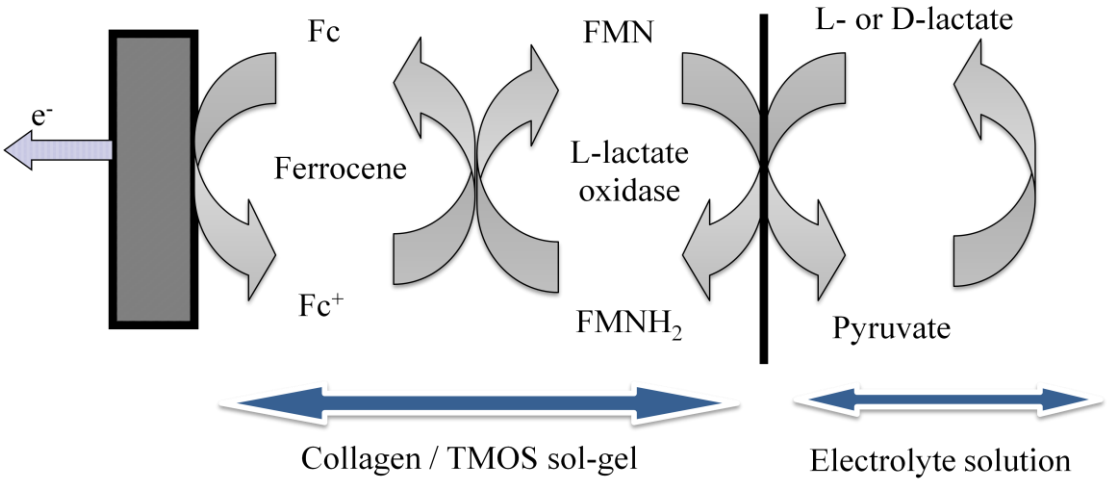

Figure 5.6: The mechanism of chiral lactate biosensors.

Both glucose and lactate have a significant influence between each another as shown in the glycolytic pathway in Figure 5.5. Glucose is a main nutrient in the human brain, while L-lactate and pyruvate are formed from glucose in an actively glycolyzing

system under anaerobic and aerobic conditions, respectively. These metabolites are of interest in many metabolic disorders, including cerebral ischemia and lactate acidosis in diabetic patients.[12] Therefore, the simultaneous on-line monitoring of glucose, L-lactate, and pyruvate in the brain would be of great benefit for studies on glucose metabolism.

In food industry, the concentration of D-glucose and L-lactate in food products has been shown to be an indicator of bacterial activity, which may result in a drastic alteration in the quality of the final product. Hence, the simultaneous measurement of these compounds is of great importance for quality control in food production.[28-29]

In this section, chiral glucose and lactate biosensors based on enzymes D-GOx and L-LOx immobilized within TMOS sol-gel, collagen and/or TMOS sol-gel matrixes in the presence of ferrocene as mediator is monitored. Glucose oxidase system was used as the benchmark due to its widely studied in terms of its physical and electrochemical behaviour. Lactate oxidase was chosen as a model enzyme because very few studies on its electrochemical activity and behaviour have been carried out, although its analyte which is lactate is of great interest in various fields and industry (Section 5.2). Collagen, a positively charged biopolymer was selected to entrap the negatively charged GOx and LOx at neutral pH, due to its good stability and biocompatibility.[30] The effect of collagen to enantioselectivity of D- and glucose as well as L- and D-lactate was also studied in further detail.

5.3 Electrochemical Studies

In this section, the GC electrode has been modified with ferrocene and entrapped GOx or LOx within sol-gel, collagen and collagen/sol-gel matrix. The biosensors were developed according to the mechanisms shown in Figure 5.3 and 5.6. The new chiral glucose and lactate biosensors were investigated in terms of the electrochemical behaviour and their amperometric responses.

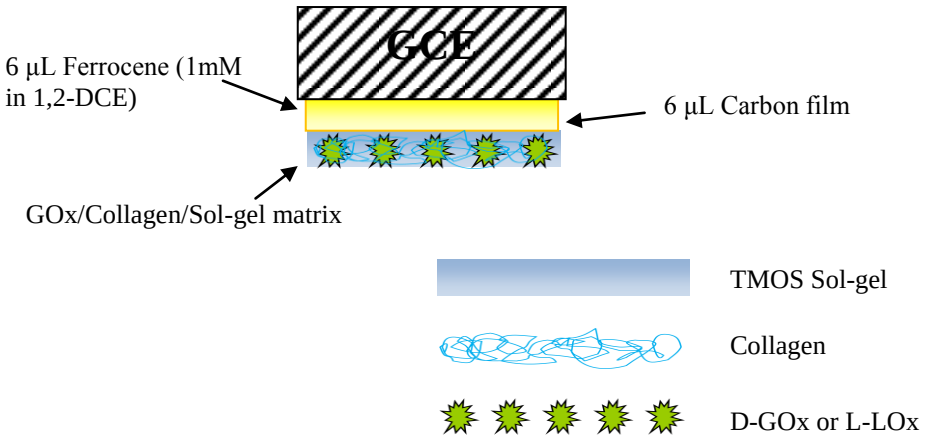

Figure 5.7: Diagram illustrated the layers on the modified GC electrode.

Cyclic voltammetry (CV) and electrochemical impedance spectroscopy (EIS) were used to characterize the modification of the GC electrodes. Figure 5.8 and 5.9 compare the CVs response at Fc/GOx electrode, entrapped within (a) sol-gel, (b) collagen and (c) collagen/sol-gel matrix in PBS (0.1 M, pH 7) containing 2 mM D- and L-glucose, respectively. Similar to that observed in Section 4.5, the shape of the CVs here have also shown a significant difference between both enantiomers of analytes in the buffer solution. When the solution was added with D-glucose, the CVs showed a sigmoidal shape (Figure 5.8), whereas it becomes peak shape when L-glucose is presence in the solution (Figure 5.9). The steady state current responses obtained for D-glucose detection indicates the typical characteristic of electrocatalytic reaction in this system. On the other hand, a pair of well-defined peak-shaped CVs observed in L-glucose detection depicts a semi-infinite linear diffusion-controlled redox process of the Fc/Fc^{+} couple at those GOx-modified electrodes. Overall, the redox peaks currents correspond to the signal to L-glucose were found higher compared to the steady state currents arises from the detection of D-glucose.

For both D- and L-stereoisomers of glucose, the highest current response was obtained with Fc/GOx/Collagen/Sol-gel electrode, indicate that this modified electrode gave a better response to both D- and L-glucose. The hybrid matrixes of collagen and TMOS sol-gel leads to better interaction between the complex and the GOx due to the microenvironment and the long-range organization developed in the hybrid complex.

The collagen/sol-gel interface had improves by hydrogen bonding and electrostatic interaction between both matrixes.[31]

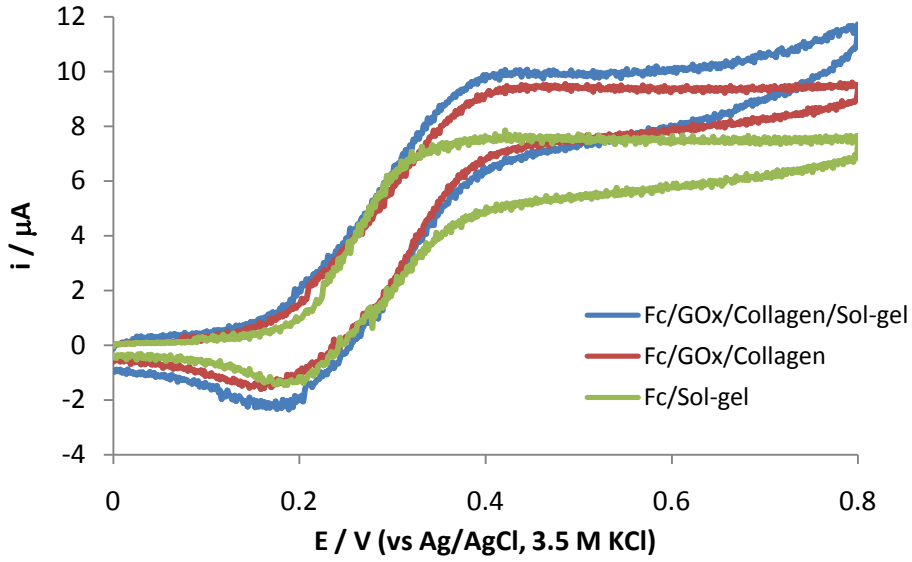

Figure 5.8: CVs of Fc/GOx electrode entrapped within sol-gel, collagen and collagen/sol-gel matrixes in 0.1 M PBS (pH 7) containing 2 mM D-glucose. Scan rate: 10 mV/s.

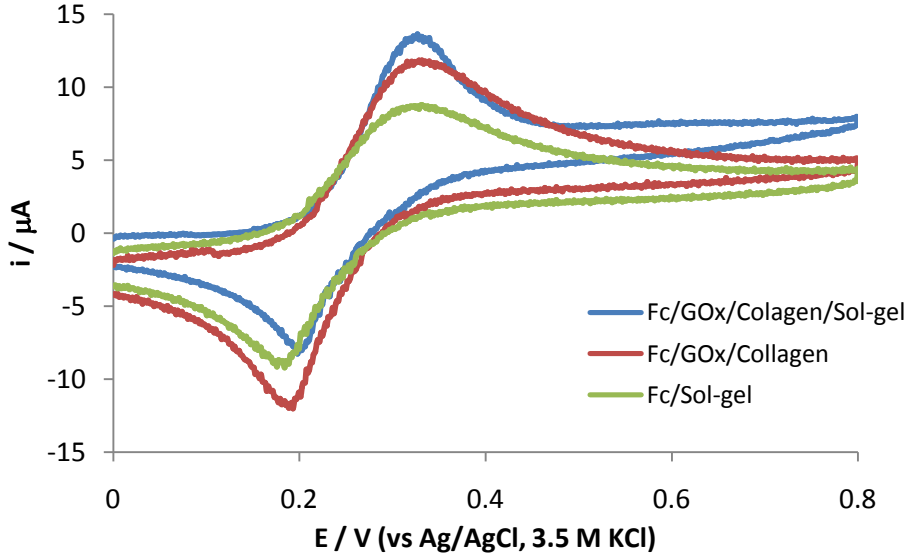

Figure 5.9: CVs of Fc/GOx electrode entrapped within sol-gel, collagen and collagen/sol-gel matrixes in 0.1 M PBS (pH 7) containing 2 mM L-glucose. Scan rate: 10 mV/s.

Figure 5.10 and 5.11 compare the CVs response at Fc/LOx electrode, entrapped within sol-gel, collagen and collagen/sol-gel matrixes in PBS (0.1 M, pH 7) containing 2 mM L- and D-lactate, respectively. The shape of the CVs seems to show a similar behaviour between those GOx- and LOx-modified electrodes. In the presence of L-lactate, the CVs of various Fc/LOx-modified electrodes showed a shape that tending towards the sigmoidal shape behaviour indicates the characteristic of electrocatalytic reaction in the L-LOx/L-lactate system. The highest oxidation current response of 6.6 μA was obtained with Fc/LOx/Collagen/Sol-gel electrode indicates a better response to L-lactate at this modified electrode.

Different characteristics of the CVs were observed when the LOx-modified electrodes were tested for the presence of D-lactate. There are well-peak shaped CVs with the characteristics of a redox reaction of Fc/Fc^+ at various Fc/LOx-modified electrodes when they were tested to detect 2 mM of D-lactate presence in the PB solution. In this L-LOx/D-lactate system, the highest redox current of 39 μA was obtained with Fc/LOx/Collagen electrode. However, by introduction of TMOS sol-gel to collagen matrix contributes to an obvious decrease in redox peak currents and decrease in peak-to-peak separation. Collagen is said to have a strong effect to increase the enantioselectivity towards D-lactate.

A further dramatic decrease in redox peak current was observed at Fc/LOx/Sol-gel electrode when used to detect D-lactate. In fact, the value of anodic peak current response to D-lactate is much lower compared to current response to L-lactate. This was in contrast to other collagen-based modified electrodes where the current responses to D-lactate was higher from the current responses to L-lactate. This different behaviour in the enantioselectivity response needs to further analyzed by using the amperometric technique.

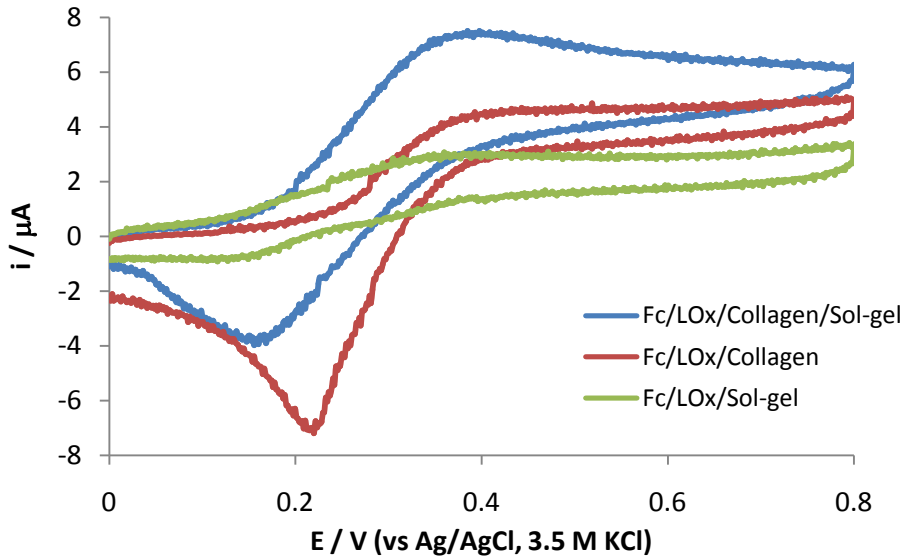

Figure 5.10: CVs of Fc/LOx electrode entrapped within sol-gel, collagen and collagen/sol-gel matrixes in 0.1 M PBS (pH 7) containing 2 mM L-lactate. Scan rate: 10 mV/s.

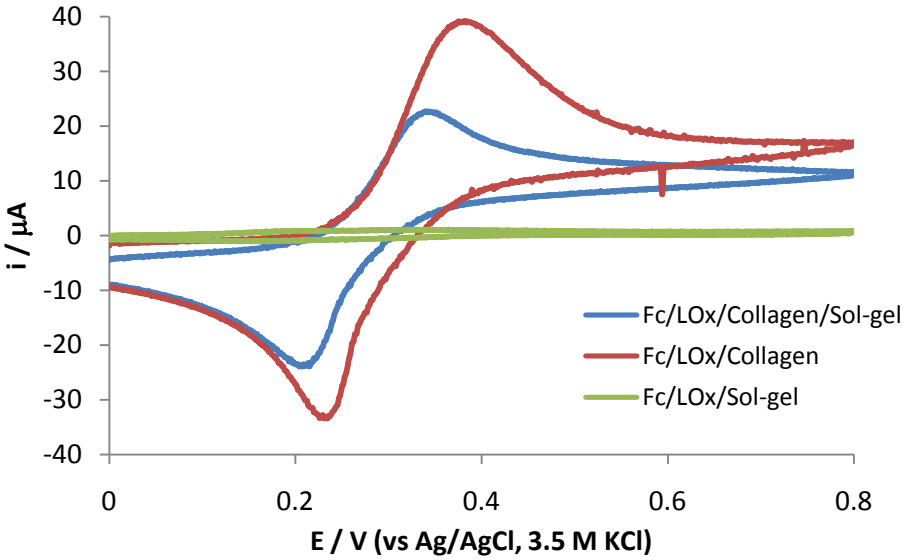

Figure 5.11: CVs of Fc/LOx electrode entrapped within sol-gel, collagen and collagen/sol-gel matrixes in 0.1 M PBS (pH 7) containing 2 mM D-lactate. Scan rate: 10 mV/s.

The process at the modified electrodes was also monitored by EIS, which is an effective method that always used for probing the interfacial properties of modified electrodes.[32-36] The Nyquist plot of impedance spectra includes a semicircle portion and a linear portion, with the former at higher frequencies corresponding to the electron transfer limited process and the latter at lower frequencies corresponding to the diffusion process. The electron transfer resistance (R_{ct}) at the electrode surface is equal to the semicircle diameter, which can be used to describe the interface properties of the electrode. Figure 5.12 displays the bare and modified GC electrodes, obtained in 5 mM $Fe(CN)_6^{3-/4-}$ and 0.1 M KCl solution. They were measured at the formal potential of the electrochemical probe.

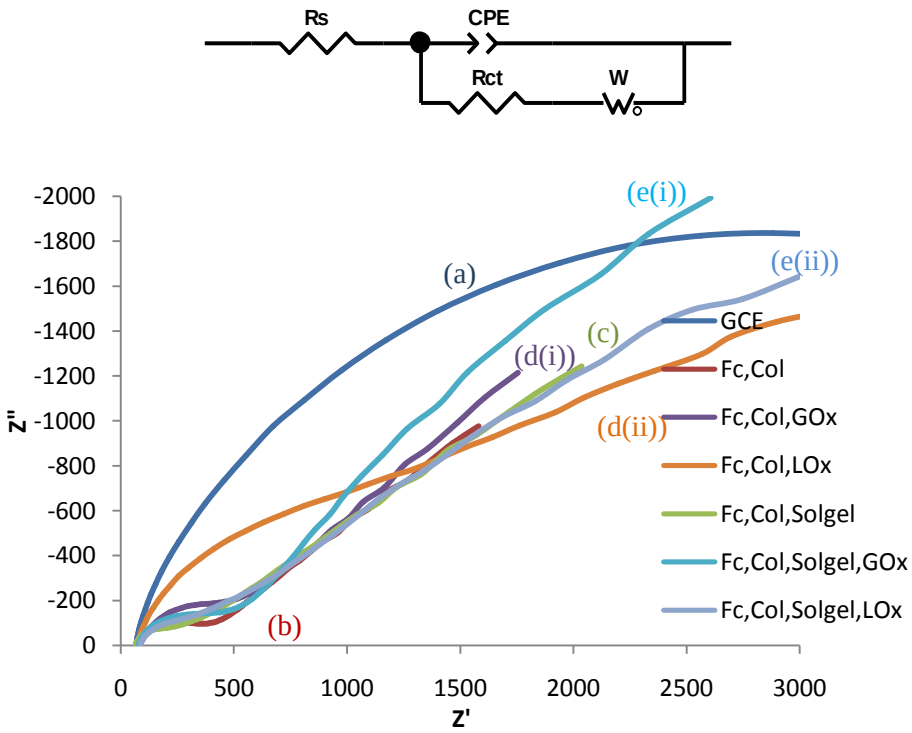

Figure 5.12: The Nyquist plot of impedance spectra obtained from bare and modified GC electrode.

As shown in Figure 5.12, the R_{ct} of the bare GC electrode can be estimated to be 745 Ω (curve a). This R_{ct} value is quite similar with the value obtained from literature (R_{ct} = 750 Ω).[37] After deposition a layer of Fc/Collagen and Fc/Collagen/Sol-gel

matrixes, the R_{ct} decreases dramatically to 257 and 147 Ω at curves b and c, respectively. This could be due to the increased conductivity of Fc-modified collagen and collagen/sol-gel film, and thus facilitated electron-transfer rate. It can be seen that the presence of TMOS sol-gel in the collagen matrix further reduces the R_{ct} suggesting that these modified electrode possess better electrocatalytic activity compared to collagen enzyme electrode. However, the R_{ct} increased to 379 and 366 Ω (curves d(i) and e(i), respectively) after deposition of GOx on both collagen and collagen/sol-gel electrodes, respectively. On the other hand, after deposition of LOx to Fc/collagen GC electrode, the defining point between semicircle and the straight-line portions become not so really clear, thus increasing the R_{ct} value to 414 Ω (curve d(ii)). This was attributed to the immobilization of LOx on the collagen matrix that hinders the access of the redox probe to the electrode surface. Again, the R_{ct} value of the collagen/sol-gel electrode also increased (180 Ω at curve e(ii)) after deposition of LOx to collagen/sol-gel electrodes although the increment was not obvious as that observed at Fc/collagen/LOx electrode. Thus, it could be suggested that Fc/collagen/sol-gel/LOx electrode posses better electrocatalytic activity compared to collagen/LOx electrode.

The different behaviour of each GOx-modified and LOx-modified GC electrodes towards both enantiomer of glucose and lactate, respectively observed in the CVs was further investigated by chronoamperometric techniques to see the current response change as a function of time. Each time corresponds to an addition of an analyte at a concentration ranging from 0.25 mM for the first 1 mM, increasing to 0.5 mM addition for the next 2 mM and increased to 1 mM addition until the final concentration giving approximately unchanged current responses in the amperometric curves. At this concentration, the biosensor is said to achieve the limit of detection. Figure 5.13(a) and (b), and 5.14(a) and (b) show the typical amperometric responses and the calibration curves, respectively of the Fc/GOx enzyme and Fc/LOx enzyme electrodes incorporated within various matrixes upon successive addition of D- and L-glucose or L- and D-lactate in PBS (0.1 M, pH 7). These amperometric responses of the GOx-modified and LOx-modified electrodes were carried out at the potential of 0.4 and 0.28 V, respectively.

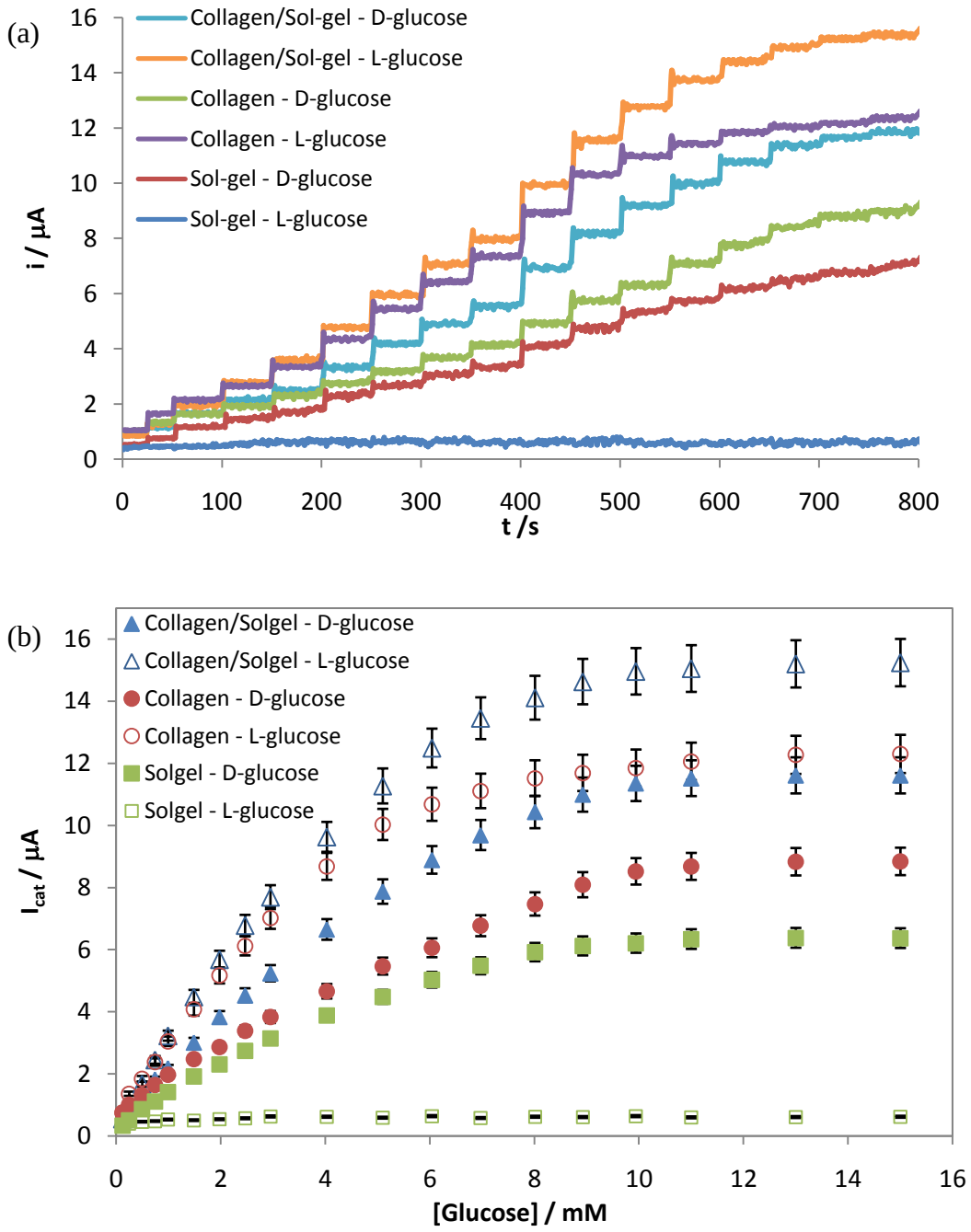

Figure 5.13: The amperometric responses (a) and the calibration curves (b) of current response of Fc/GOx enzyme electrodes incorporated within various matrixes upon successive addition of D- and L-glucose in PBS (0.1 M, pH 7). Applied potential: 0.4 V.

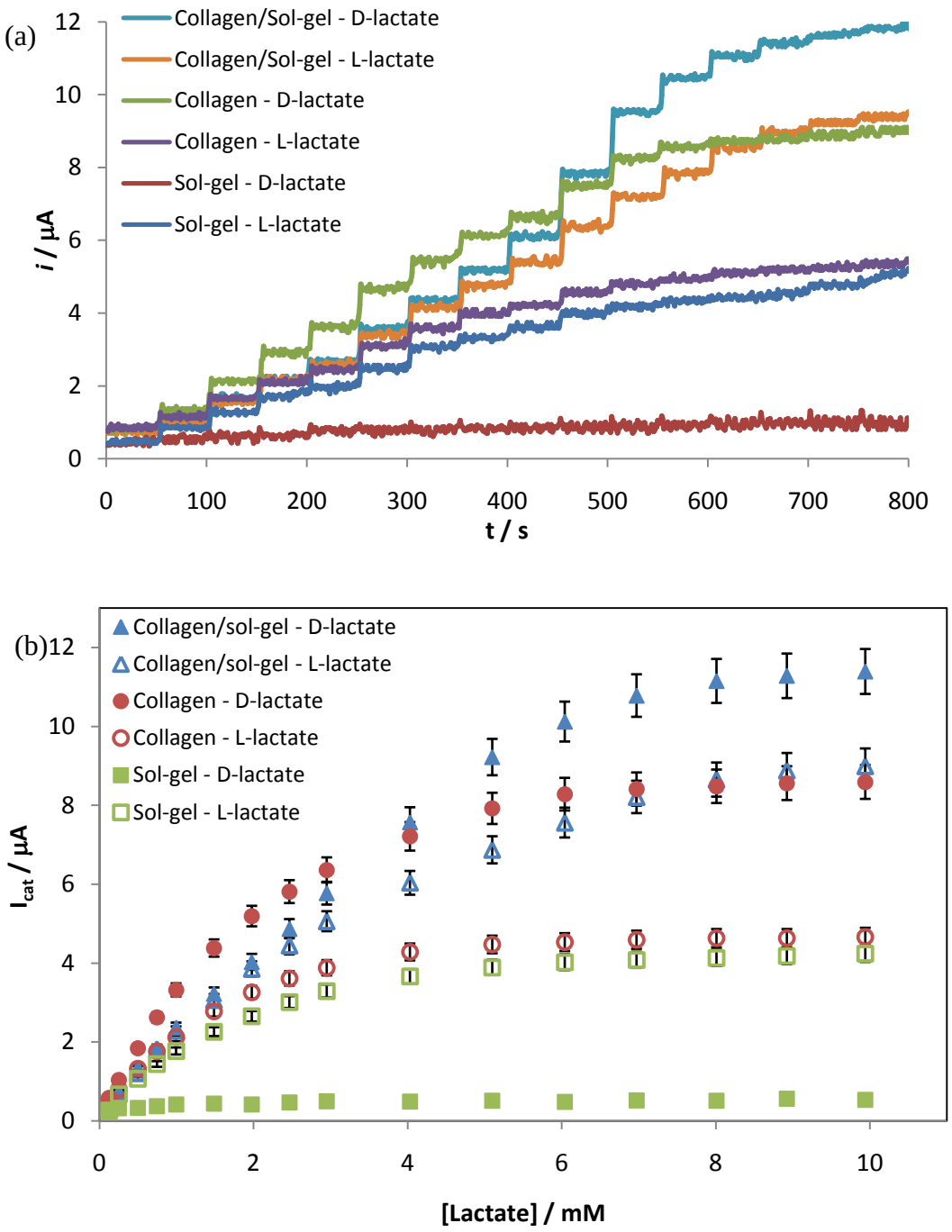

Figure 5.14: The amperometric responses (a) and the calibration curves (b) of current response of Fc/LOx enzyme electrodes incorporated within various matrixes upon successive addition of L- and D-lactate in PBS (0.1 M, pH 7). Applied potential: 0.28 V.

Amperometric measurements with the D-GOx or L-LOx enzymes incorporated in a TMOS sol-gel matrix displayed the expected behaviour with a preference for D-glucose and L-lactate, respectively. The current response of the Fc/GOx/Sol-gel electrode increased linearly with increasing concentration of D-glucose in the range from 0.1 to 8 mM as shown in Figure 5.13. It takes about 12 s for the anodic current to achieve the steady state. The similar current behaviour was also observed with Fc/LOx/Sol-gel electrode when responding to L-lactate. The current response increased up to the concentration of 2.5 mM, beyond which it remained considerably constant. The anodic current achieved steady state for about 10 s. The smaller linear range obtained with LOx-modified electrode can also be attributed to the relatively lower stability of LOx as compared to GOx.[38-39] However, by increasing the concentration of L-glucose and D-lactate in each of the tested solutions, these sol-gel modified enzyme electrodes could not responded to various concentration of both counter-stereoisomer of the analytes supporting to the fact that D-GOx and L-LOx enzymes used in these studies are very specific enzymes that could only react to D-glucose and L-lactate analyte, respectively.

Interestingly, with the introduction of collagen into the sol-gel matrix, a response to analyte of opposite chirality, *i.e*. L-glucose, for D-GOx and D-lactate for L-LOx is evident. The possible explanation to this reversal in chiral responses can be related to the K_m values obtained as calculated based on the analysis of Hanes plot. Based on the results comparing enzymes immobilized within TMOS gel in the absence and presence of collagen, it is believed that collagen itself may have an effect on chiral inversion in both glucose and lactate. These observations were further investigated by circular dichroism spectroscopy (Section 5.4) and FTIR spectroscopy (Section 5.5).

The collagen enzyme and collagen/sol-gel enzyme electrode elicits faster response times for both glucose and lactate sensors to less than 8 s. This is much faster response as compared to the sol-gel enzyme electrode used previously (12 s response to glucose and 10s response to lactate) and than the reported results for GOx (50 s) in pure silica sol-gel matrix,[40-41] (< 1 min) in the hybrid silicate sol-gel mixing with 3-aminopropyltriethoxy silane and 2-(3,4-epoxycyclohexyl)-ethyltrimethoxy silane[42], (20 s) in the silica sol-gel composite [37], (11 s) in the sol-gel derived glass with a grafting poly(vinyl alcohol) and 4-vinylpyridine [43] and (10 s) in biocomposite film composed of

chitosan, gold nanoparticles and GOx [44]. Such fast response times are quite comparable to needle enzyme electrode in collagen gel (<10 s)[45] and in chitosan/polyvinylimidazole-osmium/CNTs/LOx network nanocomposite (<7s)[27]. The fast response times can be attributed to the fast diffusion of the substrate molecule in the thin hybrid film. A short response time further proves that the Fc/Collagen/Sol-gel-based material is a promising platform for the construction of biosensors.

The linear range for pure collagen gels, of GOx was from 0.1 to 10 and 5 mM for D- and L-glucose, respectively. On the other hand, with collagen/sol-gel matrix, the linear response range of GOx was from 0.1 to 8 and 7 mM for D- and L-glucose, respectively. However, because of their higher current response to L-glucose, the sensitivity of both collagen and collagen/sol-gel based electrodes also were found higher to L-glucose. Sensitivity is defined as a measure for the current response of the biosensor to the concentration of the analyte at which the maximum linear range of the analyte concentration can be measured. With collagen gels electrode, the sensitivity of 2.67 and 0.95 μA/mM was obtained to L- and D-glucose, respectively, whereas a sensitivity of 2.42 and 1.56 μA/mM was obtained to L- and D-glucose, respectively for collagen/sol-gel-based electrode. Table 5.1 and 5.2 shows the comparison of the performance of different chiral glucose biosensors based on TMOS sol-gel, collagen and collagen/sol-gel respectively.

Table 5.1: The comparison of the performance of different chiral glucose biosensors.

GOx modified GC Electrodes	**Linear range [glucose] / mM**	**Sensitivity / μA/mM ± 0.01**	**Correlation coefficient, *R***
Sol-gel - D-glucose	6	0.99	0.982
Sol-gel - L-glucose	n.d	n.d	n.d
Collagen - D-glucose	10	1.05	0.989
Collagen - L-glucose	5	2.82	0.986
Collagen/Sol-gel - D-glucose	8	1.76	0.985
Collagen/sol-gel - L-glucose	7	2.60	0.980

Table 5.2: The comparison of the performance of different chiral lactate biosensors.

LOx modified GC Electrodes	**Linear range [lactate] / mM**	**Sensitivity / μA/mM ± 0.01**	**Correlation coefficient, *R***
Sol-gel - D-lactate	n.d	n.d	n.d
Sol-gel - L-lactate	2.5	2.05	0.977
Collagen - D-lactate	3	3.63	0.980
Collagen - L-lactate	2.5	2.22	0.972
Collagen/Sol-gel - D-lactate	5	4.27	0.997
Collagen/sol-gel - L-lactate	4	3.51	0.988

In the case of LOx/collagen- and LOx/collagen/sol-gel-modified electrodes, a similar trend in linear response range was obtained, where the response to D-lactate were wider compared to L-lactate (Table 5.2). The wide linear response range is of great interest for the application of the commercialized lactate biosensor in monitoring the physical condition of individuals who do exercise. The lactate level measurement can be used to determine appropriate training intensities and help diagnosis the endurance performance.[46-47] At rest conditions, the physiological level of lactic acid is between 0.8 to 1.5 mM in normal blood for most humans. During prolonged exercise, the lactate level increases and could reach the lactate threshold, which is the point of lactate accumulation at the onset of the anaerobic performance. The lactate threshold is commonly set at level of 4 mM. Thus, the wide linear response range of LOx/collagen/sol-gel electrode to up to 5 mM could be benefit for the use of lactate measurement up to the level of lactate threshold.

Back to the calibration curve of the steady state current versus each of glucose and lactate concentration, the current responses were increase steadily until it reaches at certain point of concentration, where no further increment of current response was observed, signifies the characteristics of Michaelis-Menten kinetics mechanism for the enzyme-catalyzed process. The Michaelis-Menten constant (K_m), which gives an

indication of the enzyme-substrate kinetics for the biosensor can be obtained from the analysis of the Hanes plot.[48]

The enzyme kinetic analysis was evaluated by using a method described by Albery and Bartlett[49] for analysing amperometric enzyme kinetics where the enzyme is entrapped behind a membrane, in our case, the enzyme was entrapped between the collagen and sol-gel matrix (Equation 5.4).

$$\frac{S_\infty}{j} = \frac{1}{k'_{ME}}\left[1 + \frac{S_\infty}{K_{ME}}\left(1 - \frac{j}{k_s S_\infty}\right)\right] \qquad (5.4)$$

where S_∞ is the bulk substrate concentration, j is the flux, k'_{ME} is the effective heterogeneous rate constant and K_{ME} is similar to the Michaelis–Menten constant in homogeneous enzyme kinetics. Starting from Hanes plot, the plot of y against б (where $y = (б^{-1} - 1)/ s_\infty$ and $б = [i/s_\infty]/[i/s_\infty]_0$) have gave a straight line with a slope of $-k_{ME}'$ / ($k_s' K_{ME}$), an intercept on the y-axis of $1/ K_{ME}$, and an intercept on the б-axis of k_s'/k_{ME}').

Table 5.3 and 5.4 show the summary of the K_{ME} values calculated by this method for each GOx- and LOx-modified electrode, respectively. The value of k_s'/k_{ME}' can be used to determine process at the electrode surface. From the results in Table 5.3 and 5.4, we can see that all of these modified electrodes have k_s'/k_{ME}' values of > 1, indicating that the diffusion of the analyte through the membrane is rate limiting. This is a desirable condition in many cases since it means that the response does not depend upon the activity of the enzyme.[48-49]

Table 5.3: The K_{ME} values calculated from the analysis of Hanes plot according to the method described by Albery and Bartlett[49] for each GOx modified electrodes.

GOx modified GC Electrodes	k_s' / k_{ME}'	K_{ME} / mM
Sol-gel - D-glucose	1.2	2.9
Sol-gel - L-glucose	n.d	n.d
Collagen - D-glucose	1.1	3.2
Collagen - L-glucose	1.5	2.4
Collagen/Sol-gel - D-glucose	1.1	3.4
Collagen/sol-gel - L-glucose	1.3	3.2

Table 5.4: The K_{ME} values calculated from the analysis of Hanes plot according to the method described by Albery and Bartlett[49] for each LOx modified electrodes.

LOx modified GC Electrodes	k_s' / k_{ME}'	K_{ME} / mM
Sol-gel - D-lactate	n.d	n.d
Sol-gel - L-lactate	1.9	1.4
Collagen - D-lactate	1.2	1.3
Collagen - L-lactate	1.4	0.8
Collagen/Sol-gel - D-lactate	1.2	3.0
Collagen/sol-gel - L-lactate	1.2	2.5

Among all the GOx-modified electrodes with D-glucose as analyte, showed the lowest calculated K_m ($K_{ME(D\text{-glucose})}$ = 2.9 ± 0.01 mmol dm^{-3}) value with the TMOS gel enzyme electrode (Table 5.3). However, with the introduction of collagen in the TMOS gel matrix, the chiral preference was dramatically changed as indicated by the lower K_m values for the response to L-glucose ($K_{ME(L\text{-glucose})}$ = 3.2 ± 0.01 mmol dm^{-3}), instead to D-glucose ($K_{ME(D\text{-glucose})}$ = 3.4 ± 0.01 mmol dm^{-3}). With pure collagen gels matrix, a chiral

inversion in the response of D-GOx was clearly observed with further reduced in the value of K_m of L-glucose ($K_{ME(L\text{-}glucose)}$ = 2.4 ± 0.01 mmol dm^{-3}) compared to D-glucose ($K_{ME(D\text{-}glucose)}$ = 3.2 ± 0.01 mmol dm^{-3}). All of the values of K_m for GOx at these modified electrodes were much lower in comparison to other reported glucose biosensor based on GOx entrapped in silica sol-gel membrane (K_m = 22 mM)[43], GOx bound to self-assembled monolayer electrode (K_m = 20 mM)[50], GOx immobilized in the silica hybrid sol-gel film (K_m = 11.8 mM)[51], GOx immobilized onto the surface of conductive polymer (K_m = 5.04 mM)[52] and for native GOx in solution (K_m = 27 mM).[53] The smaller K_m value means that the immobilized GOx possesses higher enzymatic activity and the biosensor produced exhibits a higher affinity to D- and L-glucose.

On the other hand, in the case of LOx-modified electrodes, the lower calculated K_m values were obtained L-lactate ($K_{ME(collagen/L\text{-}lactate)}$ = 0.8 ± 0.01 mmol dm^{-3} and $K_{ME(collagen/sol\text{-}gel/L\text{-}lactate)}$ = 2.5 ± 0.01 mmol dm^{-3}) instead of D-lactate ($K_{ME(collagen/L\text{-}lactate)}$ = 1.3 ± 0.01 mmol dm^{-3} and $K_{ME(collagen/sol\text{-}gel/L\text{-}lactate)}$ = 3.0 ± 0.01 mmol dm^{-3}) although their sensitivity towards L-lactate are lower than their sensitivity towards D-lactate (Table 5.2). The low K_m values obtained in response to L-lactate was explained by their faster rate of the L-LOx to catalyzes the reaction to ½ V_{max} before it became saturated earlier by further increment of L-lactate concentrations. The K_m values for LOx at the sol-gel matrix and collagen matrix electrodes seems to give much lower values in comparison to other literaturely published lactate biosensors based on the LOx co-crosslinking with glutaraldehyde and bovine serum albumin (K_m = 2.4 mM)[54], bienzymatic system of LOx and horseradish peroxidase mediated by the redox polymer (K_m = 2.8 mM)[55] and free LOx in solution (K_m = 2.8 mM)[56]. The changes in the values of K_m could be due to change in its conformational when immobilized within TMOS gel or collagen matrixes compared to its free condition.[56]

An exception to the lower K_m values occurs with LOx immobilized within collagen/sol-gel matrix, especially when it was tested to the presence of D-lactate, where the K_m value was found higher compared to the K_m value of free LOx in solution (K_m = 2.8 mM)[56]. This higher K_m value indicates that the immobilized L-LOx within collagen/sol-gel matrix have a decreased affinity towards its counter stereo-analyte, which is the D-lactate. That is further support the results obtained in the calibration curve, which shows that this modified electrode have slower rate to catalyzes the

oxidation of D-lactate to ½ V_{max}, even though it gave the highest current response compared to its response to L-lactate itself.

In the construction of enzyme electrodes, it is desirable to obtain the lowest K_m and the highest V_{max} values. The results obtained in LOx-modified electrodes were further analysed by using other kinetic analysis methods. As shown in Figure 5.14(b), the amperometric response of immobilized L-LOx seems to follow the Michaelis-Menten kinetics behaviour. One of the methods to analyze enzyme kinetic data is by linear regression. The Lineweaver-Burk plot is the most widely used for calculating the kinetics parameters by plotting the inverse of the reaction rate versus the inverse of various lactate concentrations. In this case, the inverse of the current response is plot instead of reaction rate since the reaction rate is directly proportional to the current.[38,57] The Lineweaver-Burk equation is shown as follows:

$$\frac{1}{I_{ss}} = \frac{K_m}{i_{max}}\frac{1}{C} + \frac{1}{i_{max}} \tag{5.5}$$

where I_{ss} is the steady state current after the addition of the substrate, i_{max} is the maximum current measured under substrate saturation condition, and C is the concentration of the substrate. The K_m value is calculated from the slope of K_m/i_{max} and the intercept ($1/i_{max}$) from the Lineweaver-Burk plot (Figure 5.15).

Another conversion of the Michaelis-Menten equation is a plot of substrate concentration divided by velocity (in this case, the current response) against substrate concentration. This plot is known as the Hanes plot, and it gives a direct readout of K_m value as shown in the following equation:

$$\frac{C}{I_{ss}} = \frac{C}{i_{max}} + \frac{K_m}{i_{max}} \tag{5.6}$$

where the symbols as the same as defined in Lineweaver-Burk equation, above. The K_m value is determined from the intercept on the horizontal axis of - K_m or on the vertical axis of K_m/i_{max}. Figure 5.15 and 5.16 display the Lineweaver-Burk and Hanes plots, respectively according to the data obtained from the calibration curve of LOx-modified GC electrodes (Figure 5.14(b)).

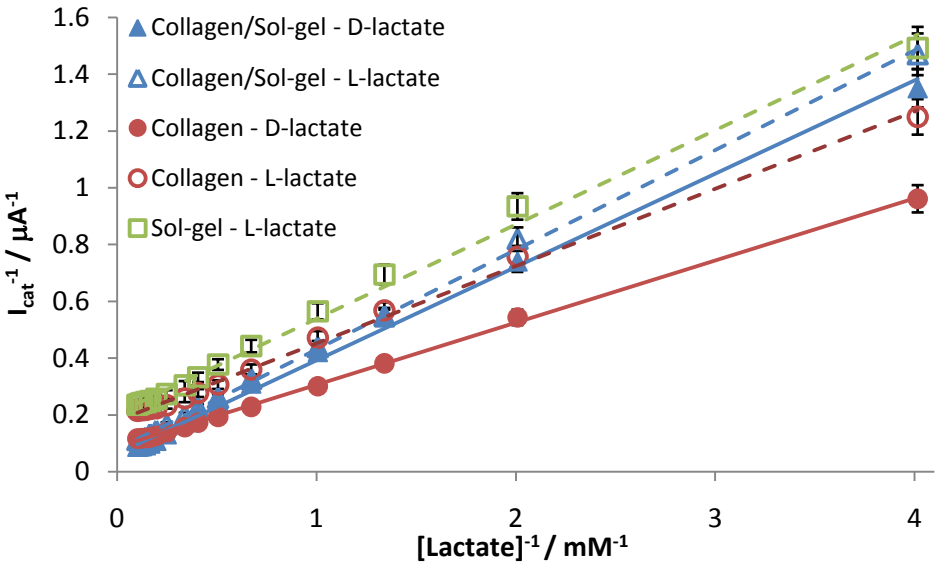

Figure 5.15: Lineweaver-Burk plots according the data obtained from the calibration curve of LOx-modified GC electrodes (Figure 5.14(b)).

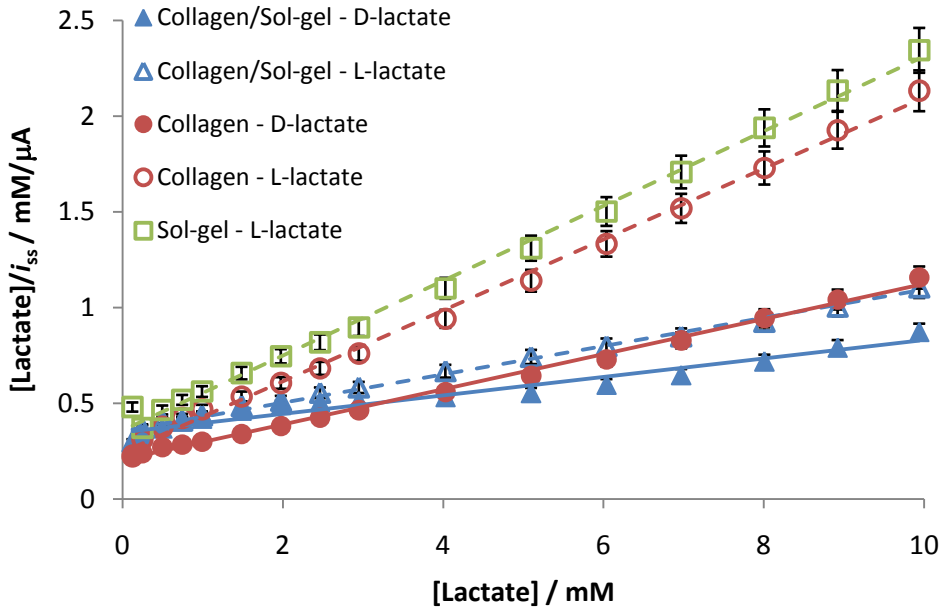

Figure 5.16: Hanes plots according the data obtained from the calibration curve of LOx-modified GC electrodes (Figure 5.14(b)).

Both Lineweaver-Burk and Hanes plots for nearly all types of LOx-modified electrodes appear linear with $R^2 \approx 0.99$. This behaviour indicating that the immobilized LOx follows the Michaelis-Menten kinetics, which is expected to occur for an enzyme catalysis-controlled amperometric biosensor.[54,58-59] However, an exception to this linearity behaviour was observed with the Hanes plot for LOx enzyme immobilized within collagen/sol-gel matrix when it was used to measure the current response to various concentration of D-lactate. The Hanes plot did not give a straight line (R^2 = 0.948) thus, it is difficult to determine the exact value of K_m for this LOx-modified electrode.

Table 5.5 summarizes the values of K_m for immobilized L-LOx within various matrices, calculated from the the Lineweaver-Burk and Hanes plots. The calculation of K_m was performed under conditions in which [lactate] << K_m so that it would be a linear trend between the steady state current and concentrations.[60]

The K_m values calculated from the Hanes plot (Table 5.5) were similar to the values obtained from the method described by Albery and Bartlett[49] (Table 5.4). On the other hand, most of the K_m values calculated by Hanes equation are noticeably smaller than the values calculated using Lineweaver-Burk equation. According to Cornish-Bowden[61], the Lineweaver-Burk plot gives a grossly misleading impression of experimental errors hence over-estimates the K_m values, compared to Hanes plot which gives fair range of errors leading to realistic K_m values. Again, the smallest K_m value was obtained with LOx/Collagen electrode when used to detect the presence of L-lactate. The smaller K_m value means that the immobilized LOx possesses a higher enzyme activity and the proposed electrode exhibits a higher affinity for lactate.

Table 5.5: Values of K_m for immobilized L-LOx within various matrixes.

LOx modified GC Electrodes	K_m / mM calculated from Lineweaver-Burk plot	K_m / mM calculated from Hanes plot
Sol-gel - D-lactate	n.d	n.d
Sol-gel - L-lactate	1.6	1.4
Collagen - D-lactate	2.5	1.4
Collagen - L-lactate	1.5	0.8
Collagen/Sol-gel - D-lactate	5.2	3.5
Collagen/sol-gel - L-lactate	4.4	2.8

It can be concluded that the collagen matrix has contributed to the chiral inversion in D-GOx and L-LOx as collagen itself is a chiral molecule. This unusual effect of collagen matrix was further analyzed by using other spectroscopic techniques.

5.4 Circular Dichroism Studies

Because of their chirality, collagen exhibits positive and negative signals that assigned as their Cotton effects. Circular dichroism (CD) studies of solutions prior to gelation with TMOS sol-gel, in pH 7 buffer showed a typical spectrum for type I collagen from rat tendon with a positive strong cotton effect at 221 nm (401 mdeg cm^2 $dmol^{-1}$), negative weak Cotton effect at 210 nm and a cross over (zero rotation) at about 213 nm, characteristic of the triple helical conformation of collagen[62]. The positive peak due to n−π* amide transition in collagen samples is the index for triple helical conformation and disappears on denaturation. The negative peak is characteristic of the so-called P_2 conformational structure (π−π* transition) and correlates with the particular structure of collagen type I molecules. The fraction of native protein was evaluated from the change in ellipticity at 221 nm.

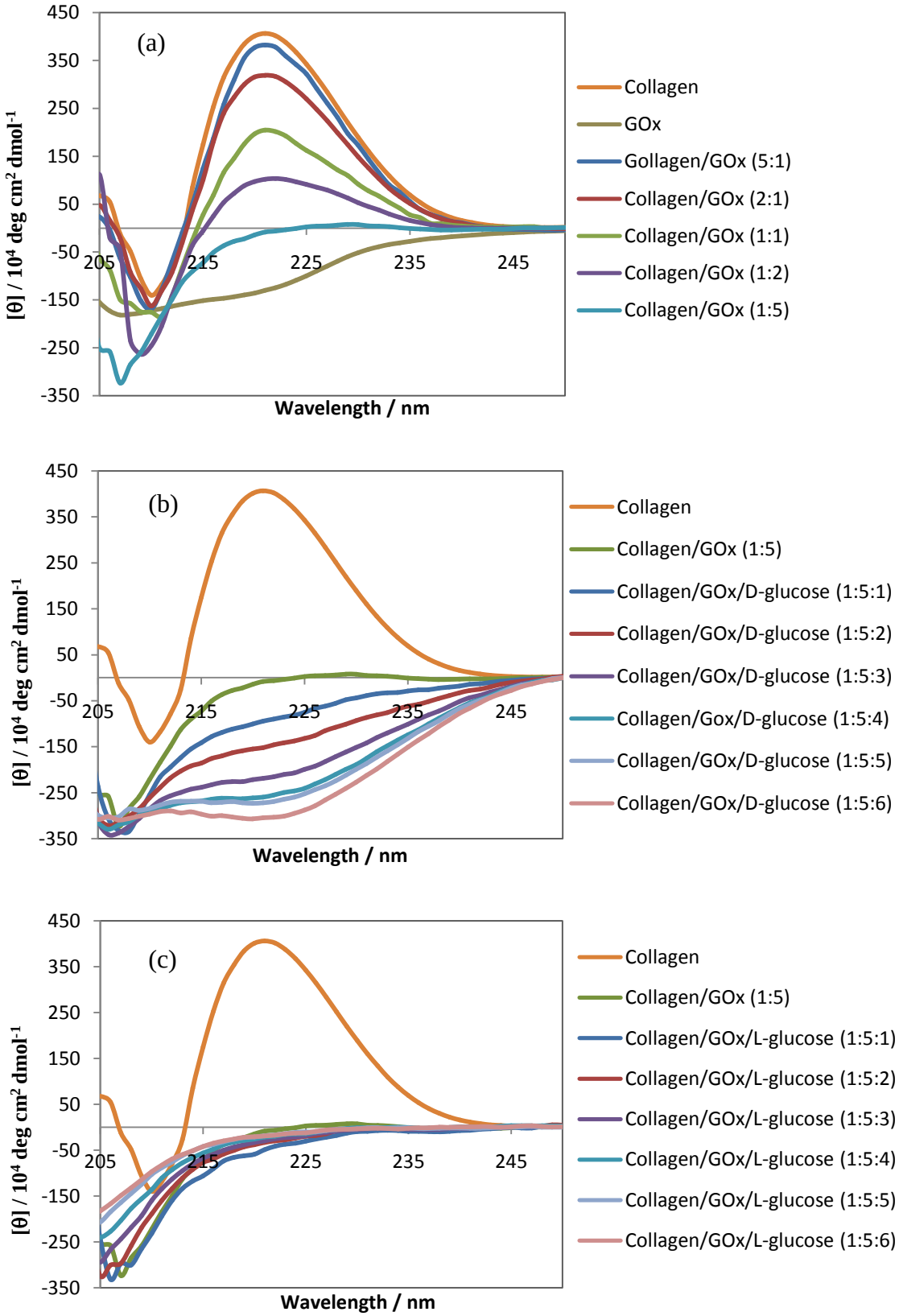

Figure 5.17: CD obtained from (a) titration of GOx to collagen, (b) titration of D-glucose to Collagen/GOx (1:5) system, and (c) titration of L-glucose to Collagen/GOx (1:5) system.

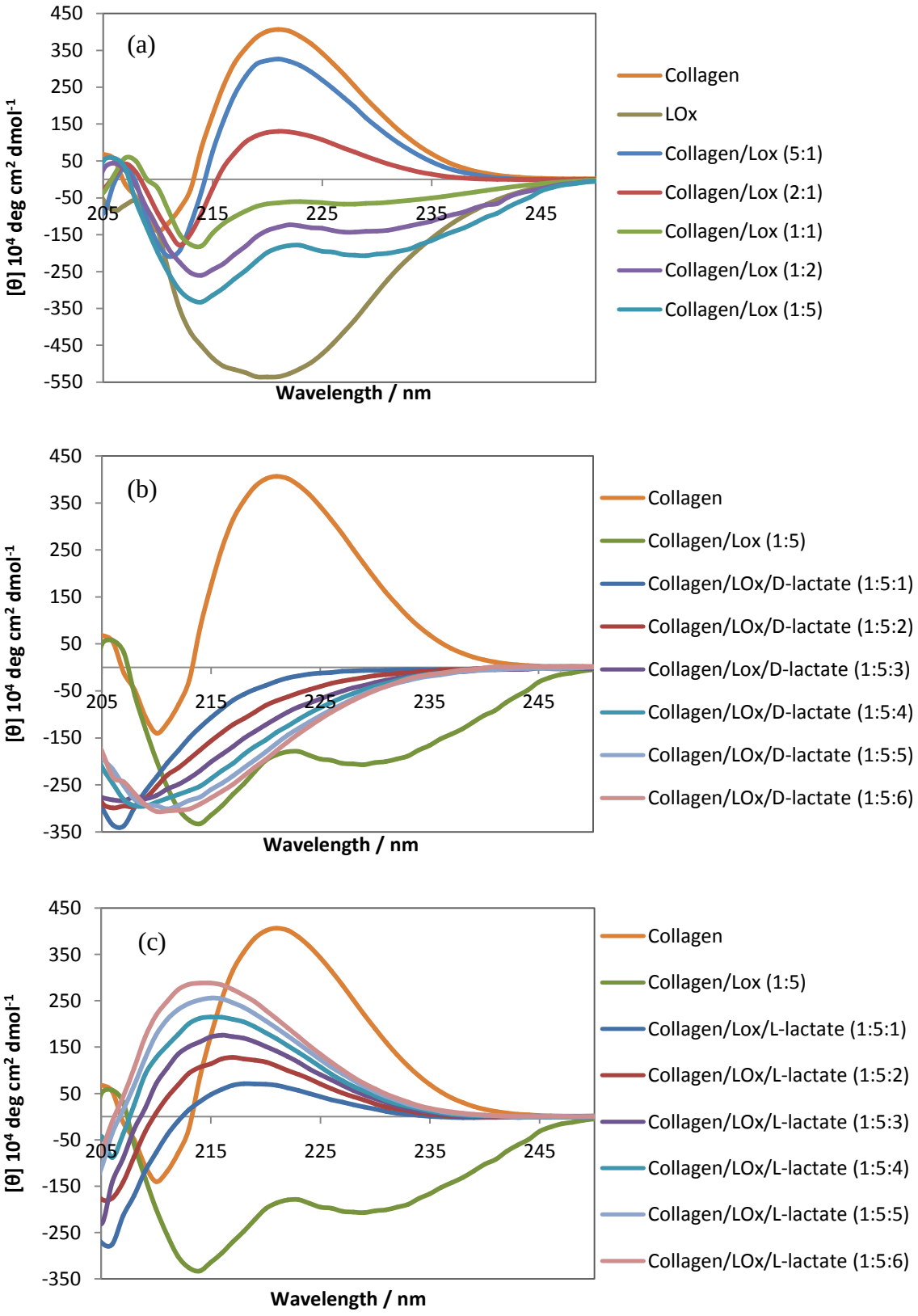

Figure 5.18: CD obtained from (a) titration of LOx to collagen, (b) titration of D-lactate to Collagen/LOx (1:5) system, and (c) titration of L-lactate to Collagen/LOx (1:5) system.

The isoelectric point of type I collagen is 8.26[62] which gives the collagen a net positive charge at pH 7.4. GOx and LOx have isoelectric points of 4.3 and 4.6, respectively,[63] giving the molecules an overall negative charge at the same pH. Electrostatic interaction between the enzymes and collagen is therefore highly likely. With increasing GOx:Collagen ratios, the peak at 221 nm (Figure 5.17) decreases indicating the decreasing the triple helical content-effects that lead to the denaturation of collagen. Collagen is a polysaccharide with 1% of equivalent amount of glucose and galactose, therefore denaturation when modified with GOx is highly possible. Stepwise addition of D-glucose shows a further decrease in the peak at 221 nm, in contrast to the addition of equivalent ratios of L-glucose. With the LOx/glucose complex addition to collagen matrix, the negative peak of the CD also shows a minor shift towards lower wavelength due to the increase in ionic strength of collagen solution.[64]

L-lactate oxidase has a negative Cotton effect compared to collagen (Figure 5.18). Increasing ratios of LOx:Collagen again decreases the peak at 221 nm indicates the denaturation of collagen. By stepwise addition of D-lactate, the CD spectrum presents only the negative peak confirming that the collagen is denatured and deleted the triple helical structure. The mixture solution now is composed of detached α-chains that exhibit a polyproline II conformation.[65] Since the hydroxyproline residues are very important for stabilizing the collagen triple helix, the modification of the residues could disturb the triple helical conformation of collagen, which might explain the loss of the optical rotation.[66] The change in collagen conformation structure has led to the changes in optical rotation of L-LOx as well, resulting to increasing the stereoselectivity towards D-lactate.

In contrast, titration of L-lactate into the 1:5 Collagen:LOx composite, reveals a tendency towards recovery of the collagen triple helical conformation, although the negative peak (205 nm) and the positive one (215 nm) are slightly blue shifted. It confirms that the Collagen/LOx/L-lactate complex recovers from denaturation to presents a triple helical structure. A possible explanation for this observation may be attributable to the interaction of L-LOx with the collagen fibres. On addition of L-lactate, the enzyme reacts with the L-lactate, allowing the collagen to relax back to its triple helix conformation. This recovery phenomenon has maintained the stability of triple helix conformation of collagen and thus, increases the activity of immobilized

LOx to possess a higher affinity towards L-lactate resulting to lower value of K_m ($K_{m(collagen/LOx - L\text{-}lactate)}$= 0.8 mM) (Table 5.4).

An enantioselective difference of $\Delta\theta_{CD}$ is observed which increases from 45 to 286 / mdeg cm^2 dmol^{-1} for collagen/GOx system (Figure 5.19) and from 98 to 388 / mdeg cm^2 dmol^{-1} for collagen/LOx system (Figure 5.20). These enantioselective differences at 221 nm are important in chiral detection and separation field industries.

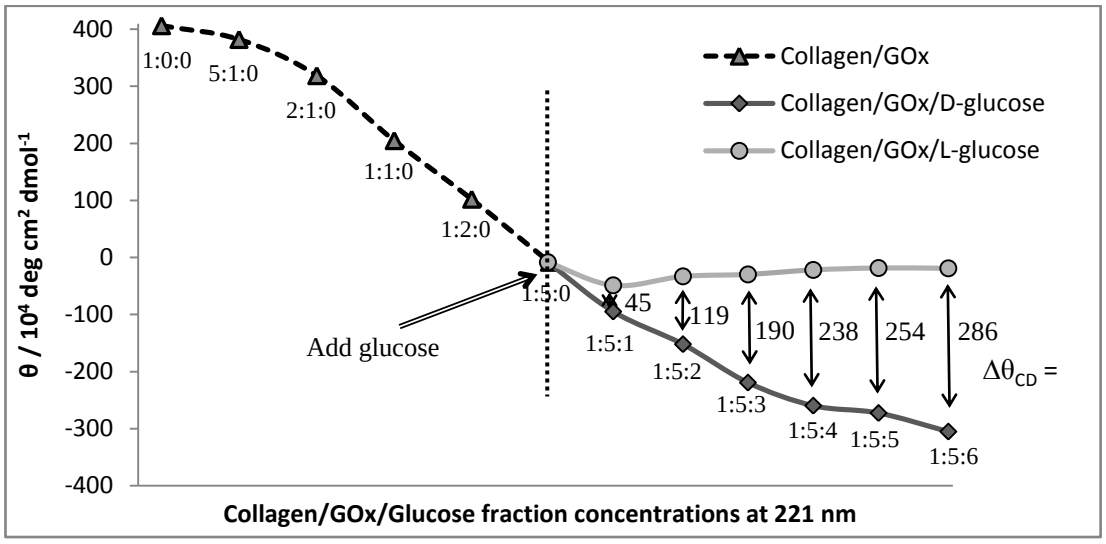

Figure 5.19: The enantioselective difference of $\Delta\theta_{CD}$ between D- and L-glucose.

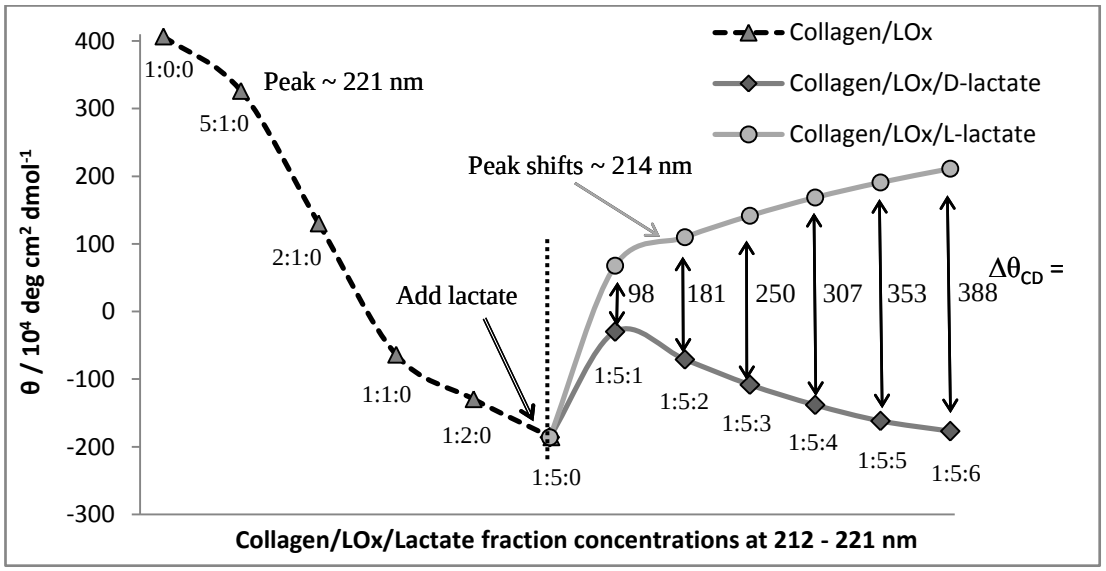

Figure 5.20: The enantioselective difference of $\Delta\theta_{CD}$ between L- and D-lactate.

5.5 Fourier Transform Infra-Red Spectroscopy

Pure type I collagen and collagen-enzyme binding were analyzed by using Fourier Transform Infra-Red (FTIR) spectroscopy to determine secondary structure of the proteins. According to Sionkowska *et al*. (2004)[67] infrared spectra of proteins indicate a number of bands attributed to the peptide bond. Amino acids in collagen molecule are known to link together through peptide bonds giving rise to several IR active vibration modes such as amide A and B (near 3330 and 3080 cm^{-1}, respectively) and amide I, II and III (near 1650, 1550 and 1250 cm^{-1}, respectively).[67] The FTIR spectra from pure collagen and modified collagen for GOx and LOx systems are show in Figure 5.21 and 5.22, respectively.

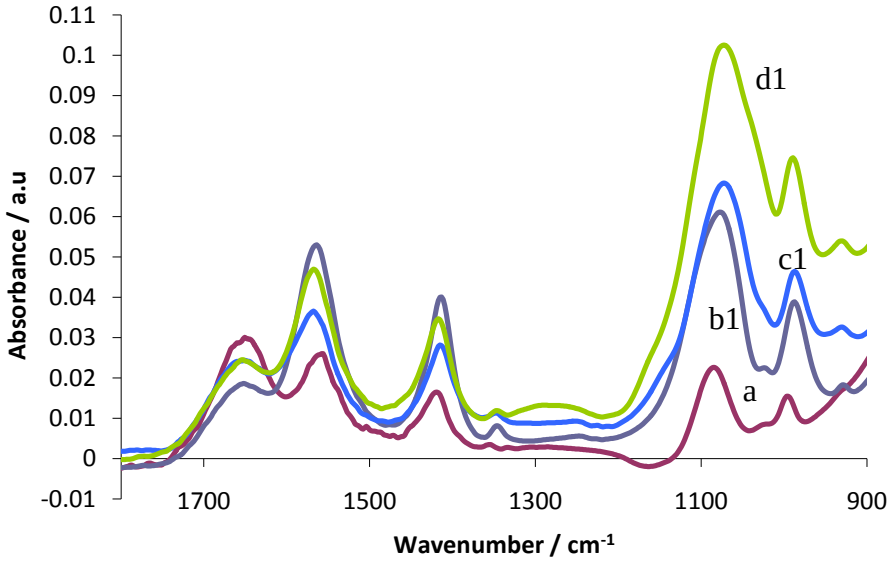

Figure 5.21: FTIR spectra of (a) collagen, (b) collagen/GOx, (c) collagen/GOx/D-glucose and (d) collagen/GOx/L-glucose.

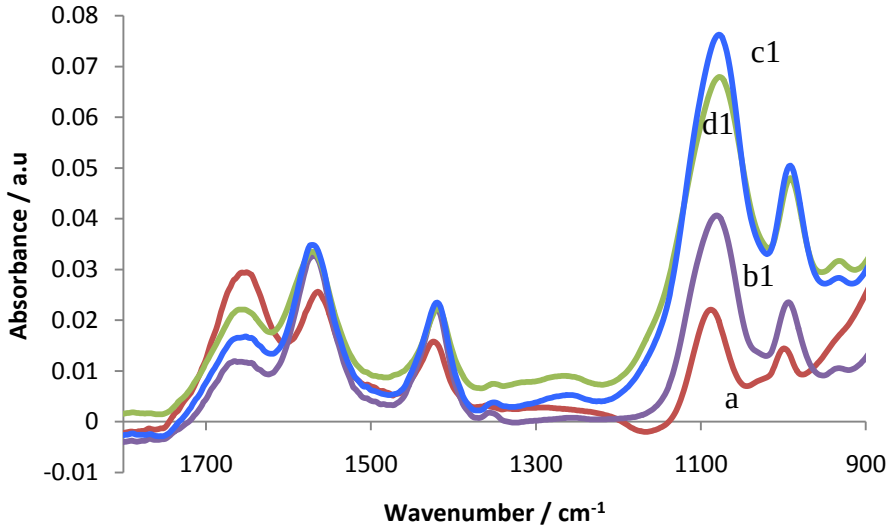

Figure 5.22: FTIR spectra of (a) collagen, (b) collagen/LOx, (c) collagen/LOx/L-lactate and (d) collagen/LOx/D-lactate.

All of the FTIR spectra of pure and complex collagen revealed the amide I and II absorptions at approximately 1650 and 1550 cm^{-1}, respectively, though varied significantly in intensity. The amide I and II band regions of collagen are directly related to polypeptide conformation. In the case of collagen, the band of interest in the FTIR spectra is the amide I band, which can be used to determine the secondary structure of collagen. The spectral component, which arises mainly from stretching vibrations of C=O bond along the polypeptide backbone, is composed of several underlying features. Each of these peaks is the characteristics of a particular secondary structure of collagen. There are also absorption peaks at 1030 and 1080 ± 5 cm^{-1} arises from the C–OH stretching vibrations of the carbohydrate moieties attached to the collagen molecule.[68-69]

The peak observed at the amide I band proves the triple helix structure of collagen (curve a). However, this triple helix structure was unfold by interaction of collagen with either GOx or LOx, shown by the reduced in absorption intensity in the FTIR spectrum of collagen/GOx or collagen/LOx matrices (curve b1 and b2). In the presence of D- and L-glucose or L- and D-lactate, this unfolding structure was found to reversing back tending towards triple helix conformation again (curves c1, c2 and d1,

d2). To further analyze the secondary structure of the collagen/enzyme composites as to determine the reversal of chiral inversion, works on deconvolution of FTIR spectra was done by using Origin pro 7.5 software (Origin-Lab, USA).

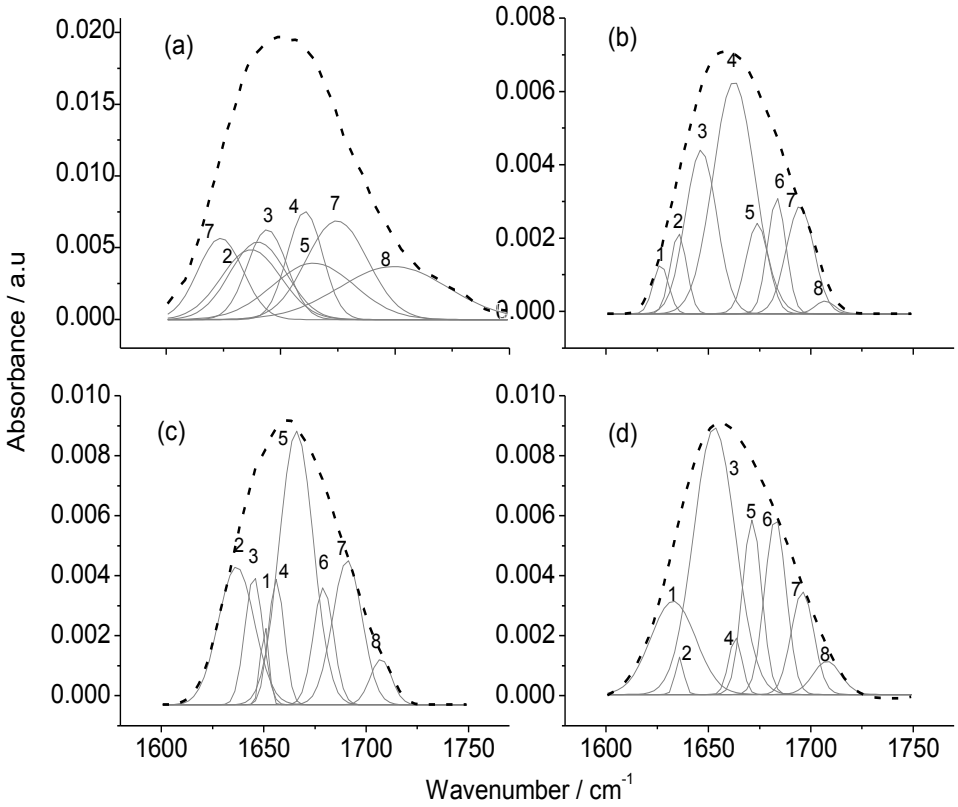

Figure 5.23: Deconvolution of the FTIR spectrums at Amide I band for (a) collagen, (b) collagen/GOx, (c) collagen/GOx/D-glucose, and (d) collagen/GOx/L-glucose systems. (1. Denatured collagen, 2. Triple helix, 3. Unordered structure, 4. α-helix, 5. B-turns, 6. Anti-parallel β-sheets, 7. Parallel β-sheets, 8. Helixes of aggregated collagen-like peptides).

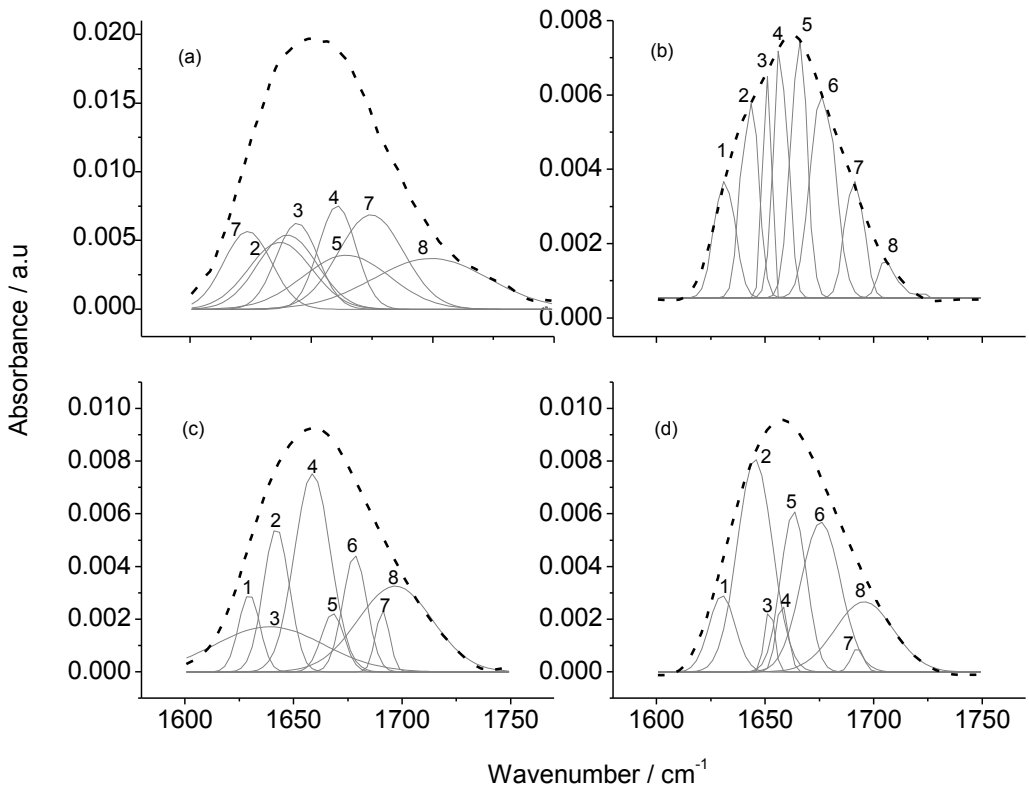

Figure 5.24: Deconvolution of the FTIR spectrums at Amide I band for (a) collagen, (b) collagen/LOx, (c) collagen/LOx/L-lactate, and (d) collagen/LOx/D-lactate systems. (1. Denatured collagen, 2. Triple helix, 3. Unordered structure, 4. α-helix, 5. B-turns, 6. Anti-parallel β-sheets, 7. Parallel β-sheets, 8. Helixes of aggregated collagen-like peptides).

Curve fitting of FTIR spectra was performed at 1750-1500 cm^{-1} spectral interval to determine the effect of the additives on the secondary structure of collagen (Figure 5.23 and 5.24). Absorption bands are assigned according to literature values [69-70]. The absorption features could be attributed as follows: triple helix at ca. 1638 cm^{-1}, unordered structure at ca. 1647 cm^{-1}, α-helix at ca. 1658 cm^{-1}, β-turns at ca. 1668 cm^{-1}, anti-parallel β-sheets at ca. 1680 cm^{-1}, denatured collagen at ca. 1683 cm^{-1}, and parallel β-sheets at ca. 1690 cm^{-1}. Spectral area per band is then used for secondary structure calculations.

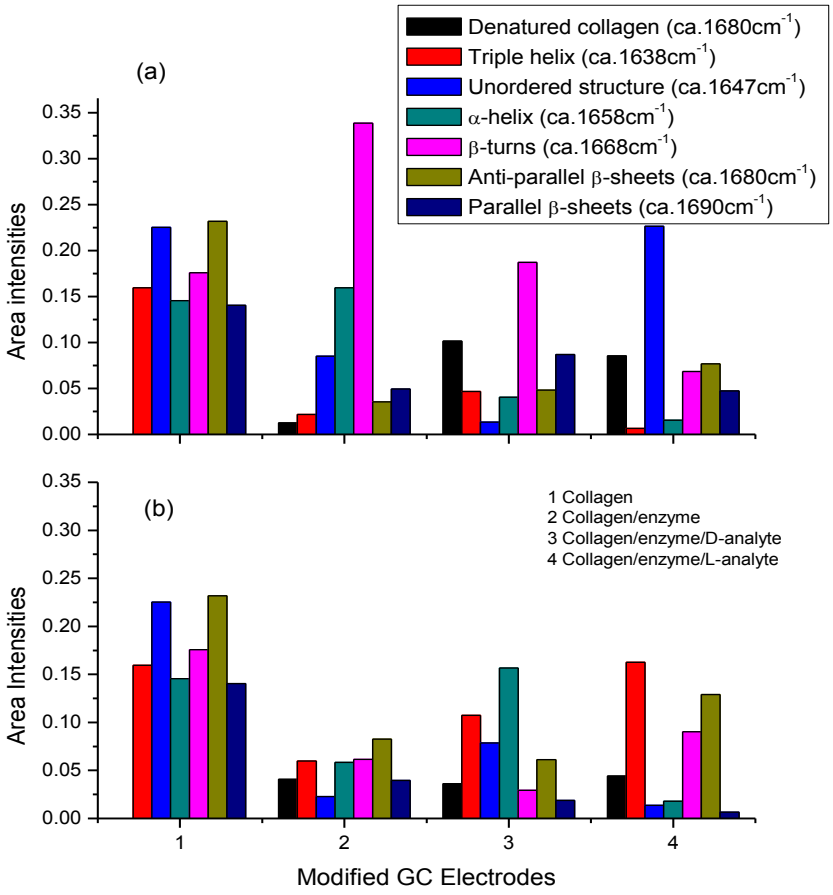

Figure 5.25: Secondary structures presence in collagen complex. (a) GOx complex system and (b) LOx complex system.

Results of the curve fitting of the FTIR spectra summarized in Figure 5.25 clearly revealed the structural differences of the collagen/enzyme composites and the effect of addition of the analytes. It was found that collagen gels possess significantly higher triple helix and β-sheets contents than collagen/enzymes mixture. In presence of either GOx or LOx to the collagen matrix, the triple helix conformation was unfolded as shown by a minimal content of triple helix and maximal content of β-turns structure at 1666 cm^{-1}. Because GOx also have a high content of secondary structure with 28% helix and 18% sheet[71], the interaction between collagen and GOx can contributed to the changes in stability of the triple helix conformation. Such interactions can be inter-chain hydrogen bonds coupled by the NH groups of a glycyl residue with the CO group of a residue in the neighbouring chain.[70]

The β-turn intensity in collagen modified with enzymes is reduced on addition of D-glucose to approximately the same intensity as the collagen matrix. However, on addition of L-glucose, the intensity is reduced to half whereas the intensity of the unordered structure at 1647 cm^{-1} is increased. Interestingly, the triple helix configuration at 1638 cm^{-1} is reduced when GOx is added. Addition of D-glucose to the collagen/GOx composite shows a slight increase in the peak intensity, whereas addition of L-glucose indicates a further decrease in the triple helix conformation (Figure 5.25(a)).

The interaction of L-LOx with the collagen matrix decreases the intensities of all the peaks observed in the FTIR spectra for pure collagen (Figure 5.25(b)). Addition of D-lactate has a major effect on the α-helix structure at 1658 cm^{-1}, whereas addition of L-lactate leads to a recovery of the triple helix configuration at 1638 cm^{-1}, supporting the observations from CD spectroscopy (Section 5.4).

5.6 Reproducibility and Stability of the Biosensor

The following studies will be focused on lactate biosensors. The reproducibility of the lactate biosensors were estimated from the response to L- and D-lactate at various LOx-modified GC electrodes prepared under the same conditions. Three successive measurements using each of the lactate biosensors were carried out at the concentration of 2 mM. The precision of the biosensor is investigated and summarized in Table 5.6. The relative standard deviation (RSD) values for all of the lactate biosensors are relatively low (less than 5%) exhibits an excellent reproducibility of the biosensors. In fact, the lowest RSD values (RSD = 0.88 – 1.06 %) were obtained at Fc/LOx/Collagen electrode suggesting that collagen has improved the reproducibility of the lactate biosensors.

Table 5.6: Precision of lactate biosensors response to 2 mM L- or D-lactate.

LOx modified GC Electrodes	**Current response, µA**			**Average current, µA**	**RSD (%)**
Sol-gel - L-lactate	2.59	2.67	2.69	2.65	2.00
Collagen - D-lactate	5.25	5.14	5.19	5.19	1.06
Collagen - L-lactate	3.28	3.23	3.28	3.26	0.88
Collagen/Sol-gel - D-lactate	4.09	4.02	3.97	4.03	1.50
Collagen/sol-gel - L-lactate	3.84	3.79	3.91	3.84	1.57

The stability of the LOx-modified electrodes was evaluated by measuring the steady state current response to 2 mM L- and D-lactate. The stability tests were investigated in which the electrode was tested every 5 days for 1 month (Figure 5.26). When not in use, the biosensors were stored in 0.1 M PBS (pH 7) at 4 ˚C to maintain its stability.

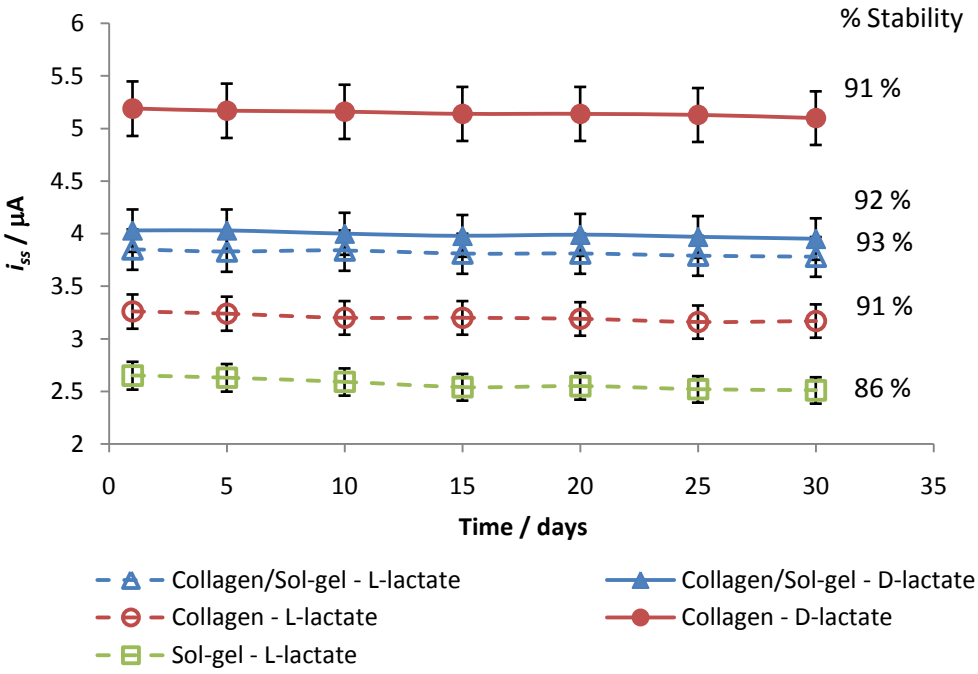

Figure 5.26: The stability of the lactate biosensors in PBS (0.1 M, pH 7) containing 2 mM L- and D-lactate, checked by performing the biosensors in every 5 days with the biosensors being stored in 0.1 M PBS (pH 7) at 4 ˚C.

The lactate biosensor based sol-gel matrixes retained about 86% of its original response after 30 days of testing. The stability of the biosensors increased up to 90% of their initial response when the biosensors were developed based on collagen matrix. These indicated an excellent long-term storage stability, which is possibly related to the biocompatibility of both collagen and sol-gel matrixes with the enzyme.

5.7 Selectivity against Interferences

In this section, the selectivity of lactate biosensor against interference was carried out with Fc/LOx/Collagen/Sol-gel electrode because of their wider linear range to response to higher range of concentration to up to the lactate threshold. Lactate is always measure as indicator for various metabolic disorders in clinical care. One of the

application is to measure toxicity for example poisoning by ethylene glycol that can produce interfering effect to blood lactate masurement.[72] Many cases have reported that ethylene glycol ingestion can give an artificial lactate elevation in point-of-care analysis.[72-76] False lactate result might led to misdiagnosis and delayed treatment that could lead to serious consequences.

Ethylene glycol is commonly found in automotive antifreeze, hydraulic brake fluid and coolant. It is a toxic, colorless, odorless, almost nonvolatile liquid with a sweet taste. Poisoning by ethylene glycol might occur in accidental paediatric ingestions, or as an inexpensive substitute for ethanol.[74] Ethylene glycol poisoning is characterized by central nervous system depression, severe metabolic acidosis, cardiovascular dysfunction, hypocalcemia, and acute kidney failure.[74,76-77] However, the ethylene glycol toxicity is mainly due to its toxic metabolites rather than to ethylene glycol itself. Glycolic acid, oxalic acid and glyoxylic acid are the metabolites that can cause toxicity, which produce from the metabolic pathway of ethylene glycol. In its metabolic pathway, ethylene glycol is converted to glycoaldehyde by alcohol dehydrogenase that is then converted to glycolic acid. The conversion of glycolic acid to glyoxylic acid is a rate-limiting step that leads to the accumulation of glycolate thereby its toxic effect.[74]

Glycolic acid ($C_2H_4O_3$) is the smallest α-hydroxyacid (AHA) that is colourless, odourless in nature, and very soluble in water. Due to its excellent capabilities to penetrate skin, glycolic acids are often used in various skin-care products to improve the skin's appearance and texture. It is also used in the textile industry as a dyeing and tanning agent, and as a monomer in the preparation of polyglycolic acid. However, it is a strong irritant and harmful if ingested or inhaled.[78] Figure 5.27(a) shows the structure of glycolic acid. The toxic metabolite, glycolate, is very similar in structure to lactate and might interferes with the measurement of whole blood lactate by some enzymatic methods, thereby falsely increasing lactate levels.[74]

Another metabolites arises from the metabolic pathway of ethylene glycol is glyoxylic acid ($C_2H_2O_3$) (Figure 5.27(b)). It is liquid in nature with a melting point of -93ºC and a boiling point of 111ºC.[79] The conjugate base of glyoxylic acid, glyoxylate is the by-product of the amidation process in biosynthesis of some amidated peptides.

Oxalic acid ($C_2H_2O_4$) (Figure 5.27(c)) is the final product of the ethylene glycol metabolism. It is a strong organic acid, with pKa_1 = 1.27 and pKa_2 = 4.28.[80] The conjugate base of oxalic acid, known as oxalate is a reducing agent that can act as an

excellent ligand for metal ions. In the body, oxalate binds with metal such as Ca^{2+} and Fe^{2+} to deposit crystals known as kidney stones, which irritate the gut and kidneys. Thus, for those people with kidney disorders or gout are typically advised to avoid foods high in oxalic acid or oxalates.

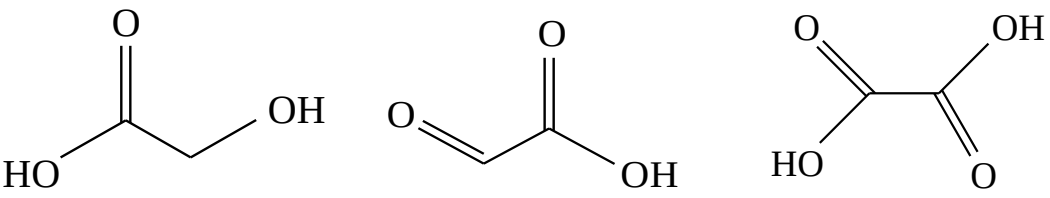

(a) (b) (c)

Figure 5.27: The structure of (a) glycolic acid, (b) glyoxylic acid, and (c) oxalic acid.

The selectivity of lactate biosensor against ethylene glycol metabolites was studied in terms of its response as monitored in the CVs of electrode to the presence of interfering acids in lactate-containing solution. The results are compared with those obtained with pure lactate solution. Figure 5.28 demonstrates the CVs of L- and D-lactate in the presence and absence of interfering acids at the Fc/LOx/Collagen/Sol-gel electrode, scanned at 25 mV/s. The current ratios known as "lactate gap" between those responses are summarized in Figure 5.29.

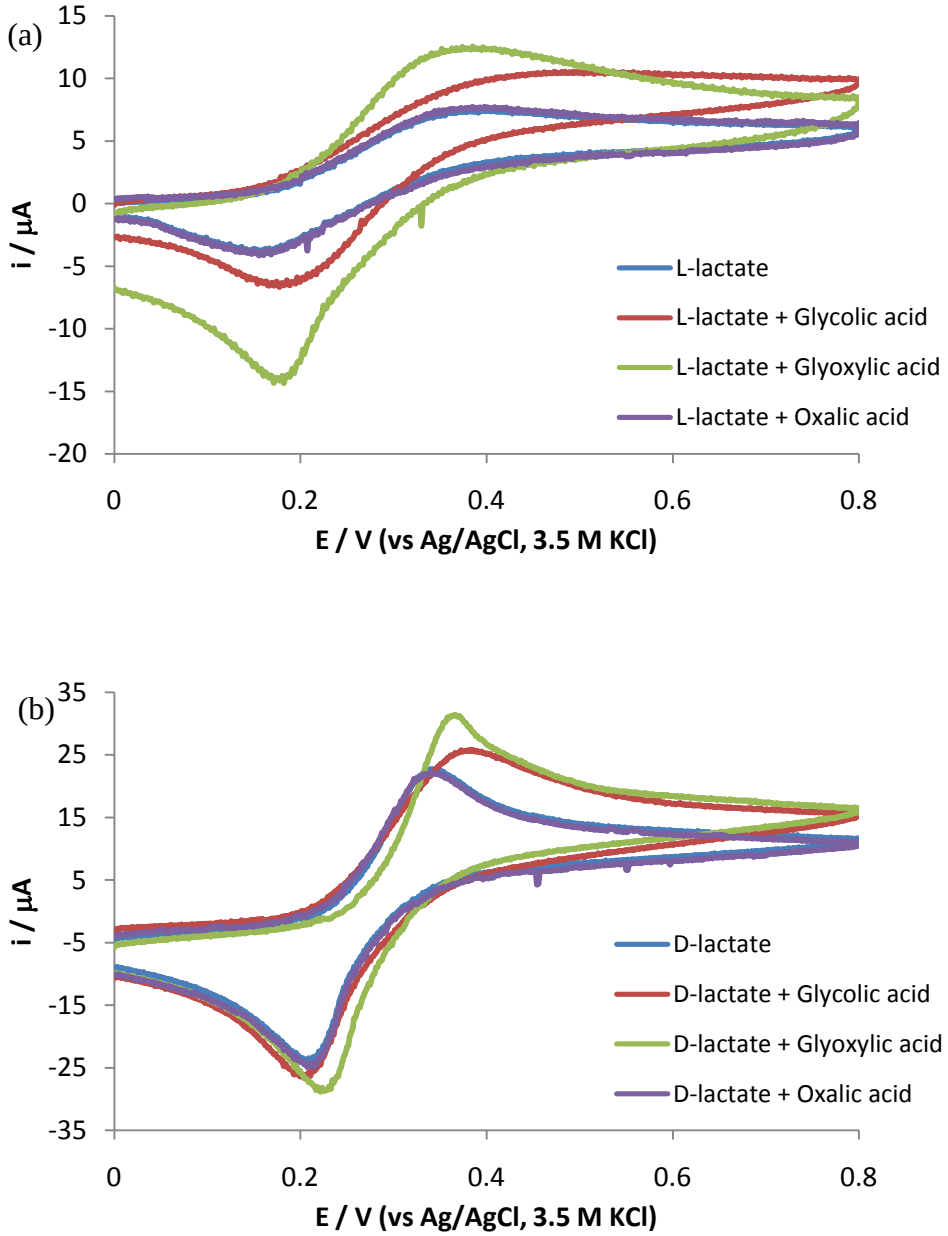

Figure 5.28: The CVs at Fc/LOx/Collagen/Sol-gel electrode for the detection of (a) L-lactate and (b) D-lactate, respectively in PBS (0.1 M, pH 7) in the absence and presence of interfering acids. Scan rate: 10 mV/s.

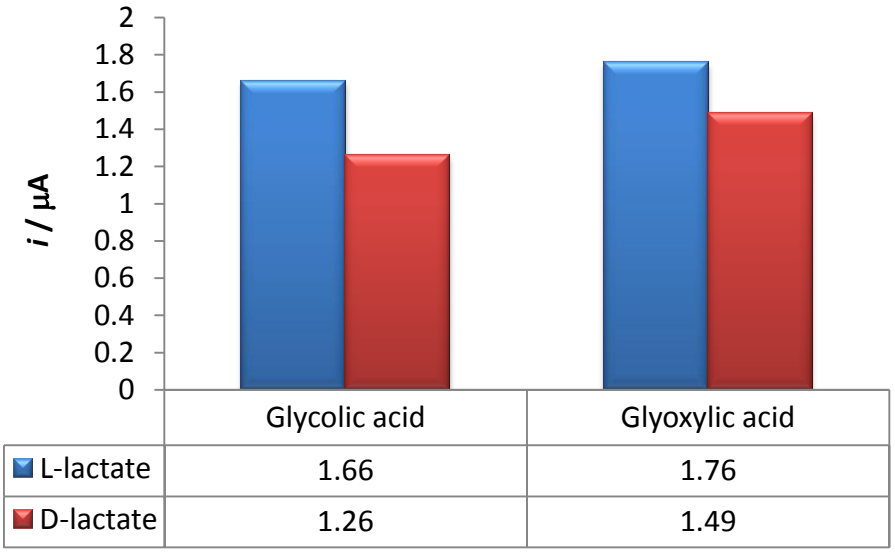

Figure 5.29: Current ratios represents "lactate gap" obtained from the CVs at Fc/LOx/Collagen/Sol-gel electrode in the presence of various interfering acids.

As shown from the current ratio, both glycolic and glyoxylic acid give positive false results in both L- and D-lactate measurements. When we added glycolic acid at 1:1 ratio to L- and D-lactate-containing solution, the current response rose to 10.53 and 25.34 µA, respectively. Similar to that, when glyoxylic acid was added, the current response rose to 11.21 and 30.1 µA, respectively. The positive false result could be due to the incomplete specificity of the analytical reagent L-LOx, allowing cross-reaction between the ethylene glycol metabolites with L-LOx.[73-74,81] An artificial elevation of lactate measurements might lead to a misdiagnosis of lactic acidosis in ethylene glycol poisoning. Once this misdiagnosis was recognized, a "lactate gap" is calculated in point-of-care testing and is used to aid in proper diagnosis and therapy. Figure 5.28 also shows that the oxalic acid had not affected the biosensor response at all. This could be due to the selectivity of this biosensor towards the final product of the ethylene glycol metabolism.

False lactate measurement might have led to misdiagnosis, inappropriate laparotomy and delayed treatment in a patient with severe acidosis.[72] The treatment of ethylene glycol ingestion is time-dependent, which delays could lead to serious consequences, including renal failure and death. The "lactate gap" is a quick and sensitive test that can be established at the point-of-care analysis to help for the lactate

acidosis treatment.[82] As long as the "lactate gap" is exist, it means that the metabolites are still exist and the treatment of ethylene glycol poisoning has to be continued. This treatment could be ended with confidence, once the gap has disappeared.

5.8 Carbon Nanotubes-based Chiral Lactate Biosensors

The studies on chiral lactate biosensors were continued by expanding the electrode modification with Single Wall Carbon Nanotubes (SWCNTs). The unique properties of carbon nanotubes such as good electrical conductivity, high stability, strong adsorptive ability, high electrocatalytic effect and fast electron-transfer rate, make them extremely attractive for fabricating biosensors.[83] It has been shown that carbon nanotubes are able to improve the direct electron transfer reaction of some important biomolecules such as glucose[83-86], NADH[87-89], cytochrome c[90-92], and lactate[21,27,93-96].

In this section, ferrocene was used to modify the carbon nanotubes by using the adsorption process. The SWCNTs were treated with concentrated nitric acid solution, and then filtered, rinsed with deionised water and dried prior to modification with ferrocene. Nitric acid causes significant destruction of carbon nanotubes and introduces –COOH groups at the ends of, or at the sidewall defects in the nanotube structure.[97-98] The final SWCNTs are negatively charged after treatment.[99] These negatively charged particle can assemble on the surface of positively charged collagen and TMOS sol-gel easily by electrostatic interaction. The SWCNTs have strong adsorptive ability and they can adsorb biomolecules stably. This make the LOx enzyme interact with the SWCNTs strongly and immobilize on the SWCNTs nanocomposite tightly via the adsorption process.[93] The pH of the enzyme solution was also kept at neutral pH, which was above the isoelectric point of LOx (pI = 4.6)[63]. The enzyme exists in the form of anion under these conditions,[83] facilitating its interaction with the collagen (pI = 8.26[62]), which makes it suitably incorporated into the nanocomposite films.

The biosensors were developed according to the scheme shown in Figure 5.30. The carbon nanotubes-based chiral lactate biosensors were investigated in terms of the

electrochemical behaviour, chronoamperometric responses as well as its morphology characteristics.

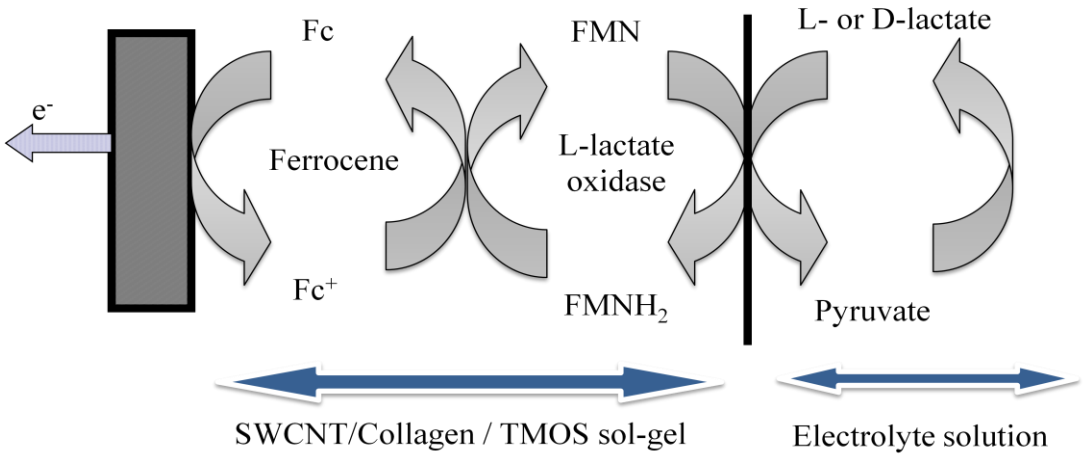

Figure 5.30: The mechanism of carbon nanotubes-based chiral lactate biosensors.

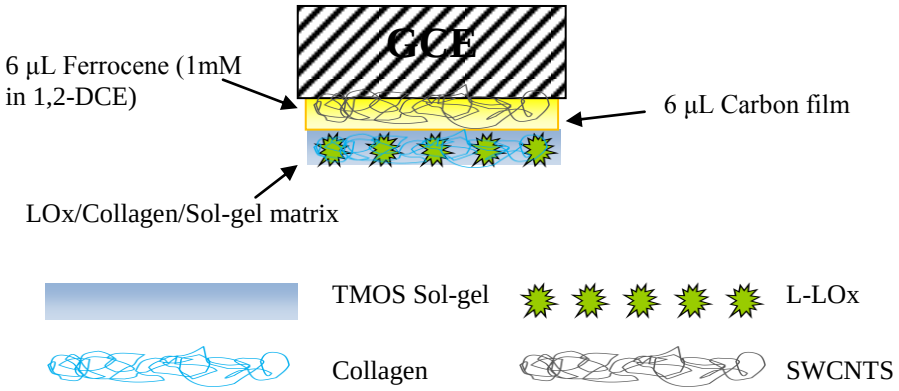

Figure 5.31: Diagram illustrated the layers on the modified GC electrode.

Cyclic voltammetry (CV) and electrochemical impedance spectroscopy (EIS) were used to characterize the modification of the GC electrodes. Figure 5.32 and 5.33 compare the CVs response at Fc/SWCNTs/LOx electrode, entrapped within (a) sol-gel, (b) collagen and (c) collagen/sol-gel matrixes in PBS (0.1 M, pH 7) containing 2 mM L- and D-lactate, respectively.

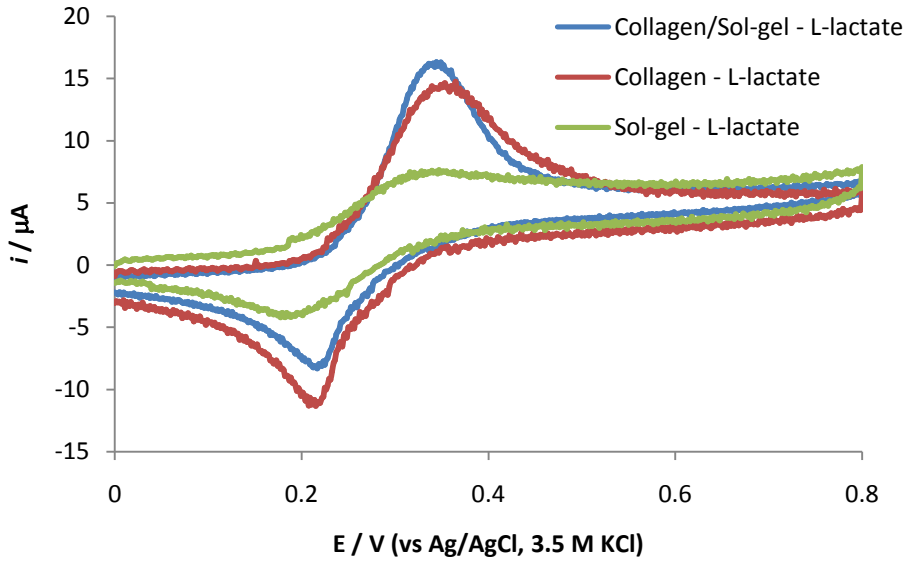

Figure 5.32: CVs of Fc/SWCNTs/LOx electrode entrapped within sol-gel, collagen and collagen/sol-gel matrixes in 0.1 M PBS (pH 7) containing 2 mM L-lactate. Scan rate: 10 mV/s.

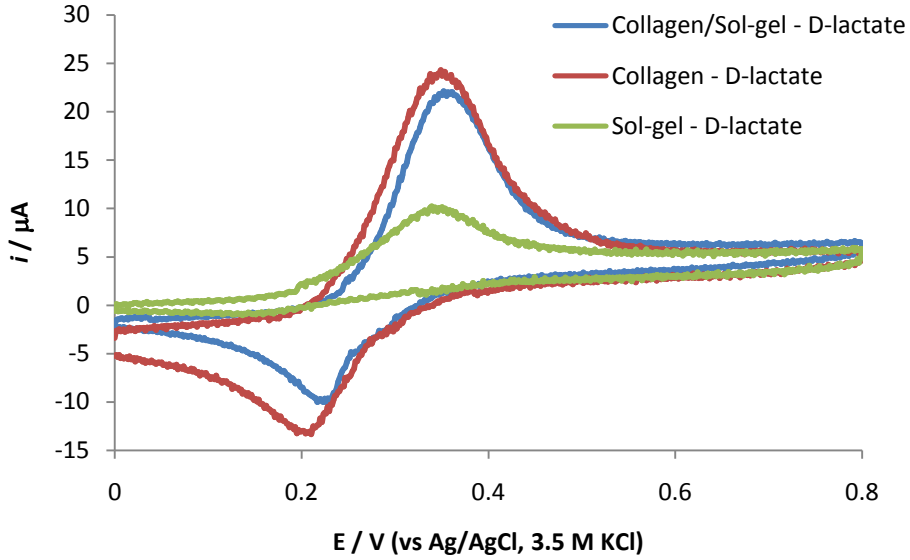

Figure 5.33: CVs of Fc/SWCNTs/LOx electrode entrapped within sol-gel, collagen and collagen/sol-gel matrixes in 0.1 M PBS (pH 7) containing 2 mM D-lactate. Scan rate: 10 mV/s.

The Fc/SWCNTs/LOx electrode, entrapped within collagen and collagen/sol-gel matrixes display a pair of well-defined redox peaks at approximately 0.35 V (E_{pa}) and 0.21 V (E_{pc}) in both L- and D-lactate-containing solutions, respectively. A pair of well-defined peak-shaped CVs observed in L- and D-lactate detection depicts a semi-infinite linear diffusion-controlled redox process of the Fc/Fc^{+} couple at the SWCNTs/LOx-modified electrodes. The formal potential of the redox process was found to be approximately 0.28 V. By introduction of TMOS sol-gel to collagen matrix, the peak separation (ΔE_p) was slightly decreased indicating a more facile electron transfer process at the hybrid complex matrix.

Further decrease in the anodic peak current was observed at Fc/SWCNTs/LOx electrode, entrapped within TMOS gel matrix. In addition, the reduction peak of the redox active species disappeared when tested to detect the presence of D-lactate, suggesting an irreversible redox reaction occurs at this electrode. SWCNTs can also improve the surface area of electrode as indicated by its higher current response in conjunction with collagen as the immobilizing matrix. Naturally, SWCNTs should electrostatically attract the positively charged collagen, and then formed a porous network nanostructure by self-assembly process. Here, the carbon nanotubes functioned as a cross-linker.[27] Figure 5.34 shows the TEM image of SWCNTs incorporated within collagen matrix.

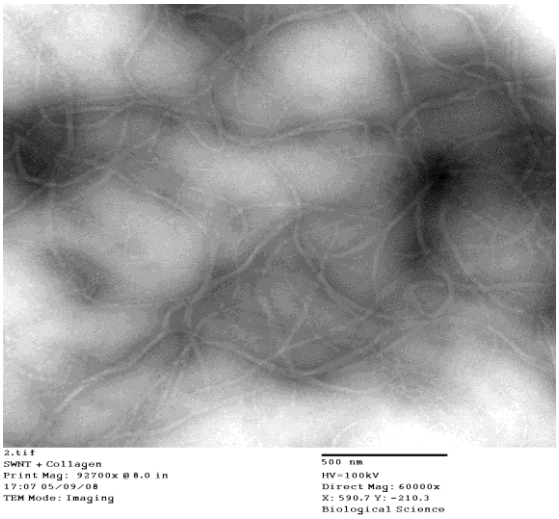

Figure 5.34: TEM image of SWCNTs incorporated within collagen matrix.

Figure 5.32 also shows that SWCNTs can enhance the current response to L-lactate in comparison to the LOx systems without carbon nanotubes (Figure 5.10). The anodic current response of SWCNTs electrode to the addition of 2 mM L-lactate increased by two fold compare to the electrode without SWCNT. This indicates that the Fc/SWCNTs/LOx electrode has better electrocatalytic activity to L-lactate, which improved the current intensities. This means the electrons could transfer occurs more kinetically favourably between the enzyme and modified electrode through the SWCNTs layer. However, the SWCNTs/LOx electrode entrapped within collagen and collagen/sol-gel matrixes had reduced the current response to D-lactate compared to the LOx-modified electrode without the presence of carbon nanotubes. This reduction in current response could be due to the adsorption competition between both negatively charged carbon nanotubes and LOx.[27] This competition could suppress the activity of LOx to tune its stereoselectivity towards D-lactate in conjunction to the effect of collagen within the composite mixture.

Another method to characterize the process at the modified electrodes is by using EIS, which is an effective method that always used for probing the interfacial properties of modified electrodes.[32-36] Figure 5.35 displays the Nyquist plot of impedance spectra obtained from various SWCNTs-modified GC electrodes, in 5 mM $Fe(CN)_6^{3-/4-}$ and 0.1 M KCl solution measured at the formal potential of the electrochemical probe.

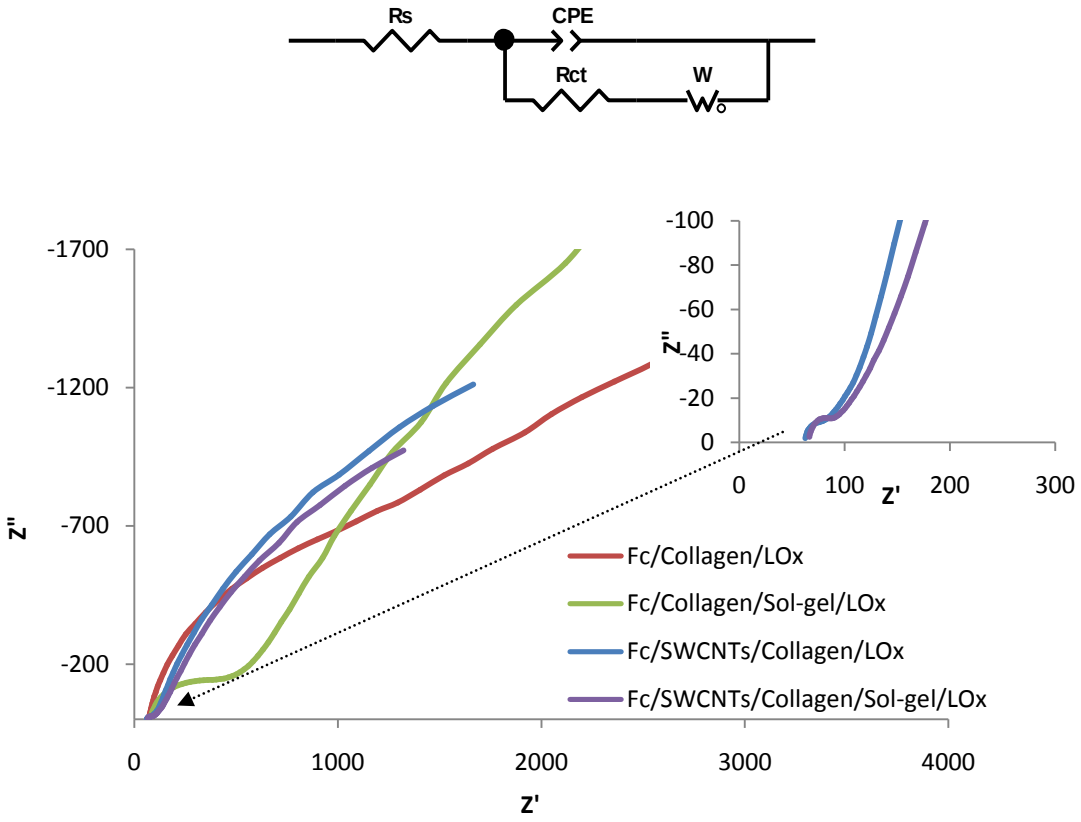

Figure 5.35: The Nyquist plot of impedance spectra obtained from various LOx-modified GC electrodes.

As shown in Figure 5.35, the impedance spectra measured at Fc/SWCNTs/Collagen/LOx and Fc/SWCNTs/Collagen/Sol-gel/LOx electrodes, respectively showed well-defined semicircles over a high frequency range followed by a straight-line portion over a lower frequency region. As calculated previously, the electron-transfer resistance (R_{ct}) was found to be 379 and 366 Ω for Fc/Collagen/LOx (red curve) and Fc/Collagen/Sol-gel/LOx (green curve) electrodes, respectively. After addition of SWCNTs, the semicircle portion become smaller and the R_{ct} reduced drastically to 24 and 33 Ω (blue and purple curves, respectively), indicating that the SWCNTs networked film provided much better electron transfer paths to have higher electrocatalytic activity. These results were in good agreement with the higher current response obtained in the CVs at SWCNTs/LOx-based electrodes (Figure 5.32 and 5.33).

The amperometric response of the SWCNTs network-based lactate biosensor was tested by sequential additions of a concentrated lactate solution into a stirred PBS (0.1 M, pH 7) at the potential of 0.28 V. The volume added to the buffer solution to

make up final concentration was varied from 0.25 mM at the first 1 mM final concentration, then increased to 0.5 mM for the next 2 mM and then continued by adding 1 mM of stock lactate solution until no further increment or small changes in current response was observed at the end of the measurement. The results shown in Figure 5.36, demonstrating the similar behaviour shows at SWCNTs/Collagen-based electrodes where the biosensors responding to both enantiomers of lactate. In the absence of collagen matrix as the enzyme immobilizing-agent, the amperometric measurement preferred to response to L-lactate instead of D-lactate. The current response of the Fc/SWCNTs/LOx/Sol-gel electrode increased linearly with increasing concentration of L-lactate in the range from 0.1 to 2 mM as shown in Figure 5.36(b). It takes about 8 s for the anodic current to achieve the steady state.

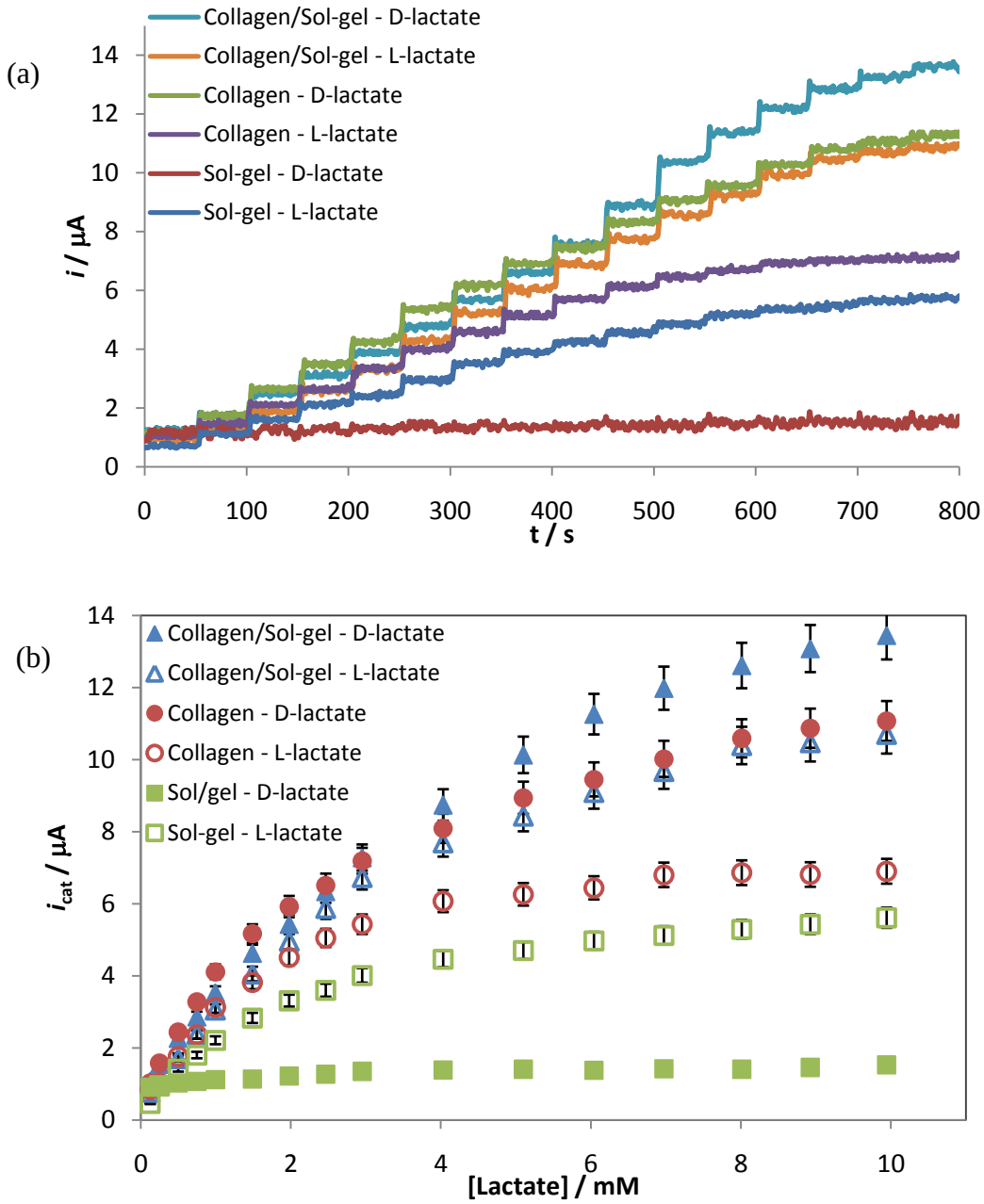

Figure 5.36: The amperometric responses (a) and the calibration curves (b) of current response of Fc/SWCNTs/LOx enzyme electrodes incorporated within various matrixes upon successive addition of L- and D-lactate in PBS (0.1 M, pH 7). Applied potential: 0.28 V.

Again, with the introduction of collagen, the chiral preference was dramatically changed to D-lactate instead of L-lactate in the SWCNTs/LOx system. Both collagen and collagen/sol-gel matrixes give a higher current response of L-LOx to D-lactate due to the effect of chiral inversion donated by collagen. It was seen that the SWCNTs

introduction as the cross-linker had enhanced the sensitivity of the biosensors in comparison with the biosensors without SWCNTs. The SWCNTs/Collagen and SWCNTs/Collagen/Sol-gel networks also have reduced the response time to lactate within less than 5 s, which is much faster response compared to the LOx-modified electrodes without incorporation with carbon nanotubes. This can be attributed to the easy diffusion of lactate, the high enzymatic reaction kinetics and the fast electrochemical reaction within the SWCNTs/LOx/Collagen and SWCNTs/LOx/Collagen/Sol-gel matrices.

However, an exceptional to this condition was obtained with Fc/SWCNTs/LOx/Collagen/Sol-gel electrode responding to D-lactate due to its wider linear range towards D-lactate concentration up to 7 mM (Table 5.7). The wider linear range could have benefits for the lactate detection in blood without further treatment.

After incorporation of SWCNTs into the composite, the sensitivity increased by approximately 50% compared to the sensitivity of the biosensors without incorporation with carbon nanotubes. The increase in sensitivity, which arises from the increase in the current response, is attributed to the ability of the SWCNTs nanocomposite to act as transducer for amperometric measurements. This is due to high conductivity and high surface area that facilitating the electron transfer. This result apparently demonstrated that the network nanostructure is more stable and could significantly reduce the measurement variations from swelling and resistance change.[27]

Table 5.7: The comparison of the performance of SWCNTs-based chiral lactate biosensors.

SWCNTs/LOx-modified GC Electrodes	**Linear range [lactate] / mM**	**Sensitivity / μA/mM ± 0.01**	**Correlation coefficient, *R***
Sol-gel - D-lactate	n.d	n.d	n.d
Sol-gel - L-lactate	2	3.27	0.984
Collagen - D-lactate	2.5	5.33	0.974
Collagen - L-lactate	2.5	3.25	0.980
Collagen/Sol-gel - D-lactate	7	2.60	0.975
Collagen/sol-gel - L-lactate	3	4.83	0.991

The calibration curve of the steady state current versus lactate concentration shows the characteristics of Michaelis-Menten kinetics mechanism. The current responses to various lactate concentrations were increased until to certain point it reaches a plateau current. This characteristic, which demonstrates the enzyme-substrate kinetics for the biosensor can be obtained from the analysis of the Hanes plot as evaluated by using a method described by Albery and Bartlett.[49] The Hanes plots and the calculated kinetic parameters are shown in Figure 5.37 and Table 5.8, respectively. The value of k'_s/k'_{ME} can be used to determine process at the electrode surface. From the results in Table 5.8, we can see that all of these SWCNTs/LOx-modified electrodes have k'_s/k'_{ME} values of > 1, indicating that the diffusion of the analyte through the membrane is rate limiting. Again, this is a desirable condition in many cases since it means that the response does not depend upon the activity of the enzyme.[48-49]

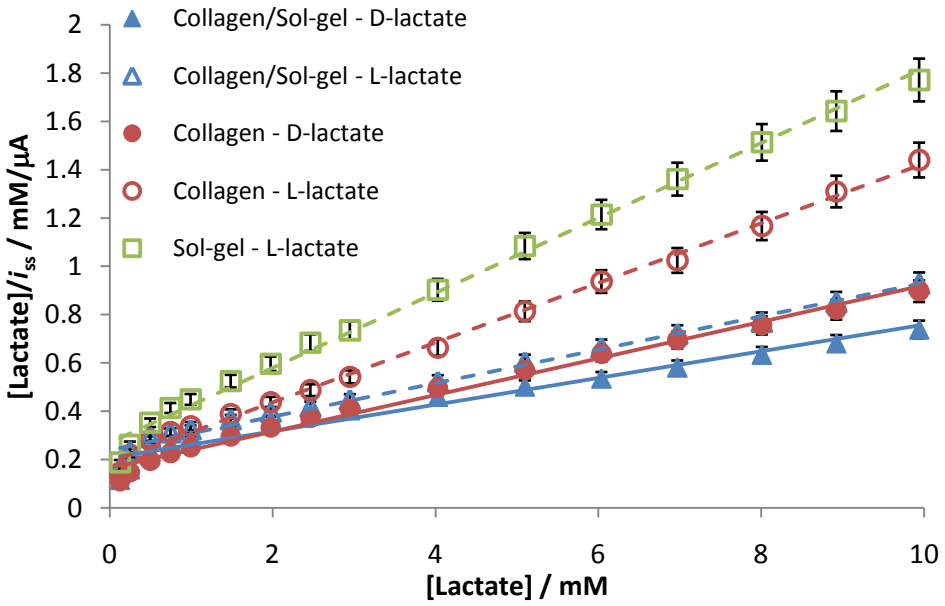

Figure 5.37: Hanes plots according to the data obtained from the calibration curve of SWCNTs/LOx-modified GC electrodes (Figure 5.34).

Table 5.8: The K_{ME} values calculated from the analysis of Hanes plot according to the method described by Albery and Bartlett[49] for each Fc/SWCNTs/LOx-modified electrodes.

LOx modified GC Electrodes	k_s' / k_{ME}'	K_{ME} / mM
Sol-gel - D-lactate	n.d	n.d
Sol-gel - L-lactate	1.4	1.8
Collagen - D-lactate	1.1	2.2
Collagen - L-lactate	1.2	1.5
Collagen/Sol-gel - D-lactate	1.1	3.7
Collagen/sol-gel - L-lactate	1.1	3.5

Similar to that observed with lactate biosensors without SWCNTs, lower calculated K_m values were obtained with L-lactate instead of D-lactate for each of the SWCNTs/LOx-modified electrodes. The lower K_m values obtained in response to L-lactate is explained by the faster rate of the L-LOx catalysis of the reaction to ½ V_{max} before it becomes saturated by further increment of L-lactate concentrations. The K_m values for LOx at the TMOS sol-gel matrix and collagen matrix electrodes seems to give much lower values compared to K_m values for the oxidation of L-lactate by free LOx in solution (K_m = 2.8 mM)[56]. The smaller K_m values indicate a high affinity of LOx entrapped within SWCNTs/sol-gel and SWCNTs/collagen composite to lactate. In fact, the smallest K_m value was obtained with the SWCNTs/LOx/Collagen composite electrode. This high affinity of LOx arises because of integration between the good biocompatibility of collagen and the good conductivity of carbon nanotubes. However, the K_m values of immobilized LOx within SWCNTs/Collagen/Sol-gel were found higher than that of free LOx. When the LOx enzyme is immobilized on solid supports with large active surface, contributed from the SWCNTs/collagen/sol-gel network, the surface groups on the support can induce conformational changes on the enzyme. This can lead to loss in the LOx activity after immobilization for reasons such as diffusion limitation of substrate and product and steric hindrance of the active site by the carrier.[96]

References

(1) Wang, J. *Chem. Rev.* **2008**, *108*, 814.

(2) Marxtibbon, S.; Katz, E.; Willner, I. *J. Am. Chem. Soc.* **1995**, *117*, 9925.

(3) Tao, G. L.; Katz, E.; Willner, I. *Chem. Commun.* **1997**, 2073.

(4) Scheele, C. *The Collected Papers of Carl Wilhelm Scheele*; 1931 edition ed.; G. Bell: London, UK, 1780.

(5) Ewaschuk, J. B.; Naylor, J. M.; Zello, G. A. *J. Nutr.* **2005**, *135*, 1619.

(6) Kim, J. W.; Dang, C. V. *Trends Biochem.Sci.* **2005**, *30*, 142.

(7) Bakker, J.; Gris, P.; Coffernils, M.; Kahn, R. J.; Vincent, J. L. *Am. J. Surg.* **1996**, *171*, 221.

(8) Baker, D. A.; Gough, D. A. *Anal. Chem.* **1995**, *67*, 1536.

(9) Smolenski, R. T.; Swierczynski, J.; Narkiewicz, M.; Zydowo, M. M. *Clin. Chim. Acta.* **1990**, *192*, 155.

(10) Mascini, M.; Moscone, D.; Palleschi, G. *Anal. Chim. Acta.* **1984**, *157*, 45.

(11) Pilloton, R.; Nwosu, T. N.; Mascini, M. *Anal. Lett.* **1988**, *21*, 727.

(12) Hillered, L.; Smith, M. L.; Siesjo, B. K. *J. Cereb. Blood Flow Metab.* **1985**, *5*, 259.

(13) Parra, A.; Casero, E.; Vazquez, L.; Pariente, F.; Lorenzo, E. *Anal. Chim. Acta.* **2006**, *555*, 308.

(14) Nikolaus, N.; Strehlitz, B. *Microchim. Acta.* **2008**, *160*, 15.

(15) Poscia, A.; Messeri, D.; Moscone, D.; Ricci, F.; Valgimigli, F. *Biosens. Bioelectron.* **2005**, *20*, 2244.

(16) Lowinsohn, D.; Bertotti, M. *Anal. Biochem.* **2007**, *365*, 260.

(17) Cai, X.; Yan, J. L.; Chu, H. H.; Wu, M. S.; Tu, Y. F. *Sens. Actuator B-Chem.* **2010**, *143*, 655.

(18) Shapiro, F.; Silanikove, N. *Food Chemistry.* **2010**, *119*, 829.

(19) Salminen, S., von Wright, A., & Ouwehand, A.C. *Lactic acid Bacteria: Microbiological and Functional Aspects*; 3rd edition ed.; Marcel Dekker, Inc.: New York, 2004.

(20) Mizutani, F.; Yabuki, S.; Hirata, Y. *Anal. Chim. Acta.* **1995**, *314*, 233.

(21) Pereira, A. C.; Aguiar, M. R.; Kisner, A.; Macedo, D. V.; Kubota, L. T. *Sens. Actuator B-Chem.* **2007**, *124*, 269.

(22) Kriz, K.; Kraft, L.; Krook, M.; Kriz, D. *J. Agric. Food Chem.* **2002**, *50*, 3419.

(23) He, X. R.; Yu, J. H.; Ge, S. G.; Zhang, X. M.; Lin, Q.; Zhu, H.; Feng, S.; Yuan, L.; Huang, J. D. *Chin. J. Anal. Chem.* **2010**, *38*, 57.

(24) Lin, C. L.; Shih, C. L.; Chau, L. K. *Anal. Chem.* **2007**, *79*, 3757.

(25) Goriushkina, T. B.; Orlova, A. P.; Smutok, O. V.; Gonchar, M. V.; Soldatkin, A. P.; Dzyadevych, S. V. *Biopolymers and Cell.* **2009**, *25*, 194.

(26) Montagne, M.; Marty, J. L. *Anal. Chim. Acta.* **1995**, *315*, 297.

(27) Cui, X. Q.; Li, C. M.; Zang, J. F.; Yu, S. C. *Biosens. Bioelectron.* **2007**, *22*, 3288.

(28) Sato, N.; Okuma, H. *Anal. Chim. Acta.* **2006**, *565*, 250.

(29) Palleschi, G.; Cubadda, R. *Ital. J. Food Sci.* **2001**, *13*, 137.

(30) Padalkar, S.; Zhao, J.; Stuart, K.; Panitch, A.; Rickus, J.; Stanciu, L. *Ultramicroscopy.* **2008**, *108*, 309.

(31) Eglin, D.; Coradin, T.; Giraud Guille, M. M.; Helary, C.; Livage, J. In *2nd International Conference on New Biomedical Materials*; Ios Press: Cardiff, WALES, 2003; Vol. 15, p 43.

(32) Ehret, R.; Baumann, W.; Brischwein, M.; Schwinde, A.; Stegbauer, K.; Wolf, B. *Biosens. Bioelectron.* **1997**, *12*, 29.

(33) Bardea, A.; Katz, E.; Willner, I. *Electroanalysis.* **2000**, *12*, 1097.

(34) Feng, C. L.; Xu, Y. H.; Song, L. M. *Sens. Actuator B-Chem.* **2000**, *66*, 190.

(35) Kang, X. H.; Mai, Z. B.; Zou, X. Y.; Cai, P. X.; Mo, J. Y. *Anal. Biochem.* **2007**, *369*, 71.

(36) Qiu, J. D.; Wang, R.; Liang, R. P.; Xia, X. H. *Biosens. Bioelectron.* **2009**, *24*, 2920.

(37) Zou, Y. J.; Xiang, C. L.; Sun, L. X.; Xu, F. *Biosens. Bioelectron.* **2008**, *23*, 1010.

(38) Ciobanu, M.; Taylor, D. E.; Wilburn, J. P.; Cliffel, D. E. *Anal. Chem.* **2008**, *80*, 2717.

(39) Wilson, R.; Turner, A. P. F. *Biosens. Bioelectron.* **1992**, *7*, 165.

(40) Narang, U.; Prasad, P. N.; Bright, F. V.; Ramanathan, K.; Kumar, N. D.; Malhotra, B. D.; Kamalasanan, M. N.; Chandra, S. *Anal. Chem.* **1994**, *66*, 3139.

(41) Wang, J.; Pamidi, P. V. A.; Park, D. S. *Electroanalysis.* **1997**, *9*, 52.

(42) Pandey, P. C.; Upadhyay, S.; Pathak, H. C. *Sens. Actuator B-Chem.* **1999**, *60*, 83.

(43) Wang, B. Q., Li, B., Deng, Q., and Dong, S.J. *Anal. Chem.* **1998**, *70*, 3170.

(44) Luo, X. L.; Xu, J. J.; Du, Y.; Chen, H. Y. *Anal. Biochem.* **2004**, *334*, 284.

(45) Rong, Z. M.; Cheema, U.; Vadgama, P. *Analyst.* **2006**, *131*, 816.

(46) Yang, M. L.; Wang, J.; Li, H. Q.; Zheng, J. G.; Wu, N. Q. N. *Nanotechnology.* **2008**, *19*.

(47) Faude, O.; Kindermann, W.; Meyer, T. *Sports Med.* **2009**, *39*, 469.

(48) Cooper, J., and Cass, T. *Biosensors: A Practical Approach*; First edition ed.; Oxford University Press: Oxford, 1990.

(49) Albery, W. J.; Bartlett, P. N. *J. Electroanal. Chem.* **1985**, *194*, 211.

(50) Murthy, A. S. N.; Sharma, J. *Anal. Chim. Acta.* **1998**, *363*, 215.

(51) Liu, S. Q.; Sun, Y. M. *Biosens. Bioelectron.* **2007**, *22*, 905.

(52) Xian, Y. Z.; Liu, F.; Feng, L. J.; Wu, F. H.; Wang, L. W.; Jin, L. T. *Electrochem. Commun.* **2007**, *9*, 773.

(53) Rogers, M. J.; Brandt, K. G. *Biochemistry.* **1971**, *10*, 4636.

(54) Palmisano, F.; Quinto, M.; Rizzi, R.; Zambonin, P. G. *Analyst.* **2001**, *126*, 866.

(55) Torriero, A. A. J.; Salinas, E.; Battaglini, F.; Raba, J. *Anal. Chim. Acta.* **2003**, *498*, 155.

(56) Suman, a. P., C.S. *Sensors & Transducers Journal.* **2007**, *79*, 1192.

(57) Bard, A. J., and Faulkner, L.R. *Electrochemical Methods: Fundamentals and Applications*; 2nd edition ed.; John Wiley & Sons Inc.: USA, 2001.

(58) Bartlett, P. N.; Whitaker, R. G. *J. Electroanal. Chem.* **1987**, *224*, 27.

(59) Bartlett, P. N.; Whitaker, R. G. *J. Electroanal. Chem.* **1987**, *224*, 37.

(60) Kothapalli, A.; Hayes, K.; Sadler, G.; Morgan, M. *J. Food Sci.* **2007**, *72*, C478.

(61) Cornish-Bowden, A.; Portland Press Ltd.: London, 1995.

(62) Zhang, Z. K.; Li, G. Y.; Shi, B. *J. Soc. Leather Technol. Chem.* **2006**, *90*, 23.

(63) Sung, W. J.; Bae, Y. H. *Sens. Actuator B-Chem.* **2006**, *114*, 164.

(64) Freudenberg, U.; Behrens, S. H.; Welzel, P. B.; Muller, M.; Grimmer, M.; Salchert, K.; Taeger, T.; Schmidt, K.; Pompe, W.; Werner, C. *Biophys. J.* **2007**, *92*, 2108.

(65) Deniset-Besseau, A.; Duboisset, J.; Benichou, E.; Hache, F.; Brevet, P. F.; Schanne-Klein, M. C. *J. Phys. Chem. B.* **2009**, *113*, 13437.

(66) Yamauchi, K.; Takeuchi, N.; Kurimoto, A.; Tanabe, T. *Biomaterials.* **2001**, *22*, 855.

(67) Sionkowska, A.; Wisniewski, M.; Skopinska, J.; Kennedy, C. J.; Wess, T. J. *J. Photochem. Photobiol. A-Chem.* **2004**, *162*, 545.

(68) Liu, K. Z.; Dixon, I. M. C.; Mantsch, H. H. *Cardiovasc. Pathol.* **1999**, *8*, 41.

(69) Petibois, C.; Gouspillou, G.; Wehbe, K.; Delage, J. P.; Deleris, G. *Anal. Bioanal. Chem.* **2006**, *386*, 1961.

(70) Habermehl, J.; Skopinska, J.; Boccafoschi, F.; Sionkowska, A.; Kaczmarek, H.; Laroche, G.; Mantovani, D. *Macromolecular Bioscience.* **2005**, *5*, 821.

(71) Hecht, H. J.; Schomburg, D.; Kalisz, H.; Schmid, R. D. *Biosens. Bioelectron.* **1993**, *8*, 197.

(72) Brindley, P. G.; Butler, M. S.; Cembrowski, G.; Brindley, D. N. *Can. Med. Assoc. J.* **2007**, *176*, 1097.

(73) Morgen, T. J.; Clark, C.; Clague, A. *Crit. Care Med.* **1999**, *27*, 2177.

(74) Woo, M. Y.; Greenway, D. C.; Nadler, S. P.; Cardinal, P. *J. Emerg. Med.* **2003**, *25*, 289.

(75) Graine, H.; Toumi, K.; Roullier, V.; Capeau, J.; Lefevre, G. *Ann. Biol. Clin.* **2007**, *65*, 421.

(76) Meng, Q. H.; Adeli, K.; Zello, G. A.; Porter, W. H.; Krahn, J. *Clin. Chim. Acta.* **2010**, *411*, 601.

(77) Eder, A. F.; McGrath, C. M.; Dowdy, Y. G.; Tomaszewski, J. E.; Rosenberg, F. M.; Wilson, R. B.; Wolf, B. A.; Shaw, L. M. *Clin. Chem.* **1998**, *44*, 168.

(78) MSDS-Glycolic-Acid; Sigma Aldrich.

(79) MSDS; Sigma Aldrich.

(80) Clarke. H.T., D., A.W. *Organic Synthetic.* **1941**, *1*, 421.

(81) Porter, W. H.; Crellin, M.; Rutter, P. W.; Oeltgen, P. *Clin. Chem.* **2000**, *46*, 874.

(82) Shirey, T.; Sivilotti, M. *Crit. Care Med.* **1999**, *27*, 2305.

(83) Zou, Y. J.; Xian, C. L.; Sun, L. X.; Xu, F. *Electrochim. Acta.* **2008**, *53*, 4089.

(84) Zhu, L. D.; Yang, R. L.; Zhai, J. G.; Tian, C. Y. *Biosens. Bioelectron.* **2007**, *23*, 528.

(85) Tsai, M. C.; Tsai, Y. C. *Sens. Actuator B-Chem.* **2009**, *141*, 592.

(86) Wang, J.; Musameh, M. *Analyst.* **2003**, *128*, 1382.

(87) Musameh, M.; Wang, J.; Merkoci, A.; Lin, Y. H. *Electrochem. Commun.* **2002**, *4*, 743.

(88) Chen, J.; Bao, J. C.; Cai, C. X.; Lu, T. H. *Chin. Chem. Lett.* **2003**, *14*, 1171.

(89) Wang, J. *Electroanalysis.* **2005**, *17*, 7.

(90) Wang, J. X.; Li, M. X.; Shi, Z. J.; Li, N. Q.; Gu, Z. N. *Anal. Chem.* **2002**, *74*, 1993.

(91) Zhao, G. C.; Yin, Z. Z.; Wei, X. W. *Front. Biosci.* **2005**, *10*, 2005.

(92) Yin, Z. Z.; Zhao, G. C.; Wei, X. W. *Chem. Lett.* **2005**, *34*, 992.

(93) Huang, J. D.; Song, Z.; Li, J.; Yang, Y.; Shi, H. B.; Wu, B. Y.; Anzai, J. I.; Osa, T.; Chen, Q. *Mater. Sci. Eng. C-Biomimetic Supramol. Syst.* **2007**, *27*, 29.

(94) Huang, J.; Li, J.; Yang, Y.; Wang, X. S.; Wu, B. Y.; Anzai, J. I.; Osa, T.; Chen, Q. *Mater. Sci. Eng. C-Biomimetic Supramol. Syst.* **2008**, *28*, 1070.

(95) Tsai, Y. C.; Chen, S. Y.; Liaw, H. W. *Sens. Actuator B-Chem.* **2007**, *125*, 474.

(96) Ma, L. J.; Wen, J. P.; Lu, W. Y.; Caiyin, Q. G.; Liang, Y. *Enzyme Microb. Technol.* **2008**, *42*, 235.

(97) Papakonstantinou, P.; Kern, R.; Irvine, J.; McAdams, E.; McLaughlin, J.; McNally, T. *Fuller. Nanotub. Carbon Nanostruct.* **2005**, *13*, 275.

(98) Lawrence, N. S.; Deo, R. P.; Wang, J. *Electroanalysis.* **2005**, *17*, 65.

(99) Xu, Z. A.; Gao, N.; Chen, H. J.; Dong, S. J. *Langmuir.* **2005**, *21*, 10808.

CHAPTER 6

APPLICATION OF CHIRAL LACTATE BIOSENSORS IN DAIRY PRODUCTS

6.1 Introduction

As explained previously in Section 5.2, lactate exists as two stereoisomers, L-lactate and D-lactate. Both enantiomers of lactate can be produced by a group of bacteria, known as lactic acid bacteria (LAB) as the major metabolic end product of carbohydrate fermentation.[1] Fermentative products such as milk, yogurt, wine, pickled vegetables and cured meats and fish produce a mixture of L- and D-lactate. While L-lactate has many nutritional advantages to human body system, D-lactate is always used as a specific indicator of bacteria fermentation to serves as an indicator for the freshness quality of fermentative products.[2-3]

In food industry, yogurt is produced by LAB fermentation of milk lactose to produce lactic acid. According to Tamime and Deeth (1980)[4], in order to be named as yogurt, a product should be made with the bacteria species' *Streptococcus salivarius* subsp. *Thermophilus* (an L-lactate producing LAB) and *Lactobacillus delbrueckii* subsp. *Bulgaricus* (a D-lactate producing LAB). A mixture of L- and D-lactate is formed with these bacteria and the preponderance of either isomer is related to the predominance of one group of bacteria over another group.

Beside the main lactate producing LAB as stated above, modern dairy products also contain added live cultures of LAB such as *Lactobacillus acidophilus*, *Lactobacillus casei* and *Bifid bacterium* species. These bacteria commonly known as probiotics, produce mostly L-lactate as the main end product.[5] Thus, a higher content of L-lactate compared to D-lactate can be expected presence in many probiotics-based dairy products in the market today. Probiotics are known to extend health benefits and therefore may be included during yoghurt manufacture to enhance its prophylactic properties.

An increase in lactate content also results from microbial contamination of dairy product. Lactate determination can therefore be very useful for the early detection of microbial contamination, especially for milk thermally treated for long-term storage.[6]

Besides dairy product, L- and D-lactate can also be found in any other foodstuffs such as in cured meat and fish. In the industry involving processed meat, D-lactate is used as an indicator for contamination of vacuum-packed chilled meat. Similarly, an increase occurrence of L-lactate is an indicator of spoilage by contamination in the egg industry. The quality of beer, fruit and vegetable juices can be assured by measurement of the D- and L-lactate content. A contamination of fruit juices with LAB often remains unnoticed for a longer time, allowing the bacteria to spread and infect huge volumes of juices.[7] The alteration of the organoleptic properties of the juice does not permit a further consumption. In the wine industry, the course of malolactic fermentation is monitored by following the falling level of L-malic acid and the increasing level of L-lactic acid. This conversion leads to a deacidification and softening of the wine's taste. However, the production of D-lactic acid, can indicate wine spoilage.[7]

This chapter will be focused on the application of lactate biosensors in milk and yogurt samples. Several examples of amperometric biosensors for L-lactate determination in milk and/or yogurt samples have been proposed.[6,8-15] Palmisano *et al*. (2001)[6] for example, have described and characterized a bilayer disposable lactate sensor that able to operate in flow injection analysis. The biosensor that was fabricated by glutaraldehyde co-crosslinking of L-lactate oxidase with bovine serum albumin was adequate for L-lactate determination in untreated milk and diluted yogurt samples. Mizutani *et al*. (1995)[10] have prepared an L-lactate sensing electrode based on a poly-L-lysine/poly(4-styrenesulfonate) complex layer containing L-LOx. The resulting electrode exhibited high performance characteristics such as rapid response (100% response in 5 s), high stability (usable for at least 8 weeks), and low interference levels. Whereas, Choi (2005)[12] has designed a long-lived L-lactate biosensor constructed from an eggshell membrane with LOx-chitosan polyelectrolyte complexes that can be used both in untreated or diluted dairy product and human serum samples.

Besides L-lactate biosensing, other papers also have presented an amperometric sensor for the detection of D-lactate by using D-lactate dehydrogenase system. In some of the cases, dilution or pretreatment of the samples is needed due to the certain limit of detection. Montagne and Marty (1995)[3] for example, have developed a bi-enzyme

sensor made from D-lactate dehydrogenase/NADH oxidase/NAD^+-dextran immobilized electrode for determination of D-lactate. The sensor can be used to measure the amount of D-lactate in dairy products such as yogurt and milk without any pretreatment, except for the cheeses, which were treated as indicated in Boerhinger kit test. The result obtained by this biosensor was in good agreement with the result obtained by using standard spectrophotometric method.

Until todate, all of the published literature related to lactate biosensor, have used stereospecifically L- or D-enzyme for the detection of its specific L- or D- enantiomer analytes. There is still no research involves selectively L- or D-lactate-based enzyme that can detect both enantiomers of lactate. For that reason, this study has been focused on simultaneously detection of both L- and D-lactate by using L-LOx system and applied the findings to real samples that contain both enantiomers of analytes. In this chapter, the amperometric biosensor based on LOx/collagen/TMOS matrix was used to simultaneously determine the content of both L- and D-lactate in dairy products and compare the results with previously reported lactate biosensors in literature.

6.2 Determination of L- and D-lactate in Food Samples.

The L- and D-lactate concentrations of commercially available milk and yogurt samples were determined by the constructed chiral lactate biosensor. Both fresh milk and yogurt were obtained directly from Tesco Extra superstore (Tesco Stores Limited, United Kingdom). The pasteurised standardised homogenised whole milk and low fat strawberry flavoured yogurt were used as the fresh milk and yogurt samples, respectively. For yogurt, sample of 1 g was diluted in 20 mL of deionised water, homogenized using a high speed stirrer and filtered. The filtered solutions were used for measurements. Fresh milk sample was analysed directly without any dilution. Both yogurt and milk samples was stored at 4 ºC and analysed within 3 days of buying it.

Chiral lactate biosensor based on LOx modified within collagen and TMOS sol-gel electrode was used thorough out this study. Standard curves of each L- and D-lactate were used as previously prepared in Section 5.3. This standard curves were obtained from the amperometric measurement by sequential addition of each L- and D-lactate

stock solution at 0.25 mM intervals. The standard curves of either L- and D-lactate were also assayed in the presence of 0.1 mM of the counter stereoisomers in all the standard points. Figure 6.1 shows the calibration standard curves of the stock solution of both L- and D-lactate in absence and presence of each of their counter stereoisomers.

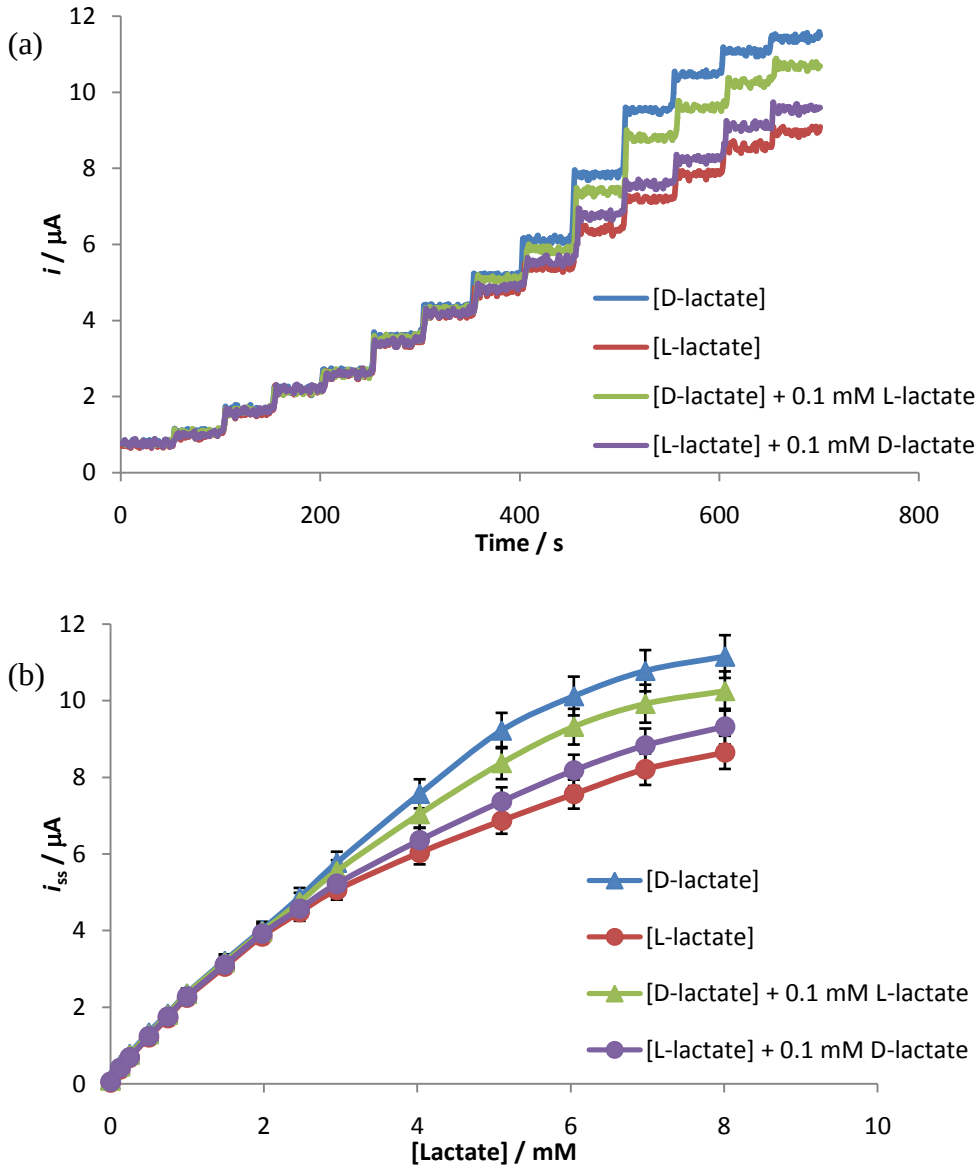

Figure 6.1: The amperometric responses (a) and the calibration curves (b) of current response of Fc/LOx/Collagen/Sol-gel GC electrodes upon successive addition of L- and D-lactate in the absence and presence of their counter stereoisomers in PBS (0.1 M, pH 7). Applied potential: 0.28 V.

The signal change of the sample solution was then measured and compared with that of sets of standard solution. Measurements were performed in triplicate and the results were averaged over three measurements. Assay repeatability of the method was analysed by calculating the R.S.D values of three replications of the measurements. The results displayed in Table 6.1 were obtained from a simple calculation as shown in Equation 6.1.

$$([\text{Sample}]_{\text{L-,D-lactate}} + 0.1\ \text{mM L-lactate}) - [\text{Sample}]_{\text{L-lactate}} = [\text{Sample}]_{\text{D-lactate}}$$

or $$([\text{Sample}]_{\text{L-,D-lactate}} + 0.1\ \text{mM D-lactate}) - [\text{Sample}]_{\text{D-lactate}} = [\text{Sample}]_{\text{L-lactate}} \quad (6.1)$$

As shown in Table 6.1, the estimation of accuracy (R.S.D) are within 1 to 3%, indicating the measurement of both L- and D-lactate content in dairy products provided consistent results over time. Both yogurt and milk are similar in terms of their higher content of L-lactate compared to D-lactate. These results were in good agreement with the findings in the literature.[16-17] In milk, L-lactate is the main stereoisomer in the systemic fluids, while D-lactate probably diffuses from the systemic fluids and originates from microbial activity in the digestive tract.[18]

Table 6.1: Results of L- and D-lactate analysis in dairy products.

Sample	L-lactate content ± 0.005 (mM)	R.S.D (%)	D-lactate content ± 0.005 (mM)	R.S.D (%)
Milk	0.135	1.5	0.02	2.8
Yogurt	72.6	1.1	25.0	3.3

Among those two dairy products, yogurt obviously had a much higher content of both L- and D-lactate compared to milk. The concentration of L- and D-lactate in the yogurt (Table 6.1) was found consistent with previous reports.[4-5,16] The preponderance

of L-lactate over D-lactate may be related to the predominance of *S. thermophilus* (an L-lactate producing LAB) over *L. delbrueckii* subsp. *Bulgaricus* (a D-lactate producing LAB) activity for most of the yogurt culturing process.[5] Because of D-lactate has no physiological significance in cell metabolism which its nutritional value only limited to improvement of casein digestion in the intestine, this predominance of L-lactate in yogurt is nutritionally advantageous for those whom consumed it. The concentration of D-lactate in yogurts could be reduced by increasing the production of *S. thermophilus* and by introduction of *Lactobacillus casei* subsp. *casei* into the culturing process.[5]

The results from this study demonstrate that the chiral lactate biosensor developed based on LOx/collagen/TMOS sol-gel matrix offers a convenient, consistent and simple method for simultaneous detection of both stereoisomers of lactate in real samples.

References

(1) Salminen, S., von Wright, A., & Ouwehand, A.C. *Lactic acid Bacteria: Microbiological and Functional Aspects*; 3rd edition ed.; Marcel Dekker, Inc.: New York, 2004.

(2) Soga, T.; Ross, G. A. *J. Chromatogr. A.* **1997**, *767*, 223.

(3) Montagne, M.; Marty, J. L. *Anal. Chim. Acta.* **1995**, *315*, 297.

(4) Tamime, A. Y.; Deeth, H. C. *J. Food Prot.* **1980**, *43*, 939.

(5) Sarkar, S. *Br. Food J.* **2008**, *110*, 717.

(6) Palmisano, F.; Quinto, M.; Rizzi, R.; Zambonin, P. G. *Analyst.* **2001**, *126*, 866.

(7) Nikolaus, N., and Strehlitz, B. *Microchim. Acta.* **2008**, *160*, 15.

(8) Pilloton, R.; Nwosu, T. N.; Mascini, M. *Anal. Lett.* **1988**, *21*, 727.

(9) Palmisano, F.; Guerrieri, A.; Quinto, M.; Zambonin, P. G. *Anal. Chem.* **1995**, *67*, 1005.

(10) Mizutani, F.; Yabuki, S.; Hirata, Y. *Anal. Chim. Acta.* **1995**, *314*, 233.

(11) Collier, W. A.; Lovejoy, P.; Hart, A. L. *Biosens. Bioelectron.* **1998**, *13*, 219.

(12) Choi, M. M. F. *Food Chemistry.* **2005**, *92*, 575.

(13) Torriero, A. A. J.; Salinas, E.; Battaglini, F.; Raba, J. *Anal. Chim. Acta.* **2003**, *498*, 155.

(14) Patel, N. G.; Erlenkotter, A.; Cammann, K.; Chemnitius, G. C. *Sens. Actuator B-Chem.* **2000**, *67*, 134.

(15) Herrero, A. M.; Requena, T.; Reviejo, A. J.; Pingarron, J. M. *European Food Research and Technology.* **2004**, *219*, 556.

(16) Shapiro, F.; Silanikove, N. *Food Chemistry.* **2010**, *119*, 829.

(17) Davis, S. R.; Farr, V. C.; Prosser, C. G.; Nicholas, G. D.; Turner, S. A.; Lee, J.; Hart, A. L. *J. Dairy Res.* **2004**, *71*, 175.

(18) Lindmark-Mansson, H.; Branning, C.; Alden, G.; Paulsson, M. *Int. Dairy J.* **2006**, *16*, 717.

CHAPTER 7

CONCLUSIONS AND FUTURE WORKS

7.1 Conclusions

This project has investigated the fabrication and characterization of biocompatible composite materials that suitable for chiral recognition. The development of good stability and reproducibility chiral biosensors was achieved. The composite materials comprised of collagen and/or TMOS sol-gel were successfully being used to immobilize both D-glucose oxidase and L-lactate oxidase, respectively. Ferrocene was also incorporated in the composite matrixes to facilitate electron transfer. Comparative amperometric measurements, CD and FTIR spectroscopy were used to evaluate the enantioselectivity of the enzymes towards both of their enantiomer analytes.

Results with the D-glucose oxidase or L-lactate oxidase enzymes incorporated in TMOS sol-gel displayed the expected behaviour with a preference for D-glucose and L-lactate, respectively. This result proved the fact that only one enantiomer of a chiral substrate, which have the same orientation with the enzyme, fit to the active site propertly to undergo the oxidation reaction. Interestingly, a reversal of chiral selectivity was observed when collagen was introduced into the sol-gel matrix, or in the collagen matrix itself. Higher response to the substrate of opposite chirality, which is L-glucose, for D-glucose oxidase and D-lactate for L-lactate oxidase is evident.

The evidence from electrochemical measurements, CD spectroscopy and FTIR spectroscopy, all point to a change in chiral selectivity when D-glucose oxidase and L-lactate oxidase interact with collagen. The isoelectric point of type 1 collagen is 8.26[1] which gives the collagen a net positive charge at pH 7. Whereas, D-glucose oxidase and L-lactate oxidase have isoelectric points of 4.3 and 4.6 respectively,[2] giving the molecules an overall negative charge at the same pH. Electrostatic interaction between the enzymes and collagen is therefore highly likely. This electrostatic interaction leads

to a modification in chiral recognition and selectivity of the enzymes. In electrochemical studies, ferrocene, the mediator may affect the chiral response due its interaction with collagen. However, in the FTIR and CD spectroscopy experiments, in which no ferrocene was added, significant chiral interactions were evident.

The response of chiral lactate biosensor was also evaluated by modification of ferrocene with SWCNTs. Electrochemical studies reveal that SWCNTs have improved the surface area of electrode by enhancing the current response towards L-lactate. The anodic current response increased by two fold compare to the electrode absence of SWCNTs. This result has support the fact that SWCNTs-based electrode has better electrocatalytic activity[3] as proved by EIS measurements.

The developed chiral lactate biosensor also might give a huge contribution in food industries, where a convenient, consistent and simple method of simultaneous detection of both L- and D-lactate is needed. This is important because the presence of both L- and D-lactate in foodstuffs have their own advantages to determine the quality of the products.

7.2 Future Works

Future work for this project would include further application of chiral lactate biosensors to other lactate-based foods real samples, for example in cured meat, fish and in fruit juices. By applying the chiral biosensor to these food samples, the ability of this biosensor to simultaneously detect the presence of both L- and D-lactate could be approved and a wider range of samples could be detected.

Beside food samples, the chiral lactate biosensor can also be applied to human fluid samples such as blood, saliva or sweat. The detection of L- and D-lactate in these samples has a significant contribution in clinical analysis and medical industries. Both L- and D-lactate are always of interest as indicator of many metabolic disorders, including cerebral ischemia of the respective tissue,[4] thus detection to the presence of these enantiomers in blood for example, is essential for the diagnosis of patient conditions.

Finally, the method in the development of chiral biosensor based on collagen as the key factor can also be used to construct other types of biosensor based on amino acid oxidases. Basically, flavoproteins such as L- and D-amino acid oxidases are the enzymes that catalyze the reaction of oxidation of L- or D-amino acids to corresponding iminoacids respectively, but they do not catalyze the reaction of opposite enantiomer. Thus, applying the constructed collagen based chiral biosensor hopefully can alter the structure of enzymes so that they will react with the enantiomer with opposite chirality as well.

References

(1) Kelly, S. M.; Jess, T. J.; Price, N. C. *BBA-Proteins Proteomics.* **2005**, *1751*, 119.

(2) Zhang, Z. K.; Li, G. Y.; Shi, B. *J. Soc. Leather Technol. Chem.* **2006**, *90*, 23.

(3) Zou, Y. J.; Xian, C. L.; Sun, L. X.; Xu, F. *Electrochim. Acta.* **2008**, *53*, 4089.

(4) Hillered, L.; Smith, M. L.; Siesjo, B. K. *J. Cereb. Blood Flow Metab.* **1985**, *5*, 259.